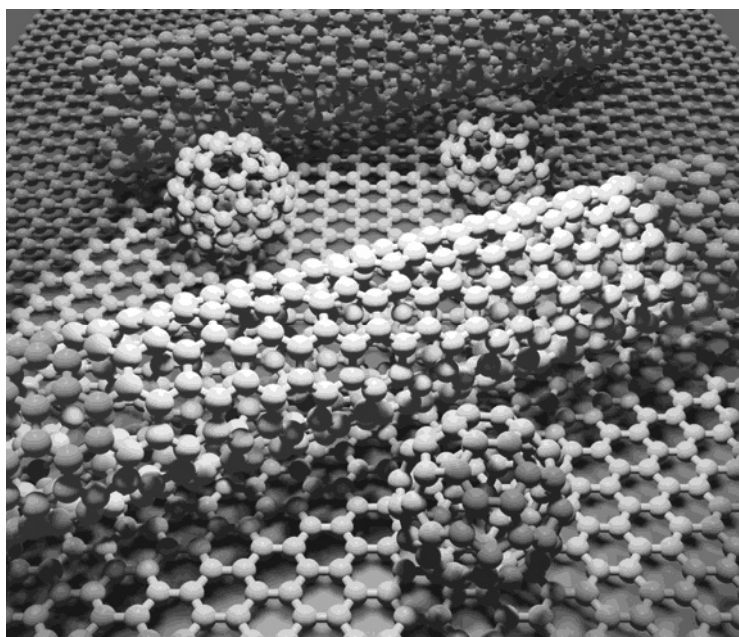


第59回
フラーレン・ナノチューブ・グラフェン
総合シンポジウム

The 59th Fullerenes-Nanotubes-Graphene General Symposium



講演要旨集

Abstracts

2020年9月16日(水) ~ 18日(金)

オンライン開催

Online Virtual Symposium



主催 フラーレン・ナノチューブ・グラフェン学会

The Fullerenes, Nanotubes and Graphene Research Society

共催

日本化学会 The Chemical Society of Japan

協賛

日本物理学会 The Physical Society of Japan

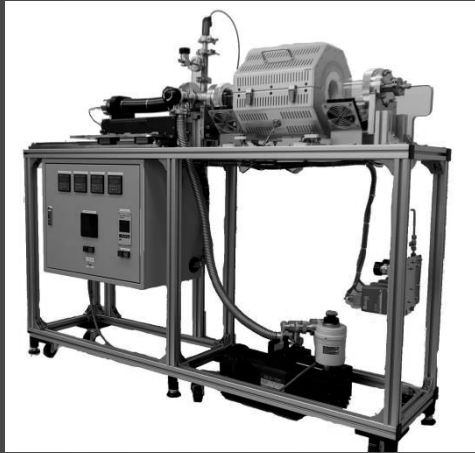
応用物理学会 The Japan Society of Applied Physics

高分子学会 The Society of Polymer Science, Japan

電気化学会 The Electrochemical Society of Japan

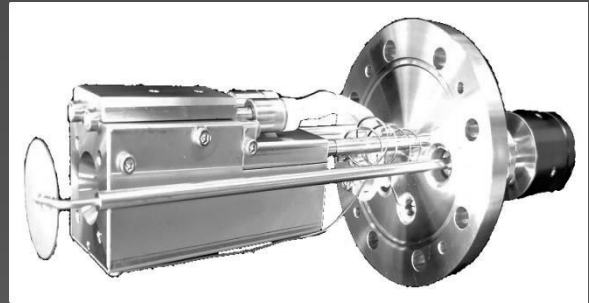
Graphene - Layered material Growth Equipment

Two-Stage Clean Thermal CVD



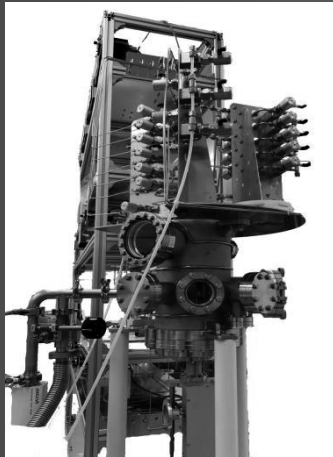
Two-stage Substrate transfer System.
1) From inside the furnace to outside
2) From inside the tube to outside

Stable Evaporation Source for MBE



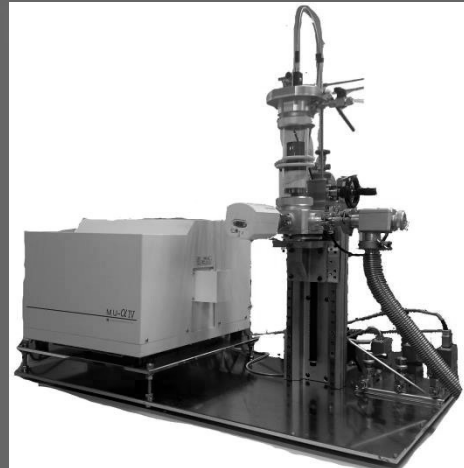
Hot lip evaporation source with
Original Special orifice for High
Vapor pressure materials.

Cold Wall type MOCVD



MOCVD equipment with a maximum
1500°C heating mechanism and
Reaction materials introduction
mechanism.

High Frequency Induction CVD



High frequency induction heating
can heat the sample mounted on the
susceptor up to 2000°C.

Kenix

2-15-501, Houjyoguchi, Himeji, Hyogo, 670-0935 JAPAN
TEL: 079-283-3150 FAX: 079-280-3002
E-mail: kenix@leto.eonet.ne.jp URL: <http://kenix.jp/>

Abstract of The 59th Fullerenes-Nanotubes-Graphene General Symposium (Online Virtual Symposium)

Sponsored by : The Fullerenes, Nanotubes and Graphene Research Society

Co-Sponsored by : The Chemical Society of Japan

Supported by : The Physical Society of Japan
The Japan Society of Applied Physics
The Society of Polymer Science, Japan
The Electrochemical Society of Japan

Date : September 16th (Wed.) – September 18th (Fri.), 2020

Presentation Time : Special Lecture (25 min presentation + 5min discussion)
Award Nominee Lecture (10 min presentation + 10min discussion)
General Lecture (10 min presentation + 5min discussion)
Poster Preview (1 min presentation without discussion)

Executive Committee : Global Innovation Center,
Kyushu University, Chikushi Campus, Fukuoka

第 59 回フラーレン・ナノチューブ・グラフェン総合シンポジウム 講演要旨集 (オンライン開催)

主催 : フラーレン・ナノチューブ・グラフェン学会

共催 : 日本化学会

協賛 : 日本物理学会、応用物理学会、高分子学会、電気化学会

日時 : 令和 2 年 9 月 16 日 (水) ~ 9 月 18 日 (金)

発表時間 : 特別講演 (発表 25 分 + 質疑応答 5 分)
受賞対象者講演 (発表 10 分 + 質疑応答 10 分)
一般講演 (発表 10 分 + 質疑応答 5 分)
ポスタープレビュー (発表 1 分・質疑応答 なし)

実行委員会 : 九州大学 筑紫キャンパス グローバルイノベーションセンター

展示団体御芳名（五十音順、敬称略）

santec（株）

テレデザイン・ジャパン（株）

（株）日本レーザー

広告掲載団体御芳名（五十音順、敬称略）

ケニックス（株）

桜木理化学機械（株）

（株）セントラル科学貿易

テレデザイン・ジャパン（株）

日本電子（株）

（株）日本レーザー

Contents

Time Table	• • • • •	i
Chairperson	• • • • •	iii
Program	Japanese • • • • •	iv
	English • • • • •	xvi
Abstracts	Special Lecture • • • • •	1
	General Lecture • • • • •	11
	Poster Preview • • • • •	47
Author Index	• • • • •	127

目次

早見表	• • • • •	i
座長一覧	• • • • •	iii
プログラム	和文 • • • • •	iv
	英文 • • • • •	xvi
講演予稿	特別講演 • • • • •	1
	一般講演 • • • • •	11
	ポスター発表 • • • • •	47
発表索引	• • • • •	127

プログラム早見表（オンライン開催）

9月16日（水）		9月17日（木）		9月18日（金）	
	接続開始 8:40-9:10		接続開始 8:45-9:00		接続開始 8:45-9:00
9:10	開会挨拶	9:00	特別講演（中野 匡規） 9:00-9:30	9:00	特別講演（中村 潤児） 9:00-9:30
9:15	特別講演（丸山 茂夫） 9:15-9:45	9:30	一般講演 2件（グラフェンの物性） 9:30-10:00	9:30	一般講演 4件 （原子層） 9:30-10:30
9:45	一般講演 3件 （ナノチューブの物性） 9:45-10:30	10:00	休憩 10:00-10:15	10:30	休憩 10:30-10:45
10:30	休憩 10:30-10:45	10:15	大澤賞・飯島賞 受賞対象者講演 4件 10:15-11:35	10:45	一般講演 2件 （ナノチューブの応用） 10:45-11:15
10:45	一般講演 3件 （グラフェン） 10:45-11:30	11:35	ポスタープレビュー （2P-1 ~ 2P-27） 11:35-12:20	11:15	ポスタープレビュー （3P-1 ~ 3P-26） 11:15-12:00
11:30	ポスタープレビュー （1P-1 ~ 1P-27） 11:30-12:15	12:20	昼食 12:20-13:30	12:00	昼食 12:00-13:00
12:15	昼食 （幹事会） 12:15-13:30	13:30	ポスターセッション 13:30-15:15	13:00	ポスターセッション 13:00-14:45
13:30	ポスターセッション 13:30-15:15	15:15	休憩 15:15-15:30	14:45	休憩 14:45-15:00
15:15	休憩 15:15-15:30	15:30	授賞式 15:30-16:00	15:00	特別講演（八木 隆多） 15:00-15:30
15:30	特別講演（池田 篤志） 15:30-16:00	16:00	総会 16:00-16:30	15:30	一般講演 4件 （ナノチューブの物性・応用） 15:30-16:30
16:00	一般講演 3件 （ナノチューブの応用） 16:00-16:45	16:30	休憩 16:30-16:45	16:30	休憩 16:30-16:45
16:45	休憩 16:45-17:00	16:45	一般講演 3件 （フラーレン・ナノ炭素粒子） 16:45-17:30	16:45	特別講演（窪田 芳之） 16:45-17:15
17:00	特別講演（田中 悟） 17:00-17:30	17:30	特別講演（速水 真也） 17:30-18:00	17:15	一般講演 2件 （ナノチューブの生成と精製） 17:15-17:45
17:30	一般講演 2件 （ナノチューブ） 17:30-18:00	18:00	一般講演 3件 （グラフェンの物性・応用） 18:00-18:45	17:45	特別講演（千賀 亮典） 17:45-18:15
18:00	休憩 18:00-18:15	18:45		18:15	
18:15	チュートリアル（松田 一成） 「ナノカーボン・原子層物質における光物性の基礎と応用」 18:15-19:45				
19:45					

特別講演 発表25分・質疑5分
 受賞対象者講演 発表10分・質疑10分
 一般講演 発表10分・質疑5分
 ポスタープレビュー 発表1分・質疑なし

Time table (Online Virtual Symposium)

Septemper 16 (Wed.)		Septemper 17 (Thu.)		Septemper 18 (Fri.)	
	Session Open (Connection Check) 8:40-9:10		Session Open (Connection Check) 8:45-9:00		Session Open (Connection Check) 8:45-9:00
9:10	Opening	9:00	Special Lecture (Masaki Nakano) 9:00-9:30	9:00	Special Lecture (Junji Nakamura) 9:00-9:30
9:15	Special Lecture (Shigeo Maruyama) 9:15-9:45	9:30	General Lectures [2] (Properties of graphene) 9:30-10:00	9:30	General Lectures [4] (Atomic Layers) 9:30-10:30
9:45	General Lectures [3] (Properties of nanotubes) 9:45-10:30	10:00	Coffee Break 10:00-10:15	10:30	Coffee Break 10:30-10:45
10:30	Coffee Break 10:30-10:45	10:15	Lectures of Osawa Award and Iijima Award Nominees [4] 10:15-11:35	10:30	Coffee Break 10:30-10:45
10:45	General Lectures [3] (Graphene) 10:45-11:30	11:35	Poster Preview (2P-1 through 2P-27) 11:35-12:20	10:45	General Lectures [2] (Applications of nanotubes) 10:45-11:15
11:30	Poster Preview (1P-1 through 1P-27) 11:30-12:15	12:20	Lunch 12:20-13:30	11:15	Poster Preview (3P-1 through 3P-26) 11:15-12:00
12:15	Lunch (Administrative meeting) 12:15-13:30	13:30	Poster Session 13:30-15:15	12:00	Lunch 12:00-13:00
13:30	Poster Session 13:30-15:15	15:15	Coffee Break 15:15-15:30	13:00	Poster Session 13:00-14:45
15:15	Coffee Break 15:15-15:30	15:30	Award Ceremony 15:30-16:00	14:45	Coffee Break 14:45-15:00
15:30	Special Lecture (Atsushi Ikeda) 15:30-16:00	16:00	General Meeting 16:00-16:30	15:00	Special Lecture (Ryuta Yagi) 15:00-15:30
16:00	General Lectures [3] (Applications of nanotubes) 16:00-16:45	16:30	Coffee Break 16:30-16:45	15:30	General Lectures [4] (Properties and Applications of nanotubes) 15:30-16:30
16:45	Coffee Break 16:45-17:00	16:45	General Lectures [3] (Fullerenes and Carbon nanoparticles) 16:45-17:30	16:30	Coffee Break 16:30-16:45
17:00	Special Lecture (Satoru Tanaka) 17:00-17:30	17:30	Special Lecture (Shinya Hayami) 17:30-18:00	16:45	Special Lecture (Yoshiyuki Kubota) 16:45-17:15
17:30	General Lectures [2] (Nanotubes) 17:30-18:00	18:00	General Lectures [3] (Graphene) 18:00-18:45	17:15	General Lectures [2] (Formation and purification of nanotubes) 17:15-17:45
18:00	Coffee Break 18:00-18:15	18:45		17:45	Special Lecture (Ryosuke Senga) 17:45-18:15
18:15	Tutorial (Kazunari Matsuda) 18:15-19:45			18:15	
19:45					

Special Lecture : 25 min (Presentation) + 5 min (Discussion)
 Award Nominee Lecture : 10 min (Presentation) + 10 min (Discussion)
 General Lecture : 10 min (Presentation) + 5 min (Discussion)
 Poster Preview : 1 min (Presentation)

座長一覧 (Chairpersons)

9月16日 (水)

(敬称略)

セッション	時 間	座 長
特別講演(丸山 茂夫)	9:15 ~ 9:45	齋藤 理一郎
一般講演	9:45 ~ 10:30	宮本 良之
一般講演	10:45 ~ 11:30	丸山 隆浩
ポスタープレビュー	11:30 ~ 12:15	蒲 江 小澤 大和
特別講演(池田 篤志)	15:30 ~ 16:00	白木 智丈
一般講演	16:00 ~ 16:45	Don Futaba
特別講演(田中 悟)	17:00 ~ 17:30	吾郷 浩樹
一般講演	17:30 ~ 18:00	野田 優
チュートリアル(松田 一成)	18:15 ~ 19:45	大野 雄高

9月17日 (木)

セッション	時 間	座 長
特別講演(中野 匡規)	9:00 ~ 9:30	北浦 良
一般講演	9:30 ~ 10:00	加藤 俊顕
一般講演(受賞対象者)	10:15 ~ 11:35	秋田 成司
ポスタープレビュー	11:35 ~ 12:20	松永 正広 吉原 直記
一般講演	16:45 ~ 17:30	松尾 豊
特別講演(速水 真也)	17:30 ~ 18:00	仁科 勇太
一般講演	18:00 ~ 18:45	柳 和宏

9月18日 (金)

セッション	時 間	座 長
特別講演(中村 潤児)	9:00 ~ 9:30	高井 和之
一般講演	9:30 ~ 10:30	宮田 耕充
一般講演	10:45 ~ 11:15	鈴木 信三
ポスタープレビュー	11:15 ~ 12:00	丸山 実那 中島 秀朗
特別講演(八木 隆多)	15:00 ~ 15:30	横井 裕之
一般講演	15:30 ~ 16:30	松田 一成
特別講演(窪田 芳之)	16:45 ~ 17:15	湯田坂 雅子
一般講演	17:15 ~ 17:45	藤ヶ谷 剛彦
特別講演(千賀 亮典)	17:45 ~ 18:15	長汐 晃輔

9月 16日 (水)

特別講演 発表 25分 ・ 質疑応答 5分
一般講演 発表 10分 ・ 質疑応答 5分
ポスタープレビュー 発表 1分 ・ 質疑応答 なし

特別講演 (9:15-9:45)

- 1S-1 一次元ヘテロナノチューブの合成と応用 1
* 丸山 茂夫

一般講演 (9:45-10:30)

ナノチューブの物性

- 1-1 ナノチューブ線材の抵抗値に見られる線形な温度特性 11
* 稲葉 工, 森本 崇宏, 山崎 悟志, 岡崎 俊也
- 1-2 単層MoS₂ナノチューブの間接-直接バンドギャップクロスオーバー 12
* 久間 馨, 丸山 実那, 岡田 晋, 千足 昇平, 丸山 茂夫
- 1-3 Diameter-dependent Photoluminescence Properties in Color Centers of Air-Suspended Single-Walled Carbon Nanotubes 13
* Daichi Kozawa, Xiaojian Wu, Akihiro Ishii, Jacob Fortner, Keigo Otsuka, Rong Xiang, Taiki Inoue, Shigeo Maruyama, YuHuang Wang, Yuichiro K. Kato

>>>>>>> 休憩 (10:30-10:45) <<<<<<<<

一般講演 (10:45-11:30)

グラフェンの物性

- 1-4 Energetics and electronic structure of bilayer graphene intercalating buckybowls 14
* Mina Maruyama, Susumu Okada

グラフェン生成

- 1-5 グラフェンナリボンを用いたサイズ制御量子ドットの直接合成 15
* 瀬尾 瑞樹, 北田 孝仁, 金子 俊郎, 大塚 朋廣, 加藤 俊顕

グラフェンの応用

- 1-6 High-order mode operation of graphene mechanical resonator 16
* Hirofumi Ikemoto, Kaito Nakagawa, Taichi Inoue, Kuniharu Takei, Takayuki Arie, Seiji Akita

ポスタープレビュー (11:30-12:15) (☆) 若手奨励賞候補

若手奨励賞候補

- 1P-1 塩化鉄を触媒前駆体に用いた多層カーボンナノチューブの成長メカニズム 47
☆ * 林 竜弘, 中野 貴之, 井上 翼
- 1P-2 Light-driven wavelength shifts of photoluminescence from single-walled carbon nanotubes by functionalization with diarylethene derivatives 48
☆ * 中川 泰人, 中嶋 琢也, 河合 壯, 藤ヶ谷 剛彦, 白木 智丈
- 1P-3 フレキシブル薄膜トランジスタに向けた架橋性アミンポリマーを用いたカーボンナノチューブ薄膜の製膜 49
☆ * 松本 海成, 上野 和樹, 廣谷 潤, 大野 雄高, 大町 遼

9月16日(水)

1P-4	局所化学修飾単層カーボンナノチューブの溶媒環境に対する励起子エネルギー変化とその構造依存性	50
☆	* 新留 嘉彬, 藤ヶ谷 剛彦, 白木 智丈	
1P-5	Visualization of thermal transports on bundled carbon nanotubes by monitoring evaporation of gold nanoparticles	51
☆	* Hiromu Hamasaki, Seiya Takimoto, Kaori Hirahara	
1P-6	単層カーボンナノチューブの低誘電率有機溶媒系におけるゼータ電位測定	52
☆	* 石井 大貴, ボラ アンガナ, 田中 直樹, 藤ヶ谷 剛彦	
1P-7	ストレプトアビジンを複合化した酸化カーボンナノチューブによる近赤外蛍光イムノアッセイ	53
☆	* 児島 敬子, 飯泉 陽子, 張 民芳, 岡崎 俊也	
1P-8	Effects of channel length on performance of transparent solar cell with monolayer WS ₂	54
☆	* Xing He, Toshiro Kaneko, Toshiaki Kato	
1P-9	Cr _{1/3} NbSe ₂ 超薄膜における面内強磁性	55
☆	* 真島 裕貴, Saika Bruno Kenichi, 松岡 秀樹, 中野 匡規, 吉田 訓, 石坂 香子, 岩佐 義宏	

ナノ炭素粒子

1P-10	Energetics and geometric structure of corannulene under an external electric field	56
	* Susumu Okada, Yanlin Gao, Mina Maruyama	

ナノチューブの生成と精製

1P-11	時間依存第一原理計算によるフェムト秒レーザー照射下でのサブナノメートル直径チューブの選択の提案	57
	* 宮本 良之	

ナノチューブの物性

1P-12	半導体型単層カーボンナノチューブの熱電物性の一次元性	58
	* 一ノ瀬 遥太, 松原 愛帆, 蓬田 陽平, 吉田 朱里, 上治 寛, 金橋 魁利, 蒲江, 竹延 大志, 山本 貴博, 柳 和宏	
1P-13	超音波照射による簡便で効果的な単層カーボンナノチューブの発光特性制御	59
	* 紺野 優以, 西野 朱音, 山田 道夫, 前田 優, 奥平 早紀, 宮内 雄平, 松田 一成, 松井 淳, 三ツ石 方也, 鈴木 光明	

ナノチューブの応用

1P-14	Utilization of transparent SWCNT films in 4-terminal perovskite-silicon tandem solar cells	60
	* Ahmed Shawky, Kosuke Akino, Takuya Matsui, Taiki Inoue, Esko Kauppinen, Shohei Chiashi, Shigeo Maruyama	
1P-15	Simple and highly efficient intermittent operation circuit for triboelectric nanogenerator	61
	* Atsushi Kawaguchi, Masahiro Matsunaga, Haruki Uchiyama, Jun Hirotsu, Yutaka Ohno	
1P-16	Carbon nanotube-Cu through-Si-via interposer with Cu-level electrical conductivity and Si-comparable thermal expansion	62
	* 陳 国海, Sundaram Rajyashree, 関口 貴子, 畠 賢治, Futaba Don N.	

9月16日(水)

- 1P-17 Electrical detection of X-ray by using coplanar CNT thin-film electrodes on PEN substrate 63
* 鈴木 慧, 松田 裕之, 石川 剛弘, 小西 輝昭, 濱野 毅, 安食 博志, 大野 雄高, 平尾 敏雄, 石井 聡

グラフェン生成

- 1P-18 ゆらぎ導入ナノバーからのグラフェンナリボン制御合成 64
* 佐藤 尚郁, 金子 俊郎, 加藤 俊顕

- 1P-19 グラフェン成長に用いるサファイア基板上巨大グレインNi薄膜の作製 65
* 中島 諒人, 櫻尾 達也, 村橋 知明, 曾我 司, 丸山 隆浩, 成塚 重弥

グラフェンの物性

- 1P-20 回転角0.5度以下での2枚グラフェンモアレ解析をコンピュータイメージングとする教育的意義 66
* 夏目 雄平, 森谷 東平

- 1P-21 Raman optothermal methods to measure interfacial thermal conductance of low-dimensional materials 67
* 李 秦宜, 高橋 厚史

グラフェンの応用

- 1P-22 Non-diffusive molecular transport in graphene liquid cells 68
* 廣川 颯汰, 手嶋 秀彰, ソリス フェルナンデス パブロ, 吾郷 浩樹, 塘 陽子, 李 秦宜, 高橋 厚史

原子層

- 1P-23 Layer-selective dopant implantation in van der Waals heterostructures 69
* Hiroto Ogura, Yuya Murai, Toshifumi Irisawa, Zheng Liu, Hiroshi Shimizu, Hong En Lim, Yusuke Nakanishi, Takahiko Endo, Ryo Kitaura, Yasumitsu Miyata

- 1P-24 TaS₂への水素吸着による電子物性への影響 70
* 石黒 康志, 児玉 尚子, Kirill Bogdanov, Alexander Baranov, 高井 和之

ナノワイヤー

- 1P-25 Simple formula of enhancement of the electric field inside a hollow metallic cylinder 71
* Yuan Tian, Muhammad Shoufie Ukhtary, Riichiro Saito

- 1P-26 Tellurization of solution-synthesized tungsten oxide nanowires 72
* Mai Nagano, Yohei Yomogida, Yasumitsu Miyata, Kazuhiro Yanagi

その他

- 1P-27 First-principles calculation of excitonic effect in Raman spectra 73
* Xiaoqi Pang, T.Hung Nguyen, Riichiro Saito

>>>>>>> 昼食 (12:15-13:30) <<<<<<<<

ポスターセッション (13:30-15:15)

>>>>>>> 休憩 (15:15-15:30) <<<<<<<<

9月16日(水)

特別講演 (15:30-16:00)

- 1S-2 リポソームに内包した光捕集分子-C₆₀誘導体二元系を用いる光線力学治療法への応用 2
* Atsushi Ikeda, Daiki Antoku, Kouta Sugikawa, Riku Kawasaki

一般講演 (16:00-16:45)

ナノチューブの応用

- 1-7 One dimensional hetero-junction diode 17
* Ya Feng, Henan Li, Taiki Inoue, Shigeo Maruyama
- 1-8 Polyaromatic Anthracene Nano-tweezer on Semiconducting Carbon Nanotubes for Growth and Bridging of Perovskite Crystal Grains in Perovskite Solar Cells 18
* 林 昊升, 田 日, 松尾 豊, 丸山 茂夫
- 1-9 Aligned carbon nanotube/polymer composite films for high thermal diffusivity 19
* Maireyee Bhattacharya, Manish Pandey, Ryo Abe, Naofumi Okamoto, Yuki Sekimoto, Masakazu Nakamura

>>>>>>> 休憩 (16:45-17:00) <<<<<<<<

特別講演 (17:00-17:30)

- 1S-3 Twisted bilayer graphene with clean interface by direct transfer of CVD graphene 3
* Satoru Tanaka, Hitoshi Imamura, Anton Visikovskiy, Ryosuke Uotani, Takashi Kajiwara, Hiroshi Ando, Takushi Iimori, Kota Iwata, Toshio Miyamachi, Kan Nakatsujii, Kazuhiko Mase, Tetsuroh Shirasawa, Fumio Komori

一般講演 (17:30-18:00)

ナノチューブの生成と精製

- 1-10 マイクロプラズマリアクターを用いた高結晶性カーボンナノチューブの気相成長と局所蒸着 20
* 辻 享志, 清水 禎樹, 金 載浩, 榑田 創, 畠 賢治, フタバドン, 桜井 俊介

内包ナノチューブ

- 1-11 振動するカーボンナノチューブ内でシャトル運動するフラーレン分子の実時間イメージング 21
* 清水 俊樹, ルングリッヒドミニク, スタックナー ジョシュア, 村山 光宏, 原野 幸治, 中村 栄一

>>>>>>> 休憩 (18:00-18:15) <<<<<<<<

チュートリアル (18:15-19:45)

- ナノカーボン・原子層物質における光物性の基礎と応用
* 松田 一成

9月17日(木)

特別講演 発表 25分 ・ 質疑応答 5分
一般講演 発表 10分 ・ 質疑応答 5分
大澤賞・飯島賞受賞対象者講演 発表 10分 ・ 質疑応答 10分
ポスタープレビュー 発表 1分 ・ 質疑応答 なし

特別講演 (9:00-9:30)

- 2S-1 MBEで切り拓くファンデルワールス界面の創発輸送現象 4
* 中野 匡規

一般講演 (9:30-10:00)

グラフェンの物性

- 2-1 構造欠陥を周期的に導入したグラフェンの電子物性 22
* 田口 裕太, 斎藤 晋
- 2-2 Control of the photoluminescence by tuning the Fermi level in single-layer graphene 23
* 犬飼 大樹, 斎藤 健輔, 小山 剛史, 河原 憲治, 吾郷 浩樹, 岸田 英夫

>>>>>>> 休憩 (10:00-10:15) <<<<<<<<

一般講演 (10:15-11:35)

大澤賞・飯島賞受賞対象者講演

- 2-3 遷移金属カルコゲナイドの一次元物質の精密合成と評価 24
* 中西 勇介, 神田 直之, 安藤 千里, 永田 雅貴, 相崎 元希, 劉 崢, 志賀 拓磨, 末永 和知, 篠原 久典, 宮田 耕充
- 2-4 Isothermal growth and stacking evolution of highly uniform AB-stacked bilayer graphene 25
* Pablo Solís-Fernández, Yuri Terao, Kenji Kawahara, Wataru Nishiyama, Teerayut Uwanno, Yung-Chang Lin, Keisuke Yamamoto, Hiroshi Nakashima, Kosuke Nagashio, Hiroki Hibino, Kazu Suenaga, Hiroki Ago
- 2-5 Concise, Single-Step Synthesis of Sulfur-Enriched Graphene: Immobilization of Molecular Clusters and Battery Applications 26
* 大町 遼, 井上 司, 畑尾 秀哉, Criado Alejandro, 篠原 久典, 吉川 浩史, Zois Syrgiannis, Maurizio Prato
- 2-6 Wafer-scale synthesis of 1D transition metal chalcogenide nanowires 27
* Hong En Lim, Yusuke Nakanishi, Zheng Liu, Jiang Pu, Takahiko Endo, Chisato Ando, Hiroshi Shimizu, Kazuhiro Yanagi, Taishi Takenobu, Yasumitsu Miyata

ポスタープレビュー (11:35-12:20) (☆) 若手奨励賞候補

若手奨励賞候補

- 2P-1 近接化学修飾可能な修飾分子の構造変化に伴う局所化学修飾単層カーボンナノチューブの発光特性変化 74
☆ * 青木 榛花, 田中 直樹, 藤ヶ谷 剛彦, 白木 智丈
- 2P-2 Temperature dependence of Seebeck coefficients in Semiconducting and Metallic Single-Wall Carbon Nanotube film. 75
☆ * Akari Yoshida, Yota Ichinose, Kengo Fukuhara, Kan Ueji, Yohei Yomogida, Kazuhiro Yanagi

9月17日(木)

2P-3	ピレン誘導体との相互作用を利用した単層カーボンナノチューブの発光特性変化	76
☆	* 余博達, 藤ヶ谷剛彦, 白木智丈	
2P-4	MoO ₃ Doping of Carbon Nanotube Top Electrodes for Highly Efficient Metal-Electrode-Free Perovskite Solar Cells	77
☆	* Seungju Seo, Il Jeon, Kosuke Akino, Hiroki Nagaya, Esko Kauppinen, Yutaka Matsuo, Shigeo Maruyama	
2P-5	脂肪酸で官能化された単層カーボンナノチューブへの血清アルブミンの吸着挙動の観察	78
☆	* 中村賢拓, 新留嘉彬, 永井薫子, 田中直樹, 白木智丈, 森健, 片山佳樹, 藤ヶ谷剛彦	
2P-6	n-type doping from sulfhydryl groups of proteins to semiconducting single-wall carbon nanotube	79
☆	* Tomohito Nakayama, Hiroataka Inoue, Yuho Shigeeda, Yasuhiko Hayashi, Takeshi Tanaka, Atsushi Hirano, Muneaki Hase	
2P-7	Time-resolved photoluminescence spectroscopy of epitaxial monolayer and bilayer graphene on SiC	80
☆	* Kensuke Saito, Jianfeng Bao, Wataru Norimatsu, Michiko Kusunoki, Hideo Kishida, Takeshi Koyama	
2P-8	A controllable post doping method for TMD atomic layers	81
☆	* 村井雄也, 吉田昭二, 劉崢, 入沢寿史, 清水宏, 遠藤尚彦, 宮田耕充, 北浦良	
2P-9	3次元構造を有するNbSe ₂ 薄膜の超伝導特性	82
☆	* 高橋統吾, 安藤千里, 斎藤光史, 宮田耕充, 中西勇介, 蒲江, 竹延大志	
ナノ炭素粒子		
2P-10	Crystallinity dependence on mechanical properties of aerographite particles	83
	* Li Yuexuan, Hamasaki Hiromu, Hirahara Kaori	
ナノチューブの生成と精製		
2P-11	High-density CNT forest by multiple coating of iron oxide nano-colloid for dry-spinnable CNT forest	84
	* 田畑良篤, 中野貴之, 井上翼	
2P-12	アルカンの活性化とCNTのCVD合成	85
	* Pengfei Chen, Mengju Yang, Rei Nakagawa, Hisashi Sugime, Hitoshi Mazaki, Suguru Noda	
ナノチューブの物性		
2P-13	Growth mechanism of one-dimensional heterostructures	86
	* Yongjia Zheng, Yang Qian, Ming Liu, Akihito Kumamoto, Yuichi Ikuhara, Esko I. Kauppinen, Shohei Chiashi, Taiki Inoue, Rong Xiang, Shigeo Maruyama	
2P-14	高空間分解SEM-EDSを用いたナノ炭素材料の表面状態イメージング評価	87
	* 中島秀朗, 森本崇宏, 周英, 小橋和文, 山田健郎, 岡崎俊也	

ナノチューブの応用

- 2P-15 Foot Pressure Sensor System Made from MWCNT Coated Cotton Fibers to Monitor Human Activities and Sports Performance 88
* Md. Abdul Momin, Mohammad Jellur Rahman, Tetsu Mieno
- 2P-16 3電極構造を用いた気体放電によるカーボンナノチューブフィラメント生成効率の向上 89
* 羽山 廣, 眞方 総一郎, 佐藤 英樹
- 2P-17 Quantitative study of sheet thermal conductance of Single-Walled carbon nanotube film 90
* Pengyingkai Wang, Yongjia Zheng, Taiki Inoue, Rong Xiang, Shohei Chiashi, Makoto Watanabe, Shigeo Maruyama

グラフェン生成

- 2P-18 In-situ X-ray diffraction monitor of multi-layer graphene precipitated from nanodiamonds 91
* 檜尾 達也, 中島 諒人, 上田 悠貴, 丸山 隆浩, 成塚 重弥
- 2P-19 非破壊・均一・連続生産可能な黒鉛シートの電気化学的手法による機能化 92
* 仁科 勇太, Campeon Benoit, 古茂田 将人

グラフェンの物性

- 2P-20 分子動力学計算におけるグラフェンの過渡フォノンスペクトルによるフォノン散乱の分解 93
* ゴロツキヒナ タチアナ, 外園 翔平
- 2P-21 Raman spectroscopy of graphene oxide and reduced graphene oxide flakes on Si-based substrates 94
* K. Kanishka H. De Silva, Seiya Suzuki, Pamarti Viswanath, Masamichi Yoshimura

グラフェンの応用

- 2P-22 マイクロ波プラズマCVD法による水素発生反応のための電気触媒としてのMo₂C/C複合膜の合成 95
* 沼田 駿佑, 緒方 啓典

原子層

- 2P-23 Anomalous electroluminescence from WS₂/WSe₂ in-plane heterostructures 96
* Naoki Wada, Jiang Pu, Tomoyuki Yamada, Wenjin Zhang, Zheng Liu, Yusuke Nakanishi, Yutaka Maniwa, Kazunari Matsuda, Yuhei Miyauchi, Taishi Takenobu, Yasumitsu Miyata
- 2P-24 Effects of defect formation in monolayer MoS₂ by low energy Ar⁺ ion beam irradiation 97
* Yangzhou Zhao, Hiroki Yokota, Haruna Ichikawa, Yasushi Ishiguro, Kazuyuki Takai

ナノワイヤー

- 2P-25 酸化ニオブナノワイヤのセレン化によるNbSe₂ナノワイヤの合成 98
* 田中 涼雅, 蓬田 陽平, 宮田 耕充, 柳 和宏

その他

- 2P-26 Polarized Raman spectra of LaAlSi 99
* Tong Wang, Xiaoqi Pang, Nguyen T. Hung, Riichiro Saito
- 2P-27 Electronic and geometric structures of carbon nano-boxes of centrohexaquinane 100
* 藤井 康丸, 丸山 実那, 岡田 晋

9月 17日 (木)

>>>>>>> 昼食 (12:20-13:30) <<<<<<<<

ポスターセッション (13:30-15:15)

>>>>>>> 休憩 (15:15-15:30) <<<<<<<<

授賞式 (15:30-16:00)

総会 (16:00-16:30)

>>>>>>> 休憩 (16:30-16:45) <<<<<<<<

一般講演 (16:45-17:30)

フラーレンの化学

- 2-7 C₆₀分子の赤外分光:実験室検出から宇宙存在度まで 28
* 若林 知成

ナノ炭素粒子

- 2-8 爆轟法ナノダイヤモンドの一次粒子確認 29
* 大澤 映二, バーナード アマンダ S., 田中 利彦

フラーレンの応用

- 2-9 Stereoselective synthesis and HIV/HCV enzyme inhibition activity of proline-type fullerene derivatives 30
* 片岸 大紀, 大江 知之, 高橋 恭子, 中村 成夫, 増野 匡彦

特別講演 (17:30-18:00)

- 2S-2 酸化グラフェンの機能開拓 5
* 速水 真也

一般講演 (18:00-18:45)

グラフェンの応用

- 2-10 The Effect of Heteroatom Doped Reduced Graphene Oxide in Enhancement of Thermoelectric Performance 31
* Mariamu Ali, Mohsen Khozami, Mohsen Ghali, Nageh Shaalan, Koichi Nakamura, Ahmed AbdElMoneim

グラフェンの物性

- 2-11 Molecular Modification of Graphene on Metal Substrate: Electrochemical Defect Insertion and Evaluation of Surface Defects 32
* Tomohiro Fukushima, Takaha Komai, Kei Murakoshi

- 2-12 Molecular Modification of Graphene on Metal Substrate: Electrochemical Defect Insertion for Controlled Proton Permeation 33
* Takaha Komai, Tomohiro Fukushima, Kei Murakoshi

9月18日(金)

特別講演 発表 25分・質疑応答 5分
一般講演 発表 10分・質疑応答 5分
ポスタープレビュー 発表 1分・質疑応答 なし

特別講演 (9:00-9:30)

- 3S-1 燃料電池用窒素ドーパカーボン触媒の活性点 6
* 中村 潤児

一般講演 (9:30-10:30)

原子層

- 3-1 2D tin layers on SiC(0001) 34
* Anton Visikovskiy, 安藤 寛, 林 真吾, 小森 文夫, 矢治 光一郎, 田中 悟
- 3-2 Strain effect on circularly-polarized electroluminescence in transition metal dichalcogenides 35
* 汪 萨克,, 齋藤 理一郎
- 3-3 Operando electrical characterization of methane oxidation with atomically thin films of IrO₂ nanosheets 36
* 野内 亮, 石原 良晃, 杉本 涉
- 3-4 Electrical control of resonance frequency for drum-type hBN nano-electro-mechanical resonator with photothermal actuation 37
* Yusuke Morimoto, Kuniharu Takei, Takayuki Arie, Seiji Akita

>>>>>>> 休憩 (10:30-10:45) <<<<<<<<

一般講演 (10:45-11:15)

ナノチューブの応用

- 3-5 Promising next-gen Cu-substitutes: Lightweight Cu/Carbon Nanotube Composite Electric Conductors 38
* Rajyashree Sundaram, Guohai Chen, Takeo Yamada, Don Futaba, Kenji Hata, Ken Kokubo, Atsuko Sekiguchi
- 3-6 Anthracene-assisted deterministic transfer of optical-quality carbon nanotubes 39
* 大塚 慶吾, 加藤 雄一郎

ポスタープレビュー (11:15-12:00) (☆) 若手奨励賞候補

若手奨励賞候補

- 3P-1 吸着等温線測定による炭素材料表面におけるポリベンゾイミダゾール吸着状態の解明 101
☆ * 嘉陽 奈々, 藤ヶ谷 剛彦
- 3P-2 Understanding the Effect of Sulfur on the Synthesis of Carbon Nanotubes 102
☆ * 仲川 黎, 江戸 倫子, 杉目 恒志, 野田 優
- 3P-3 Directional exciton diffusion in pentacene-decorated carbon nanotubes 103
☆ * 李 臻, 大塚 慶吾, 山下 大喜, 加藤 雄一郎
- 3P-4 アジド化合物を利用した局所化学修飾単層カーボンナノチューブの合成と発光特性 104
☆ * 林 啓太, 藤ヶ谷 剛彦, 白木 智丈

9月18日(金)

3P-5	Temperature dependence of Raman G-band shift in defective single-walled carbon nanotubes	105
☆	* 遠藤 雅典, 内山 晴貴, 大野 雄高, 廣谷 潤	
3P-6	蒸着による単層カーボンナノチューブシートのn型化	106
☆	* 山口 凌平, 織田 海斗, 富田 基裕, 渡邊 孝信, 藤ヶ谷 剛彦	
3P-7	Growth of Monolayer MoS ₂ Lateral p-n Junction with p-type Substitutional Nb Doping	107
☆	* 岡田 光博, 入沢 寿史, 岡田 直也, 張 文馨, 清水 哲夫, 久保 利隆, 石原 正統	
3P-8	異方性のある光学的・電子的特性をもつ二次元シリコンフォスファイド	108
☆	* 小林 幹旺, 篠北 啓介, 宮内 雄平, 松田 一成	
3P-9	WTeナノワイヤネットワークの電子輸送特性	109
☆	* Hiroshi Shimizu, Jiang Pu, Hong En Lim, Yusuke Nakanishi, Zheng Liu, Takahiko Endo, Taishi Takenobu, Yasumitsu Miyata	

フラーレンの応用

3P-10	Preparation of ruthenium oxide-[C ₆₀]fullerene nanowhisker composites and their photocatalytic activity for degradation of azo dyes	110
	* Jeong Won Ko, Sugyeong Jeon, Weon Bae Ko	

ナノチューブの応用

3P-11	CNT/copper composite yarn made from metallic nanoparticle-decorated spin-capable CNT forest	111
	* 田中 孝祐, 中野 貴之, 井上 翼	

ナノチューブの物性

3P-12	h-BN上へのガス配向成長CNTのラマン分光測定	112
	* 佐藤 周, 四元 聡, 番場 雅典, 井ノ上 泰輝, 丸山 茂夫, 千足 昇平	
3P-13	Fermi-level dependence of high-harmonic generation in semiconducting single-walled carbon nanotubes with different bandgaps	113
	* 西留 比呂幸, 永井 恒平, 内田 健人, 一ノ瀬 遥太, 枝 淳子, 大久保 瞳, 蓬田 陽平, 田中 耕一郎, 柳 和宏	

ナノチューブの応用

3P-14	炭素材料上におけるPtナノ粒子の状態とメタノール酸化に対する電極触媒特性に及ぼす堆積法の影響	114
	* 阿部 雄帆, 緒方 啓典	
3P-15	F4-TCNQ Vapor-doped Single Walled Carbon Nanotubes for Thermoelectric Applications	115
	* Mariamu Ali, Naofumi Okamoto, Ryo Abe, Ahmed AbdelMoneim, Masakazu Nakamura	
3P-16	Operation speed enhancement in carbon nanotube thin film transistors by self-aligned process	116
	* Saya Ishimaru, Taiga Kashima, Hiromichi Kataura, Yuuka Ohno	
3P-17	Radical polymerization in the presence of carbon nanotubes (CNTs): Radical scavenging by CNTs	117
	* 清水 太陽, 岸 良一, 山田 健郎, 畠 賢治	

9月18日(金)

グラフェン生成

- 3P-18 Effect of Chemical Etching Treatment on Copper Foils for Single-Layer Graphene CVD Growth 118
* Naoki Yoshihara, Masaru Noda

グラフェンの物性

- 3P-19 Thermal transport property of suspended twisted bilayer graphene 119
* 土井 惇太郎, 毛利 真一郎, 荒木 努
- 3P-20 Carrier control in bilayer graphene dual-gate field effect transistors by interlayer atomic arrangement 120
* 高 燕林, 岡田 晋

グラフェンの応用

- 3P-21 Difference of functional groups in Graphene oxide in terms of chemical activity 121
* 近藤 里駆, 松尾 吉晃, 高井 和之

原子層

- 3P-22 ナノスケール二次元超構造のテラレーメイド創出 122
* 一瀬 七海, 飯田 智士, 劉 崢, 北浦 良
- 3P-23 Chemically tuned p- and n-type WSe₂ monolayers with improved carrier mobility for electronic applications 123
* Hyun Goo Ji, Pablo Solís-Fernández, Daisuke Yoshimura, Mina Maruyama, Takahiko Endo, Yasumitsu Miyata, Susumu Okada, Hiroki Ago

ナノワイヤー

- 3P-24 Electrical Conductivity of Chemical-Vapor-Deposition Grown WTe Nanowire Bundles 124
* Chisato Ando, Yusuke Nakanishi, Hiroshi Shimizu, Hong En Lim, Zheng Liu, Takahiko Endo, Yasumitsu Miyata

その他

- 3P-25 First-principle calculation of the electronic state of a 2D covalent network of 1,3,5-triamino benzene and benzene-1,3,5-tricarboxaldehyde 125
* Hiroyuki Yokoi
- 3P-26 Two-channel model for low thermal conductivity of Mg₃Bi₂ 126
* Nguyen Tuan Hung, Riichiro Saito

>>>>>>> 昼食 (12:00-13:00) <<<<<<<<

ポスターセッション (13:00-14:45)

>>>>>>> 休憩 (14:45-15:00) <<<<<<<<

特別講演 (15:00-15:30)

- 3S-2 多層グラフェンの電子構造 7
* 八木 隆多

9月18日(金)

一般講演 (15:30-16:30)

ナノチューブの物性

- 3-7 ドープしたカーボンナノチューブにおける円偏光二色性 40
* 齋藤 理一郎, Ukhtary Md. Shoufie, Wang Sake, 前田 大聖, 岩崎 佑哉
- 3-8 単一構造カーボンナノチューブ薄膜の広帯域複素屈折率スペクトル 41
* 西原 大志, 高倉 章, 松田 一成, 田中 丈士, 片浦 弘道, 宮内 雄平
- 3-9 Unravelling the Thermal Conductivity of Semiconducting Carbon Nanotubes Film with Different Doping Levels 42
* 上治 寛, 松岡 勇也, 八木 貴志, 蓬田 陽平, 一ノ瀬 遥太, 吉田 朱里, 柳 和宏

ナノチューブの応用

- 3-10 ポリラジカルによるカーボンナノチューブの電子ドーピング 43
* 田中 直樹, 浜砂 碧, 藤ヶ谷 剛彦

>>>>>>> 休憩 (16:30-16:45) <<<<<<<<

特別講演 (16:45-17:15)

- 3S-3 導電性カーボンナノチューブコートPETテープに乗せた神経組織の高解像度電子顕微鏡撮影とその解析法 8
* 窪田 芳之

一般講演 (17:15-17:45)

ナノチューブの生成と精製

- 3-11 液中のCNT凝集体の空隙率とサイズの分析法。遠心沈降を活用する一般的方法 44
* 加藤 雄一, 森本 崇宏, 小橋 和文, 岡崎 俊也
- 3-12 XPS investigation revealing the activation of iron catalyst by a small amount of noble metals without reducing gas towards the synthesis of tall carbon nanotube forest 45
* 桜井 俊介, 何 金萍, 畠 賢治, Futaba Don

特別講演 (17:45-18:15)

- 3S-4 電子顕微鏡を使った二次元材料の局所振動特性評価 9
* 千賀 亮典, 末永和知, Thomas Pichler

September 16th, Wed.

Special Lecture: 25min (Presentation) + 5min (Discussion)
General Lecture: 10min (Presentation) + 5min (Discussion)
Poster Preview: 1min (Presentation)

Special Lecture (9:15–9:45)

- 1S-1 Hetero-nanotubes based on single-walled carbon nanotubes 1
* *Shigeo Maruyama,*

General Lecture (9:45–10:30)

Properties of nanotubes

- 1-1 Linear Temperature Dependence of Nanotube Yarn Resistance 11
* *Takumi Inaba, Takahiro Morimoto, Satoshi Yamazaki, Toshiya Okazaki*
- 1-2 Indirect to direct band gap crossover of single walled MoS₂ nanotubes 12
* *Kaoru Hisama, Mina Maruyama, Susumu Okada, Shohei Chiashi, Shigeo Maruyama*
- 1-3 Diameter-dependent Photoluminescence Properties in Color Centers of Air-Suspended Single-Walled Carbon Nanotubes 13
* *Daichi Kozawa, Xiaojian Wu, Akihiro Ishii, Jacob Fortner, Keigo Otsuka, Rong Xiang, Taiki Inoue, Shigeo Maruyama, YuHuang Wang, Yuichiro K. Kato*

>>>>>>> Coffee Break (10:30–10:45) <<<<<<<<

General Lecture (10:45–11:30)

Properties of graphene

- 1-4 Energetics and electronic structure of bilayer graphene intercalating buckybowls 14
* *Mina Maruyama, Susumu Okada*

Graphene synthesis

- 1-5 Direct synthesis of size-controlled quantum dots with graphene nanoribbon 15
* *Mizuki Seo, Takahito Kitada, Toshiro Kaneko, Tomohiro Otsuka, Toshiaki Kato*

Applications of graphene

- 1-6 High-order mode operation of graphene mechanical resonator 16
* *Hirofumi Ikemoto, Kaito Nakagawa, Taichi Inoue, Kuniharu Takei, Takayuki Arie, Seiji Akita*

Poster Preview (11:30–12:15) (★)Candidates for the Young Scientist Poster Award
Candidates for the Young Scientist Poster Award

- 1P-1 MWCNT growth mechanism using FeCl₂ catalyst precursor 47
★ * *Tatsuhiko Hayashi, Takayuki Nakano, Yoku Inoue*
- 1P-2 Light-driven wavelength shifts of photoluminescence from single-walled carbon nanotubes by functionalization with diarylethene derivatives 48
★ * *Yasuto Nakagawa, Takuya Nakashima, Tsuyoshi Kawai, Tsuyohiko Fujigaya, Tomohiro Shiraki*

September 16th, Wed.

1P-3	Fabrication of Carbon Nanotube Thin Films for Flexible Transistor Applications using a Cross-linked Amine Polymer	49
☆	* <i>Kaisei Matsumoto, Kazuki Ueno, Jun Hirotsu, Yutaka Ohno, Haruka Omachi</i>	
1P-4	Structure-dependent solvatochromic shifts of excitonic photoluminescence from locally functionalized single-walled carbon nanotubes	50
☆	* <i>Yoshiaki Niidome, Tsuyohiko Fujigaya, Tomohiro Shiraki</i>	
1P-5	Visualization of thermal transports on bundled carbon nanotubes by monitoring evaporation of gold nanoparticles	51
☆	* <i>Hiromu Hamasaki, Seiya Takimoto, Kaori Hirahara</i>	
1P-6	Measurement of Zeta potential of single-walled carbon nanotubes in non-polar organic solvent	52
☆	* <i>Taiki Ishii, Angana Borah, Naoki Tanaka, Tsuyohiko Fujigaya</i>	
1P-7	Near-Infrared Fluorescence Immunoassay Using Streptavidin-Conjugated Oxygen-Doped Carbon Nanotubes	53
☆	* <i>Keiko Kojima, Yoko Iizumi, Minfang Zhang, Toshiya Okazaki</i>	
1P-8	Effects of channel length on performance of transparent solar cell with monolayer WS ₂	54
☆	* <i>Xing He, Toshiro Kaneko, Toshiaki Kato</i>	
1P-9	Robust easy-plane 2D ferromagnetism in Cr _{1/3} NbSe ₂ ultrathin films	55
☆	* <i>Yuki Majima, Bruno Kenichi Saika, Hideki Matsuoka, Masaki Nakano, Satoshi Yoshida, Kyoko Ishizaka, Yoshihiro Iwasa</i>	
Carbon nanoparticles		
1P-10	Energetics and geometric structure of corannulene under an external electric field	56
	* <i>Susumu Okada, Yanlin Gao, Mina Maruyama</i>	
Formation and purification of nanotubes		
1P-11	Survival of Sub-nm Carbon Nanotubes under Femtosecond Laser Shot: A TDDFT Study	57
	* <i>Yoshiyuki Miyamoto</i>	
Properties of nanotubes		
1P-12	One dimensionality of the thermoelectric properties in semiconducting single walled carbon nanotubes	58
	* <i>Yota Ichinose, Manaho Matsubara, Yohei Yomogida, Akari Yoshida, Kan Ueji, Kaito Kanahashi, Jiang Pu, Taishi Takenobu, Takahiro Yamamoto, Kazuhiro Yanagi</i>	
1P-13	Simple and Effective Method to Control Photoluminescence Properties of Single-walled Carbon Nanotubes by Ultrasonic Irradiation	59
	* <i>Yui Konno, Akane Nishino, Michio Yamada, Yutaka Maeda, Saki Okudaira, Yuhei Miyauchi, Kazunari Matsuda, Jun Matsui, Masaya Mitsuishi, Mitsuaki Suzuki</i>	

Applications of nanotubes

- 1P-14 Utilization of transparent SWCNT films in 4-terminal perovskite-silicon tandem solar cells 60
* *Ahmed Shawky, Kosuke Akino, Takuya Matsui, Taiki Inoue, Esko Kauppinen, Shohei Chiashi, Shigeo Maruyama*
- 1P-15 Simple and highly efficient intermittent operation circuit for triboelectric nanogenerator 61
* *Atsushi Kawaguchi, Masahiro Matsunaga, Haruki Uchiyama, Jun Hirotsani, Yutaka*
- 1P-16 Carbon nanotube-Cu through-Si-via interposer with Cu-level electrical conductivity and Si-comparable thermal expansion 62
* *Guohai Chen, Rajyashree Sundaram, Atsuko Sekiguchi, Kenji Hata, Don N. Futaba*
- 1P-17 Electrical detection of X-ray by using coplanar CNT thin-film electrodes on PEN substrate 63
* *Satoru Suzuki, Hiroyuki Matsuda, Takahiro Ishikawa, Teruaki Konishi, Tsuyoshi Hamano, Hiroshi Ajiki, Yutaka Ohno, Toshio Hirao, Satoshi Ishii*

Graphene synthesis

- 1P-18 Controlled synthesis of graphene nanoribbons from fluctuation-induced nanobar 64
* *Naofumi Sato, Toshiro Kaneko, Toshiaki Kato*
- 1P-19 Fabrication of large Ni grain on sapphire substrate for graphene growth 65
* *Asato Nakashima, Tatsuya Kashio, Tomoaki Murahashi, Tsukasa Soga, Takahiro Maruyama, Shigeya Naritsuka*

Properties of graphene

- 1P-20 The Instructive Aspect of Moire-Patten Analysis of Rotation Less Than 0.5-degree on Twisted Bilayer Graphene by Tool for Computer Imaging 66
* *Yuhei Natsume, Tohei Moritani*
- 1P-21 Raman optothermal methods to measure interfacial thermal conductance of low-dimensional materials 67
* *Qin-Yi Li, Koji Takahashi*

Applications of graphene

- 1P-22 Non-diffusive molecular transport in graphene liquid cells 68
* *Sota Hirokawa, Hideaki Teshima, Pablo Solís-Fernández, Hiroki Ago, Yoko Tomo, Qin-Yi Li, Koji Takahashi*

Atomic Layers

- 1P-23 Layer-selective dopant implantation in van der Waals heterostructures 69
* *Hiroto Ogura, Yuya Murai, Toshifumi Irisawa, Zheng Liu, Hiroshi Shimizu, Hong En Lim, Yusuke Nakanishi, Takahiko Endo, Ryo Kitaura, Yasumitsu Miyata*

September 16th, Wed.

- 1P-24 Hydrogen adsorption effects on the electronic properties of TaS₂ 70
* *Yasushi Ishiguro, Naoko Kodama, Kirill Bogdanov, Alexander Baranov, Kazuyuki Takai*

Nanowires

- 1P-25 Simple formula of enhancement of the electric field inside a hollow metallic cylinder 71
* *Yuan Tian, Muhammad Shoufie Ukhtary, Riichiro Saito*
- 1P-26 Tellurization of solution-synthesized tungsten oxide nanowires 72
* *Mai Nagano, Yohei Yomogida, Yasumitsu Miyata, Kazuhiro Yanagi*

Other topics

- 1P-27 First-principles calculation of excitonic effect in Raman spectra 73
* *Xiaoqi Pang, T.Hung Nguyen, Riichiro Saito*

>>>>>>> Lunch Time (12:15–13:30) <<<<<<<<

Poster Session (13:30–15:15)

>>>>>>> Coffee Break (15:15–15:30) <<<<<<<<

Special Lecture (15:30–16:00)

- 1S-2 Improvement of photodynamic activity by dyad systems of fullerene derivative and photo-antenna molecule incorporated into liposomes 2
* *Atsushi Ikeda, Daiki Antoku, Kouta Sugikawa, Riku Kawasaki*

General Lecture (16:00–16:45)

Applications of nanotubes

- 1-7 One dimensional hetero-junction diode 17
* *Ya Feng, Henan Li, Taiki Inoue, Shigeo Maruyama*
- 1-8 Polyaromatic Anthracene Nano-tweezer on Semiconducting Carbon Nanotubes for Growth and Bridging of Perovskite Crystal Grains in Perovskite Solar Cells 18
* *Hao-Sheng Lin, IL Jeon, Yutaka Matsuo, Shigeo Maruyama*
- 1-9 Aligned carbon nanotube/polymer composite films for high thermal diffusivity 19
* *Maireyee Bhattacharya, Manish Pandey, Ryo Abe, Naofumi Okamoto, Yuki Sekimoto, Masakazu Nakamura*

>>>>>>> Coffee Break (16:45–17:00) <<<<<<<<

Special Lecture (17:00–17:30)

- 1S-3 Twisted bilayer graphene with clean interface by direct transfer of CVD graphene 3
* *Satoru Tanaka, Hitoshi Imamura, Anton Visikovskiy, Ryosuke Uotani, Takashi Kajiwara, Hiroshi Ando, Takushi Iimori, Kota Iwata, Toshio Miyamachi, Kan Nakatsuji, Kazuhiko Mase, Tetsuroh Shirasawa, Fumio Komori*

September 16th, Wed.

General Lecture (17:30–18:00)

Formation and purification of nanotubes

- 1-10 Gas-phase growth and localized deposition of highly crystalline carbon nanotubes using a microplasma reactor 20
* *Takashi Tsuji, Yoshiki Shimizu, Jaeho Kim, Hajime Sakakita, Kenji Hata, Don Futaba, Shunsuke Sakurai*

Endohedral nanotubes

- 1-11 Real-time Video Imaging of a Shuttling Fullerene Molecule in a Vibrating Carbon Nanotube 21
* *Toshiki Shimizu, Dominik Lungerich, Joshua Stuckner, Mitsuhiro Murayama, Koji Harano, Eiichi Nakamura*

>>>>>>> **Coffee Break (18:00–18:15)** <<<<<<<<

Tutorial (18:15–19:45)

Fundamental and application of optical physics in nano-carbon and atomically thin materials
* *Kazunari Matsuda*

September 17th, Thu.

Special Lecture: 25min (Presentation) + 5min (Discussion)
General Lecture: 10min (Presentation) + 5min (Discussion)
Award Nominee Lecture: 10min (Presentation) + 10min (Discussion)
Poster Preview: 1min (Presentation)

Special Lecture (9:00–9:30)

- 2S-1 Emergent transport phenomena at van der Waals interfaces explored by MBE 4
* *Masaki Nakano*

General Lecture (9:30–10:00)

Properties of graphene

- 2-1 Electronic properties of graphene with structural defects arranged periodically 22
* *Yuta Taguchi, Susumu Saito*
- 2-2 Control of the photoluminescence by tuning the Fermi level in single-layer graphene 23
* *Daiki Inukai, Kensuke Saito, Takeshi Koyama, Kenji Kawahara, Hiroki Ago, Hideo Kishida*

>>>>>>> Coffee Break (10:00–10:15) <<<<<<<<

General Lecture (10:15–11:35)

Lectures of Osawa Award and Iijima Award Nominees

- 2-3 Bottom-Up Growth of One-dimensional Transition Metal Chalcogenides and Their Characterization 24
* *Yusuke Nakanishi, Naoyuki Kanda, Chisato Ando, Masa Nagata, Motoki Aizaki, Zheng Liu, Takuma Shiga, Kazu Suenaga, Hisanori Shinohara, Yasumitsu Miyata*
- 2-4 Isothermal growth and stacking evolution of highly uniform AB-stacked bilayer 25
* *Pablo Solís-Fernández, Yuri Terao, Kenji Kawahara, Wataru Nishiyama, Teerayut Uwanno, Yung-Chang Lin, Keisuke Yamamoto, Hiroshi Nakashima, Kosuke Nagashio, Hiroki Hibino, Kazu Suenaga, Hiroki Ago*
- 2-5 Concise, Single-Step Synthesis of Sulfur-Enriched Graphene: Immobilization of Molecular Clusters and Battery Applications 26
* *Haruka Omachi, Tsukasa Inoue, Shunya Hatao, Criado Alejandro, Hisanori Shinohara, Hirofumi Yoshikawa, Zois Syrgiannis, Maurizio Prato*
- 2-6 Wafer-scale synthesis of 1D transition metal chalcogenide nanowires 27
* *Hong En Lim, Yusuke Nakanishi, Zheng Liu, Jiang Pu, Takahiko Endo, Chisato Ando, Hiroshi Shimizu, Kazuhiro Yanagi, Taishi Takenobu, Yasumitsu Miyata*

**Poster Preview (11:35–12:20) (★)Candidates for the Young Scientist Poster Award
Candidates for the Young Scientist Poster Award**

- 2P-1 Photoluminescence property changes of locally functionalized single-walled carbon nanotubes using structural differences of proximal modifiers 74
☆ * *Haruka Aoki, Naoki Tanaka, Tsuyohiko Fujigaya, Tomohiro Shiraki*

September 17th, Thu.

2P-2	Temperature dependence of Seebeck coefficients in Semiconducting and Metallic Single-Wall Carbon Nanotube film.	75
☆	<i>* Akari Yoshida, Yota Ichinose, Kengo Fukuhara, Kan Ueji, Yohei Yomogida, Kazuhiro Yanagi</i>	
2P-3	Effects of pyrene derivatives on photoluminescence properties of single-walled carbon nanotubes	76
☆	<i>* Boda Yu, Tsuyohiko Fujigaya, Tomohiro Shiraki</i>	
2P-4	MoO ₃ Doping of Carbon Nanotube Top Electrodes for Highly Efficient Metal-Electrode-Free Perovskite Solar Cells	77
☆	<i>* Seungju Seo, Il Jeon, Kosuke Akino, Hiroki Nagaya, Esko Kauppinen, Yutaka Matsuo, Shigeo Maruyama</i>	
2P-5	Monitoring of adsorption behavior of serum albumin onto the single-walled carbon nanotube functionalized with fatty acid	78
☆	<i>* Kenta Nakamura, Yoshiaki Niidome, Yukiko Nagai, Naoki Tanaka, Tomohiro Shiraki, Takeshi Mori, Yoshiki Katayama, Tsuyohiko Fujigaya</i>	
2P-6	n-type doping from sulfhydryl groups of proteins to semiconducting single-wall carbon nanotube	79
☆	<i>* Tomohito Nakayama, Hirotaka Inoue, Yuho Shigeeda, Yasuhiko Hayashi, Takeshi Tanaka, Atsushi Hirano, Muneaki Hase</i>	
2P-7	Time-resolved photoluminescence spectroscopy of epitaxial monolayer and bilayer graphene on SiC	80
☆	<i>* Kensuke Saito, Jianfeng Bao, Wataru Norimatsu, Michiko Kusunoki, Hideo Kishida, Takeshi Koyama</i>	
2P-8	A controllable post doping method for TMD atomic layers	81
☆	<i>* Yuya Murai, Shoji Yoshida, Zheng Liu, Toshifumi Irisawa, Hiroshi Shimizu, Takahiko Endo, Yasumitsu Miyata, Ryo Kitaura</i>	
2P-9	Superconducting properties in three-dimensional networks of NbSe ₂ films	82
☆	<i>* Togo Takahashi, Chisato Ando, Mitsufumi Saito, Yasumitsu Miyata, Yusuke Nakanishi, Jiang Pu, Taishi Takenobu</i>	
Carbon nanoparticles		
2P-10	Crystallinity dependence on mechanical properties of aerographite particles	83
	<i>* Yuexuan Li, Hiromu Hamasaki, Kaori Hirahara</i>	
Formation and purification of nanotubes		
2P-11	High-density CNT forest by multiple coating of iron oxide nano-colloid for dry-spinnable CNT forest	84
	<i>* Kento Tabata, Takayuki Nakano, Yoku Inoue</i>	

September 17th, Thu.

2P-12	Activation of Alkane for CVD Growth of Single-Wall Carbon Nanotubes <i>* Pengfei Chen, Mengju Yang, Rei Nakagawa, Hisashi Sugime, Hitoshi Mazaki, Suguru Noda</i>	85
Properties of nanotubes		
2P-13	Growth mechanism of one-dimensional heterostructures <i>* Yongjia Zheng, Yang Qian, Ming Liu, Akihito Kumamoto, Yuichi Ikuhara, Esko I. Kauppinen, Shohei Chiashi, Taiki Inoue, Rong Xiang, Shigeo Maruyama</i>	86
2P-14	Imaging of functional group distribution on carbon nanomaterials with highly spatially resolved SEM-EDS <i>* Hideaki Nakajima, Takahiro Morimoto, Ying Zhou, Kazufumi Kobashi, Takeo Yamada, Toshiya Okazaki</i>	87
Applications of nanotubes		
2P-15	Foot Pressure Sensor System Made from MWCNT Coated Cotton Fibers to Monitor Human Activities and Sports Performance <i>* Md. Abdul Momin, Mohammad Jellur Rahman, Tetsu Mieno</i>	88
2P-16	Improvement of carbon nanotube filament formation efficiency by gas discharge breakdown using triode electrode configuration <i>* Hiro Hayama, Soichiro Magata, Hideki Sato</i>	89
2P-17	Quantitative study of sheet thermal conductance of Single-Walled carbon nanotube film <i>* Pengyingkai Wang, Yongjia Zheng, Taiki Inoue, Rong Xiang, Shohei Chiashi, Makoto Watanabe, Shigeo Maruyama</i>	90
Graphene synthesis		
2P-18	In-situ X-ray diffraction monitor of multi-layer graphene precipitated from nanodiamonds <i>* Tatsuya Kashio, Asato Nakashima, Yuki Ueda, Takahiro Maruyama, Shigeya Naritsuka</i>	91
2P-19	Non-destructive, Uniform, and Continuous Electrochemical Functionalization of Graphite Sheet <i>* Yuta Nishina, Benoit Campeon, Masato Komoda</i>	92
Properties of graphene		
2P-20	Resolution of the phonon scattering by transient phonon spectra of graphene in molecular dynamics calculations <i>* Tatiana Zolotoukhna, Shohei Hokazono</i>	93
2P-21	Raman spectroscopy of graphene oxide and reduced graphene oxide flakes on Si-based substrates <i>* K. Kanishka H. De Silva, Seiya Suzuki, Pamarti Viswanath, Masamichi Yoshimura</i>	94

September 17th, Thu.

Applications of graphene

- 2P-22 Synthesis of Mo₂C/C composite films as electrocatalyst for the hydrogen evolution reaction by microwave-plasma CVD method 95
* *Shunsuke Numata , Hironori Ogata*

Atomic Layers

- 2P-23 Anomalous electroluminescence from WS₂/WSe₂ in-plane heterostructures 96
* *Naoki Wada, Jiang Pu, Tomoyuki Yamada, Wenjin Zhang, Zheng Liu, Yusuke Nakanishi, Yutaka Maniwa, Kazunari Matsuda, Yuhei Miyauchi, Taishi Takenobu, Yasumitsu Miyata*
- 2P-24 Effects of defect formation in monolayer MoS₂ by low energy Ar⁺ ion beam irradiation 97
* *Yangzhou Zhao, Hiroki Yokota, Haruna Ichikawa, Yasushi Ishiguro, Kazuyuki Takai*

Nanowires

- 2P-25 Synthesis of NbSe₂ nanowires by selenization of niobium oxide nanowires 98
* *Ryoga Tanaka, Yohei Yomogida, Yasumitsu Miyata, Kazuhiro Yanagi*

Other topics

- 2P-26 Polarized Raman spectra of LaAlSi 99
* *Tong Wang, Xiaoqi Pang, Nguyen T. Hung, Riichiro Saito*
- 2P-27 Electronic and geometric structures of carbon nano-boxes of centrohexaquinane 100
* *Yasumaru Fujii, Mina Maruyama, Susumu Okada*

>>>>>>> Lunch Time (12:20-13:30) <<<<<<<<<

Poster Session (13:30-15:15)

>>>>>>> Coffee Break (15:15-15:30) <<<<<<<<<

Awards Ceremony (15:30-16:00)

General Meeting (16:00-16:30)

>>>>>>> Coffee Break (16:30-16:45) <<<<<<<<<

General Lecture (16:45-17:30)

Chemistry of fullerenes

- 2-7 Infrared spectroscopy of C₆₀ molecules: From the laboratory detection to cosmic abundances 28
* *Tomonari Wakabayashi*

Carbon nanoparticles

- 2-8 Primary Particles of Detonation Nanodiamond Finally Identified 29
* *Eiji Osawa, Amanda S. Barnard, Toshihiko Tanaka*

September 17th, Thu.

Applications of fullerenes

- 2-9 Stereoselective synthesis and HIV/HCV enzyme inhibition activity of proline-type fullerene derivatives 30
* *Daiki Katagishi, Tomoyuki Ohe, Kyoko Takahashi, Shigeo Nakamura, Tadahiko Mashino*

Special Lecture (17:30-18:00)

- 2S-2 Graphene oxide as a super material 5
* *Shinya Hayami*

General Lecture (18:00-18:45)

Applications of graphene

- 2-10 The Effect of Heteroatom Doped Reduced Graphene Oxide in Enhancement of Thermoelectric Performance 31
* *Mariam Ali, Mohsen Khozami, Mohsen Ghali, Nageh Shaalan, Koichi Nakamura, Ahmed AbdElMoneim*

Properties of graphene

- 2-11 Molecular Modification of Graphene on Metal Substrate: Electrochemical Defect Insertion and Evaluation of Surface Defects 32
* *Tomohiro Fukushima, Takaha Komai, Kei Murakoshi*
- 2-12 Molecular Modification of Graphene on Metal Substrate: Electrochemical Defect Insertion for Controlled Proton Permeation 33
* *Takaha Komai, Tomohiro Fukushima, Kei Murakoshi*

September 18th, Fri.

Special Lecture: 25min (Presentation) + 5min (Discussion)
General Lecture: 10min (Presentation) + 5min (Discussion)
Poster Preview: 1min (Presentation)

Special Lecture (9:00–9:30)

- 3S-1 Active site of nitrogen-doped carbon catalysts for fuel cell 6
* *Junji Nakamura*

General Lecture (9:30–10:30)

Atomic Layers

- 3-1 2D tin layers on SiC(0001) 34
* *Anton Visikovskiy, Hiroshi Ando, Shingo Hayashi, Fumio Komori, Koichiro Yaji, Satoru Tanaka*
- 3-2 Strain effect on circularly-polarized electroluminescence in transition metal dichalcogenides 35
* *Sake Wang, M. Shoufie Ukhtary, Riichiro Saito*
- 3-3 Operando electrical characterization of methane oxidation with atomically thin films of IrO₂ nanosheets 36
* *Ryo Nouchi, Yoshiaki Ishihara, Wataru Sugimoto*
- 3-4 Electrical control of resonance frequency for drum-type hBN nano-electro-mechanical resonator with photothermal actuation 37
* *Yusuke Morimoto, Kuniharu Takei, Takayuki Arie, Seiji Akita*

>>>>>>> **Coffee Break (10:30–10:45)** <<<<<<<<

General Lecture (10:45–11:15)

Applications of nanotubes

- 3-5 Promising next-gen Cu-substitutes: Lightweight Cu/Carbon Nanotube Composite Electric Conductors 38
* *Rajyashree Sundaram, Guohai Chen, Takeo Yamada, Don Futaba, Kenji Hata, Ken Kokubo, Atsuko Sekiguchi*
- 3-6 Anthracene-assisted deterministic transfer of optical-quality carbon nanotubes 39
* *Keigo Otsuka, Yuichiro K. Kato*

Poster Preview (11:15–12:00) (★)Candidates for the Young Scientist Poster Award

- 3P-1 Elucidation of adsorption state of polybenzimidazole on carbon surface by adsorption isotherm measurement 101
★ * *Nana Kayo, Tsuyohiko Fujigaya*
- 3P-2 Understanding the Effect of Sulfur on the Synthesis of Carbon Nanotubes 102
★ * *Rei Nakagawa, Michiko Edo, Hisashi Sugime, Suguru Noda*

September 18th, Fri.

3P-3	Directional exciton diffusion in pentacene-decorated carbon nanotubes	103
☆	<i>* Zhen Li, Keigo Otsuka, Daiki Yamashita, Yuichiro Kato</i>	
3P-4	Locally functionalized single-walled carbon nanotubes synthesized by azide compounds and their photoluminescence properties	104
☆	<i>* Keita Hayashi, Tsuyohiko Fujigaya, Tomohiro Shiraki</i>	
3P-5	Temperature dependence of Raman G-band shift in defective single-walled carbon nanotubes	105
☆	<i>* Masanori Endo, Haruki Uchiyama, Yutaka Ohno, Jun Hirotsani</i>	
3P-6	Doping of single-walled carbon nanotube by thermal evaporation method	106
☆	<i>* Ryohei Yamaguchi, Kaito Oda, Motohiro Tomita, Takano Watanabe, Tsuyohiko Fujigaya</i>	
3P-7	Growth of Monolayer MoS ₂ Lateral p-n Junction with p-type Substitutional Nb Doping	107
☆	<i>* Mitsuhiro Okada, Toshifumi Irisawa, Naoya Okada, Wen-Hsin Chang, Tetsuo Shimizu, Toshitaka Kubo, Masatou Ishihara</i>	
3P-8	Two-dimensional silicon phosphide with anisotropic optical and electronic properties	108
☆	<i>* Mikio Kobayashi, Keisuke Shinokita, Yuhei Miyauchi, Kazunari Matsuda</i>	
3P-9	Electron transport properties of WTe nanowire networks	109
☆	<i>* Hiroshi Shimizu, Jiang Pu, Hong En Lim, Yusuke Nakanishi, Zheng Liu, Takahiko Endo, Taishi Takenobu, Yasumitsu Miyata</i>	
Applications of fullerenes		
3P-10	Preparation of ruthenium oxide-[C ₆₀]fullerene nanowhisker composites and their photocatalytic activity for degradation of azo dyes	110
	<i>* Jeong Won Ko, Sugyeong Jeon, Weon Bae Ko</i>	
Applications of nanotubes		
3P-11	CNT/copper composite yarn made from metallic nanoparticle-decorated spin-capable CNT forest	111
	<i>* Kosuke Tanaka, Takayuki Nakano, Yoku Inoue</i>	
Properties of nanotubes		
3P-12	Raman scattering spectroscopy of gas-flow oriented single-walled carbon nanotubes on hexagonal boron-nitride	112
	<i>* Shu Sato, Satoshi Yotsumoto, Masanori Bamba, Taiki Inoue, Shigeo Maruyama, Shohei Chiashi</i>	
3P-13	Fermi-level dependence of high-harmonic generation in semiconducting single-walled carbon nanotubes with different bandgaps	113
	<i>* Hiroyuki Nishidome, Kohei Nagai, Kento Uchida, Yota Ichinose, Junko Eda, Hitomi Okubo, Yohei Yomogida, Koichiro Tanaka, Kazuhiro Yanagi</i>	

Applications of nanotubes

- 3P-14 Effects of deposition method on the states of Pt nanoparticles on carbon materials and their electrocatalytic properties toward methanol oxidation 114
** Yuho Abe, Hironori Ogata*
- 3P-15 F4-TCNQ Vapor-doped Single Walled Carbon Nanotubes for Thermoelectric 115
** Mariamu Ali, Naofumi Okamoto, Ryo Abe, Ahmed AbdelMoneim, Masakazu Nakamura*
- 3P-16 Operation speed enhancement in carbon nanotube thin film transistors by self-aligned process 116
** Saya Ishimaru, Taiga Kashima, Hiromichi Kataura, Yuuka Ohno*
- 3P-17 Radical polymerization in the presence of carbon nanotubes (CNTs): Radical scavenging by CNTs 117
** Taiyo Shimizu, Ryoichi Kishi, Takeo Yamada, Kenji Hata*

Graphene synthesis

- 3P-18 Effect of Chemical Etching Treatment on Copper Foils for Single-Layer Graphene CVD Growth 118
** Naoki Yoshihara, Masaru Noda*

Properties of graphene

- 3P-19 Thermal transport property of suspended twisted bilayer graphene 119
** Doi Juntaro, Mouri Shinichiro, Araki Tsutomu*
- 3P-20 Carrier control in bilayer graphene dual-gate field effect transistors by interlayer atomic arrangement 120
** Gao Yanlin, Okada Susumu*

Applications of graphene

- 3P-21 Difference of functional groups in Graphene oxide in terms of chemical activity 121
** Riku Kondo, Yoshiaki Matsuo, Kazuyuki Takai*

Atomic Layers

- 3P-22 Tailor-made two-dimensional nano-scale super-structures 122
** Nanami Ichinose, Satoshi Iida, Liu Zheng, Ryo Kitaura*
- 3P-23 Chemically tuned p- and n-type WSe₂ monolayers with improved carrier mobility for electronic applications 123
** Hyun Goo Ji, Pablo Solís-Fernández, Daisuke Yoshimura, Mina Maruyama, Takahiko Endo, Yasumitsu Miyata, Susumu Okada, Hiroki Ago*

Nanowires

- 3P-24 Electrical Conductivity of Chemical-Vapor-Deposition Grown WTe Nanowire Bundles 124
** Chisato Ando, Yusuke Nakanishi, Hiroshi Shimizu, Hong En Lim, Zheng Liu, Takahiko Endo, Yasumitsu Miyata*

September 18th, Fri.

Other topics

3P-25 First-principle calculation of the electronic state of a 2D covalent network of 1,3,5-triamino benzene and benzene-1,3,5-tricarboxaldehyde 125
* *Hiroyuki Yokoi*

3P-26 Two-channel model for low thermal conductivity of Mg_3Bi_2 126
* *Nguyen Tuan Hung, Riichiro Saito*

>>>>>>> Lunch Time (12:00–13:00) <<<<<<<<<

Poster Session (13:00–14:45)

>>>>>>> Coffee Break (14:45–15:00) <<<<<<<<<

Special Lecture (15:00–15:30)

3S-2 Electronic band structure and transport phenomena in graphene with multiple layers 7
* *Ryuta Yagi*

General Lecture (15:30–16:30)

Properties of nanotubes

3-7 Circular dichroism in doped carbon nanotubes 40
* *Riichiro Saito, Md. Shoufie Ukhtary, Sake Wang, Taisei Maeda, Yuya Iwasaki*

3-8 Broadband complex refractive index spectra of single-chirality-enriched carbon nanotube membranes 41
* *Taishi Nishihara, Akira Takakura, Kazunari Matsuda, Takeshi Tanaka, Hiromichi Kataura, Yuhei Miyauchi*

3-9 Unravelling the Thermal Conductivity of Semiconducting Carbon Nanotubes Film with Different Doping Levels 42
* *Kan Ueji, Yuya Matsuoka, Takashi Yagi, Yohei Yomogida, Yota Ichinose, Akari Yoshida, Kazuhiro Yanagi*

Applications of nanotubes

3-10 The first electron-doping of single-walled carbon nanotube by captodatively stabilized boryl radical compounds 43
* *Naoki Tanaka, Aoi Hamasuna, Tsuyohiko Fujigaya*

>>>>>>> Coffee Break (16:30–16:45) <<<<<<<<<

Special Lecture (16:45–17:15)

3S-3 High resolution electron micrographs of serial brain tissue sections on conductive carbon nanotube coated PET tape and neural microcircuit analysis 8
* *Yoshiyuki Kubota*

September 18th, Fri.

General Lecture (17:15–17:45)

Formation and purification of nanotubes

- 3-11 Porosity and Size Analysis of Carbon Nanotube Aggregates by Centrifugal Sedimentation 44
** Yuichi Kato, Takahiro Morimoto, Kazufumi Kobashi, Toshiya Okazaki*
- 3-12 XPS investigation revealing the activation of iron catalyst by a small amount of noble metals without reducing gas towards the synthesis of tall carbon nanotube forest 45
** Shunsuke Sakurai, Jinping He, Kenji Hata, Don Futaba*

Special Lecture (17:45–18:15)

- 3S-4 Nanoscale optical and vibrational spectroscopy of low-dimensional materials in electron microscope 9
** Ryosuke Senga, Kazu Suenaga, Thomas Pichler*

特別講演
Special Lecture

1 S - 1 ~ 1 S - 3
2 S - 1 ~ 2 S - 2
3 S - 1 ~ 3 S - 4

Hetero-nanotubes based on single-walled carbon nanotubes

○Shigeo Maruyama¹

¹ *Department of Mechanical Engineering, The University of Tokyo, Tokyo 113-8656, Japan*

We have synthesized a new coaxial nanotube structure, in which mono- or few-layer hexagonal boron nitride nanotube (BNNT) seamlessly wrap around a single-walled carbon nanotube (SWCNT); SWCNT@BNNT [1]. We named these as one-dimensional van der Waals hetero-structures, because we found no correlation between chiral angle of inner SWCNT and outer BNNT for ‘double-walled’ SWCNT@BNNT. We have further developed the 1D coating CVD of transition metal dichalcogenide nanotubes, such as MoS₂ nanotubes (MoS₂-NT) [1]. These nanotubes can be labelled as SWCNT@BNNT@MoS₂ as in Fig. 1. Because BNNT is thermally more stable than SWCNT, we can remove SWCNT from SWCNT@BNNT by a gentle oxidation process. Hence, we can produce BNNT with inner diameter determined by the original SWCNT. Then, the MoS₂ CVD can result BNNT@MoS₂-NT. More recently, we have realized the CVD growth of SWCNT around SWCNT@BNNT or SWCNT, which will result SWCNT@BNNT@SWCNT or DWCNT. We can demonstrate DWCNT with inner SW¹³CNT and outer SW¹²CNT. BNNT growth on chirality-selected SWCNT is also possible. These hetero-nanotubes are characterized by HR-TEM, STEM-EELS, absorption, Raman and photoluminescence (PL) spectroscopy.

We found the bright PL from MoS₂ nanotubes for BNNT@MoS₂-NT. From DFT calculations, we expect that the K point direct band gap for 2D MoS₂ should appear for MoS₂-NT with larger diameter such as 4 nm. The PL from MoS₂-NT was quenched by inner SWCNT (metallic or small band-gap semiconductor) in the hetero-nanotube, SWCNT@BNNT@MoS₂-NT. For the devices with hetero-nanotubes, we need to start from suspended SWCNTs. We will demonstrate the growth of suspended hetero-nanotubes between silicon pillars and the transfer to Si/SiO₂ substrate for device fabrications. Furthermore, we will discuss thermal properties of BNNT coated SWCNT film [2] and solar cell application of hetero-nanotubes [3].

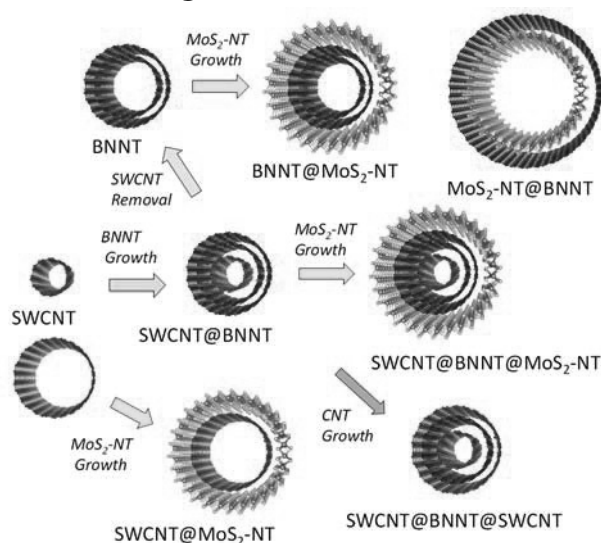


Fig. 1 Various structures of hetero-nanotubes

[1] R. Xiang, T. Inoue, Y. Zheng, A. Kumamoto, Y. Qian, Y. Sato, M. Liu, D. Tang, D. Gokhale, J. Guo, K. Hisama, S. Yotsumoto, T. Ogamoto, H. Arai, Y. Kobayashi, H. Zhang, B. Hou, A. Anissimov, M. Maruyama, Y. Miyata, S. Okada, S. Chiashi, Y. Li, E. I. Kauppinen, Y. Ikuhara, K. Suenaga, S. Maruyama, *Science* **367** (2020), 537.

[2] P. Wang, Y. Zheng, T. Inoue, R. Xiang, A. Shawky, M. Watanabe, A. Anisimov, E. I. Kauppinen, S. Chiashi, S. Maruyama, *ACS Nano* **14** (2020) 4298.

[3] Y. Qian, S. Seo, I. Jeon, H. Lin, S. Okawa, Y. Zheng, A. Shawky, A. Anisimov, E. I. Kauppinen, J. Kong, R. Xiang, Y. Matsuo, S. Maruyama, *Appl. Phys. Express* **13** (2020) 75009.

Corresponding Author: Shigeo Maruyama, Tel: +81-3-5841-6421, Fax: +81-3-5800-6983

Web: <http://www.photon.t.u-tokyo.ac.jp/~maruyama/>, E-mail: maruyama@photon.t.u-tokyo.ac.jp

Improvement of photodynamic activity by dyad systems of fullerene derivative and photo-antenna molecule incorporated into liposomes

○Atsushi Ikeda, Daiki Antoku, Kouta Sugikawa, Riku Kawasaki

Applied Chemistry Program, Graduate School of Advanced Science and Engineering, Hiroshima University, 1-4-1 Kagamiyama, Higashi-Hiroshima, Hiroshima 739-8527, Japan

Photodynamic therapy (PDT) is a next-generation non-invasive treatment for various types of tumors. Fullerenes and their derivatives have attracted significant attention as photosensitizers (PS) of PDT, because of the formation of a long-lived triplet excited state and the photoproduction ability of ROS with high quantum yields. However, the lipid-membrane-incorporating C₆₀ (LMIC₆₀) showed very low photodynamic activity toward HeLa cells under photoirradiation over 600 nm, because light absorption by C₆₀ between 600–700 nm is too low. We have reported previously that a solution to this problem is the coexistence of light-harvesting antenna molecules and pristine C₆₀ in lipid membrane bilayers by a biomimetic photosynthesis approach (Fig. 1a) [1]. However, the location of the light-harvesting moiety in the antenna molecules exists in the neighborhood of the liposomal surface, whereas C₆₀ is located in the hydrophobic core of the lipid bilayer. Consequently, the long distance between antenna molecules and C₆₀ is disadvantageous for energy transfer between these molecules. We hypothesize that energy transfer would be improved noticeably if the location of C₆₀ could be shifted to the neighborhood of the liposomal surface. In this report, a C₆₀ derivative with an ammonium moiety was used to locate C₆₀ in the neighborhood of the liposomal membrane surface (Fig. 1b). The photodynamic activity of the LMIC₆₀ derivative with an antenna molecule was compared with that of LMIC₆₀ and LMIC₇₀ with an antenna molecule. We found that the photodynamic activity of the LMIC₆₀ derivative was approximately 3.5 times higher than that of photofrin, which is the main drug currently in clinical use as a photosensitizer [2,3]. These findings have potentially important implications for the use of fullerene-based materials in biological, medicinal and materials chemistry applications.

Furthermore, I will declare that dyad systems of C₆₀-1 and photo-antenna molecule have great potential for use in the photo dynamically influenced elimination of bacterial content [4].

[1] A. Ikeda, M. Akiyama, T. Ogawa, T. Takeya, *ACS Med. Chem. Lett.*, **1**, 115 (2010).

[2] D. Antoku, S. Satake, T. Mae, K. Sugikawa, H. Funabashi, A. Kuroda, A. Ikeda, *Chem.-Eur. J.*, **24**, 7335 (2018).

[3] D. Antoku, K. Sugikawa, A. Ikeda, *Chem.-Eur. J.*, **25**, 1854 (2019).

[4] R. Kawasaki, D. Antoku, R. Ohdake, K. Sugikawa, A. Ikeda, to be submitted.

Corresponding Author: A. Ikeda

Tel: +81-82-424-7734, Fax: +81-82-424-5494,

Web: <https://ikedalab.wixsite.com/mysite>

E-mail: aiked@hiroshima-u.ac.jp

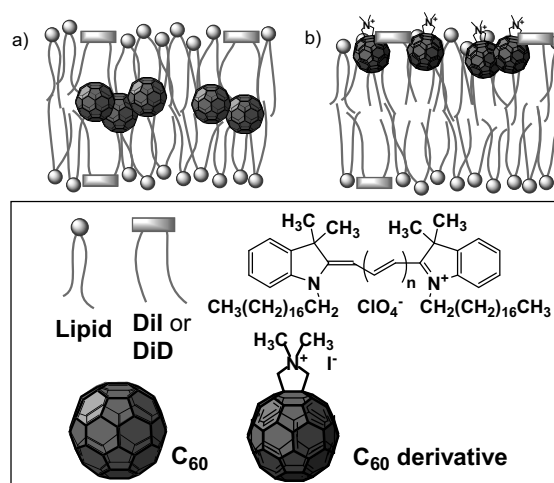


Fig. 1 Schematic illustrations a) C₆₀ and b) C₆₀ derivative in liposome-DiI or DiD and structures of fullerenes and photo-antenna molecules.

Twisted bilayer graphene with clean interface by direct transfer of CVD graphene

○Satoru Tanaka¹, Hitoshi Imamura¹, Anton Visikovskiy¹, Ryosuke Uotani¹, Takashi Kajiwara¹, Hiroshi Ando², Takushi Iimori², Kota Iwata², Toshio Miyamachi², Kan Nakatsuji², Kazuhiko Mase³, Tetsuroh Shirasawa⁴, Fumio Komori²

¹*Department of Applied Quantum Physics and Nuclear Engineering, Kyushu University, Fukuoka 819-0395, Japan*

²*The Institute for Solid State Physics, The University of Tokyo, Kashiwa 277-8581, Japan*

³*Department of Materials Science and Engineering, Tokyo Institute of Technology, Yokohama 226-8502, Japan*

⁴*Institute of Materials Structure Science, High Energy Accelerator Research Organization (KEK), Tsukuba 305-0044, Japan*

⁵*SOKENDAI (The Graduate University for Advanced Studies), Tsukuba 305-0801, Japan*

⁶*National Metrology Institute of Japan, National Institute of Advanced Industrial Science and Technology, Tsukuba 305-0395, Japan*

Twisted bilayer graphene (TBG) shows a variety of electronic characteristics depending on its interlayer twist angle due to moiré potential. The TBG with 1.08° , called the ‘magic-angle’, is predicted to produce an isolated flat-band resulting in emerged superconductivity [1]. Since the twist angle sensitively affects the electronic structures it requires precise control during sample preparation. Generally, samples are evaluated by STM or Landau level spectroscopy (LSS) [2] mainly because of very small size of TBG area, unable to be measured by macroscopic methods utilizing X-ray and electron beams. Not only the twist angle but the quality and cleanness of the interface are also significant parameters since the electronic properties are modified through interlayer interaction. Therefore, large area and clean interface TBGs are demanded for any purposes including device fabrication. We have developed a direct transfer method of the CVD grown graphene sheets on SiC substrates in vacuum. The CVD graphene exhibit unique (3x3) buffer layer on SiC, which enables to peel the sheet off much easier compared to those on the $(6\sqrt{3}\times 6\sqrt{3})R30^\circ$ (6R3) buffer layer observed in traditionally used thermal decomposition of SiC [3].

[1] Y. Cao *et al.*, Nature 556, 7699 (2018).

[2] L. Yang *et al.*, Phys. Rev. B 92, 20 (2015).

[3] W. Kim *et al.*, Science 342, 833(2013).

Corresponding Author: S. Tanaka

Tel: +81-92-802-3535

E-mail: stanaka@nucl.kyushu-u.ac.jp

Emergent transport phenomena at van der Waals interfaces explored by MBE

○Masaki Nakano^{1,2}

¹ *QPEC and Department of Applied Physics, The University of Tokyo, Tokyo 113-8656, Japan*

² *RIKEN Center for Emergent Matter Science (CEMS), Wako 351-0198, Japan*

Since the discovery of graphene, a family of layered materials with nanometer-scale thickness called ‘2D materials’ and their integrated superstructures named ‘van der Waals (vdW) heterostructures’ have become an invaluable material platform for condensed-matter research, providing intriguing properties and functionalities that are missing in their 3D bulk counterparts. There, the most-frequently-used sample fabrication method has been ‘top-down’ mechanical exfoliation combined with the pick-up and transfer methods, while ‘bottom-up’ molecular-beam epitaxy (MBE) should provide a complementary and unique approach in 2D materials research. Successful examples are the application of MBE-grown monolayer films to spectroscopic studies like ARPES and STM/STS measurements that require large-area monolayer films, unveiling fundamental aspects of a variety of 2D materials emerging at the monolayer limit. From materials science viewpoint, however, one of the biggest advantages of the MBE-based approach apart from large-area synthesis should be that we can design and create novel material systems that could not be achieved by simple exfoliation based on bulk crystals, although such attempts are almost missing in this rising research field.

We have recently established a versatile route to layer-by-layer epitaxial growth of a wide variety of 2D materials on insulating substrates by MBE [1], opening a door for exploration of emergent transport phenomena arising with reducing thickness [2-6] even based on hardly-cleavable [2-4] and/or thermodynamically-metastable [5, 6] compounds as well as at the interface between dissimilar materials [7, 8]. In this presentation, we will introduce our recent achievements in particular on the emergent transport phenomena at the vdW interfaces. The first topic is for the vdW heterostructures composed of insulating 2D materials [7], where we found emergent electrical conduction despite that the individual materials are highly insulating, which could be simply understood by taking into account the band alignment at the interface and the relevant interface charge transfer. The second topic is for the vdW heterostructures made of metallic 2D material and itinerant 2D ferromagnet [8], where we found significant modulation of the magnetic properties including the magnetic anisotropy as well as the transition temperature, which could be naturally understood by considering a new-type of magnetic proximity effect mediated by Zeeman-type spin-orbit interaction.

[1] M. Nakano *et al.*, *Nano Lett.* **17**, 5595 (2017); [2] Y. Wang *et al.*, *Appl. Phys. Lett.* **113**, 073101 (2018);

[3] M. Nakano *et al.*, *Nano Lett.* **19**, 8806 (2019); [4] H. Matsuoka *et al.*, *Phys. Rev. Res.* **2**, 012064(R) (2020);

[5] Y. Tanaka *et al.*, *Nano Lett.* **20**, 1725 (2020); [6] S. Yoshida *et al.*, *submitted*;

[7] Y. Kashiwabara *et al.*, *Adv. Funct. Mater.* **29**, 1900354 (2019); [8] H. Matsuoka *et al.*, *submitted*.

Corresponding Author: M. Nakano

Tel: +81-3-5841-6871, Fax: +81-3-5841-6822,

Web: <http://www.qpec.t.u-tokyo.ac.jp/nakano-lab/>

E-mail: nakano@ap.t.u-tokyo.ac.jp

Graphene oxide as a super material

○Shinya Hayami^{1,2}

¹ *Department of Chemistry, Faculty of Advanced Science and Technology, Kumamoto University, Kumamoto 860-8555, Japan*

² *Institute of Industrial Nanomaterials (IINa), Kumamoto University, Kumamoto, 860-8555, Japan*

In a time when there is a strong demand for innovation in energy, medical, and environmental issues, carbon materials are becoming increasingly valuable due to their metal-free, low cost, and lightweight nature. We are focusing on graphene oxide (GO) as a super material. Originally, the fabrication of graphene was done by exfoliating and transcribing graphite with adhesive tape, which is a less productive and less reproducible method. On the other hand, the synthesis of GO by chemical monolayer exfoliation, electrochemical or pulsed plasma synthesis has made it possible to fabricate GO and its reduced form, rGO, at low cost and in large quantities. Our research goal is to precisely control the properties of GO, rGO, and their hybrids to solve energy, medical, and environmental problems in cooperation with domestic companies. In addition, GO and rGO are highly practical materials that will truly contribute to the development of domestic industry.

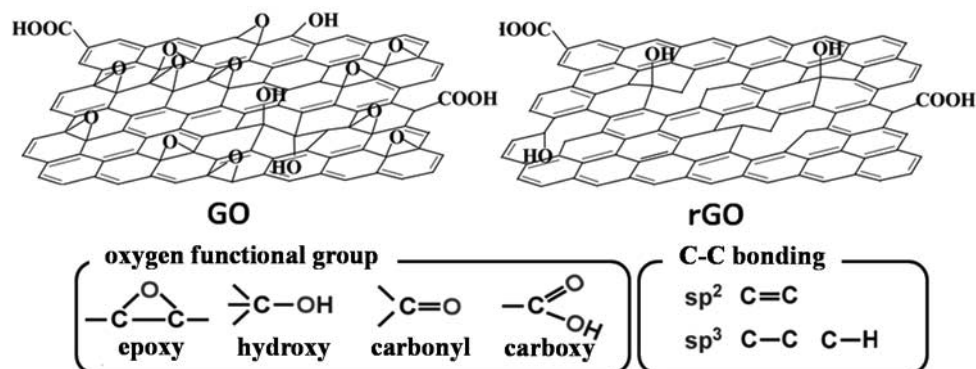


Fig. 1 Structure of GO and rGO.

Corresponding Author: S. Hayami

Tel: +81-96-342-3469, Fax: +81-96-342-3469

Web: <http://www.sci.kumamoto-u.ac.jp/~hayami/index.html>

E-mail: hayami@kumamoto-u.ac.jp

Active site of nitrogen-doped carbon catalysts for fuel cell

○Junji Nakamura¹¹ Faculty of Pure and Applied Sciences, Tsukuba Research Center for Energy Materials Science (TREMS), University of Tsukuba, 1-1-1 Tennodai, Tsukuba 305-8573, Ibaraki, Japan

Nitrogen-doped graphitic carbons as non-Pt catalysts for oxygen reduction reaction (ORR) have been paid much attention in recent years because commercialization of fuel cells requires less expensive and abundant catalytic materials. Identification of the active site of nitrogen-doped carbon materials for ORR is thus urgently required, but still under debate. Currently, the debate focuses on whether the active site is created by pyridinic N (N bonded to two carbon atoms) or graphitic N (N bonded to three carbon atoms, also called substituted N or quaternary N). To determine the active site conclusively, we prepared model catalysts of highly oriented pyrolytic graphite (HOPG) with pyridinic N (pyri-HOPG) or graphitic N (grap-HOPG). The active sites and adsorption properties were examined by ORR and post-ORR X-ray photoelectron spectroscopy (XPS). We have thus determined the active nitrogen species in carbon [1,2]. The graphitic-N doping was performed by mild bombardment with a nitrogen ion beam. To prepare the pyri-HOPG samples, edge patterning was first performed by bombarding the sample with an Ar⁺ ion beam through a slit-patterned Ni mask as shown in Fig.1 A-D. The edged HOPG samples were then exposed to NH₃ at 973 K. The catalytic performances of the model catalysts were measured by cyclic voltammetry (CV) in acidic electrolyte (0.1 M H₂SO₄). It was found that the pyri-HOPG model catalyst shows high activity at high voltages, compared to the very low ORR activities of the N-free model catalysts (Fig.1 E, F). Since the pyri-HOPG sample is nearly free of graphitic N, the ORR results indicate that it is pyridinic N rather than the graphitic N that reduces the ORR overpotential and creates the active site. It is thus concluded that the ORR active sites in nitrogen-doped carbon materials are created by pyridinic N.

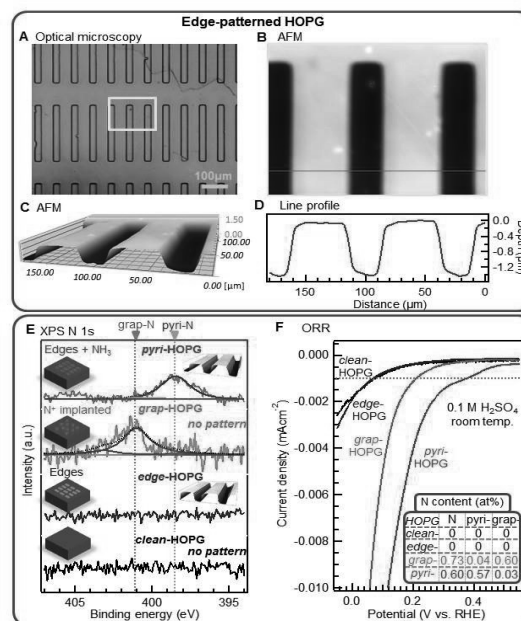


Figure.1 Structural and elemental characterization of four types of N-HOPG model catalysts and their ORR performance. (A) Optical image of patterned edge-N⁺-HOPG. (B) The AFM image obtained from the region indicated by the yellow rectangle in (A). (C) 3D representation of (B). (D) Line profile of the AFM image obtained along the blue line in (B). (E) N 1s XPS spectra of model catalysts. (F) ORR results for model catalysts corresponding to (E). Nitrogen contents of the model catalysts are shown as inset in (F).

[1] D. Guo, R. Shibuya, C. Akiba, S. Saji, T. Kondo, J. Nakamura, *Science*, **351**, 361 (2016).

[2] S. K. Singh, K. Takeyasu, J. Nakamura, *Advanced Materials*, 1804297 (2018).

Electronic band structure and transport phenomena in graphene with multiple layers

Ryuta Yagi

Graduate School of Advanced Science and Engineering, Hiroshima University, Higashi-Hiroshima 839-8530, Japan.

Since the discovery of graphene, a number of researches have been done to elucidate fundamental physics and practical applications. Most of the researches on physical properties of graphene have been performed in mono- or bilayer graphene. While graphite, the opposite limit of graphene with vast number of layers, has also been studied extensively to date, the properties of a few to several layer graphene are not fully understood. New physical phenomena and new practical applications are expected in this system. In this talk, experimental studies of electronic band structure and some transport phenomena, performed by using high-mobility graphene sample, are presented. Landau levels that appear as quantum oscillations of resistivity in magnetic field, reflect the electronic band structure. Maps of the resistivity as a function of magnetic field and carrier density (Landau fan diagrams) visualized detailed band structure which is specific to specific number of layers and stacking [1]; the band structures were much complicated than the well-known simplified band model based on a mass less band and massive bands. Moreover, the band structure was drastically changed by a perpendicular electric field. In particular, mini-Dirac cones were formed, and semi-metallic band structure tended to disappear [2, 3]. These were visualized on maps of resistivity as a function of perpendicular electric field and carrier density. The mini-Dirac cones are essentially due to trigonal warping of the band structure, which becomes increasingly important in graphene with multiple layers. The Fermi surfaces are trigonally deformed circles, and therefore, the electron trajectories in a magnetic field become trigonally warped circles. This was observed via ballistic transport experiments by using antidot lattices [4]. The effect of trigonal warping also emerged in a specific resistivity peak structure in a moiré superlattice of *h*-BN-graphene heterostructure.

[1] R. Yagi *et al.*, *Sci. Rep.* **8**, 13018 (2018).

[2] T. Hirahara *et al.*, *Sci. Rep.* **8**, 13992 (2018), T. Nakasuga *et al.* *Phys. Rev. B* **99** 035440 (2019).

[3] K. Horii *et al.*, *Phys. Rev. B* **100**, 245420 (2019).

[4] T. Oka *et al.*, *Phys. Rev. B* **99**, 035440 (2019), S. Tajima *et al.*, *J. Phys. Soc. Jpn.* **89**, 044703 (2020).

Corresponding Author: R. Yagi

Tel: +81-82-424-7041

Web: <http://home.hiroshima-u.ac.jp/~yagi/index.html>

E-mail: yagi@hiroshima-u.ac.jp

High resolution electron micrographs of serial brain tissue sections on conductive carbon nanotube coated PET tape and neural microcircuit analysis

○Yoshiyuki Kubota^{1,2}

¹ Division of Cerebral Circuitry, National Institute for Physiological Sciences, Okazaki
444-8787, Japan

² Department of Physiological Sciences, SOKENDAI, Okazaki 444-8787, Japan

The electron microscopy (EM)-based reconstruction of neuronal circuits from serial ultrathin sections has attracted considerable recent attention, despite the emergence of super resolution microscopy, because EM is a reliable method for the diverse-scale analysis of dense nanoscale details in biological structures. Here, we focus on the automated tape-collecting ultramicrotome (ATUM) method which allows the collection of many serial ultrathin sections of consistent quality quickly and automatically by producing ultrathin sections on a tape that can be repeatedly imaged using SEM. Currently, the most commonly used tape for ATUM is carbon coated (cc)-Kapton tape (polyimide film, DuPont, Wilmington, USA), but it has deficiencies due to a relatively high sheet resistance (19-6530 Mohm/sq), non-uniform carbon coating that causes mottled surface resistance, and scratching. Moreover, there is no assurance of a regular supply of high-quality cc-Kapton tape due to inconsistent industrial production procedures. Therefore, an improved alternative tape would have a valuable role the field of ATUM-based EM. In this study, we address these issues by introducing an improved tape and tissue staining protocol. We screened candidates and found that plasma-hydrophilized-carbon nanotube (CNT) tape is optimal due to its extremely high surface conductivity (240-500 ohm/sq) and low endogenous signal, and it can provide high quality images of tissue sections with SEM. The ATUM-SEM method impressively alters current research strategy using an electron microscope on functional architecture of the brain microcircuit.

[1] Kubota Y et al., *Front. Neural Circuits*, fncir.2018.00098 (2018)

[2] 窪田芳之, 電子顕微鏡を使った革新的脳組織解析法—コネクトーム研究; 実験医学増刊「脳神経回路と高次脳機能 スクラップ&ビルドによる心の発達と脳疾患の謎を解く」(榎本和生, 岡部繁男編集) 羊土社、東京、p158-164, ISBN 978-4-7581-0372-5 (2018)

[3] Kubota Y et al., *Nature Communications*, **9**, 437 (2018)

Corresponding Author: Y. Kubota

Tel: +81-564-59-5282, Fax: +81-564-59-5284,

E-mail: yoshiy@nips.ac.jp

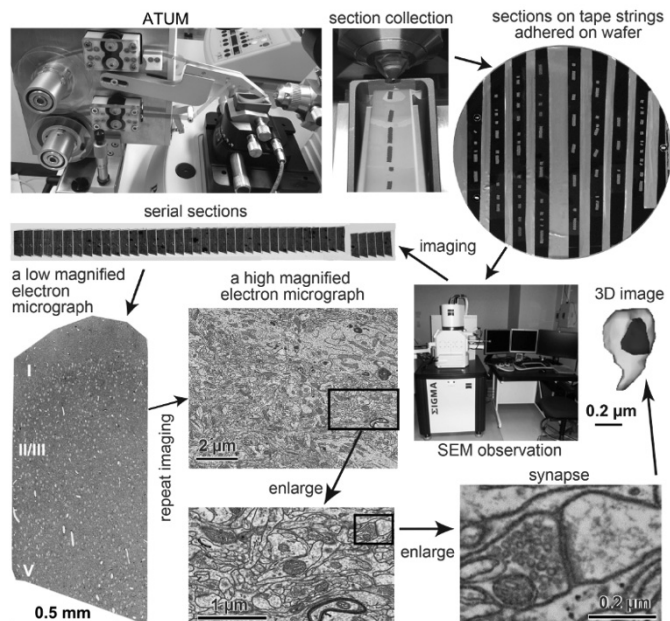


Figure 1 Pipeline of the ATUM-SEM method

Nanoscale optical and vibrational spectroscopy of low-dimensional materials in electron microscope

○Ryosuke Senga¹, Kazu Suenaga¹, Thomas Pichler²

¹ Nanomaterial research institute, AIST, Tsukuba 305-8565, Japan

² Faculty of Physics, University of Vienna, Vienna, Austria

Excitations of quasiparticles govern physical properties of low-dimensional materials. Especially their behaviors at non-perfect structures like boundaries, edges, defects or irregular stacking sequence are undoubtedly important to understand the performance of nanodevices consisting of nanomaterials. However, such local information has been usually averaged in conventional inelastic scattering techniques using x-ray, neutron and light sources because of their diffraction limit. Here we demonstrate the nanoscale optical and vibrational spectroscopy of 1D/2D materials by using a monochromatic electron source mounted in a scanning transmission electron microscope. Its energy resolution, better than 30 meV, allows to access the quasiparticle excitations (i.e. phonon, exciton and plasmon) of low-dimensional materials by electron energy-loss spectroscopy (EELS). The spatial and momentum resolutions balance each other and can be finely tuned with magnetic/electrostatic lenses. For instance, an atomically thin probe can be formed with an integration of large momentum space. This allows us to extract local information from single defects. Indeed, we have successfully measured the optical gap transitions from a defect of an individual semiconducting carbon nanotube [1,2]. In contrast, an electron probe with a higher momentum resolution can provide a full phonon dispersion of 2D materials (Fig. 1) such as hexagonal boron nitride or graphene at a few tens nanometer scale [3]. Thus, the propagation of each phonon mode at defects such as edges in graphene has been unambiguously visualized. This local spectroscopy with a large flexibility will open up a wide possibility to unravel the defect physics of quantum matters.

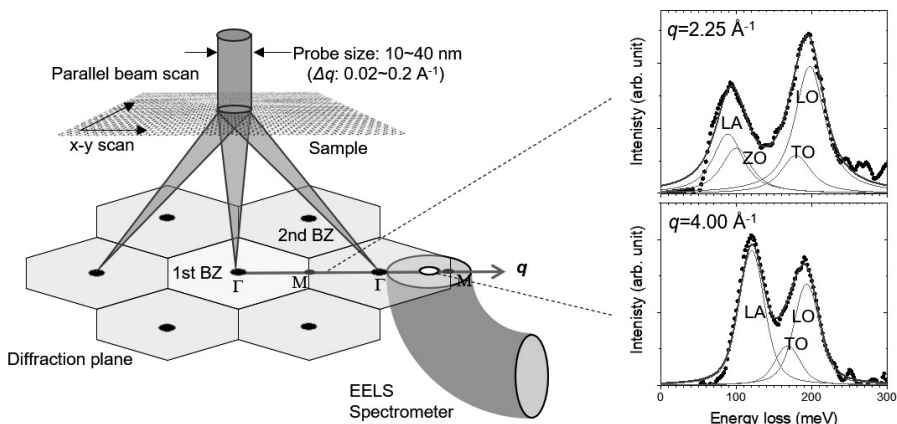


Fig. 1 Experimental setup for the momentum-resolved EELS and examples of momentum-resolved EEL spectra taken at $q=2.25$ and 4.00 \AA^{-1} along the GMGM direction. The spectrometer entrance aperture is placed at a given position in the diffraction plane including the first, second, or third Brillouin zones.

[1] R. Senga, T. Pichler and K. Suenaga *Nano Letters* **16**, 3661 (2016).

[2] R. Senga *et al.*, *Nano Letters* **18**, 3920 (2018).

[3] R. Senga *et al.*, *Nature* **573**, 247 (2019)

Corresponding Author: R. Senga

Tel: +81-29-862-6518

E-mail: ryosuke-senga@aist.go.jp

~ **Memo** ~

一般講演
General Lecture

1-1 ~ 1-11

2-1 ~ 2-12

3-1 ~ 3-12

Linear Temperature Dependence of Nanotube Yarn Resistance

○Takumi Inaba¹, Takahiro Morimoto¹, Satoshi Yamazaki², and Toshiya Okazaki¹

¹ CNT-Application Research Center, National Institute of Advanced Industrial Science and Technology AIST, Tsukuba 305-8565, Japan

² Research Association of High-Throughput Design and Development for Advanced Functional Materials (ADMAT), Tsukuba 305-8565, Japan

Carbon nanotube yarns (CNT-yarns) are expected to be used for light weight and high conductive electric cables. Specific electronic conductivity of novel CNT-yarns is close to that of copper [1]. However, no electronic conduction models were proposed for a temperature range as wide as possible (e.g. 1-1300 K), which makes ambiguity remained in the guidelines to further increase the electronic conductivity. This is likely due to absence of a model for a linear temperature dependence of the resistance that is observed near room temperature and has a negative temperature coefficient. The linearity is considered unique from a general material science perspectives. Therefore, the identification of the model is of great importance for studies of CNT as well as general material science.

Figure 1(a) shows a resistance-temperature plot acquired from a CNT-yarn made of multi-walled carbon nanotubes (MWCNTs). The solid line the result of curve fitting with the function $R(T) \propto T^\beta$. The curve fitting resulted in $\beta=1.00$, and showed the clear linearity. Although a model of the linearity for CNTs was not identified, there exist a theoretical study that predict the linearity for graphene [2], in which the linearity was attributed to the scattering by the exchange field that Friedel oscillations cause. Presumably, relatively flat regions around outermost walls of MWCNTs (see Fig. 1(b)) in the yarn can realize graphene-like conduction paths and caused the linearity.

We will discuss adaptation of the model to CNT-yarns with showing the results of few-walled CNTs, magnetoresistance measurements, and defects introduction.

This presentation is based on results obtained from a project, JPNP16010, commissioned by the New Energy and Industrial Technology Development Organization (NEDO).

[1] D. E. Tsentalovich, *et al.*, ACS Appl. Mater. Interfaces 9, 36189 (2017)

[2] V. V. Cheianov, *et al.*, Phys. Rev. Lett. 97, 226801 (2006)

Corresponding Author: T. Inaba, E-mail: takumi.inaba@aist.go.jp

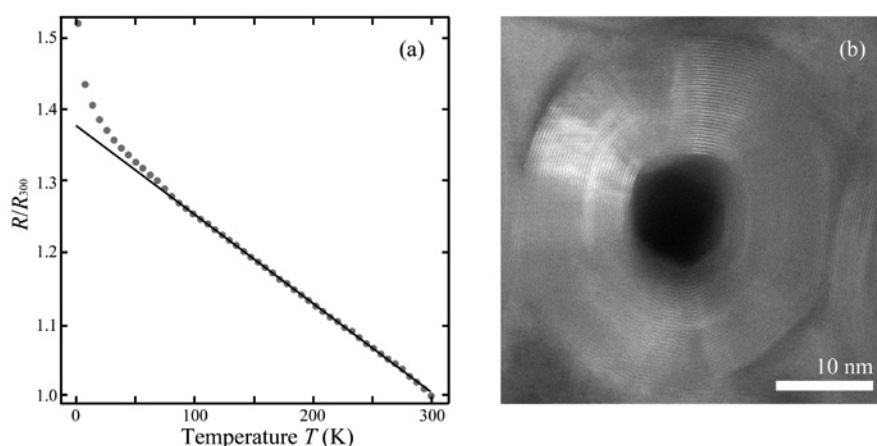


FIG. 1. (a) Normalized resistance of the yarn as a function of temperature. (b) Cross sectional STEM image of the MWCNT comprising the yarn.

Indirect to direct band gap crossover of single walled MoS₂ nanotubes

○Kaoru Hisama¹, Mina Maruyama², Susumu Okada², Shohei Chiashi¹
and Shigeo Maruyama¹

¹ Department of Mechanical Engineering, The University of Tokyo, Tokyo 113-8656, Japan

² Department of Physics, University of Tsukuba, Tsukuba 305-8571, Japan

Molybdenum disulfide (MoS₂) is known to form tubular structure, owing to its honeycomb covalent network with three-atom thickness. Semiconducting electronic structure of monolayer sheet of MoS₂ also makes MoS₂ nanotubes (MoS₂ NTs) semiconductors irrespective of their diameter and helicity. Several theoretical works predicted that MoS₂ NTs have indirect band gaps except with zigzag chiral indices [1-3]. This indirect band gap structure is ascribed to strain effect due to curvature, because the band edge alignment of MoS₂ NTs asymptotically corresponds to the direct band gap at the K point of monolayer MoS₂ sheet, with increasing their diameter. Thus, in this work, we aim to reveal this indirect to direct band gap crossover of armchair MoS₂ NTs in a wide diameter range using the density functional theory.

Although a small diameter (12,12) NT is a semiconductor with an indirect band gap between Γ and approximately $k = 2\pi/3$ where K point in 2D BZ is folded [Fig. 1(a)], a large diameter (30,30) NT is a semiconductor with a direct band gap at approximately $k = 2\pi/3$ [Fig. 1(b)]. To study the critical diameter at which the band gap crossover occurs, we investigated the energy difference between the highest occupied states at near the Γ point, E_0^{HO} and at $k = 2\pi/3$, E_K^{HO} of MoS₂ NTs in terms of their diameter. Figure 1(c) showed that the crossover occurred at the diameter of approximately 5 nm. This result suggests that photoluminescence is observed in MoS₂ NTs with the diameter 5 nm or larger.

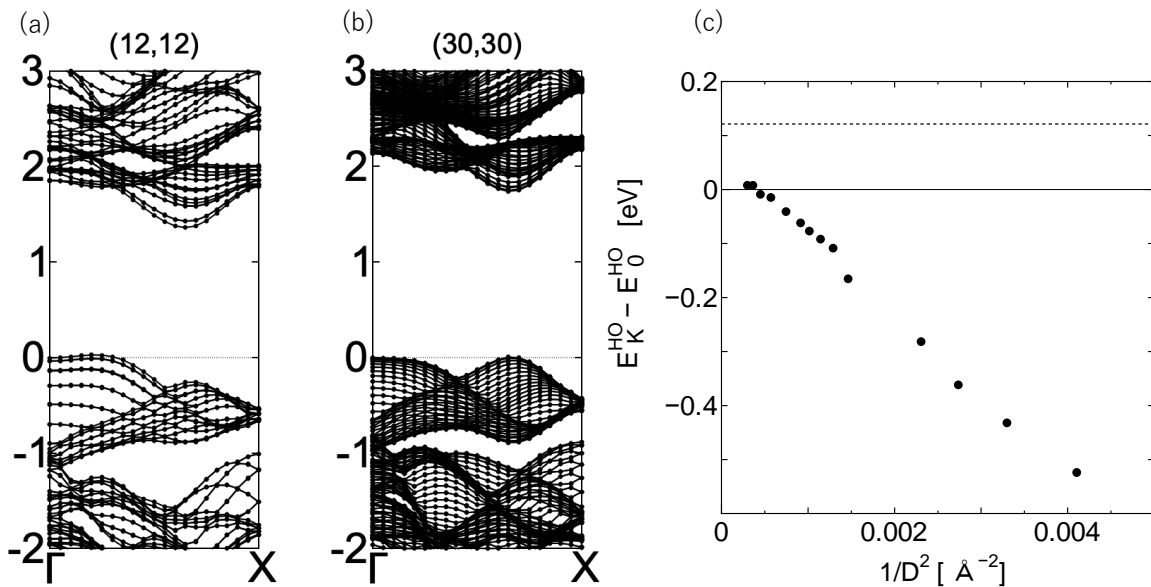


Figure 1 Electronic structure of (a) (12,12) and (b) (30,30) MoS₂ NT. (c) $E_K^{\text{HO}} - E_0^{\text{HO}}$ as a function of squared inverse of diameter. Dotted line in (c) shows the value of 2D monolayer MoS₂.

[1] G. Seifert, *et al.*, *Phys. Rev. Lett.* **85**, 146 (2000). [2] D. B. Zhang, *et al.*, *Phys. Rev. Lett.* **104**, 065502 (2010).

[3] N. Zibouche *et al.*, *Euro. Phys. J. B*, **85**, 49 (2012).

Corresponding Author: Susumu Okada E-mail: sokada@comas.frsc.tsukuba.ac.jp

Diameter-dependent Photoluminescence Properties in Color Centers of Air-Suspended Single-Walled Carbon Nanotubes

○ Daichi Kozawa¹, Xiaojian Wu², Akihiro Ishii^{1,3}, Jacob Fortner², Keigo Otsuka³, Rong Xiang⁴, Taiki Inoue⁴, Shigeo Maruyama^{4,5}, YuHuang Wang^{2,6}, Yuichiro K. Kato^{1,3}

¹ *Quantum Optoelectronics Research Team, RIKEN Center for Advanced Photonics*

² *Department of Chemistry and Biochemistry, University of Maryland, College Park*

³ *Nanoscale Quantum Photonics Laboratory, RIKEN Cluster for Pioneering Research*

⁴ *Department of Mechanical Engineering, The University of Tokyo*

⁵ *Energy NanoEngineering Laboratory, National Institute of Advanced Industrial Science and Technology (AIST)*

⁶ *Maryland NanoCenter, University of Maryland, College Park*

Color centers in single-walled carbon nanotubes are of interest because of their single-photon emission at room temperature in the telecom range [1, 2], but the lack of vapor-phase reaction route for forming the color centers hinders the use of the excellent optical properties of air-suspended carbon nanotubes. We herein demonstrate the functionalization of air-suspended carbon nanotubes using iodobenzene as a precursor. We rationally design the chemical reaction procedure without compromising the suspended structure. Formed phenyl group serves as a color center and exhibits localized exciton emission peaks E_{11}^* and E_{11}^{*-} in addition to the free exciton emission peak E_{11} . We characterize representative 12 chiralities to reveal the diameter-dependent reactivity and optical property of the color centers. We quantitatively describe the reactivity, where a strain of nanotube curvature promotes the reaction. The trapping potential of E_{11}^* and E_{11}^{*-} excitons also shows the diameter dependence, which we discuss in the presentation. These findings should lead to further development of quantum photon sources that utilize color centers in carbon nanotubes.

This work was supported in part by RIKEN (Special Postdoctoral Researcher Program), MIC (SCOPE 191503001), JSPS (KAKENHI JP15H05760, JP18H05329, 20K15112, 20K15137, 20H02558), and MEXT (Nanotechnology Platform). We thank the Advanced Manufacturing Support Team at RIKEN for technical assistance.

[1] A. Ishii, X. He, N. F. Hartmann, H. Machiya, H. Htoon, S. K. Doorn, and Y. K. Kato, *Nano Lett.* **18**, 3873 (2018).

[2] X. He, N. F. Hartmann, X. Ma, Y. Kim, R. Ihly, J. L. Blackburn, W. Gao, J. Kono, Y. Yomogida, A. Hirano, T. Tanaka, H. Kataura, H. Htoon, and S. K. Doorn, *Nat. Photonics* **11**, 577 (2017).

Corresponding Author: Y. K. Kato

Tel: +81-48-462-1449,

Web: <http://katogroup.riken.jp/en/>

E-mail: yuichiro.kato@riken.jp

Energetics and electronic structure of bilayer graphene intercalating buckybowls

○Mina Maruyama, Susumu Okada

Department of Physics, University of Tsukuba, Tsukuba 305-8571, Japan

Atomic layer materials opened new paradigm of science and technology of intercalation compounds where the thickness and constituent materials/layers are arbitrarily tailored. Because of interaction between constituents, physical and chemical properties of such compounds exceeded the simple sum of those of each constituent material. Bilayer graphene is an ultimate host material to form such intercalation compound by intercalating guest materials into the two-dimensional space with nanometer thickness. In such confined nanospace, guest materials occasionally possessed unusual geometric and electronic structures those are absent in their bulk phases. In this work, we elucidate energetics and electronic structure of bilayer graphene intercalating sumanene [Fig. 1] to investigate the bowl-to-flat conformation change of sumanene between graphene layers, using the density functional theory with the generalized gradient approximation with van der Waals correction.

Our calculation shows that sumanene retained the bowl shape as its ground state conformation between graphene layers of which total energy is lower by approximately 0.4 eV/molecule than that with flat molecular conformation [Fig. 2]. By analyzing the energy potential landscape, we found that sumanene turned into flat conformation by applying pressure of 0.6-0.8 GPa normal to graphene layer, depending on the interlayer stacking. Sumanene molecule with bowl shape leads to electron and hole doping into bilayer graphene owing to the strong electron polarity of molecule arose from pentagonal ring and edge C-H bond.

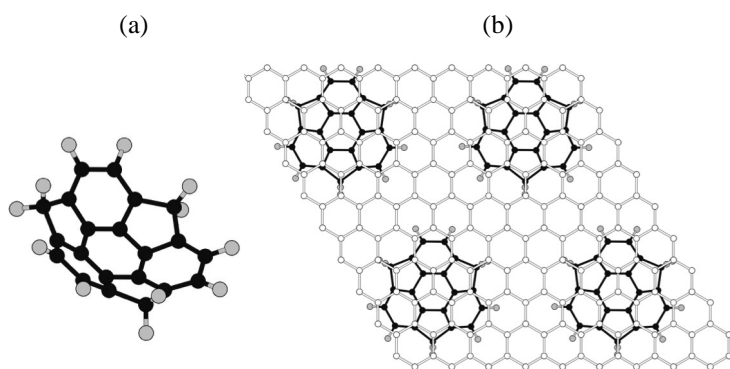


Fig. 1 Geometric structures of (a) sumanene molecule and (b) sumanene intercalated bilayer graphene.

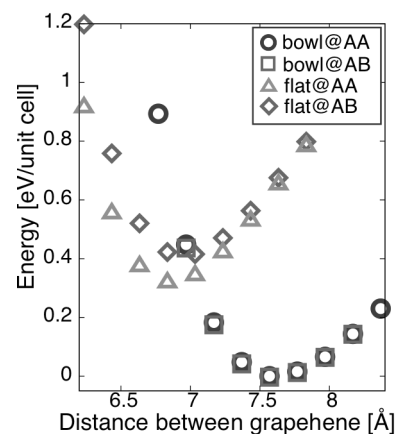


Fig. 2 Total energy of sumanene intercalated bilayer graphene as a function of interlayer spacing.

Corresponding Author: M. Maruyama

Tel: +81-29-853-5921, Fax: +81-29-853-5924,

E-mail: mmaruyama@comas.frsc.tsukuba.ac.jp

Direct synthesis of size-controlled quantum dots with graphene nanoribbon

○Mizuki Seo¹, Takahito Kitada², Toshiro Kaneko¹, Tomohiro Otsuka², and Toshiaki Kato^{1,3}

¹ Graduate School of Engineering, Tohoku University, Sendai 980-8579, Japan

² RIEC, Tohoku University, Sendai 980-8577, Japan

³ JST-PRESTO

Graphene is one of the topical nanomaterials attracting intense attentions as next generation electronic materials due to its superior electrical conductivity, mechanically flexible structure and high optical transparency. While graphene has 2-dimensional sheet structure and shows metallic like behaviour, it has been discovered that graphene nanoribbon (GNR) has finite bandgap, which can be obtained by making graphene into 1-dimensional structure. This discovery made GNR conspicuous material mainly in semiconductor device field around the world.

So far, we have succeeded for the first time in the integrated synthesis [1-3] of suspended GNR by combining our original plasma CVD process [4] and the original idea of using the nanobar structure as a catalyst. Furthermore, previous studies have revealed that GNR behaves as a quantum dot. However, the quantum dot size is much smaller than that of whole GNR, indicating spontaneous defects may be the origin of quantum dot. Hence, it is very difficult to control the dot size and density, which is critical subject for the future application as quantum devices.

The simplest way to control the size and density of quantum dot within GNR is making whole GNR as a single quantum dot. Then, we attempted to control the size and density of GNR quantum dots by optimizing the unique nanobar structure and synthesis conditions. Based on the systematic investigations, it is found that periodic Coulomb oscillation and clear Coulomb diamond feature was observed at cryogenic temperature (4.2 K) (Fig.1). The size of quantum dot was estimated from this Coulomb diamond feature. It was found that the quantum dot size is almost same with that of the whole GNR, indicating that whole GNR region was used as a single quantum dot. Since the size of whole GNR can be controlled by initial nanobar structure, our method can be useful to apply for the future quantum device applications with GNRs.

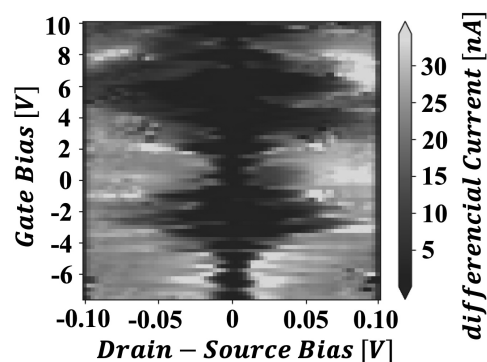


Fig.1 Typical Coulomb diamond feature of GNR device measured at cryogenic temperature (4.2K).

[1] T. Kato and R. Hatakeyama, *Nature Nanotechnology* **7**, 651 (2012).

[2] H. Suzuki, T. Kaneko, Y. Shibuta, M. Ohno, Y. Maekawa and T. Kato, *Nature Communications* **7**, 11797 (2016).

[3] H. Suzuki, N. Ogura, T. Kaneko, and T. Kato, *Scientific Reports* **8**, 11819 (2018).

[4] T. Kato and R. Hatakeyama, *ACS Nano* **6**, 8508 (2012).

Corresponding Author: M. Seo

Tel: +81-22-795-7046,

E-mail: mizuki.seo.s1@dc.tohoku.ac.jp

High-order mode operation of graphene mechanical resonator

○Hirofumi Ikemoto,¹ Kaito Nakagawa,¹ Taichi Inoue,¹ Kuniharu Takei,¹ Takayuki Arie,¹ Seiji Akita¹

¹*Department of Physics and Electronics, Osaka Prefecture University, Sakai 599-8531, Japan*

Mode coupling of nano-electro-mechanical resonators (NEMR) are one of emerging components for ultralow power information processing mimicking the superposition of states. Here, we investigate the higher mode oscillation of a suspended graphene NEMR (G-NEMR) with a metal local gate structure.

The sample fabrication procedure is as follows. First, a Cr / Au as a gate electrode was deposited on n+Si/SiO₂ substrate followed by spin-coating of spin-on-glass (SOG) as an additional oxide layer. Then, the graphene synthesized by the CVD was transferred on it and was etched by O₂ plasma to form the graphene stripe with the width of 2 μm . To form the suspended ribbon structure, the SOG under the graphene was etched by BHF and dried using the supercritical drying method to fabricate $2 \times 2 \mu\text{m}^2$ G-NEMRs with a local metal gate (Fig. 1.).

In the G-NEMR, with the channel length $L = 2 \mu\text{m}$ using the global gate structure (without the metallic local gate), the resonance was observed at $V_{\text{GS}} > 12 \text{ V}$ (Fig. 2.). However, in this structure, it was difficult to measure higher mode resonance above 100 MHz even when a back gate voltage of $V_{\text{GS}} = 30 \text{ V}$ was applied because of the large parasitic capacitance and high impedance of n+Si against the higher frequency. On the contrary, in this study, the same size G-NEMR with the local gate showed the resonance mode higher than 100 MHz at $V_{\text{GS}} = 30 \text{ V}$ (Fig. 3.). This is due to the successful decrease of the impedance and parasitic capacitance of the gate electrode. Thus, we have successfully measured the higher mode resonance on the G-NEMR with the metallic local gate.

Acknowledgements This work was partially supported by KAKENHI Grant Numbers 15H05869, 16H00920, 16K14259, 16H06504, and 17H01040.

Corresponding Author: S. Akita, Tel: +81-72-254- 9261, E-mail: akita@pe.osakafu-u.ac.jp

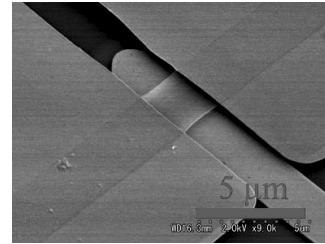


Fig. 1. SEM image of a double clamped graphene resonator using local gate ($2 \times 2 \mu\text{m}^2$)

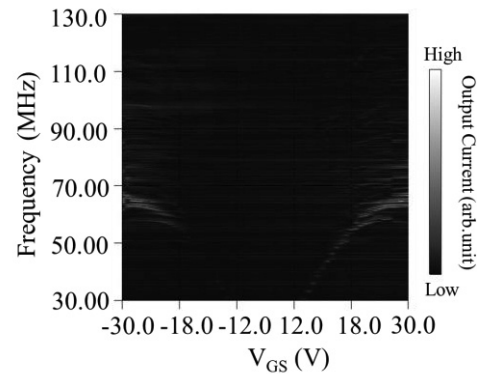


Fig. 2. Frequency dependence of gate voltage. (Global gate: $2 \times 2 \mu\text{m}^2$)

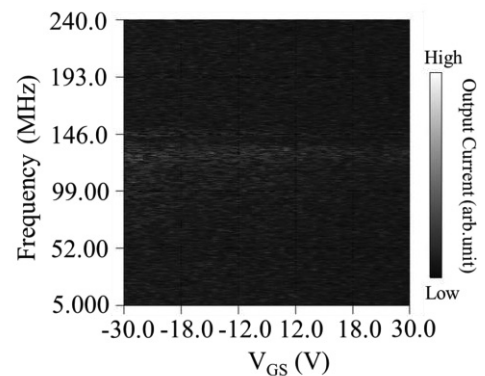


Fig. 3. Frequency dependence of gate voltage. (Local gate: $2 \times 2 \mu\text{m}^2$)

One dimensional hetero-junction diode

○Ya Feng, Henan Li, Taiki Inoue, Shigeo Maruyama

*Department of Mechanical Engineering, School of Engineering, The University of Tokyo,
Tokyo 113-8656, Japan*

The synthesis of one-dimensional van der Waals heterostructure was realized recently [1], which opens up new possibilities for potential applications in electronics and optoelectronics as the two-dimensional counterpart has demonstrated extensively. The natural doping results in p-type carbon nanotube transistors [2], while n-type for molybdenum disulfide transistors [3]. Therefore, the coaxial one-dimensional heterostructure of single walled carbon nanotube (SWNT)-boron nitride nanotube (BNNT)-molybdenum disulfide nanotube (MoS₂NT) would form a p-i-n junction; and if opposite potential polarity is applied on SWNT and MoS₂NT respectively, as shown in the schematic of Fig. 1, the forward bias would allow the flow of current while the reverse bias would block it. The current work is providing such a one-dimensional heterojunction diode as demonstrated in the graph of Fig. 1.

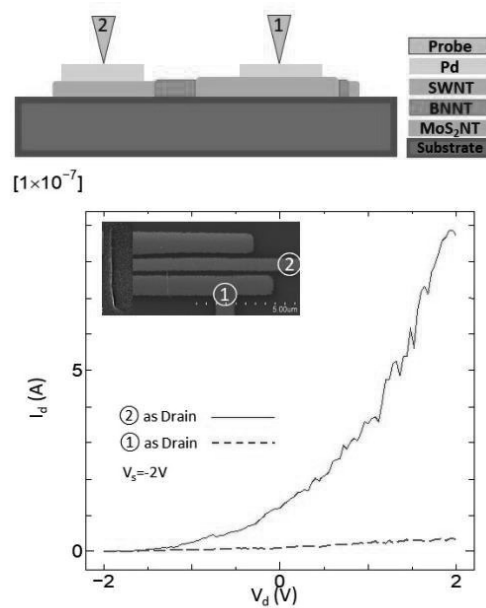


Figure 1 The top panel illustrates schematic of the device; the bottom graph demonstrates rectifying effect and SEM image of the device is shown in the inset.

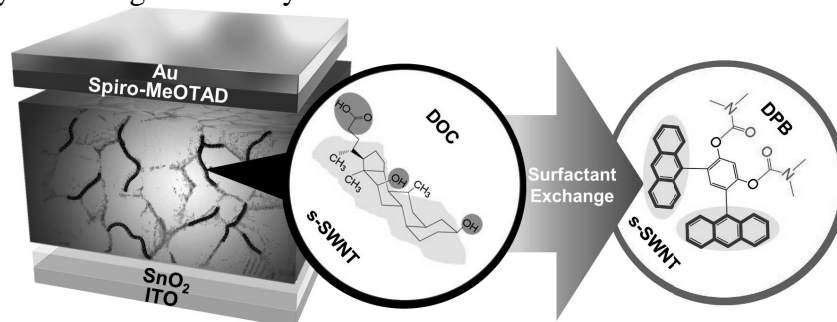
- [1] R. Xiang *et al.*, *Science*, **367**, 6477 (2020).
- [2] C. Qiu *et al.*, *Science*, **355**, 6322 (2017).
- [3] S. Desai *et al.*, *Science*, **354**, 6308 (2016).

Polyaromatic Anthracene Nano-tweezer on Semiconducting Carbon Nanotubes for Growth and Bridging of Perovskite Crystal Grains in Perovskite Solar Cells

○Hao-Sheng Lin¹, Il Jeon¹, Yutaka Matsuo¹, Shigeo Maruyama¹

¹Department of Mechanical Engineering, The University of Tokyo, Tokyo 113-8656, Japan

Polyaromatic anthracene, which contains a bent polyaromatic group on one end and a functional group on the other end, has been reported to clench SWNTs. While the polyaromatic end induces strong π - π interaction with the SWNTs, the functional end can easily be modified chemically. In our group, the modified polyaromatic anthracenes were used as charge-transporting layers in optoelectronics, harnessing their bandgaps and high mobility arising from the conjugated sp^2 bonds. Hence, we designed and synthesized 4,6-di(anthracen-9-yl)-1,3-phenylene bis(dimethylcarbamate) (DPB), which is essentially polyaromatic anthracene with two urea-analogues functional groups. Subsequently, we used them as new surfactants for s-SWNTs in the PSC application. DPB successfully attached to s-SWNTs and replaced DOC surfactants as confirmed by photoluminescence (PL) and UV-visible absorption spectroscopy (UV-Vis). DPB-attached s-SWNTs showed much higher solubility in both DMF and dimethyl sulfoxide (DMSO) than the DOC-attached s-SWNTs. Accordingly, higher concentration of s-SWNTs could be added to the perovskite precursor solution. The DPB on SWNTs expectedly manifested a stronger interaction on Pb^{2+} than DOC owing to the strongly electron donating nature of the lone pair electrons on the carbamate group enhanced by its configurational orientation facing outwards. DPB-attached s-SWNT-added perovskite films exhibited excellent charge-selectivity and reduced charge trap density. The suitable molecular energy levels and higher mobility of DPB compared with DOC led to higher device performance. DPB-attached s-SWNTs-added PSCs exhibited a PCE of 20.7%, which is higher than those of DOC-attached s-SWNT-added PSCs (19.7%) and pristine PSCs (18.4%). All of the three photovoltaic parameters, namely, high short-circuit current density (J_{SC}), open-circuit voltage (V_{OC}), and filling factor (FF) contributed to the high power conversion efficiency (PCE) of the DPB-attached s-SWNTs-added PSCs. The high J_{SC} came from the large perovskite crystal size of over 500 nm. The high V_{OC} came from strong passivation effect of the DPB-attached s-SWNTs. The high FF came from the improved carrier mobility and charge selectivity of DPBs on s-SWNTs.



Corresponding Author: S. Maruyama

Tel: +81-3-5841-6408

E-mail: maruyama@photon.t.u-tokyo.ac.jp

Aligned carbon nanotube/polymer composite films for high thermal diffusivity

○Maireyee Bhattacharya, Manish Pandey, Ryo Abe, Naofumi Okamoto, Yuki Sekimoto, Masakazu Nakamura

*Division of Materials Science, Nara Institute of Science and Technology,
8916-5 Takayama-cho, Ikoma, Nara 630-0192, Japan*

Isolated carbon nanotubes (CNTs) exhibit exceptionally high electrical, mechanical, and thermal properties [1, 2]. But the practical application of individual CNTs is limited by the difficulties of handling them at nanometer scale. CNT networks at bulk, on the other hand, are generally random. Therefore, a technique is highly sought after that can help retain the intrinsic anisotropic properties of single CNTs at bulk by enforcing alignment among them in the CNT network.

Recently, we reported a new method of fabricating scalable ribbon-like CNT/polymer composite films using a programmed robotic dispenser [3]. This method can easily produce controlled orientation of the CNTs in the CNT/polymer composite along the drawing direction of the ribbon. In this work, we conducted several investigations related to the optimization of the controlling factors that were crucial to improve the alignment and will be reported in detail. We have found that the choice of substrate, its surface energy and casting parameters play crucial role. It is proposed that during the flow of the CNT polymer dispersion through the narrow needle, the shear stress at the inner wall of the needle tends to direct the longitudinal axis of the CNTs parallel to the flow direction. The dispersion is then dispensed on to a suitable substrate where the streamlined orientation is preserved. The effect of various drawing conditions on this orientation control mechanism will also be discussed. The degree of orientation was evaluated using polarized Raman mapping. The axial alignment of CNT bundles along the drawing direction was further confirmed by scanning electron microscope images over the surface as well as deeper inside the film. Finally, the effect of alignment on thermal diffusivity of CNT ribbons will also be reported.

This work was supported by JST CREST Grant Number JPMJCR18I3, Japan.

- [1] Shokrieh *et al.* *Mech Compos Mater* **46**, 155 (2010).
- [2] Z. Han, Alberto Fina, *Prog. Polym. Sci.* **36**, 914 (2011).
- [3] Pandey *et al.* *Appl. Phys. Express* **13**, 065503 (2020).

Corresponding Author: M. Nakamura
Tel: +81- 743-72-6031, Fax: +81-743-72-6047,
E-mail: mnakamura@ms.naist.jp

Gas-phase growth and localized deposition of highly crystalline carbon nanotubes using a microplasma reactor

○Takashi Tsuji¹, Yoshiki Shimizu^{2,3}, Jaeho Kim⁴, Hajime Sakakita⁴, Kenji Hata¹, Don N. Futaba¹, Shunsuke Sakurai¹

¹*CNT-Application Research Center, National Institute of Advanced Industrial Science and Technology (AIST), Ibaraki 305-8565, Japan*

²*Nanomaterials Research Institute, National Institute of Advanced Industrial Science and Technology (AIST), Tsukuba, Ibaraki 305-8565, Japan*

³*AIST-UTokyo Advanced Operando-Measurement Technology Open Innovation Laboratory (OPERANDO-OIL), National Institute of Advanced Industrial Science and Technology (AIST), Kashiwa, Chiba 227-8589, Japan*

⁴*Innovative Plasma Processing Group, Research Institute for Advanced electronics and Photonics, National Institute of Advanced Industrial Science and Technology (AIST), Ibaraki 305-8568, Japan*

Physical vapor deposition (PVD) process based on plasma technology such as arc discharge [1] and thermal plasma jet [2] has enabled the production of highly crystalline carbon nanotubes (CNTs). The PVD process operates by generating high temperature (> 4000 K) which is used for the vaporization of the solid feedstock and catalyst particle nucleation, and the CNTs precipitate during the cooling of the ambient gases at ~ 1000 – 2000 K [3]. Compared to the chemical vapor deposition process, temperature control of the CNT growth zone is not as direct and simple. In addition, plasma-based growth reactor is large, and requires large amounts of power (> 1 kW), therefore, downsizing this technology would be beneficial for the development of new type of plasma-based CNT growth methods, where gas temperature can be controlled to roughly match the CNT growth temperature (1000–2000 K).

In this study, we have developed a compact, microplasma-assisted gas-phase CNT growth method which enables the localized deposition of high quality CNTs. By utilizing a microplasma generated by ultrahigh frequency (< 40 W) in a ceramic tube (i.d.: 0.8 mm) and flowing catalyst precursor (FeCp_2) and carbon feedstock (CH_4), we demonstrated that highly crystalline CNTs possessing an average diameter of ~ 2 nm and average length of ~ 2 μm could be grown in gas-phase. The Raman G/D-ratio was measured to exceed 100. In addition, through this approach, the growth rate was estimated to be more than 1000 $\mu\text{m/s}$, which ranks among the highest for CNT growth. These results demonstrate that microplasma reactors can serve as an efficient reaction hub for each of the necessary steps for gas phase CNT growth: decomposition of catalyst precursor and carbon feedstock, nucleation of the Fe catalyst nanoparticles, and nucleation and growth of the CNTs. Furthermore, being in gas phase and channeled through a small diameter ceramic tube, the grown CNTs could be localized onto a substrate located downstream in the reactor.

[1] C. Journet *et al.*, *Nature*, **388**, 756 (1997).

[2] K. S. Kim *et al.*, *J. Phys. D. Appl. Phys.*, **40**, 2375 (2007).

[3] M. Kundrapu *et al.*, *IEEE Trans. Plasma Sci.*, **39**, 2876 (2011).

Corresponding Author: T. Tsuji

Tel: +81-29-861-0254, Fax: +81-29-861-4851

E-mail: takashi.tsuji@aist.go.jp

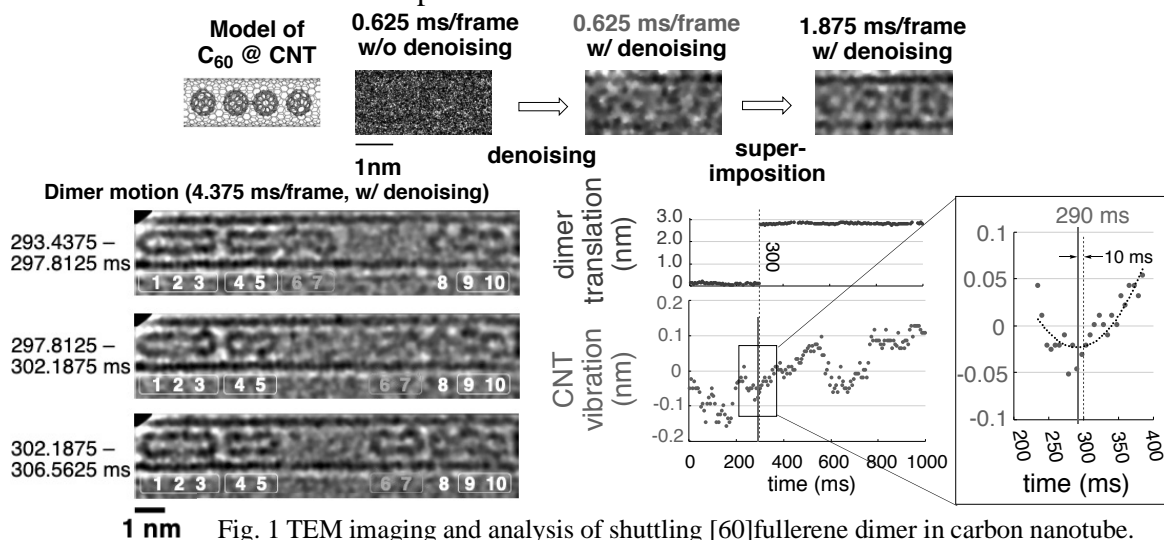
Real-time Video Imaging of a Shuttling Fullerene Molecule in a Vibrating Carbon Nanotube

○Toshiki Shimizu¹, Dominik Lungerich¹, Joshua Stuckner², Mitsuhiro Murayama², Koji Harano¹, and Eiichi Nakamura¹

¹ *Department of Chemistry, The University of Tokyo, 7-3-1 Hongo, Bunkyo-ku, Tokyo 113-0033, Japan*

² *Materials Science and Engineering Department, Virginia Tech, Blacksburg, VA 24061, USA*

Time-resolved imaging of molecular dynamics is of great importance to unveil behavior of an individual molecule in the nanoscale system and thus to apply for nanodevices. Especially, the recent advances in atomic-resolution electron microscopy is tremendous and it is one of the best approaches to observe molecules in situ, whose mechanics is non-linear, stochastic, and non-repeatable. However, conventional dynamic imaging for nanoscale mechanical events has achieved time resolution only down to tens of milliseconds. Here, we succeeded in recording of world's fastest video of a single molecular shuttle at the time resolution of sub-millisecond. [60]fullerenes (C₆₀) encapsulated in carbon nanotubes (CNT) [1] reacted each other under electron beam to form a C₆₀ dimer or oligomer, and it moved back and forth in CNT during TEM observation. In this work, we analyzed these mechanical motions more deeply with sub-millisecond sub-Å precision in situ video imaging [2]. Rich molecular dynamics of a single fullerene molecule shuttling, rotating, and interacting with a vibrating CNT were revealed by using an electron microscope, a fast camera, and a denoising algorithm [3]. As a result, we found the molecule and the CNT container as a whole behave as a mechanical coupled oscillator, where the molecular motion is coupled with the mechanical motion of CNT.



1 nm Fig. 1 TEM imaging and analysis of shuttling [60]fullerene dimer in carbon nanotube.

[1] S. Okada *et al.*, *J. Am. Chem. Soc.*, **139**, 18281 (2017).

[2] T. Shimizu *et al.*, *Bull. Chem. Soc. Jpn.* (2020). doi: 10.1246/bcsj.20200134

[3] J. Stuckner *et al.*, *Microsc. Microanal.* (2020). doi: 10.1017/S1431927620001750

Corresponding Author: K. Harano/ E. Nakamura

Tel: +81-03-5841-4369, Fax: +81-03-5841-4369

Web: <http://www.chem.s.u-tokyo.ac.jp/~common/NakamuraLab.html>

E-mail: harano@chem.s.u-tokyo.ac.jp / nakamura@chem.s.u-tokyo.ac.jp

Electronic properties of graphene with structural defects arranged periodically

○Yuta Taguchi¹, Susumu Saito¹

¹*Department of Physics, Tokyo Institute of Technology, 2-12-1 Oh-okayama, Meguro-ku, Tokyo 152-8551, Japan*

Graphene, a single metallic sheet of a hexagonal carbon network, has attracted much attention since it possesses unique properties such as high carrier mobility and high heat conductivity. However, pristine graphene cannot be used for ordinary electronic devices where a high on/off ratio is required because it does not have a band gap. To expand the possibility of application, modifications of the geometric structure of pristine graphene should be promising methods since previous theoretical studies show that periodically modified graphene sometimes has a band gap[1,2].

We study the electronic properties of graphene with structural defects in the shape of truncated triangles arranged periodically using the local density approximation (LDA) within the framework of the density-functional theory (DFT). We consider two sizes of structural defects(Hole1 and Hole2) and arrange either Hole1 or Hole2 defects in the system[Fig. 1 , Fig. 2]. There are two structural defects in one supercell and we consider one arrangement of defects: sides of regular triangles face each other. We find that all systems in this study should be semiconductors with band gap of 0.1 eV to 1.3 eV. We also find that nearly flat bands (dispersion is less than 0.05 eV) usually appear at the valence band top or the conduction band bottom in the electronic structure of the system in which Hole1s are arranged [Fig. 1]. The existence of nearly flat bands implies the possibility of ferromagnetic behavior if property doped with carriers. In the electronic structure of the system in which Hole2s are arranged, nearly flat bands hardly appear at the valence-band top nor the conduction-band bottom[Fig. 2]. In this presentation, details of the electronic structures and spatial distributions of the valence band top and conduction band bottom will be discussed.

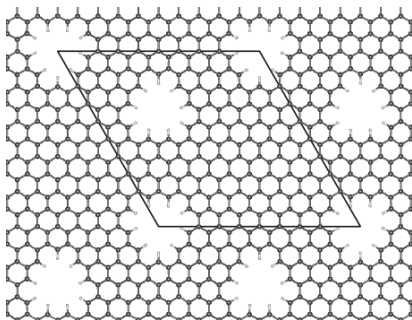


Figure 1 Super honeycomb lattice arrangement of Hole1s.

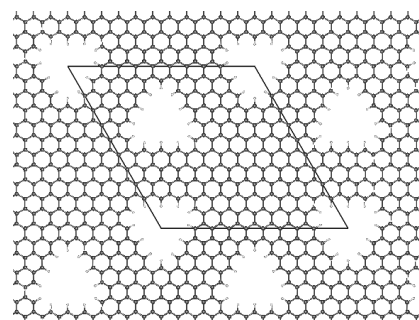


Figure 2 Super honeycomb lattice arrangement of Hole2s.

[1] T. Matsumoto and S. Saito, J. Phys. Soc. Jpn. **71**, 2765 (2002)

[2]M. Sakurai, Y. Sakai, and S. Saito, J. Phys: Conf. Ser. **302**, 012018 (2011)

Corresponding Author: Y. Taguchi

E-mail: taguchi.y@stat.phys.titech.ac.jp

Control of the photoluminescence by tuning the Fermi level in single-layer graphene

○Daiki Inukai¹, Kensuke Saito¹, Takeshi Koyama¹, Kenji Kawahara², Hiroki Ago², and Hideo Kishida¹

¹Department of Applied Physics, Nagoya University, Nagoya, Aichi 464-8603, Japan

²Global Innovation Center, Kyushu University, Kasuga, Fukuoka 816-8580, Japan

Luminescence devices based on single-layer graphene were reported [1,2]. It has been revealed that the origin of the luminescence of graphene is free electron-hole recombination [3,4]. The photoexcited electrons relax immediately after photoexcitation due to the strong coupling with the optical phonons, so that the decay time of the luminescence is in the range of several hundreds of femtoseconds. Moreover, the interaction between the graphene and the substrate affects the lifetime of the luminescence [5]. However, the Fermi level dependence of the luminescence from graphene was not revealed. Fundamental understandings of the Fermi level dependence of the luminescence are required for a wide range of applications of luminescence devices.

In this research, we investigated the Fermi level dependence of the photoluminescence (PL) from graphene. The Fermi level of the graphene was controlled with the carrier doping achieved by the electrochemical doping. The graphene was transferred onto an ITO/SiO₂ substrate. We prepared a planner type doping cell using an ionic liquid 1-ethyl-3-methylimidazolium bis(trifluoromethylsulfonyl)imid ([EMIM][TFSI]). Here, applying a voltage to ITO electrodes enables carrier injection into graphene. We conducted the time-resolved PL experiment using the mode-locked Ti-sapphire pulse laser (1.55 eV, 82 MHz, 100 fs). The time evolution of PL at 0.9 eV was observed by the frequency up-conversion method [6,7]. The dots in Figure 1 show an experimental PL decay curve of graphene with an excitation density of 3.45×10^{-2} J/m². As the PL decay curve has a tail after 200 fs, it looks like the sum of two exponential functions. In order to consider the mechanism of the PL, we fitted the experimental result using two exponential functions. Here, the time constants of the two exponential functions are $\tau_1 = 10$ fs and $\tau_2 = 170$ fs, respectively. The decay and intensity of PL were changed by the applied voltage. We will discuss the Fermi level dependence of the luminescence.

[1] Y. Miyoshi *et al.*, Nat. Commun. **9**, 1279 (2018).

[2] Y. D. Kim *et al.*, Nano Lett. **18**, 934 (2018).

[3] C. H. Lui *et al.*, Phys. Rev. Lett. **105**, 127404 (2010).

[4] T.-W. Liu *et al.*, Phys. Rev. B **82**, 081408 (2010).

[5] H. Imaeda *et al.*, J. Phys. Chem. C **122**, 19273 (2018).

[6] T. Koyama *et al.*, Phys. Chem. Chem. Phys. **14**, 1070 (2012).

[7] T. Koyama *et al.*, ACS Nano **7**, 2335 (2013).

Corresponding Authors: T. Koyama and H. Kishida

Web: <http://www.op.ap.pse.nagoya-u.ac.jp/>

E-mail: koyama@nuap.nagoya-u.ac.jp;

kishida@nagoya-u.jp

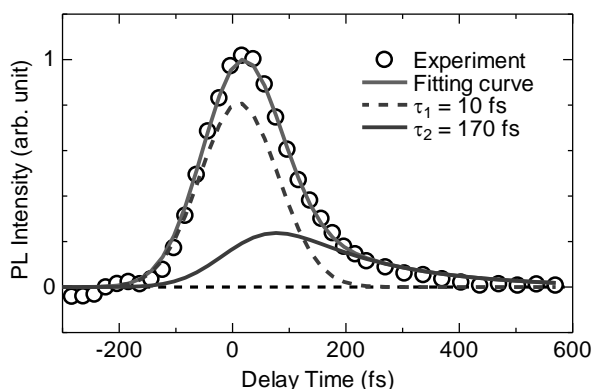


Figure 1. Experimental result of the PL from graphene and fitting result using two exponential functions.

Bottom-Up Growth of One-dimensional Transition Metal Chalcogenides and Their Characterization

○Yusuke Nakanishi¹, Naoyuki Kanda^{1,2}, Chisato Ando¹, Masa Nagata², Zheng Liu³, Takuma Shiga⁴, Kazu Suenaga⁵, Hisanori Shinohara², and Yasumitsu Miyata¹

¹ Department of Physics, Tokyo Metropolitan University, Tokyo 192-0397, Japan.

² Department of Chemistry, Nagoya University, Nagoya 464-8602, Japan.

³ National Institute of Advanced Industrial Science & Technology, Nagoya 463-8560, Japan.

⁴ Department of Mechanical Engineering, The University of Tokyo, Tokyo 113-8656, Japan.

⁵ National Institute of Advanced Industrial Science & Technology, Tsukuba 464-8602, Japan.

Since the discovery of buckminsterfullerene in 1985, nanocarbon materials have played a crucial role in modern materials science. Recently, significant efforts have been redirected towards exploring ‘post-nanocarbons’. Over the past decade, 2D layers of transition metal dichalcogenides (TMDs) have been widely recognized as ‘beyond graphene’ owing to their versatile chemistry and physics. On the other hand, their 1D counterparts such as transition metal *monochalcogenide* (TMM) nanowires could exhibit the unique electrical and optical properties, significantly distinct from 2D TMDs as well as 1D nanocarbons [1]. However, exploring the potential of TMM nanowires has been hampered by their limited availability. Although these materials have been prepared by using chemical and lithographic methods [2], the reliable production of well-defined TMM nanowires remains a significant challenge.

Here we report atomically precise fabrication of TMM nanowires by vapor-phase reactions. Chemical reactions confined within carbon nanotubes promotes the growth of single TMM nanowires to prevent oxidation, allowing their easy handling and characterization [3]. We revealed that the choice of suitable metal oxides as a precursor provides feasible yields for their characterization. Atomic-level transmission electron microscopy revealed their unusual torsional waves not seen in the bulk (Figure 1). Furthermore, we have recently achieved wafer-scale growth of bundled WTe nanowires by chemical vapor deposition, and demonstrated their highly conductive properties [4]. Our findings suggest that TMM nanowires could provide new building blocks for future flexible nanoelectronics.

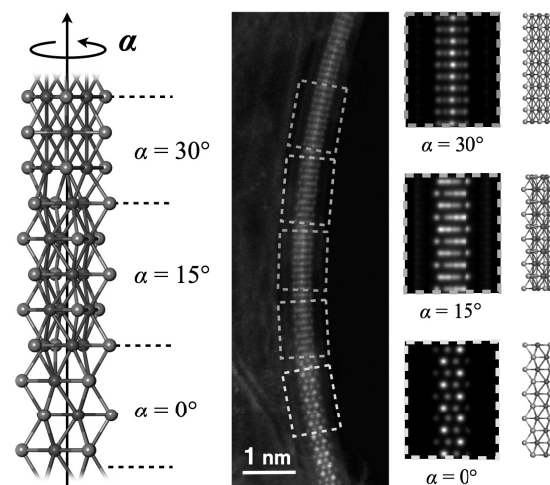


Fig. 1 Schematics of a single-wired MoTe twisting inside a carbon nanotube.

[1] I. Popov *et al. Phys. Rev. Lett.* **99**, 085503 (2007); I. Popov *et al. Nano Lett.* **8**, 4093 (2008)

[2] J. Kibsgaard *et al. Nano Lett.* **8**, 3928 (2008); J. Lin *et al. Nat. Nanotechnol.* **9**, 436 (2014)

[3] M. Nagata *et al. Nano Lett.* **19**, 4845 (2019); N. Kanda *et al. Nanoscale* in press (2020)

[4] H.-E. Lim *et al. Submitted*

Corresponding Author: Yusuke Nakanishi

Tel: +81-42-677-2498

E-mail: naka24ysk@tmu.ac.jp

Isothermal growth and stacking evolution of highly uniform AB-stacked bilayer graphene

○ Pablo Solís-Fernández^{1,*}, Yuri Terao¹, Kenji Kawahara¹, Wataru Nishiyama², Teerayut Uwanno², Yung-Chang Lin³, Keisuke Yamamoto¹, Hiroshi Nakashima¹, Kosuke Nagashio², Hiroki Hibino⁴, Kazu Suenaga³, Hiroki Ago^{1,3,*}

¹ Kyushu University, Fukuoka 816-8580, Japan

² University of Tokyo, Tokyo 113-8656, Japan

³ AIST, Tsukuba 305-8565, Japan

⁴ Kwansai Gakuin University, Hyogo 669-1337, Japan

There is an intimate correlation between the stacking order and the electronic properties of bilayer graphene (BLG). This allows realizing unique physical properties by precisely controlling the stacking order. AB-stacked BLG (AB-BLG) in particular possess a great technological importance for electronic and optoelectronic applications, owing to its ability to provide a tunable band gap [1]. Current methods to produce AB-BLG generally suffer from inhomogeneous layer thickness and/or coexistence with twist BLG areas [2]. Here, we demonstrate a method based on the chemical vapor deposition (CVD) on Cu-Ni thin films to synthesize large-area AB-BLG virtually devoid of twisted areas [3]. Our findings proved that the reaction time can be used to control the stacking order, with the amount of AB-stacked BLG gradually increasing with the CVD time (Fig. 1a). This evolution is explained by a catalyst-assisted continuous BLG reconstruction driven by carbon dissolution-segregation processes. Large areas of AB-BLG can thus be obtained, with the only limitation of the size of the CVD furnace employed (inset of Fig. 1a). The stacking order was followed by different techniques, including Raman spectroscopy (Fig. 1b), scanning tunneling microscopy (STM) (Fig. 1c), scanning transmission electron microscopy (STEM) and low-energy electron diffraction (LEED). The opening of a band gap was successfully observed by electrical measurements on dual-gate field-effect transistors (FETs) (Fig. 1d). The concept of the continuous reconstruction offers a new strategy to both obtain highly pure AB-BLG and to control the stacking order of catalytically grown 2D materials.

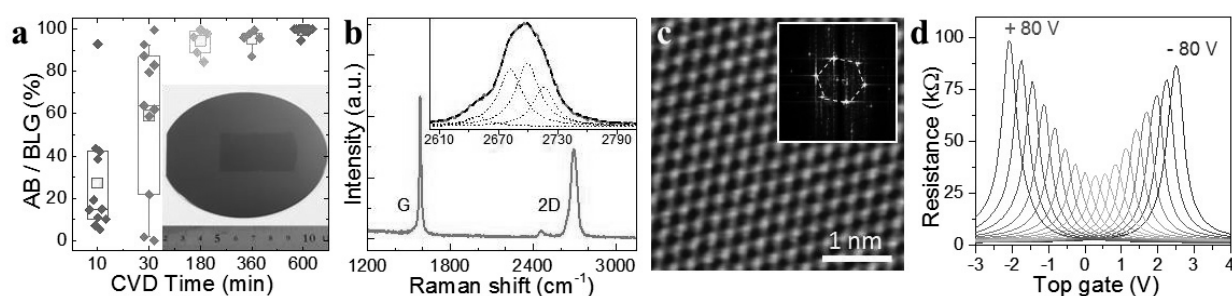


Figure 1. (a) Evolution of the AB stacking ratio with CVD time. Inset shows a large area BLG on a SiO₂ substrate. (b) Raman spectrum of the AB-BLG. Inset shows an enlargement of the 2D band, fitted by 4 Lorentzian peaks. (c) STM image of the AB-BLG. Inset shows the FFT of the STM image. (d) Resistance of an AB-BLG FET as a function of the top gate voltage, for different applied back-gate voltages. The numbers indicate the value of the back-gate voltage for the corresponding curve.

[1] T. Ohta *et al.*, *Science*, **313**, 951 (2009).

[2] Y. Takesaki *et al.*, *Chem. Mater.*, **28**, 4583 (2016).

[3] P. Solís-Fernández *et al.*, *ACS Nano*, **14**, 6834 (2020).

Corresponding Author: P. Solís-Fernández

Tel: +81-92-583-8975, Fax: +81-92-583-8975, E-mail: ps-fernandez@gic.kyushu-u.ac.jp

Concise, Single-Step Synthesis of Sulfur-Enriched Graphene: Immobilization of Molecular Clusters and Battery Applications

○Haruka Omachi^{1,2}, Tsukasa Inoue², Shunya Hatao³, Criado Alejandro⁴, Hisanori Shinohara², Hirofumi Yoshikawa³, Zois Syrgiannis⁴, Maurizio Prato^{4,5,6}

¹ *Research Center for Materials Science, Nagoya University, Nagoya 464-8602, Japan*

² *Department of Chemistry, Nagoya University, Nagoya, 464-8602, Japan.*

³ *Department of Nanotechnology for Sustainable Energy, School of Science and Technology, Kwansei Gakuin University, Sanda, 669-1337, Japan*

⁴ *Carbon Bionanotechnology Group, CICbiomaGUNE, Gipuzkoa, Spain*

⁵ *Center of Excellence for Nanostructured Materials (CENMAT), INSTM, Dipartimento di Scienze Chimiche e Farmaceutiche, Università di Trieste, Trieste, Italy*

⁶ *Basque Foundation for Science, Ikerbasque, Spain*

The concise synthesis of sulfur-enriched graphene for battery applications is reported (Fig 1a)[1]. The direct treatment of graphene oxide (GO) with the commercially available Lawesson's reagent produced sulfur-enriched-reduced GO (S-rGO). Various techniques, such as X-ray photoelectron spectroscopy (XPS), confirmed the occurrence of both sulfur functionalization and GO reduction. Also fabricated was a nanohybrid material by using S-rGO with polyoxometalate (POM) as a cathode-active material for a rechargeable battery. Transmission electron microscopy (TEM) revealed that POM clusters were individually immobilized on the S-rGO surface. This battery, based on a POM/S-rGO complex, exhibited greater cycling stability for the charge-discharge process than a battery with nanohybrid materials positioned between the POM and nonenriched rGO (Fig 1b). These results demonstrate that the use of sulfur-containing groups on a graphene surface can be extended to applications such as the catalysis of electro-chemical reactions and electrodes in other battery systems.

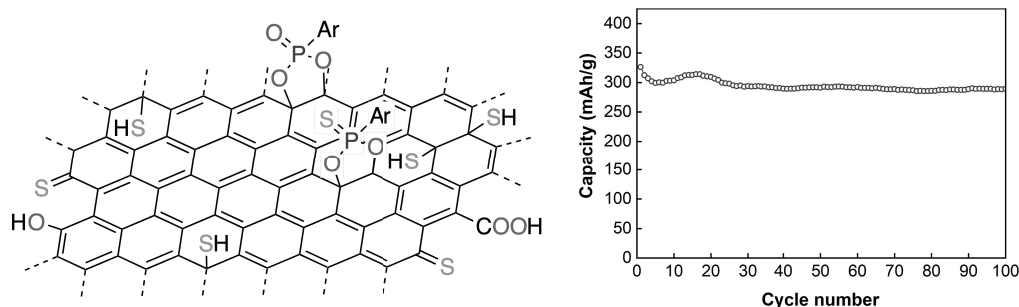


Fig 1. (a) Chemical structure of sulfur-enriched-reduced GO S-rGO. (b) Cycle performance of the discharge capacity for MCBs comprised of POM/S-rGO

[1] H. Omachi, T. Inoue, S. Hatao, H. Shinohara, A. Criado, H. Yoshikawa, Z. Syrgiannis, M. Prato, *Angew. Chem. Int. Ed.* **2020**, *59*, 7836–7841.

Corresponding Author: H. Omachi

Tel: +81-52-789-3660

Web: <https://sites.google.com/view/haruka-omachi/>

E-mail: omachi@chem.nagoya-u.ac.jp

Wafer-scale synthesis of 1D transition metal chalcogenide nanowires

○ Hong En Lim¹, Yusuke Nakanishi¹, Zheng Liu², Jiang Pu³, Takahiko Endo¹, Chisato Ando¹, Hiroshi Shimizu¹, Kazuhiro Yanagi¹, Taishi Takenobu³, Yasumitsu Miyata¹

¹ Department of Physics, Tokyo Metropolitan University, Tokyo, 192-0397, Japan

² Innovative Functional Materials Research Institute, National Institute of Advanced Industrial Science and Technology (AIST), Nagoya, 463-8560, Japan

³ Department of Applied Physics, Nagoya University, Nagoya, 464-8603, Japan.

Realizing large-scale fabrication is crucial to escalate progress in fundamental studies and applications of functional nanomaterials. Transition metal chalcogenide (TMC) nanowires [1-3], MX with 1D metallic nature [4-6], are considered useful for future nanoelectronics applications. However, their mass synthesis has never been achieved. Herein, we report a wafer-scale growth of highly-crystalline TMC nanowires, WTe and MoTe specifically, with controlled orientation and geometrical structures by chemical vapor deposition (CVD). Depending on crystallographic structure of the supporting surfaces, aligned, atomically thin 2D sheets or disordered 3D bundles network, both consisted of individual TMC nanowires, were selectively formed. They show excellent conducting properties with anisotropic 1D optical response. Besides, these 1D nanowires could be readily converted into 2D transition metal dichalcogenides, MX_2 of either $2H$ or T_d configurations. We offer not only the controlled and large-scale growth of conductive 1D nanowire thin films but also the fabrication of narrow 2D compounds. This provides an access to study on material science, physics and applications of nanowire-based van der Waals 2D and 3D crystals.

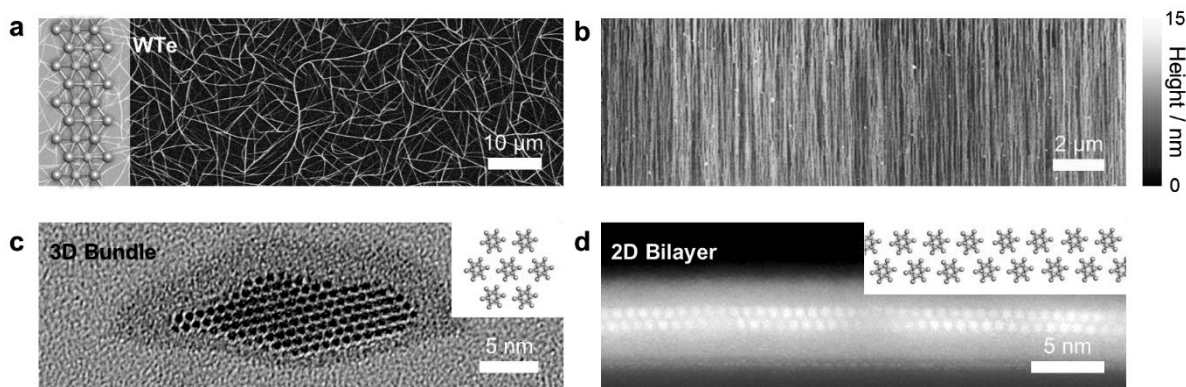


Fig. 1 **a**, Scanning electron microscope (SEM) image of a random WTe network grown on SiO_2/Si substrate. **b**, Atomic force microscope (AFM) topographic image of an aligned WTe network grown on a -sapphire substrate. **c**, Cross-section transmission electron microscope (TEM) and **d**, high-angle annular dark field (HAADF) scanning TEM images for the WTe nanowires fabricated on SiO_2/Si and a -sapphire substrates with either 3D or 2D configuration, respectively. Insets showing the corresponding 3D and 2D WTe assemblies.

[1] J. M. Tarascon, J. Electrochem. Soc. **132**, 2089 (1985) [2] J. Lin *et al.*, Nat. Nanotechnol. **9**, 436-442 (2014) [3] M. Nagata *et al.*, Nano Lett. **19**, 4845-4851 (2019) [4] L. Venkataraman & C. M. Lieber, Phys. Rev. Lett. **83**, 5334-5337 (1999) [5] L. Venkataraman, Y. S. Hong & P. Kim, Phys. Rev. Lett. **96**, 076601 (2006) [6] Y. Xia *et al.*, Nano Lett., **20**, 2094-2099 (2020) [7] H. E. Lim *et al.*, Submitted (2020).

Corresponding Authors: H. E. Lim, Y. Miyata

Tel: +81-42-677-2508,

Web: <http://www.comp.tmu.ac.jp/nanotube/index.html> E-mail: lim@tmu.ac.jp; ymiyata@tmu.ac.jp

Infrared spectroscopy of C₆₀ molecules: From the laboratory detection to cosmic abundances

○Tomonari Wakabayashi

Department of Chemistry, Kindai University, Higashi-Osaka 577-8502, Japan

The mass spectroscopic detection of C₆₀: buckminsterfullerene in 1985 [1] triggered the series of theoretical predictions on molecular vibrations [2], leading to the identification of the infrared (IR) absorption features as evidence for the presence of macroscopic quantities of C₆₀ molecules in 1990 [3]. The bands of the same four IR-active T_{1u} modes of C₆₀ in I_h symmetry have been observed also in the IR emission spectra in the laboratory [4] and in space [5]. The detection of C₆₀ and related species such as C₇₀ in young planetary nebulae in 2010 [5] facilitated the basic research on cosmic abundances of the molecule [6]. A fundamental figure necessary for the estimation of the molecular abundance is the band strength which is identical with the integrated absorption intensity per unit concentration and unit length. We have been tackling this issue along the interpretation of the split IR absorption bands of the four T_{1u} modes ($\nu = 1$) of matrix-isolated C₆₀ molecules in cryogenic solid pH₂, oD₂, and Ne, where more than 300 distinct isotopomers of ¹³C_n¹²C_{60-n} ($n = 0-3$) are involved [7]. It is confirmed by rigorous calculations that the band strength averaged over statistically random isotopomeric distributions for 0.5-3.5% ¹³C abundances is more or less the same as that of the single I_h-C₆₀ species, *i.e.*, 84.7 km/mol for T_{1u}(1) at 530 cm⁻¹, 33.8 km/mol for T_{1u}(2) at 578 cm⁻¹, 27.1 km/mol for T_{1u}(3) at 1185 cm⁻¹, and 35.4 km/mol for T_{1u}(4) at 1432 cm⁻¹ for the absorption. For the emission in planetary nebulae, vibrational temperature, statistical weights in the vibrationally excited states, and thermal populations are relevant in which the triply degenerate T_{1u} modes are somewhat tricky. A brief description for the golden anniversary of the prediction of aromatic stability of C₆₀ will also be presented [8].

- [1] H. W. Kroto, J. R. Heath, S. C. O'Brien, R. F. Curl, and R. E. Smalley, *Nature* **318**, 162 (1985).
 [2] (a) M. D. Stanton and R. E. Newton, *J. Phys. Chem.* **92**, 2141 (1988); (b) D. E. Weeks and W. G. Harter, *Chem. Phys. Lett.* **144**, 366 (1988); (c) Z. Slanina, J. M. Rudziński, M. Togashi, and E. Osawa, *J. Mol. Struct. Theochem* **202**, 169 (1989).
 [3] (a) W. Krätschmer, K. Fostiropoulos, and D. R. Huffman, *Chem. Phys. Lett.* **170**, 167 (1990); (b) W. Krätschmer, L. D. Lamb, K. Fostiropoulos, and D. R. Huffman, *Nature* **347**, 354 (1990).
 [4] C. I. Frum, R. Engelman Jr., H. G. Hedderich, P. F. Bernath, L. D. Lamb, and D. R. Huffman, *Chem. Phys. Lett.* **176**, 504 (1991).
 [5] J. Cami, J. Bernard-Salas, E. Peebles, and S. E. Malek, *Science* **329**, 1180 (2010).
 [6] S. Iglesias-Groth, F. Cataldo, and A. Manchado, *Mon. Not. R. Astron. Soc.* **413**, 213 (2011).
 [7] (a) N. Sogoshi, Y. Kato, T. Wakabayashi, T. Momose, S. Tam, M. E. DeRose, and M. E. Fajardo, *J. Phys. Chem. A* **104**, 3733 (1996); (b) T. Wakabayashi, T. Momose, and M. E. Fajardo, *J. Chem. Phys.* **151**, 234301 (2019).
 [8] (a) E. Osawa, *Kagaku* (Kyoto) **25**, 854 (1970); (b) The 58th FNTG General Symposium, Commemorative Session 2C-1–2C-6, Abstract Book p.p. 11–16 (2020).

Corresponding Author: T. Wakabayashi

Tel: +81-6-4307-3408, Fax: +81-6-6723-2721,

Web: <https://www.chem.kindai.ac.jp/laboratory/wakabayashi/>

E-mail: wakaba@chem.kindai.ac.jp

Primary Particles of Detonation Nanodiamond Finally Identified

○Eiji Ōsawa^{1*}, Amanda S. Barnard², and Toshihiko Tanaka³

¹*NanoCarbon Res. Inst., Asama Res. Ext. Center, Shinshu Univ., Ueda 386-8567, Japan.*

²*Res. School of Comput. Sci., Aust. Nat. Univ., Canberra, Australia.*

³*Depart. Chem. and Biochem., Nat Inst. Technol., Fukushima Coll., Iwaki, 970-8034, Japan*

Following our preliminary announcements[1] we report herewith full results from our long work to isolate and characterize the primary particles of detonation nanodiamonds (PPDND). If we count from the discovery of DND by Danilenko in 1963[2], it took well over half a century to solve this difficult problem.

Attractive interfacial Coulombic interactions (ICI) between the closest pair of facets in the neighboring particles are the major causes of tight agglutination among PPDNDs in the crude DND[3]. According to SCC-DFTB calculations, the strongest of such bonds could be as tight as covalent C-C bonds[4]. Thus, we can imagine how highly destructive shock could our stirred-media milling produce.

Taguchi's quality engineering method was used to simultaneously optimize the operation conditions of the mill, but to our surprise, the only parameter that should carefully adjusted turned out to be the initial concentration of agglutinates, and the optimized concentration proved unexpectedly low 4.0 w/v%! Hydration of solvent water on the charged nano-surface of PPDND was found responsible for the unusual behaviors of PPDND. The novel feature of nano-hydration was later studied in detail by Petit[5] and Kaneko[6].

Surface and internal structures of PPDND have been studied by both experiments, especially with the aid of LDI-TOF-MS[7], and SCC-DFTB calculations[3,4]. Briefly, the surface shell consists of graphene patches on top and a thin amorphous diamond layer is formed immediately below. Detailed features in the shell will be given in the lecture. Inner core is a pure diamond. A few indirect pieces of evidence will be presented to conclude that the core diamond consists of exactly 1000 carbon atoms in the shape of a hexahedron with circumscribing sphere diameter of 2.2nm.

Size of PPDND is, as we have reported before[1], 2.6 ± 0.5 nm by DLS method in water. There is still no absolute proof to ensure this value corresponding to the true PPDND, but for a couple of indirect evidence. First it perfectly matches with those of meteoritic, especially Allende, nanodiamonds discovered by R. S. Lewis in 1987[8]. Second, we have never observed detonation nanodiamonds smaller than this value with statistical significance.

Finally, the almost perfect agreements between average experimental structural features and the corresponding numbers from quantum-chemical calculation cannot be overemphasized.

[1] S. Sasaki, Abstract No. 17, p-PM3-8, in *JSAP-MRS Meeting*, Doshisha University, Sept. 16-20, 2013.

[2] V. V. Danilenko, 'Nanocarbon phase diagram and conditions for detonation nanodiamond formation.' In "Synthesis and Applications of Ultrananocrystalline Diamond", D. M. Gruen, *et al.* (Eds.), Springer, p. 181, 2005.

[3] A. S. Barnard, M. Sternberg, *J. Mater. Chem.* **17**, 4811 (2007).

[4] A. S. Barnard, *J. Mater. Chem.* **18**, 4038 (2008).

[5] T. Petit *et al.*, *J. Phys. Chem. Lett.* **6**, 2909 (2015).

[6] E. Z. Pina-Salazar, T. Sakai, E. Osawa, R. Futamura, K. Kaneko, *J. Colloid. & Interface Sci.*, **549**, 133 (2019).

[7] M. Fukaya, *et al.*, FNTG 50th General Symposium, Feb.19-22, 2016, Univ. Tokyo.

[8] R. S. Lewis, E. Anders, B. T. Draine, *Nature*, **339**, 117 (1989).

*Corresponding Author: E. Osawa, Tel: +81-268-75-8381, <http://nano-carbon.jp/>, E-mail: osawa@nano-carbon.jp.

Stereoselective synthesis and HIV/HCV enzyme inhibition activity of proline-type fullerene derivatives

○Daiki Katagishi¹, Tomoyuki Ohe¹, Kyoko Takahashi¹, Shigeo Nakamura²,
Tadahiko Mashino¹

¹ Department of Pharmaceutical Sciences, Faculty of Pharmacy, Keio University, 1-5-30
Shibakoen, Minato-ku, Tokyo 105-8512, Japan

² Department of Chemistry, Nippon Medical School, 1-7-1 Sakaminami-cho, Musashino,
Tokyo 180-0023, Japan

A lot of diseases are caused by viral infection of humans. Although many drugs are currently used as antiviral therapy, many problems still remain. For this reason, it has been an urgent challenge to develop a novel type of antiviral drugs. In this context, fullerenes may become novel drugs due to its unique structures. However, its poor water solubility is a barrier in the aim of pharmaceutical usage. To overcome this, many water-soluble derivatives have been synthesized and their biological activities have been studied.

We have previously reported water-soluble proline-type C₆₀ derivatives show inhibition activities against HIV protease (HIV-PR), HIV reverse transcriptase (HIV-RT), HCV NS3/4A protease (HCV-NS3/4A), and HCV NS5B polymerase (HCV-NS5B). Some of them have stereoisomers, but we have not evaluated the activities of their respective enantiomers due to the difficulties in obtaining them. In this study, we stereoselectively synthesized two enantiomers of the proline-type C₆₀ derivatives *cis*-1~3 (Scheme 1) and evaluated their inhibition activities against the above-mentioned four enzymes.

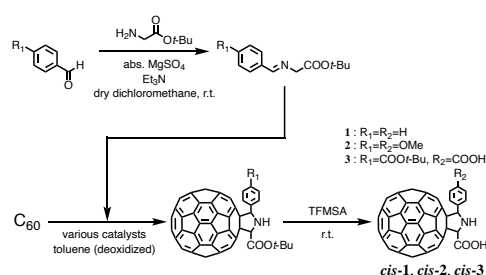
First, we synthesized α -imino esters as precursors from glycine *tert*-butyl ester and corresponding benzaldehyde derivatives. Then, *tert*-butyl esters of *cis*-1~3 were synthesized via the 1,3-dipolar cycloaddition in the presence of asymmetric catalysts [1]. Finally, by deprotection of *tert*-butyl group, each enantiomer of carboxylic acids *cis*-1~3 was obtained. The obtained compounds were identified by ESI-MS and ¹H NMR. The absolute configuration was determined by circular dichroism (CD) in accordance with the sector rule [2]. Furthermore, the enantiomeric excess was calculated by HPLC with chiral column. HIV-PR and HCV-NS3/4A inhibition activities were evaluated by the quantitative analyses of peptide fragments cleaved by the enzymes with LC-MS. HIV-RT and HCV-NS5B inhibition activities were evaluated by measuring radioactivities of nucleotides incorporated by the enzymes. *cis*-1 against HIV-PR and *cis*-2 and *cis*-3 against HCV-NS5B showed different inhibition activities between two enantiomers.

This is the first report to show enantiomers of C₆₀ derivatives have different biological activities. It is suggested that structural design considering absolute configuration is important for the development of fullerenes as medicines.

[1] J. Marco-Martínez *et al.*, *Angew. Chem. Int. Ed.*, **56**, 2136 (2017).

[2] J. Marco-Martínez *et al.*, *Angew. Chem. Int. Ed.*, **52**, 5115 (2013).

Corresponding Author: Tomoyuki Ohe; Tadahiko Mashino
Tel: +81 35 400 2691; +81 35 400 2694, Fax: +81 35 400 2691,
E-mail: ohe-tm@pha.keio.ac.jp; mashino-td@pha.keio.ac.jp



Scheme 1 Stereoselective synthesis of *cis*-1~3

The Effect of Heteroatom Doped Reduced Graphene Oxide in Enhancement of Thermoelectric Performance

○Mariamu Kassim Ali¹, Mohsen Khozami¹, Mohsen Ghali², Nageh Shaalan³, Koichi Nakamura⁴, Ahmed Abd El-Moneim^{1,2}

¹Department of Materials Science and Engineering, Egypt-Japan University of Science and Technology, New Borg El Arab City, Alexandria 21934, Egypt

²School of Basic and Applied Science, Egypt-Japan University of Science and Technology, New Borg El Arab City, Alexandria 21934, Egypt

³Department of Physics, College of Science, King Faisal University, Al-Hasa 31982, P.O. Box 400, Saudi Arabia

⁴Department of Mechanical and Electrical System Engineering, Kyoto University of Advanced Science, Kyoto 615-8577, Japan

Carbon-based materials and in particular, graphene have sparked a special interest due to their outstanding electronic and mechanical properties [1]. The zero-band gap nature of graphene however limits its usage in many applications and so numerous chemical functionalization processes such as doping with heteroatoms such as like nitrogen, sulfur, boron and more recently co-doping have been adopted to open the band gap and tailor its electronic properties [2]. Other low performing such as polymers have utilized graphene in order to enhance their T.E characteristics. In this study, heteroatom-doped reduced graphene oxide was used to improve the T.E properties of polyaniline.

The heteroatom doped rGO was fabricated via hydrothermal process after which the nanocomposites were prepared via chemical oxidative polymerization. Structural characterization carried out confirmed the successful doping of the rGO and its incorporation into the polyaniline. Additionally, TEM results proved the successful enwrapping of the basal rGO sheets with polyaniline due to the strong π - π stacking.

Thermoelectric analysis further revealed a negative Seebeck coefficient which indicates n-type transport characteristics. The graphene-based nanocomposites were shown to have an enhanced thermoelectric behavior compared to pristine material which is proof that rGO can be used for enhancing T.E performance.

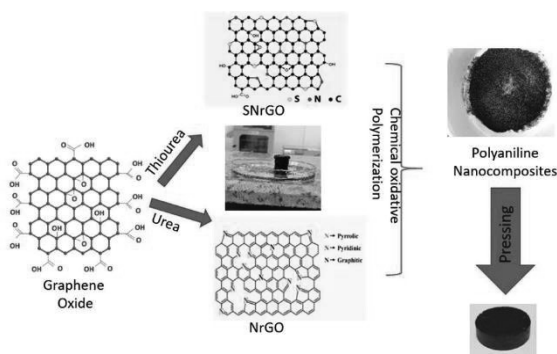


Fig. 1 Schematic of the heteroatom doping of graphene oxide and preparation of nanocomposites

[1] Novoselov, K.S., et al., A roadmap for graphene. Nature, 2012. **490** (7419): p.192-200.

[2] Liu, H., Y. Liu, and D. Zhu, Chemical doping of graphene. Journal of materials chemistry, 2011. **21** (10): p. 3335-3345

Corresponding Author: M. Kassim Ali

Tel: +20 102 409 3749

E-mail: mariam.kassim@ejust.edu.eg

Molecular Modification of Graphene on Metal Substrate: Electrochemical Defect Insertion and Evaluation of Surface Defects

○Tomohiro Fukushima, Takaha Komai, Kei Murakoshi

*Department of Chemistry, Faculty of Science, Hokkaido University,
Sapporo 060-0810, Japan*

The structure of graphene is crucial for the determining their properties. In order to control the structural- and electronic-properties of graphene, the modification of chemical structure is required. Conventionally, diazonium grafting method is utilized for the functionalization of graphene due to the reduction potential of diazonium salts. However, due to relatively negative electrochemical potential of reactant to the Fermi level, spontaneous exothermic reaction between graphene and diazonium salt occurred. The control of the surface grafted amounts are still difficult. Here, we utilize the electrochemical methods for the modification of the surface by using anodic oxidation of phenyl hydrazine derivatives.

Graphene on the metal surfaces were prepared by the chemical vapor deposition methods, and the crystallinity of graphene was characterized by confirmation of G band and 2D band from the Raman spectroscopy (excitation wavelength 514 nm, laser intensity 0.5 mW). All the electrochemical experiments were conducted by using HSV-110 potentiostat. Ag/AgCl and Pt electrodes were used as reference and counter electrodes, respectively. Cu underpotential deposition was conducted by using 1 mM CuSO₄ and 0.05 M H₂SO₄ solution with the sweep rate of 50 mV/s. Due to the possibility for the oxidation of graphene, potential range was set lower than one of the open circuit potential (0.5 V). Molecular modification of graphene/Au(111) surface was by cyclic voltammogram by using 0.1 M NaClO₄ and 2 mM phenylhydrazine derivatives.

Electrochemical measurements were conducted in 0.1 M NaClO₄ in the presence of 2 mM phenylhydrazine as shown in Figure 1. In the absence of phenylhydrazine, anodic current was not observed. On the other hand, in the presence of phenylhydrazine, anodic current was observed from -0.2 V vs. Ag/AgCl. The anodic feature was different from second cycle suggesting that deposition of phenyl groups on G/Au electrode (Ph-G/Au). Figure 2 shows the Raman spectra of G/Au and Ph-G/Au. G band (1580 cm⁻¹) and 2D band (2700 cm⁻¹) were observed for the as-prepared G/Au electrode. On the other hand, D band (1350 cm⁻¹) was additionally observed for Ph-G/Au. Raman spectroscopy revealed that successful modification of graphene surface by phenylhydrazine. Additionally, underpotential deposition showed that the surface of electrode is still covered with graphene after electrochemical treatments. These results propose the new preparation method for molecularly-modified graphene even on metal surface.

[1] T. Fukushima, K. Murakoshi, *Current Opinion in Electrochemistry*, **17**, 158 (2019).

Corresponding Author: T. Fukushima

Tel: +81-11-706-4811, Fax: +81-11-706-4811,

Web: <https://wwwchem.sci.hokudai.ac.jp/~pc/>, E-mail: tfuku@sci.hokudai.ac.jp

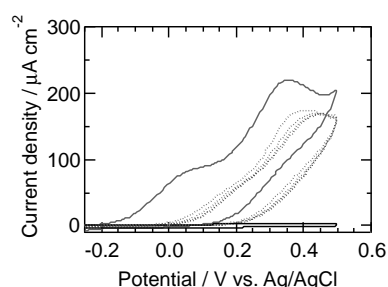


Figure 1. Cyclic voltammogram of G/Au in the absence (black) and presence of phenylhydrazine (red) in 0.1 M NaClO₄. Sweep rate: 50 mV/s.

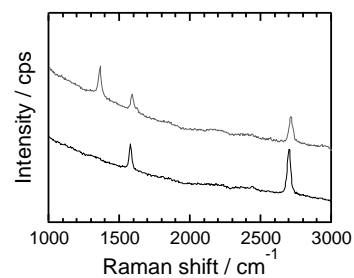


Figure 2. Raman spectra of G/Au (black, bottom) and Ph-G/Au (red, top) (514 nm, 0.5 mW).

Molecular Modification of Graphene on Metal Substrate: Electrochemical Defect Insertion for Controlled Proton Permeation

○Takaha Komai, Tomohiro Fukushima, Kei Murakoshi

*Department of Chemistry, Faculty of Science, Hokkaido University,
Sapporo 060-0810, Japan*

The electronic and chemical properties of graphene can be modulated through the interfacial interaction.[1] Recently, Geim *et al.*, reported that graphene can be uniquely used as proton permeable membrane.[2] The structural control of the proton permeability can be useful for the applications such as the separator for electrochemical systems. However, it is still difficult to control the structure of graphene. Here, we show that molecular modification of graphene surface can modulate the proton permeability from in-situ Raman spectroscopy under electrochemical potential control.

Graphene on Au surfaces (denoted as G/Au) were prepared by the chemical vapor deposition methods, and the crystallinity of graphene was characterized by confirmation of G band and 2D band from the Raman spectroscopy (excitation wavelength 514 nm, laser intensity 0.5 mW). All the electrochemical experiments were conducted by using HSV-110 potentiostat. Ag/AgCl and Pt electrodes were used as reference and counter electrodes, respectively. Molecular modification of graphene/Au(111) surface was by electrochemical anodization by using 2 mM phenylhydrazine derivatives in 0.1 M NaClO₄. The modified electrode was denoted as Ph-G/Au. In-situ electrochemical Raman spectroscopy was conducted by using 0.1 M KOH.

Figure 1 and 2 show the electrochemical potential-dependent G band and 2D band position of G/Au and Ph-G/Au electrode. Due to the modification of electronic structure and intercalants between G/Au alters the position of G band and 2D bands. G band and 2D band remains similar position upto -1 V. G band position, which suggests the electronic structure of graphene, suddenly shifts at -1.2 V. 2D band suddenly dropped at -1.2 V and -1.9 V and reversibly. Due to the electrochemical reaction, hydrogen evolution was observed in cyclic voltammograms. The observed 2D band shift is due to the intercalation of H₂ molecules between graphene and Au possibly due to the proton tunneling. Importantly, the permeation was controlled by the electrochemical potential for anodization. This study demonstrates successful modification of the graphene properties for controlled proton permeation.

[1] (a) T. Fukushima, K. Murakoshi, *Current Opinion in Electrochemistry*, **17**, 158 (2019). (b) J. Kim, T. Fukushima, K. Murakoshi *et al.*, *Materials*, **12**, 211(1-8) (2019).

[2] M. Lozada-Hidalgo, H. A. Wu, A. K. Geim *et al.*, *Nature* **516**, 227(2014).

Corresponding Author: T. Komai

Tel: +81-11-706-4811, Fax: +81-11-706-4811,

E-mail: t_komai_731@frontier.hokudai.ac.jp

Web: <https://wwwchem.sci.hokudai.ac.jp/~pc/>

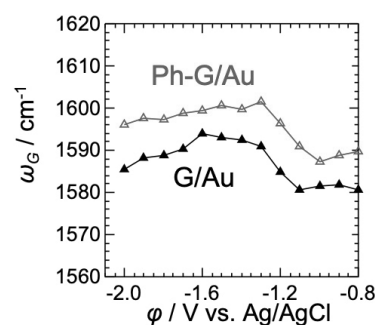


Fig.1 Dependence of G band peak position on electrochemical potential.

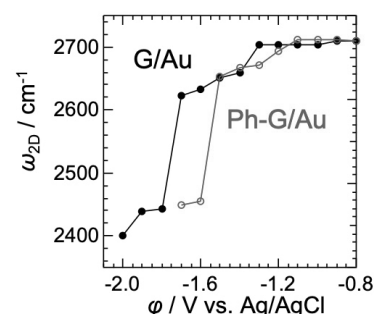


Fig.2 Dependence of 2D band peak position on electrochemical potential.

2D tin layers on SiC(0001)

○Anton Visikovskiy¹, Hiroshi Ando¹, Shingo Hayashi¹, Fumio Komori², Koichiro Yaji²,
Satoru Tanaka¹

¹Dept. of Applied Quantum Physics, Kyushu University, Fukuoka 819-0395, Japan

²Institute for Solid State Physics, University of Tokyo, Kashiwa 277-0882, Japan

Graphene is a fascinating 2D material. However, due to small spin-orbit interaction (SOI) in carbon atoms, band spin polarization is usually very small in normal graphene layer, which limits its use for spintronics devices. Sn is a heavy group IV element with substantial SOI, and it would be interesting to see if 2D materials made of Sn are possible to be realized and what properties they would exhibit. In our work we address the issue of stability and electronic properties of 2D Sn layers on SiC(0001) by *ab initio* calculations and experimental measurements.

Our DFT calculations show that layer with honeycomb structure similar to graphene (it is called stanene in case of Sn atoms) is stable when grown on top of Si₂N₃/SiC(0001), while on bare SiC(0001) the more dense (1x1), unusual for group IV element, triangular structure has better energy stability. While growth of 2D triangular structure on bare SiC can be hindered by thermal growth dynamics and result in clustering, one of the solution would be to intercalate Sn atoms into graphene/SiC(0001) interface, which suppresses 3D growth and promote layered. This approach was realized experimentally with a very good agreement between experimental results and computational data [1,2]. Both triangular and honeycomb structures are found to have very interesting band dispersion with spin-polarized states in form of Rashba and Zeeman splitting.

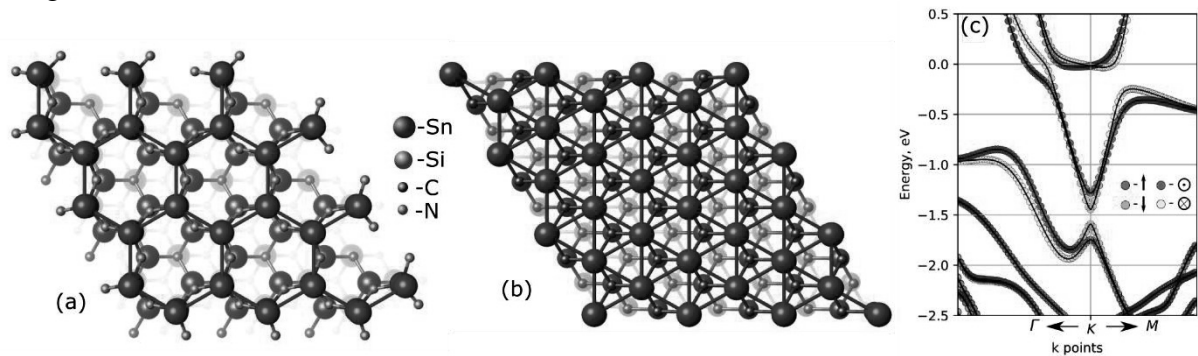


Fig. 1 (a) Honeycomb Sn layer (stanene) on Si₂N₃/SiC(0001). (b) Triangular Sn layer on SiC(0001). (c) The electronic structure around K point of structure (b) with color coding of spin directions, both Zeeman and Rashba type spin splitting occur.

[1] S. Hayashi et al. Appl. Phys. Express, **11**, 015202 (2018).

[2] K. Yaji et al. Phys. Rev. Lett., **122**, 126403 (2019).

Corresponding Author: A. Visikovskiy

Tel: +81-92-802-3536

Web: <http://www.qpn.kyushu-u.ac.jp/Tanaka/Welcome.php>

E-mail: anton_v@nucl.kyushu-u.ac.jp

Strain effect on circularly-polarized electroluminescence in transition metal dichalcogenides

Sake Wang, M. Shoufie Ukhtary, Riichiro Saito

Department of Physics, Tohoku University, Sendai 980-8578, Japan

Transition metal dichalcogenide (TMD) has attracted much attention as a two-dimensional (2D) direct-gap semiconductor [1]. Since the TMD possesses broken inversion symmetry [1], a left- (or right-) handed circularly-polarized light (LCP or RCP) is emitted in the K (or K') valley in the hexagonal Brillouin zone, which is known as the valley polarization [2]. If photoemission from the K and K' valleys is not equal to each other, we observe a circularly-polarized light which is important in optoelectronics.

Zhang *et al.* [3] have fabricated a light-emitting diode (LED) in a p-i-n junction of tungsten diselenide. The LED emits circularly-polarized electroluminescence (EL) by applying in-plane electric field between the source and drain electrodes. Since the EL photon is emitted in the overlapping region of the occupied \mathbf{k} states by an electron (e) in the conduction band and a hole (h) in the valence band as shown in Fig.1(a1), the circularly-polarized EL occurs when the two overlapping regions in the K and K' valleys are not equivalent to each other. This situation occurs when we apply the electric field, \mathbf{E} , in the direction of k_x [Fig.1(a2)] in which the overlapping regions change the area since the (e) or (h) states shift to left or right both for the K and K' valleys. In order to get the inequivalent area of the two overlapping regions, we need so-called trigonal warping (TW) effect [4] in the valence band which we exaggeratedly show as a triangle in Fig.1.

However, since the TW effect is not effective especially for a small circle near the K (K') point, we cannot get the large difference of the overlapping area. Here we consider the strain effect on the energy dispersion in which the (e) and (h) circles are originally mutually shifted in the case of $E=0$ as shown in Fig.1(b1) which has the time-reversal symmetry [5, 6]. When we apply the electric field, the overlapping regions become more inequivalent than the case of the TW effect as shown in Fig.1(b2), since the direction of the original shift is selected to the direction of the electric field. We show even 100% circular polarization without losing the EL intensity, which is much larger than the circular polarization caused by the TW effect. We hope that the theoretical prediction will be observed by the experiment.

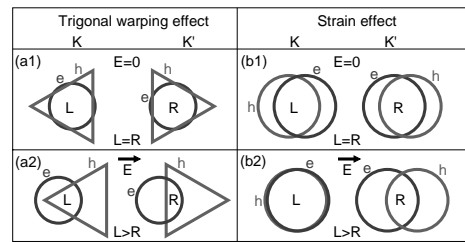


Fig.1 Occurrence of circularly-polarized EL: (a1) the overlapping region of hole (h) and electron (e) occupied regions emits LCP (L) or RCP (R) in the K or K' valley, respectively. Here the triangle shape for (h) represents the trigonal warping effect. When the electric field is zero $E=0$, the two regions have the same area, $L=R$. (a2) For $E \neq 0$, (h) [or (e)] shifts to right (left) from which we get $L>R$. (b1) When we apply the strain, (h) and (e) are originally shifted in the K and K' valleys, which gives $L=R$. (b2) For $E \neq 0$, we get $L>R$ more effectively than the case of (a2).

- [1] D. Xiao *et al.*, Phys. Rev. Lett. **108**, 196802 (2012).
- [2] S. Wang, F. R. Pratama, M. S. Ukhtary, and R. Saito, Phys. Rev. B **101**, 081414(R) (2020).
- [3] Y. J. Zhang *et al.*, Science **344**, 725 (2014).
- [4] A. Kormányos *et al.*, Phys. Rev. B **88**, 045416 (2013).
- [5] H. Rostami *et al.*, Phys. Rev. B **92**, 195402 (2015).
- [6] S. Wang, M. S. Ukhtary, and R. Saito, Phys. Rev. Research (in press).

Corresponding Author: Sake Wang

E-mail: sake@flex.phys.tohoku.ac.jp

Operando electrical characterization of methane oxidation with atomically thin films of IrO₂ nanosheets

○Ryo Nouchi^{1,2}, Yoshiaki Ishihara¹, Wataru Sugimoto³

¹ Dept. of Physics and Electronics, Osaka Prefecture University, Sakai 599-8570, Japan

² PRESTO, Japan Science and Technology Agency, Kawaguchi 332-0012, Japan

³ Research Initiative for Supra-Materials (RISM) and Faculty of Textile Science and Technology, Shinshu University, Ueda 386-8567, Japan

Methane (CH₄) is the main component of natural gas such as shale gas and now regarded as an alternative carbon source to petroleum for producing value-added chemicals such as methanol, formaldehyde and ethylene. Oxidation (dehydrogenation) is the initial step to produce the chemicals, but CH₄ possesses the most stable C–H bond among all hydrocarbons. Thus, a lot of efforts have been devoted to finding a material that enables facile dehydrogenation of CH₄. Recently, Weaver *et al.* reported that CH₄ undergoes dehydrogenation at low temperatures on a surface of iridium dioxide single crystals [1].

Operando monitoring of the reaction is effective in confirming whether such reaction actually occurs. Herein, we employed a change in electrical resistance as a facile platform for monitoring chemical reactions [Fig. 1(a)]. However, a reaction-induced change in resistance is hard to be detected because the high bulk conductivity of the IrO₂ single crystals masks the resistance change. Thus, an ultrathin sensing layer is desired to enhance the surface sensitivity. In this study, atomically thin films of IrO₂ nanosheets were fabricated on a SiO₂/Si substrate by the layer-by-layer method using a colloidal suspension of the nanosheet [2]. We observed a clear decrease in resistance upon CH₄ exposure, which is ascribable to (partial) reduction of the IrO₂ nanosheets (bulk resistivity: IrO₂ > Ir [3]) [Fig. 1(b)]. The resistance decrease was found to be suppressed upon co-exposure of O₂ [Fig. 1(c)], which can be understood as immediate healing of oxygen vacancies formed by the reduction by CH₄.

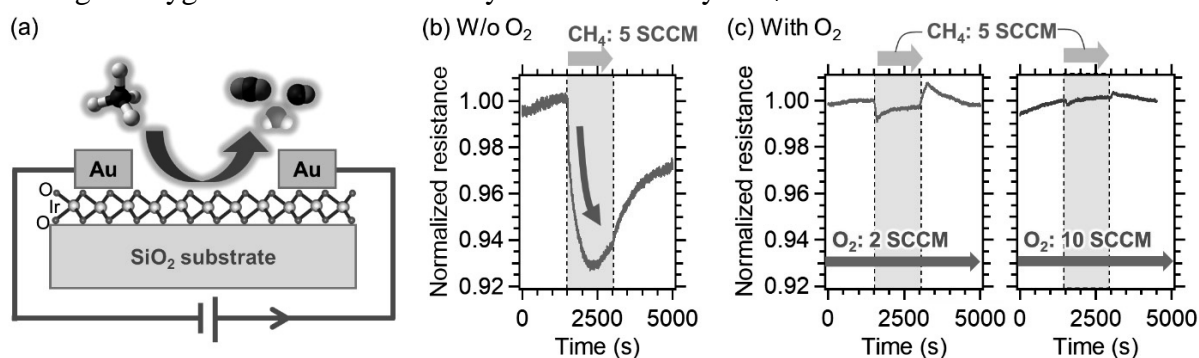


Fig. 1 (a) Schematic diagram of resistance change of IrO₂ nanosheet films upon CH₄ exposure. Resistance change (b) without and (c) with co-exposure of O₂.

[1] Z. Liang, J. F. Weaver *et al.*, *Science* **356**, 299 (2017).

[2] D. Takimoto, W. Sugimoto *et al.*, *Electrocatalysis* **8**, 144 (2017).

[3] S.-W. Kim *et al.*, *J. Appl. Phys.* **103**, 023517 (2008).

Corresponding Author: R. Nouchi

Tel: +81-72-254-8394, Fax: +81-72-254-8394,

E-mail: r-nouchi@pe.osakafu-u.ac.jp

Electrical control of resonance frequency for drum-type hBN nano-electro-mechanical resonator with photothermal actuation

[○]Yusuke Morimoto¹, Kuniharu Takei¹, Takayuki Arie¹, Seiji Akita¹

¹Department of Physics and Electronics, Osaka Prefecture University, 1-1 Gakuencho, Nakaku, Sakai, Japan

Nano-electro-mechanical resonator (NEMR) made of hexagonal boron nitride (hBN) that is transparent in the visible light region can be expected to realize the precious measurement of optical force acting on photoresponsive nanomaterials on hBN. It is important to control only the resonance frequency with the constant oscillation amplitude. In this study, in order to address this issue, the electrical tuning of the resonance frequency of drum-type hBN NEMRs with photothermal actuation is investigated.

The bulk h-BN was transferred onto the n⁺Si/SiO₂ substrate by PDMS gel stamping method, and the lower SiO₂ part was etched with BHF to produce a suspended drum-type (6 μm diameter) structure (Figure 1). The drum was driven by a photothermal method by irradiation of intensity modulated laser on the electrode of the drum edge, where DC voltage (V_{DC}) was applied between the substrate (n⁺Si) and the Au electrode. The resonance curves were measured in vacuum.

The resonance frequency and Q factor were 22.72 MHz and 260, respectively without DC bias. The amplitude at resonance increased with increasing the excitation laser intensity. When a DC voltage was applied, the resonance frequency increases up to 0.5% with increasing the DC voltage to 2 V as shown in Fig. 2(a). This is most likely due to the increase in tension induced by the deformation of suspended part of Au electrodes. Further application of DC voltage induces the electrical softening on the hBN due to the non-uniformity of electric field distribution. As shown in Fig. 2(b), the oscillation amplitude at resonance keeps constant even under different V_{DC} (< 2.5 V). Thus, we have successfully demonstrated the electrical control of resonance frequency for the drum-type hBN NEMR with photothermal actuation.

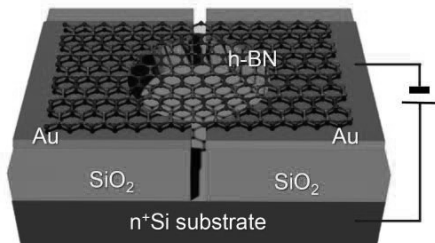


Figure 1: Schematic illustration of the DC biased drum type hBN NEMR.

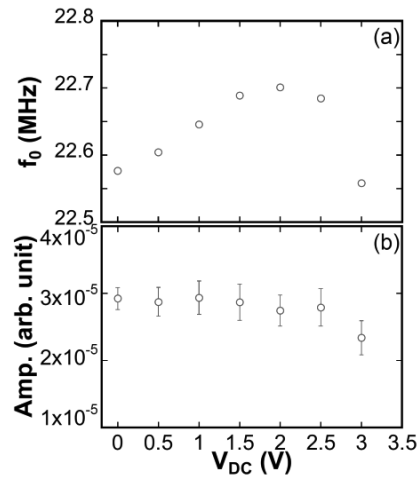


Figure 2: DC bias V_{DC} dependences of (a) resonance frequency and (b) oscillation amplitude of photo-thermally actuated drum type hBN NEMR.

Acknowledgements This work was partially supported by KAKENHI Grant Numbers 15H05869, 16H00920, 16K14259, 16H06504, and 17H01040.

Corresponding Author: S.Akita, Tel: +81-72-254- 9261, E-mail: akita@pe.osakafu-u.ac.jp

Promising next-gen Cu-substitutes: Lightweight Cu/Carbon Nanotube Composite Electric Conductors

○Rajyashree Sundaram¹, Guohai Chen¹, Takeo Yamada¹, Don Futaba¹, Kenji Hata¹, Ken Kokubo¹, Atsuko Sekiguchi¹

¹National Institute of Advanced Industrial Science and Technology (AIST), CNT application research center, Central 5, 1-1-1 Higashi, Tsukuba 305-8565, Japan

We present recent progress in developing copper-matrix carbon nanotube (Cu/CNT) composites as realistic next-gen electric conductors substituting copper [1]. Neat CNT materials are yet to fulfil demands for lightweight electrical conductors that surpass Cu for sustainable future technologies. Despite advances, best CNT assembly conductivities are 10 times lower than that of copper [2]. We believe this deficiency can be overcome by copper-CNT hybrids.

We introduce our homogeneously mixed Cu/CNT composites at least 2/3rd as light as copper [3-6] with competitive electrical conductivities, heat-/current-stabilities and tensile strengths. We could fabricate the composites in a variety of structures ranging from macroscale wires and sheets to microscale pillars. Our composite room temperature electrical conductivities are $1-3 \times 10^5$ S/cm (vs. 5.9×10^5 S/cm for Cu) with temperature coefficients of resistivity (TCR) 10% of Cu-TCR, and current carrying capacities (CCC) rivalling Cu. Our Cu/CNT show coefficients of thermal expansion (CTE) of ~ 4 ppm/K, closer to Si-CTE (~ 3 ppm/K) and much lower than Cu-CTE (~ 17 ppm/K). We observe Cu/CNT performances to depend on Cu spatial distribution and CNT attributes, indicating possibilities for performance-tuning.

With overall composite performances competitive to Cu, Cu/CNT holds promising application-potential as a Cu-substitute. Our lightweight conducting Cu/CNT wires could replace heavy copper electrical wiring in aircrafts and automobiles to achieve better fuel efficiencies and reduced CO₂ emissions. The composite's lower TCR vs. Cu (i.e., temperature-stable conductivity) also makes it a more reliable electrical conductor than Cu for high-temperature operation e.g., in motor windings. In addition, applying our Cu/CNT with CTE \sim Si and CCC rivalling Cu as interconnects could enable smaller and more powerful electronics with reduced delamination and current-failure.

- [1] R. Sundaram *et al.* Royal Society Open Science, **5(11)**, 1-21 (2018).
- [2] D. E. Tsentelovich *et al.* ACS Applied Materials & Interfaces, **9 (41)**, 36189 (2017).
- [3] R. Sundaram *et al.* Scientific Reports, **7(1)**, 9267 (2017).
- [4] R. Sundaram *et al.* Materials Today Communications, **13**, 119 (2017).
- [5] R. Sundaram *et al.* Japanese Journal of Applied Physics, **57(4)**, 04FP08 (2018).
- [6] R. Sundaram *et al.* Journal of Materials Research and Technology, **9(3)**, 6944 (2020).

Corresponding Author: R. Sundaram, A. Sekiguchi

Tel: +81-029-861-0487, +81-029-861-4611 Fax: +81-029-851-5425

Web: https://unit.aist.go.jp/cnta/index_en.html

E-mail: Rajyashree-meenukshisundaram@aist.go.jp, atsuko-sekiguchi@aist.go.jp

Anthracene-assisted deterministic transfer of optical-quality carbon nanotubes

○Keigo Otsuka¹, Yuichiro K. Kato^{1,2}

¹ *Nanoscale Quantum Photonics Laboratory, RIKEN Cluster for Pioneering Research, Saitama 351-0198, Japan*

² *Quantum Optoelectronics Research Team, RIKEN Center for Advanced Photonics, Saitama 351-0198, Japan*

Carbon nanotubes are unusual nanomaterials with a high reproducibility in atomic structures defined by two integers (chirality) and promising as quantum light sources that can be incorporated into electrical devices and photonic circuits [1,2]. Although the tunability of optical transition energies depending on the tube chirality and surrounding environments could be of great benefit, the realization of applications has been hampered by the lack of their proper control while keeping the nanotubes brightly fluorescent.

Here, we report on a dry stamping technique using single-crystalline anthracene as a medium to transfer nanotubes on flat substrates and over trenches. The anthracene crystals sublime by mild heating, leaving behind clean nanotubes and thus enabling bright photoluminescence. Since this transfer process is compatible with confocal optical measurements, a nanotube with a desired chirality can be selected and placed at a designated position with a sub-micron accuracy under in-situ photoluminescence monitoring. By repeating the deterministic transfer, we demonstrate an assembly of crossed structure from selected nanotubes, where intertube exciton transfer is observed at a single junction. Our method will facilitate fabrication of photonic and optoelectronic devices that use atomically defined nanomaterials, as well as basic study on complex but well-controlled heterostructures of carbon nanotubes and other nanomaterials.

Part of this study is supported by JSPS (KAKENHI JP20H02558, JP19J00894, JP20K15137), MIC (SCOPE 191503001), and MEXT (Nanotechnology Platform JPMXP09F19UT0075). K.O. is supported by JSPS (Research Fellowship for Young Scientists). We thank T. Inoue and S. Maruyama for the use of the CVD furnace and the thermal evaporator, as well as the Advanced Manufacturing Support Team at RIKEN for technical assistance.

[1] R. Miura, S. Imamura, R. Ohta, A. Ishii, X. Liu, T. Shimada, S. Iwamoto, Y. Arakawa, and Y.K. Kato, *Nat. Commun.* **5**, 5580 (2014).

[2] F. Pyatkov, V. Fütterling, S. Khasminkaya, B. S. Flavel, F. Henrich, M. M. Kappes, R. Krupke, and W. H. P. Pernice, *Nat. Photonics* **10**, 420 (2016).

Corresponding Author: Yuichiro K. Kato

Tel: +81-48-462-1449

Web: <http://katogroup.riken.jp>

E-mail: yuichiro.kato@riken.jp

Circular dichroism in doped carbon nanotubes

○Riichiro Saito, Md. Shoufie Ukhtary, Sake Wang, Taisei Maeda, Yuya Iwasaki

¹*Department of physics, Tohoku University, Sendai 980-8578, Japan*

In a doped carbon nanotube, we have observed an optical absorption spectrum for the polarization of light in the direction perpendicular to the nanotube axis as a function of the Fermi energy [1]. The occurrence of the optical absorption is understood by the excitation of azimuthal surface plasmon of a doped carbon nanotube [2]. Circular dichroism (CD) is defined by inequivalent optical absorption for left-handed or right-handed circularly polarized light. The occurrence of the CD in a chiral nanotube is related to the lack of the mirror symmetry of the lattice structure [3]. Thus when the handedness of the chiral nanotube (either left-handed or right-handed nanotube) is exchanged, sign of the CD value is exchanged accordingly. The measurement of CD is an important characterization tool for identifying the enantiomer [4].

Since circular dichroism of undoped, “chiral” carbon nanotube is observed for enantiomer separated nanotubes [4] and since the CD spectra as a function of the wavelength of the light is well characterized theoretically [3], it is thus important for us to investigate the circular dichroism of doped carbon nanotubes theoretically. Since there are free carriers in the doped carbon nanotubes, the optical absorption of doped graphene nanotubes is calculated by the matrix element of current density with which the optical conductivity is calculated within linear response theory (or the Kubo formula) [5]. In this presentation, we would like to discuss the origin of off-diagonal optical conductivity for the occurrence of CD and show some calculated results of CD of doped carbon nanotubes as a function of (n,m) [6].

This work is supported JSPS KAKENHI No. JPB18H01810.

References: Related papers are given in the references.

- [1] D. Satco, et al., ACS Appl. Electron. Mater., **2**, 195-203, (2020)
- [2] M. S. Ukhtary, R. Saito, Carbon (review), 167, 455, (2020). D. Satco, et al., Phys. Rev. B, **99**, 075403, (2019).
- [3] N. Sato, Y. Tatsumi, R. Saito, Phys. Rev. B, **95**, 155436, (2017) .
- [4] X. Wei, T. Tanaka, Y. Yomogida, N. Sato, R. Saito, H. Kataura, Nat. Comm. **7**, 12899 (2016).
- [5] R. Saito et al. unpublished.
- [6] Y. Iwasaki, Master thesis, Tohoku University (2019).

Corresponding Author: Riichiro Saito
Tel: +81-22-795-7754, Fax: +81-22-795-6447,
Web: <http://flex.phys.tohoku.ac.jp/>
E-mail: rsaito@flex.phys.tohoku.ac.jp

Broadband complex refractive index spectra of single-chirality-enriched carbon nanotube membranes

○Taishi Nishihara¹, Akira Takakura¹, Kazunari Matsuda¹, Takeshi Tanaka², Hiromichi Kataura², and Yuhei Miyauchi^{1*}

¹*Institute of Advanced Energy, Kyoto University, Uji, Kyoto 611-0011, Japan.*

²*Nanomaterials Research Institute, AIST, Tsukuba, Ibaraki 305-8565, Japan.*

Carbon nanotubes have attracted much attentions because of their distinct physical properties since their discovery [1]. Previous experiments using individual carbon nanotubes have demonstrated high electrical/thermal conductivities [2,3], strong light-matter interaction arising from excitons [4,5], structure-dependent tensile strengths with ultrahigh strength-to-weight ratio [6], and high thermal stability [5]; these exceptional properties potentially provide various promising applications for electronics, photonics, structural materials, and thermal management. Fabrication of macroscopically assembled carbon nanotubes with keeping their excellent physical properties are strongly desired, and determination of their fundamental physical property values is prerequisite for the developing future devices using carbon nanotubes. However, in regard to macroscopic nanotube assemblies enriched with a single chirality, most of their fundamental physical property values remains to be clarified yet. In particular, systematic knowledge on their broadband complex refractive index spectra and their chirality dependence, which is essential for designing devices using carbon nanotubes as optofunctional materials, has still been limited.

Here, we report broadband complex refractive index spectra of single-chirality-enriched carbon nanotube membranes. Free-standing and on-sapphire nanotube membranes were fabricated via filtration of nanotube solution prepared by separation method using gel chromatography [7,8]. The thicknesses of the nanotube membranes were determined as ~100 nm using a step meter and an atomic force microscope. We measured reflection and transmission spectra in far-infrared-to-visible wavelength region using the combination of Fourier transform infrared spectrometer (0.06–1.77 eV) and a home-made optical setup (1.1–3.1 eV). The fitting analyses of the optical spectra reveal that the real and imaginary parts of the complex refractive indices at the first subband exciton resonance (S_{11}) are ~2.4 and ~1.2, respectively (Fig. 1). Furthermore, we obtained an empirical expression that comprehensively reproduces the complex refractive index spectra of various chiral structures; this facilitates designing various nanotube-membrane-based optical devices.

- [1] S. Iijima, *Nature* **354**, 56 (1991).
- [2] S. J. Tans *et al.*, *Nature* **386**, 474 (1997).
- [3] C. Yu *et al.*, *Nano Lett.* **5**, 1842 (2005).
- [4] M.Y. Sfeir *et al.*, *Science* **312**, 554 (2006).
- [5] T. Nishihara *et al.*, *Nat. Commun.* **9**, 3144 (2018).
- [6] A. Takakura *et al.*, *Nat. Commun.* **10**, 3040 (2019).
- [7] H. Liu *et al.*, *Nat. Commun.* **2**, 309 (2011).
- [8] Y. Yomogida *et al.*, *Nat. Commun.* **7**, 12056 (2016).

Corresponding Author: Y. Miyauchi
Tel: +81-774-38-3463
E-mail: miyauchi@iae.kyoto-u.ac.jp

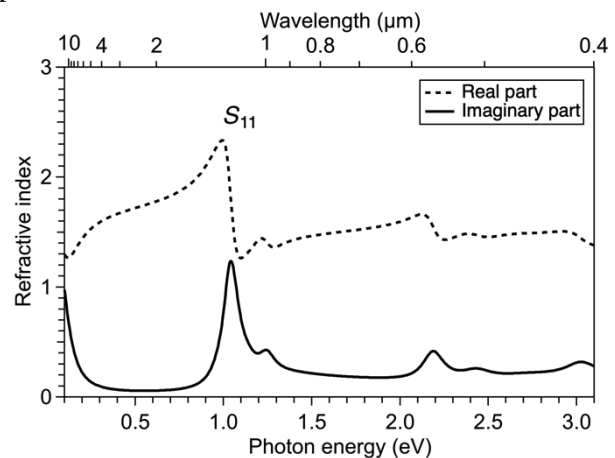


Fig. 1 Experimentally determined complex refractive index spectrum of a membrane enriched with (9,2) nanotubes.

Unravelling the Thermal Conductivity of Semiconducting Carbon Nanotubes Film with Different Doping Levels

○Kan Ueji¹, Yuya Matsuoka¹, Takashi Yagi², Yohei Yomogida¹, Yota Ichinose¹, Akari Yoshida¹, and Kazuhiro Yanagi¹

¹ *Department of Physics, Tokyo Metropolitan University, Hachioji, Tokyo 192-0397 Japan*

² *National Metrology Institute of Japan, National Institute of Advanced Industrial Science and Technology, Tsukuba, Ibaraki, 305-8563, Japan*

Flexible thin films, such as carbon-based materials, are promising candidates for flexible electronics, sensors, and batteries. Although numerous studies on flexible materials have focused on their electrical characteristics and methods for improving the electrical performance, recently the thermal management of flexible thin films attracts a lot of interest for the maximization of their device performances [1]. Therefore, the evaluation of the thermal conductivity of flexible devices is one of important subjects. The time-domain thermoreflectance (TDTR) method is an ultrafast laser-based technique (pump-probe method) that can measure the thermal conductivity of nanoscale materials using an aluminum (Al) layer as a thermal transducer. Several studies [2-3] elucidated the thermal conductivity of thin films with different potentials using Al as not only thermal transducers but also as electrodes through electrochemical procedures. However, use of Al electrodes limits target materials because Al is electro-chemically reactive. Therefore, we have developed a unique TDTR system in which a stable gold (Au) thin film is utilized as a thermal transducer instead of Al, thus making it possible to measure the thermal conductivity of a wide range of flexible materials. In this study, we investigated the relationships between the doping level and the thermal conductivity of semiconducting single-walled carbon nanotube (SWCNT) films by combining our TDTR system with the electrolyte gating system.

A typical electrolyte gating method with stable Au electrodes controls doping level of semiconducting SWCNT films. The films have ambipolar characteristic with a clear on/off ratio ($\sim 10^3$). Simultaneously, our developed TDTR system can evaluate the thermal conductivity of SWCNT films perpendicular to the sample. Figure 1 shows the thermal conductivity perpendicular to the semiconducting SWCNT film as a function of carrier density. The thermal conductivity of SWCNT films is almost identical irrespective of the carrier densities and electrical conductivity; thus implying that carrier transport does not contribute to the thermal conductivity perpendicular to the sample, suggesting that many inter-tube junctions prevent coherent charge carrier transport [4]. The details of this study will be discussed in the presentation.

References;

- [1] A. L. Moore *et al.*, *Materials today* **17**, 163–174 (2014).
- [2] A. Sood *et al.*, *Nature communications* **9**, 1–9 (2018).
- [3] J. Cho *et al.*, *Nature communications* **5**, 1–6 (2014).
- [4] K. Ueji *et al.*, to be submitted. (2020)

Corresponding Author: K. Ueji and K. Yanagi

E-mail: kueji@tmu.ac.jp and yanagi-kazuhiro@tmu.ac.jp

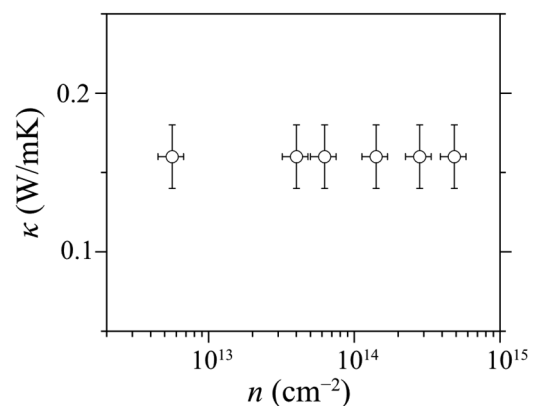


Figure 1. The thermal conductivity (κ) of SWCNT film as a function of its carrier density (n).

First electron-doping of single-walled carbon nanotube by captodatively stabilized boryl radical compounds

○Naoki Tanaka^{1,2}, Aoi Hamasuna¹, Tsuyohiko Fujigaya^{1,2,3}

¹ Department of Applied Chemistry, Graduate School of Engineering, Kyushu University, Fukuoka 819-0395, Japan

² International Institute for Carbon-Neutral Energy Research (WPI-I2CNER), Kyushu University, Fukuoka 819-0395, Japan

³ Center for Molecular Systems (CMS), Kyushu University, Fukuoka 819-0395, Japan

Chemical doping of single-walled carbon nanotubes (SWNTs) by using electron donor and acceptor molecules is a crucial method for controlling the frontier orbital energy gap, leading to promising materials for thermoelectric conversion devices with flexibility, stability, and light weight [1]. Typically, organic boron-containing compounds can serve as hole dopants for SWNT because of an electron deficient of the boron [2]. Recently, the reductive boron compounds such as boryl lithium and boryl radical compounds have been developed in organoboron chemistry field since the 2000s [3,4]. Here we demonstrate that the boryl radical compound show a good one-electron reduction for SWNT, giving rise to n-type Seebeck coefficient in SWNT sheet (**Fig. 1a**).

The absorption spectra of the SWNT sheet, after immersing in a solution of a boryl radical compound, showed that the conducting subband of semiconducting CNTs peaks almost completely disappeared, clearly indicating the occurrence of effective electron-doping of SWNT by boryl radical. In fact, the Seebeck coefficient of a n-doped SWNT sheet was negative (**Fig. 1b**). On the other hand, the electrical conductivity of the SWNT sheet was increased compared with pristine SWNT film (**Fig. 1c**). In this presentation, we will detail the above experiments as well as electric structure of the counter cation of the doped SWNT sheet.

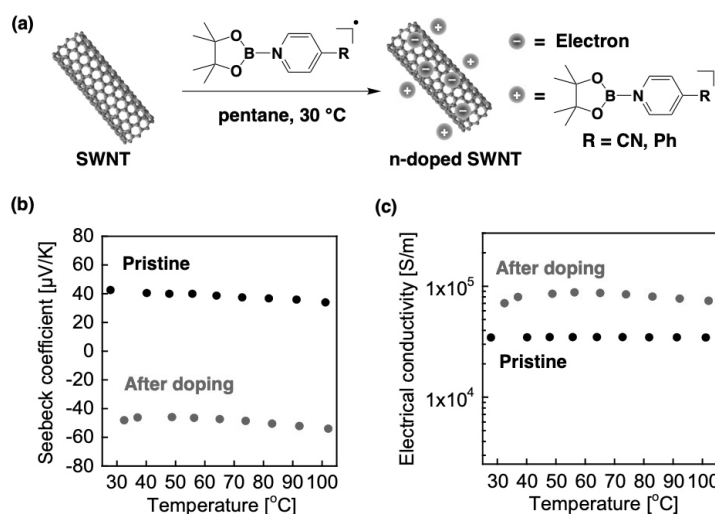


Fig. 1 (a) Schematic illustration of this work. Temperature dependence of (b) Seebeck coefficient and (c) electrical conductivity of the pristine film (Black dots) and the SWNT film after doping (Red dots).

[1] N. T. Hung, A. R. T. Nugraha and R. Saito, *Energies* **2019**, *12*, 4561.

[2] Y. Shoji, T. Fukushima, T. Takenobu et al., *Applied Physics Express* **2017**, *10*, 035101.

[3] Y. Segawa, M. Yamashita, K. Nozaki, *Science* **2006**, *314*, 113.

[4] C. Zhu, S. Li et al., *Angew. Chem. Int. Ed.* **2016**, *55*, 5985.

Corresponding Author: N. Tanaka

Tel: +81-92-845-2840, Fax: +81-92-845-2842,

Web: <http://www.chem.kyushu-u.ac.jp/~fifth/jp/> E-mail: tanaka.naoki.468@m.kyushu-u.ac.jp

Porosity and Size Analysis of Carbon Nanotube Aggregates by Centrifugal Sedimentation

○Yuichi Kato¹, Takahiro Morimoto², Kazufumi Kobashi², Toshiya Okazaki²

1 Nanomaterials Research Institute, National Institute of Advanced Industrial Science and Technology (AIST), Osaka 563-8577, Japan

2 CNT-Application Research Center, AIST, Tsukuba 305-8565, Japan

Fine tuning of the structure for disentangled carbon nanotube (CNT) agglomerates is important to enhance the CNT composite material's performance. Quantitative analysis of porosity (ϕ) in liquid of the CNT agglomerates (when we disentangle CNTs, ϕ of CNT agglomerates increases) has been limited despite its importance. Recently, we proposed an analysis of ϕ and sedimentation particle size (D) of the agglomerates by centrifugal sedimentation.[1] We consider "inner fluid buoyancy", that is the buoyancy caused by the smaller fluid density inside the agglomerate that sediments in a density gradient than the fluid outside (Fig. 1). For instance, we obtained ϕ : 0.9994 and D : 20 μm as for our CNT agglomerates.[1] Here we introduce (A) how to analyze ϕ and D by sedimentation. Moreover, we report (B) generality of the inner fluid buoyancy and discuss accuracy of the analysis.

(A) If neither ϕ nor D is known, you can estimate both simultaneously with equation (1).

$$\frac{1}{D_{STD}^2} \frac{t}{t_{STD}} \frac{\Delta\rho}{\Delta\rho_{STD}} = \frac{1}{D^2(1-\phi)} \left(1 + \phi D^4 \frac{\frac{\partial\rho_f}{\partial R} R \omega^2}{1080\eta D_d} \right) \quad (1)$$

where t is sedimentation time, $\Delta\rho$ is the difference between apparent density and fluid density, $\frac{\partial\rho_f}{\partial R}$ is density gradient, η is viscosity, and D_d is diffusion constant of solute. The subscript STD indicates that the value is from a standard particle. You should measure t for different values of ω . If either ϕ or D is known, the other is measured at the lowest possible ω using the minimum necessary $\frac{\partial\rho_f}{\partial R}$ to stabilize the sedimentation.

(B) We measured t of nylon-6 porous particles in density gradient at different values of ω . Inner fluid buoyancy explains sedimentation of the particles well. Both estimated values of ϕ and D with equation (1) were reasonable. This result supports generality of the inner fluid buoyancy. We will discuss accuracy of the analysis and validate steady-state approximation, which is a prerequisite for equation 1.

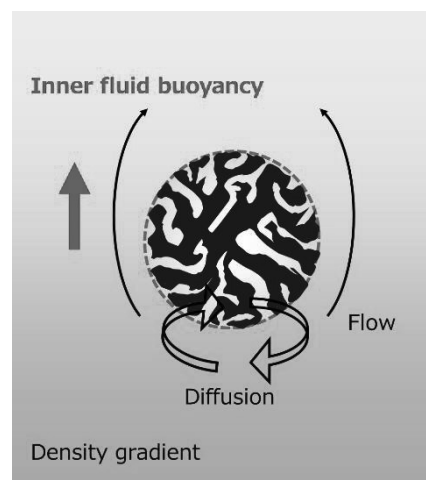


Fig. 1 Schematic illustration of inner fluid buoyancy.

[1] Y. Kato, T. Morimoto, K. Kobashi, T. Yamada, T. Okazaki, K. Hata, *The Journal of Physical Chemistry C* **123** (2019) 21252-21256.

Corresponding Author: Yuichi Kato

Tel: +81-29-861-9275

E-mail: yuichi.katou@aist.go.jp

XPS investigation revealing the activation of iron catalyst by a small amount of noble metals without reducing gas towards the synthesis of tall carbon nanotube forest

○Shunsuke Sakurai, Jinping He, Kenji Hata, Don N. Futaba

CNT Application Center, National Institute of Advanced Industrial Science and Technology (AIST), 1-1-1 Higashi, Tsukuba, Ibaraki, 305-8565, Japan

For the synthesis of vertically-aligned carbon nanotube (CNT) by chemical vapor deposition (CVD) method, the importance of reducing gases such as hydrogen (H_2) to prepare catalyst nanoparticle array of transition metal such as iron (Fe) has been frequently investigated [1,2]. In the previous meeting, we reported an unexpected effect of noble metals (NM = iridium, rhodium, and platinum) added into Fe catalyst with a small fraction on the CNT synthesis efficiency during the process without any reducing gases. Here we report XPS investigation revealing the reduction of electronics status of Fe atoms triggered by the appearance of metallic NM atoms.

Height of CNT grown without H_2 reached to c.a. 500 μm only by <0.5 at% addition of NM atoms as shown in Figure 1. XPS spectra of the catalyst substrate after annealing in helium ambient shows the appearance of Fe^{2+} peak around 709 eV by adding small amount of iridium (Figure 2). The ratio of Fe^{2+} status drastically increased and saturated around 30% by adding 0.3 at% iridium. Further analysis on the effect of annealing temperature showed Fe^{2+} status observed by annealing at $>500^\circ C$, where metallic status of iridium atoms observed from Ir4f peaks was also observed. Those results suggested the small amount of metallic noble metal atoms located on the surface of oxidized iron can trigger the reduction of iron, and results in the activation of iron catalyst for CNT growth. This work was supported by JSPS KAKENHI Grant Number JP17K14090.

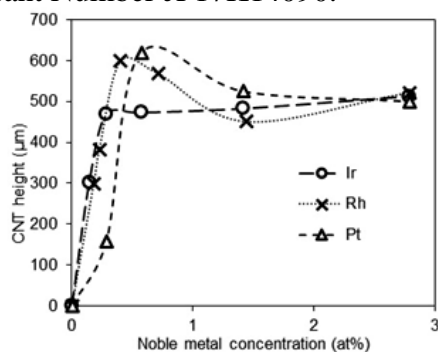


Fig. 1 CNT height vs noble metal concentration.

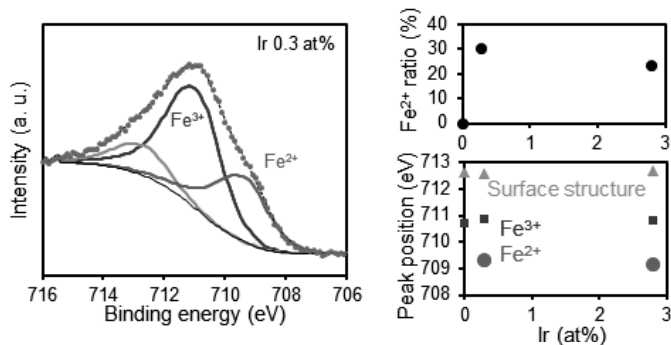


Fig. 2 (a) XPS spectra (Fe2p) from the sample with 0.3at% iridium. (b) Fe^{2+} ratio and (c) peak positions vs iridium concentration.

[1] S. Sakurai, H. Nishino, D. N. Futaba, S. Yasuda, T. Yamada, A. Maigne, Y. Matsuo, E. Nakamura, M. Yumura, and K. Hata, *J. Am. Chem. Soc.* **134**, 2148 (2012).

[2] S. Sakurai, M. Inaguma, D. N. Futaba, M. Yumura, K. Hata *Small* **9**(21), 3584 (2013).

[3] S. Sakurai *et al.* Abstracts of the 52nd Fullerene-Nanotubes-Graphene General Symposium (2017).

Corresponding Author: S. Sakurai

Tel: +81-29-861-6205, Fax: +81-29-861-4851,

E-mail: shunsuke-sakurai@aist.go.jp

~ Memo ~

ポスター発表
Poster Preview

1 P-1 ~ 1 P-27

2 P-1 ~ 2 P-27

3 P-1 ~ 3 P-26

MWCNT growth mechanism using FeCl₂ catalyst precursor

°Tatsuhiko Hayashi, Takayuki Nakano, Yoku Inoue

Department of Electronics and Materials Science, Shizuoka Univ., Hamamatsu 432-8561, Japan

So far, we have developed a chloride-mediated chemical vapor deposition (CM-CVD) method using iron chloride as a catalyst precursor for the synthesis of carbon nanotubes. The CNT forest synthesized by this method has a high growth rate, density, and orientation. The CNT grows higher than 2 mm with keeping high spin-capability [1]. However, the growth mechanism of CNT has not been clarified in detail. In this study, we investigated the growth mechanism by observing the cross-section of the CNT forest using a transmission electron microscope (TEM).

CNTs were synthesized on a heat-treated Si substrate. The CNT was grown at 820° C at a pressure of 20 Torr with FeCl₂ of 120 mg. C₂H₂ of 200 sccm was used for feedstock and Ar of 300 sccm for carrier gas. The catalyst behavior at the substrate interface was investigated by TEM observation of the cross-section of samples with different growth times.

Figure 1 shows the cross-sectional TEM image and EDS image of the CNT synthesized on the substrate. It is observed that the tip of the catalyst is absorbed in the hollow part of the CNT from the substrate. It was also found that the iron layer was uniformly deposited on the substrate surface. Figure 2 shows cross-sectional TEM images of CNTs synthesized with growth times of 30 seconds, 1 minute, and 2 minutes, respectively. The catalyst tip is sharpened in the hollow part of CNT. It was found that as the CNTs grow over time, the absorption of catalyst into the hollow CNTs progresses further. From this observation, it is expected that the catalyst is well melted, and thus the diffusion rate of carbon inside catalyst is increased. This is considered to lead to suppression of amorphous carbon deposition on the catalyst surface. The above expectation can be attributed to the fact that by the CM-CVD method, CNTs grow at high speed, and the forest has a long catalyst life, resulting in a long length and high spinnability.

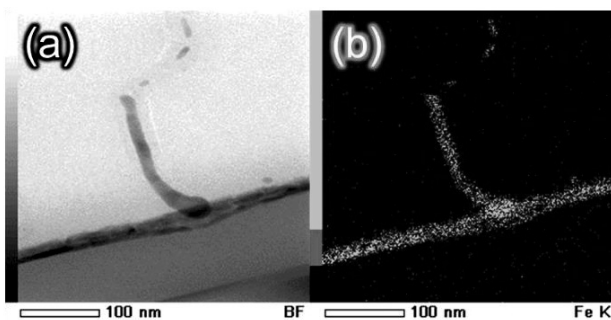


Fig1. Cross-sectional STEM image of a MWCNT grown on SiO₂/Si substrate with a growth time of 2min. (a)STEM image (b)STEM-EDS image of Fe

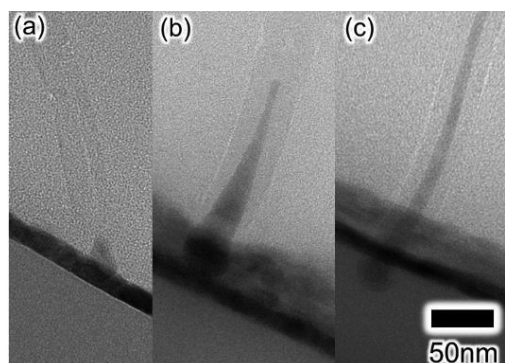


Fig2. Cross-sectional TEM image of a MWCNT grown on SiO₂/Si substrate with different growth times (a)30s (b)1min (c)2min

[1] Y.Inoue, et al, Appl. Phys. Lett, **92**, 213113 (2008)

Corresponding Author: Yoku Inoue

Tel: +81-53-478-1356

Web: <http://cnt.eng.shizuoka.ac.jp/>

E-mail: inoue.yoku@shizuoka.ac.jp

Light-driven wavelength shifts of photoluminescence from single-walled carbon nanotubes by functionalization with diarylethene derivatives

○Yasuto Nakagawa¹, Takuya Nakashima³,
Tsuyoshi Kawai³, Tsuyohiko Fujigaya^{1,2,4}, Tomohiro Shiraki^{1,2}

¹ Department of Applied Chemistry, Kyushu University, Fukuoka 819-0395, Japan

² WPI-ICNER, Kyushu University, Fukuoka 819-0395, Japan

³ Division of Materials Science, Nara Institute of Science and Technology, Nara 630-0192, Japan

⁴ Center for Molecular Systems, Kyushu University, Fukuoka 819-0395, Japan

Local chemical functionalization of single-walled carbon nanotubes (SWNTs) has achieved defect doping to enhance their near-infrared (NIR) photoluminescence (PL) properties[1-4]. The locally functionalized SWNTs (lf-SWNTs) show new red-shifted PL (E_{11}^*) with enhanced quantum yields compared to the original PL (E_{11}) of pristine SWNTs. One of characteristic features of the lf-SWNTs is that the E_{11}^* PL wavelength can be modulated depending on the functionalized molecular structures on their doped sites. For example, protonation of amine groups by pH variation[2] and selective molecular binding based on molecular recognition and dynamic covalent bonding[3,4] at the functionalized aryl groups of lf-SWNTs have been reported to induce E_{11}^* PL wavelength changes.

In this study, we synthesize lf-SWNTs functionalized with diarylethene derivatives (DAE) that show photoisomerization properties[5]. For the synthesis of DAE-functionalized lf-SWNTs (lf-SWNTs-DAE), a diazonium salt having a DAE moiety (DAE-Dz) was synthesized and reacted with the SWNTs solubilized in a sodium dodecylbenzenesulfonate micellar solution. In the PL spectrum of the lf-SWNTs-DAE (Figure 1), peaks were observed at 980 nm and 1142 nm. The former one is assigned to E_{11} PL and the latter one, which has appeared after the local chemical functionalization, is assignable to E_{11}^* PL of the lf-SWNTs-DAE. When the lf-SWNTs-DAE solution was irradiated with UV light, E_{11}^* PL peak was red-shifted by 3 nm. In contrast, when irradiating with visible light to the solution, the E_{11}^* PL peak was blue-shifted to the initial wavelength position. These observations indicated the reversible switching of the E_{11}^* PL wavelength for the lf-SWNTs-DAE triggered by photoisomerization. Moreover, the photoswitching behavior was repeatedly observed over 5 times. The developed photoswitching function is expected to produce functionalized lf-SWNTs for advanced applications such as bio/medical imaging and quantum communications.

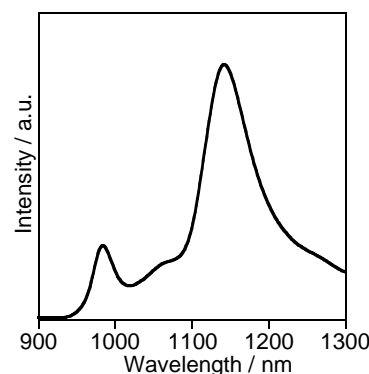


Figure 1 PL spectrum of lf-SWNTs-DAE. $\lambda_{\text{exc}} = 570$ nm.

[1] Y. Wang *et al.*, *Nat. Chem.* **2013**, 5, 840. [2] Y. Wang *et al.*, *J. Phys. Chem.* **2015**, 119, 3733.

[3] T. Shiraki *et al.*, *Chem. Comm.* **2016**, 52, 12972. [4] T. Shiraki *et al.*, *Chem. Eur. J.* **2018**, 24, 19162.

[5] T. Kawai *et al.*, *Eur. J. Org. Chem.* **2017**, 17, 2451.

Corresponding Author: T. Shiraki

Tel/Fax: +81-92-802-2841/ +81-92-802-2841

Web: <http://www.chem.kyushu-u.ac.jp/~fifth/jp/>

E-mail: shiraki.tomohiro.992@m.kyushu-u.ac.jp

Fabrication of Carbon Nanotube Thin Films for Flexible Transistor Applications using a Cross-linked Amine Polymer

○Kaisei Matsumoto¹, Kazuki Ueno¹, Jun Hirotsu², Yutaka Ohno^{2,3}, and Haruka Omachi^{1,4}

¹ Department of Chemistry, Graduate School of Science, Nagoya University, Nagoya 464-8602, Japan

² Department of Electronics, Graduate School of Engineering, Nagoya University, Nagoya 464-8601, Japan

³ Institute of Materials and Systems for Sustainability, Nagoya University, Nagoya 464-8601, Japan

⁴ Research Center for Materials Science, Nagoya University, Nagoya, 464-8602, Japan

Owing to their remarkable properties, single-walled carbon nanotube thin film transistors (SWCNT-TFTs) are expected to be used in various flexible electronics applications. To fabricate SWCNT channel layers for TFTs, solution-based film formation on a self-assembled monolayer (SAM) covered with amino groups is commonly used. However, this method uses highly oxidized surfaces, which is not suitable for flexible polymeric substrates.

Herein, we report a solution-based SWCNT film fabrication using methoxycarbonyl polyallylamine (Moc-PAA)[1]. The NH₂-terminated surface of the cross-linked Moc-PAA layer enables the formation of highly dense and uniform SWCNT networks on both rigid and flexible substrates (Fig. 1a). TFTs that use the fabricated SWCNT thin film exhibited excellent performance with small variations (Fig. 1b). The presented simple method to access SWCNT thin film accelerates the realization of flexible nanoelectronics.

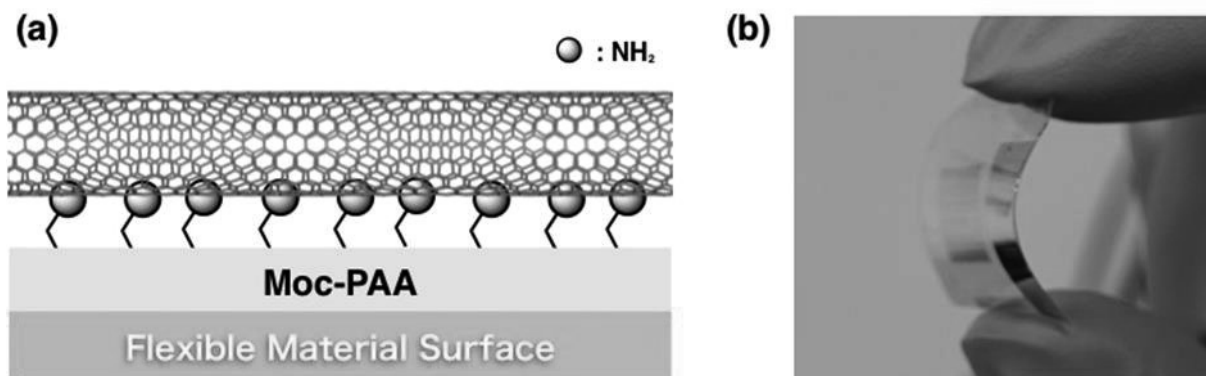


Fig. 1 (a) Schematic diagram of the fabrication of the SWCNTs thin film on the Moc-PAA layer. (b) Photograph of SWCNT TFT on the flexible PEN substrate.

[1] K. Matsumoto, K. Ueno, J. Hirotsu, Y. Ohno, H. Omachi, *Chem. Eur. J.*, **26**, 6118 (2020).

Corresponding Author: H. Omachi

Tel: +81-52-789-3660,

Web: <https://sites.google.com/view/haruka-omachi/>

E-mail: omachi@chem.nagoya-u.ac.jp

Structure-dependent solvatochromic shifts of excitonic photoluminescence from locally functionalized single-walled carbon nanotubes

○Yoshiaki Niidome¹, Tsuyohiko Fujigaya^{1,2,3}, Tomohiro Shiraki^{1,2}

¹ Department of Applied Chemistry, Kyushu University, Fukuoka 819-0395, Japan

² WPI-ICNER, Kyushu University, Fukuoka 819-0395, Japan

³ Center for Molecular Systems, Kyushu University, Fukuoka 819-0395, Japan

Single-walled carbon nanotubes (SWNTs) with semiconducting features show near infrared photoluminescence (PL) and whose property is determined by the exciton that is a bound state of an electron and a hole by Coulombic interactions. The excitonic PL energies are sensitively changed depending on the surrounding environments [1]. Recently, doping of structural defects such as oxygen or sp^3 carbon to the crystalline lattice of the carbon network of SWNTs has been reported by local chemical functionalization to improve the excitonic PL properties[2,3]. The locally functionalized SWNTs (lf-SWNTs) emit red-shifted and brighter E_{11}^* PL compared to original E_{11} PL of pristine SWNTs. It is due to the creation of the doped sites that work as new emissive sites with narrower bandgaps and exciton trapping features. Very recently, we have reported that the sp^3 carbon doped sites of aryl modified lf-SWNTs showed highly sensitive PL energy changes based on solvent environments compared to E_{11} PL of pristine SWNTs[4]. The finding indicates that excitonic properties in the lf-SWNTs would be remarkably modulated by the defect doping effects.

Here, we examined solvatochromic shifts of the E_{11}^* PL from oxygen-doped lf-SWNTs (lf-SWNTs-O) (Fig. 1). lf-SWNTs-O were synthesized through the reaction between ozone and the solubilized SWNTs in D_2O using sodium dodecylbenzenesulfate micelles. Various organic solvent environments were created by mixing a water-immiscible organic solvent into the aqueous lf-SWNTs-O solution[4,5]. From the PL spectral changes of the lf-SWNTs-O after the solvent injection, the E_{11}^* PL was found to be red-shifted with dependence on the mixed organic solvents. The E_{11}^* PL from ether-type doped sites (~ 1125 nm) showed larger shifts compared to those of the E_{11} PL. In sharp contrast, the E_{11}^* PL from the epoxide-type doped sites (~ 1250 nm) of the lf-SWNTs-O was insensitive to the solvent environment changes. These results indicate that the excitonic PL properties strongly depend on the doped site structures of lf-SWNTs. In this presentation, comparison with the E_{11}^* PL shifts of sp^3 carbon doped sites of lf-SWNTs will be also discussed.

- [1] Y. Ohno *et al.* Phys. Status Solidi B. **244**, 4002 (2007).
- [2] R. B. Weisman *et al.* Science. **330**, 1656 (2010).
- [3] Y. Wang *et al.* Nat. Chem. **7**, 715 (2013).
- [4] T. Shiraki *et al.* Chem. Commun. **55**, 3662 (2019).
- [5] K. J. Ziegler *et al.* Phys. Chem. Chem. Phys. **12**, 6990 (2010).

Corresponding Author: T. Shiraki

Tel/Fax: +81-92-802-2841

E-mail: shirak.tomohiro.992@m.kyushu-u.ac.jp

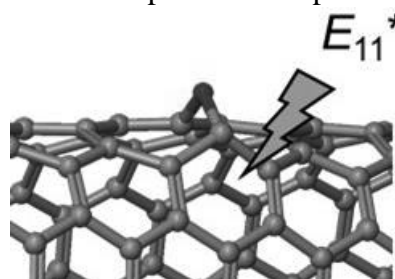


Fig. 1. Schematic image of lf-SWNTs-O with the ether-type doped site and E_{11}^* PL emission.

Visualization of thermal transports on bundled carbon nanotubes by monitoring evaporation of gold nanoparticles

○Hiromu Hamasaki¹, Seiya Takimoto¹ and Kaori Hirahara²

¹ Dept. of Mechanical Engineering, Osaka University, Osaka 565-0871, Japan

² Dept. of Mechanical Engineering and Center for Atomic and Molecular Technologies, Osaka University, Osaka 565-0871, Japan

Thermal conductivity is one of the most fascinating property of single walled carbon nanotubes (SWCNTs). Most assemblies of SWCNTs (ropes, films and so on) consist of the bundles, therefore the thermal transport of assemblies should strongly depend on properties of the bundles. Bundles of SWCNTs are common structure often seen in the synthesized CNTs. In a close-pack bundle, parallelly aligned CNTs are tightly bound each other by van der Waals force. Previously, thermal conductivities of single bundles parallel to axial direction of CNTs have been investigated [1]. However, that along the perpendicular direction was still unclear. This may be because a single bundle size along perpendicular direction is much smaller than parallel direction. In order to investigate thermal conductivity along the perpendicular direction, we conducted visualization of the thermal transport in a bundle of SWCNTs by in-situ transmission electron microscopy (TEM).

Prior to TEM observation, gold nanoparticles were deposited on SWCNTs bundles (MEIJO-SO) by vapor deposition. The diameter of gold particles was less than 10 nm. In TEM, an electrode probe tip was made contact to a bundle protruded from an edge of the substrate, and voltage was applied between the tip and substrate. Joule heat generated mainly at the contact point flowed toward the end of free-standing bundle, and we visualized how heat is transported in the bundle by monitoring the evaporation of gold particles. As the result, significant anisotropy for thermal transport between parallel and perpendicular direction to the bundle was observed as shown in Fig. 1. Thermal conductivity in the perpendicular direction was estimated from the experimental results with the aid of calculations, to be $\sim 1/500$ of that in parallel direction.

This work was supported by JST CREST Grant Number JPMJCR17I5, Japan.

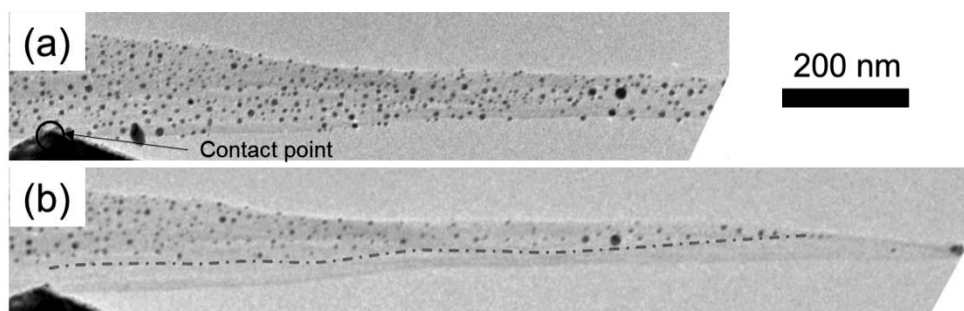


Fig. 1 TEM images of the bundle after heating with (a) 90 μ A and (b) 135 μ A.

[1] Y. Feng *et al.*, Appl. Phys. Lett., **112**, 191904 (2018).

Corresponding Author: H. Hamasaki

Tel: +81-6-6879-7307

E-mail: hamasaki@ne.mech.eng.osaka-u.ac.jp

Measurement of Zeta potential of single-walled carbon nanotubes in non-polar organic solvent

○Taiki Ishii¹, Angana Borah¹, Naoki Tanaka^{1,2}, Tsuyohiko Fujigaya^{1,2,3}

¹Department of Applied Chemistry, Kyushu University, Fukuoka 819-0395, Japan

²WPI-I2CNER, Kyushu University, Fukuoka 819-0395, Japan

³CMS, Kyushu University, Fukuoka 819-0395, Japan

Single-walled carbon nanotubes (SWNTs) are promising material for electronic and mechanical materials for next generation owing to their excellent properties. They are synthesized as mixtures of semiconducting SWNTs (s-SWNTs) and metallic SWNTs (m-SWNT). Up to date, various separation method of s-SWNTs and m-SWNTs such as chromatography and electric-field-induced layer formation (ELF) method were realized mainly in aqueous system [1,2], while an extraction of only s-SWNTs was realized in non-polar organic solvents such as toluene [3,4] have been reported. However, the mechanism of these separation and extraction methods had not been understood. Recently, in the ELF method, separation mechanism was explained that the degree of negative charge was smaller for m-SWNTs than s-SWNTs due to the hole doping and the difference of the surface charge between s-SWNTs and m-SWNTs in water played an critical role in response to an applied electric field [5]. We consider that the similar mechanism was applied for extraction method in organic solvent.

In this study, we measured the surface charge of s-SWNTs and m-SWNTs in organic solvent to investigate the mechanism of the extraction in organic solvent, in which the Zeta potential measurements were used to monitor the surface charge of the SWNTs. For the s- and m-SWNTs, commercially available m-SWNTs (NanoIntegris) and s-SWNTs sorted by Flavin extraction method [4]. We found that the Zeta potential of the m-SWNTs was approximately 11.9 mV, while that of s-SWNTs was 32.0 mV. Since the dispersion stability test showed the aggregation only for the m-SWNTs, we consider that the lower charge repulsion of m-SWNTs in non-polar solvents resulted in the aggregation of m-SWNTs and extraction of s-SWNT was realized.

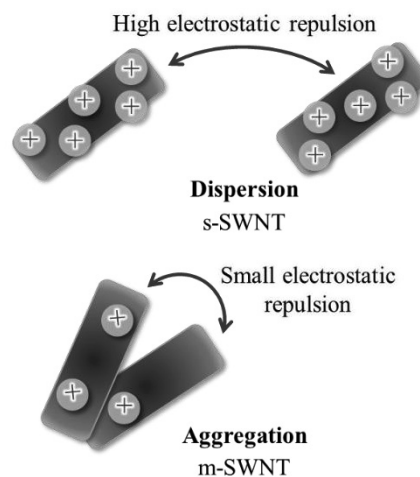


Fig. 1 Illustration of the possible difference of dispersion stability between s-SWNT and m-SWNT.

[1] H. Liu *et al.*, Nat. Commun., **2**, 309 (2011).

[2] M. S. Arnold *et al.*, Nat. Nanotechnol., **1**, 60 (2006).

[3] F. Chen *et al.*, Nano Lett. **7**, 10 (2007)

[4] Y. Kato *et al.*, Chem. Lett., **44**, 556 (2015).

[5] Y. Kuwahara *et al.*, J. Phys. Chem. C., **123**, 6 (2019)

Corresponding Author: T. Fujigaya

Tel/Fax: +81-92-802-2842,

Web: <http://www.chem.kyushu-u.ac.jp/~fifth/jp/>

E-mail: fujigaya.tsuyohiko.948@m.kyushu-u.ac.jp

Near-Infrared Fluorescence Immunoassay Using Streptavidin-Conjugated Oxygen-Doped Carbon Nanotubes

○Keiko Kojima^{1,2}, Yoko Iizumi², Minfang Zhang², and Toshiya Okazaki^{2,1}

¹Department of Chemistry, The University of Tsukuba, Tsukuba 305-8577, Japan

² CNT-Application Research Center, National Institute of Advanced Industrial Science and Technology (AIST), Tsukuba 305-8565, Japan

Single-walled carbon nanotubes (CNTs) have been introduced to near-infrared (NIR) immunoassay systems for recent years. Compared with other NIR molecules and materials, CNTs have several advantages such as strong emissions, large Stokes-shifts and high photostabilities as NIR labels. Previously, our research group reported that immunoprecipitation (IP) was successfully conducted between IgG-conjugated CNTs and protein G magnetic beads. Although the system can ideally measure target analytes at concentrations as low as 600 pmol/L, the practical reaction efficiency was insufficient, around ~18% [1].

To improve the IP reaction yield, we here made the streptavidin-conjugated oxygen-doped CNTs (o-CNT-SA) that can selectively bind with biotin molecules. The o-CNTs [2] were coated by streptavidin which combined with phospholipid polyethylene glycol (SA-PEG). While IgG forms a 1:1 complex with an antigen, SA can bind biotin molecules at four sites. Some amounts of phospholipid polyethylene glycol (PL-PEG) were added to stabilize the dispersion state of o-CNT-SA. For assessing the IP reactivity, the fluorescent intensity ratio between the eluted solution and the original o-CNT-SA dispersion was calculated (Fig. 1). Figure 2 shows the NIR fluorescence spectra observed from the eluted and the original o-CNT-SA solutions. By adjusting the concentrations of o-CNTs, SA-PEG and PL-PEG, the IP reaction yield increased up to 78%. In this symposium, we will show the detailed experimental procedures and discuss the proper structure of the o-CNT-SA NIR label based on the obtained results.

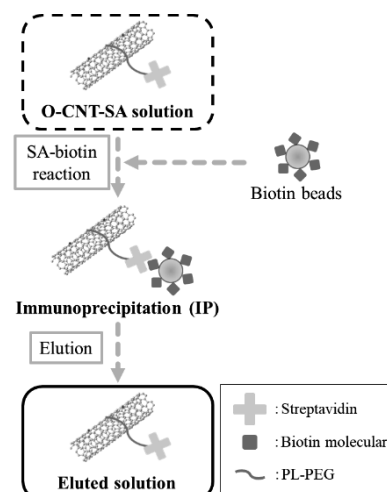


Fig. 1. Flow-chart of the present IP experiment.

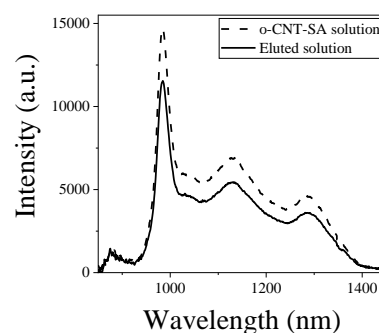


Fig. 2. Fluorescence spectra observed from the original o-CNT-SA and the eluted solutions.

[1] Y. Iizumi *et al.*, ACS Appl. Mater. Interfaces, 5, 7665 (2013).

[2] Y. Iizumi *et al.*, Sci. Rep., 8, 6272 (2018).

Corresponding Author: T. Okazaki, E-mail: toshi.okazaki@aist.go.jp

Effects of channel length on performance of transparent solar cell with monolayer WS₂

○X. He¹, T. Kaneko¹, and T. Kato^{1,2}

¹Graduate School of Engineering, Tohoku University, Sendai 980-8579, Japan

²JST-PRESTO

Layered transition metal dichalcogenide (TMD) is known as a true 2D material with excellent semiconducting properties. TMD is one of the most attractive materials for future transparent and flexible optoelectrical devices due to their atomically thin structure, band gap in visible light range, and high optical transparency. Those merits of TMD have not been applied for transparent and flexible solar cell, which is attracted intense attention as a next-generation energy harvesting technology.

Recently, we have developed a new fabrication process of TMD-based solar cell [1]. In our process, Schottky type device configuration is utilized, which can be simply formed by asymmetrically contacting electrodes and TMD. The power conversion efficiency clearly depended on the work function difference between two electrodes (ΔWF), and a higher efficiency could be obtained with higher ΔWF (Pd-Ni). Based on the optimizations of electrodes and distance, the power conversion efficiency (PCE) can be reached up to 0.7 %, which is the highest value for solar cell with similar TMD thickness [1].

To further improve the PCE, optimization of device structures is important. As one of the key parameters, we focus on the channel length (L_{ch}) between Schottky- and Ohmic-side electrodes (Fig.1) We found that the best L_{ch} showing highest PCE (L_{chbst}) strongly depends on the kinds of electrodes and layer numbers of WS₂. For the Ni electrode, L_{chbst} is ~ 4 μm , while Cu shows much shorter L_{chbst} (~ 0.5 μm). Double and triple-layer WS₂ also show shorter L_{chbst} than that of monolayer WS₂ even with Ni electrode. These can be attributed to the Fermi pinning effect, which exists when electrode is in contact with the two-dimensional WS₂. Stronger pinning effect (Ni or monolayer) may have relatively longer L_{chbst} than that (Cu or few layer) with weaker pinning effects. This finding is very important for further improving the performances of the transparent and flexible solar cell.

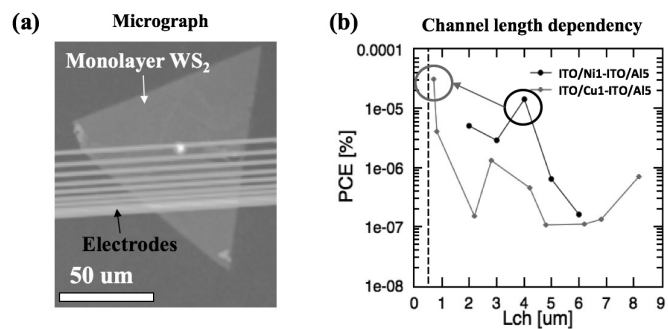


Fig.1 (a) Typical optical image of Schottky solar cell device with monolayer WS₂. (b) The dependence of PCE on different L_{ch} for Ni and Cu electrode devices.

[1] T. Akama, W. Okita, R. Nagai, C. Li, T. Kaneko, and T. Kato, Sci. Reports **7**, 11967 (2017).

Corresponding Author: Xing He

Tel: +81-22-795-7046, Fax: +81-22-263-9225, E-mail: he.xing.q7@dc.tohoku.ac.jp

Robust easy-plane 2D ferromagnetism in $\text{Cr}_{1/3}\text{NbSe}_2$ ultrathin films

○Yuki Majima¹, Bruno Kenichi Saika¹, Hideki Matsuoka¹, Masaki Nakano^{1,2}, Satoshi Yoshida¹, Kyoko Ishizaka^{1,2}, Yoshihiro Iwasa^{1,2}

¹ *Department of Applied Physics, University of Tokyo, Tokyo 113-8656, Japan*

² *RIKEN Center for Emergent Matter Science, Saitama 351-0198, Japan*

In transition-metal dichalcogenides (TMDCs), there have been found many interesting physical properties, such as valley-contrasting optical phenomena^[1], 2D superconductivity^[2] and so on. In addition, the van der Waals gaps in TMDCs allow intercalation of a wide variety of atoms or molecules. In particular, when the magnetic ions are intercalated, various magnetic ordering can be formed dependent on their intercalation level, although their properties at the 2D limit are so far less studied probably due to technical difficulty in exfoliation. Our group instead has employed molecular-beam epitaxy (MBE) and demonstrated that V_5Se_8 thin films, in which V atoms are self-intercalated into the host VSe_2 , display intrinsic ferromagnetism^[3], while the bulk counterpart is an antiferromagnet.

In this work, we succeeded in synthesizing epitaxial thin films of $\text{Cr}_{1/3}\text{NbSe}_2$. Figure 1 shows (a) the crystal structure of $\text{Cr}_{1/3}\text{NbSe}_2$ and (b) the magnetization-temperature relation of the 6 nm-thick film. We found that the film shows ferromagnetism at the Curie temperature of 100 K with strong easy-plane anisotropy. Also we found that controlling the intercalation level is possible just by tuning the film growth condition. In the presentation, we will report the MBE growth process in detail and discuss their structural, electrical and magnetic properties.

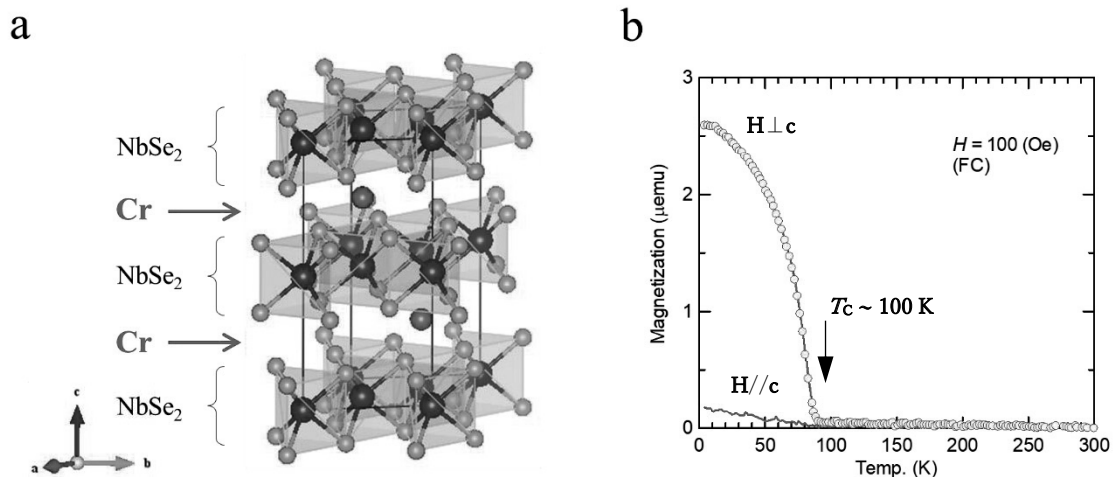


Fig. 1 (a) Crystal structure of $\text{Cr}_{1/3}\text{NbSe}_2$. Mother material (NbSe_2) and intercalated Cr atoms are also indicated.

(b) Magnetization-temperature relation of the 6 nm-thick film.

[1] J. R. Schaibley *et al.*, *Nature Reviews Materials* **1**, 16055 (2016).

[2] Y. Saito *et al.*, *Nature Reviews Materials* **2**, 16094 (2017).

[3] M. Nakano *et al.*, *Nano Lett.* **19**, 8806 (2019).

Corresponding Author: M. Nakano

Tel: +81-03-5841-6871, Fax: +81-03-5841-6822, E-mail: nakano@ap.t.u-tokyo.ac.jp

Energetics and geometric structure of corannulene under an external electric field

Susumu Okada, Yanlin Gao, and Mina Maruyama

Department of Physics, University of Tsukuba, Tennodai, Tsukuba 305-8571, Japan

An electric field plays crucial role to control the electronic structure of semiconducting materials by tuning their Fermi level energy. Simultaneously, the electric field causes the unintentional structural modulation in semiconducting and insulating materials, which seriously deteriorate device performance. Furthermore, the electric field was able to cause isomerization of small molecules on metal surfaces. For instance, *trans-sis* isomerization of azobenzene has occurred using STM. These facts implies that the electric field also play decisive role to determine the atomistic structures of nanoscale materials.

Thus, in this work, we aim to investigate the geometric structures of corannulene ($C_{20}H_{10}$) under the static electric field, using the density functional theory. Because corannulene has C-H bond at its edge and bowl shape structure, we investigate the possibility of molecular orientation control and bowl-to-bowl conformation change by the electric field. Our calculation demonstrated that corannulene molecule change its orientation from normal to parallel to field with increasing the field strength. Furthermore, under the strong perpendicular electric field, of which direction is opposite to the CH dipole, corannulene undergoes bowl-to-bowl conformation change via a flat conformation under the critical electric field of approximately 0.14 V/nm. By applying the opposite field, the apex of corannulene is steeper than that under the zero-field.

Corresponding Author: Susumu Okada (sokada@comas.frsc.tsukuba.ac.jp)

Survival of Sub-nm Carbon Nanotubes under Femtosecond Laser Shot: A TDDFT Study

○Yoshiyuki Miyamoto¹

¹ *Research Center for Computational Design of Advanced Functional Materials, National Institute of Advanced Industrial Science and Technology (AIST), Central 2, 1-1-1 Umezono, Tsukuba 305-8568, Japan*

Selection of narrow carbon nanotubes (CNTs) with diameters less than 1 nm is useful for semiconductor technologies thanks to their substantial energy bandgap. Yet, such thin CNTs are unstable due to their internal strain energy [1], thus thermal processes are not feasible to synthesize narrow CNTs. Chemical vapor deposition on catalytic alloys with specific surface condition [2] can make CNTs with unique chiral index with diameter less than 1 nm, but this technique does not suit for massive production. On the other hand, current work theoretically proposes application of linearly polarized femtosecond laser to select thin CNTs from CNT arrays with polarization vector of laser perpendicular to tube axes.

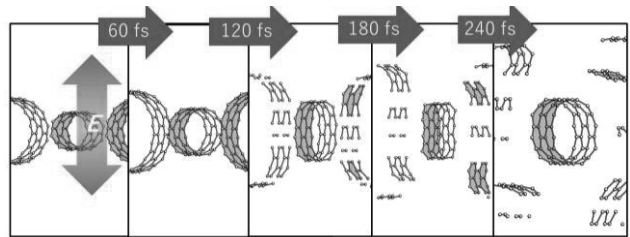


Fig. 1. Survival of (8,0) CNTs in an array of (8,0) and (14,0) CNTs. Blue arrows denote the simulation time and a red arrow denotes the polarization vector of the laser. All figures are from direction nearly parallel to tube axes and part of periodic structures of the CNT arrays are displayed.

Figure 1 demonstrates the ab-initio electron-ion dynamics of an array of (8,0) and (14,0) CNTs showing breakage of the (14,0) tubes but survival of the (8,0) tubes. This simulation assumed laser wavelength 800 nm and the pulse width 10 fs with maximum laser field as 5 V/\AA which is under accessible condition with current laser technology. The similar selection in armchair CNTs will also be demonstrated and physical origin of the selection will be discussed [3]. The calculation was performed by time-dependent density functional theory [4] using the code FPSEID [5].

This work has been performed under supports from the TACMI (Technical Alliance for Cool laser Machining with Intelligence) project commissioned by the New Energy and Industrial Technology Development Organization (NEDO), and from JSPS KAKENHI grant number JP19K05103. All calculations presented here were performed by using supercomputer systems in Cyberscience Center in Tohoku University and Cybermedia Center in Osaka University.

[1] D. Sánchez-Portal *et al.*, Phys. Rev. B **59**, 12678 (1999).

[2] F. Yang *et al.*, Nature **512**, 64 (2014).

[3] Y. Miyamoto, Nano Lett. **20**, 4416 (2020).

[4] E. Runge and E. K. U. Gross, Phys. Rev. Lett **52**, 997 (1984).

[5] O. Sugino and Y. Miyamoto, Phys. Rev. B **59**, 2579 (1999).

Corresponding Author: Y. Miyamoto

Tel: +81-29-849-1498, Fax: +81-29-861-3171,

Web: (our department home page is under construction)

E-mail: yoshi-miyamoto@aist.go.jp

One dimensionality of the thermoelectric properties in semiconducting single walled carbon nanotubes

○Yota Ichinose¹, Manaho Matsubara², Yohei Yomogida¹, Akari Yoshida¹, Kan Ueji¹, Kaito Kanahashi³, Jiang Pu⁴, Taishi Takenobu⁴, Takahiro Yamamoto², and Kazuhiro Yanagi¹

¹Department of Physics, Tokyo Metropolitan University, Tokyo, Japan

²Department of Physics, Tokyo University of Science, Shinjuku, Tokyo, Japan

³Department of Advanced Science and Engineering, Waseda University, Tokyo, Japan

⁴Department of Applied Physics, Nagoya University, Nagoya, Japan

Thermoelectrics is an important technology for the efficient conversion of waste heat to electrical power. Theoretical studies suggested that lowering the dimensionalities can enhance thermoelectric (TE) performance due to the following two factors, (1) the quantum confinement effect and (2) the reduction of thermal conductivity.¹ The enhancement of TE performance by the reduction of thermal conductivity has been confirmed, however, experimental verification of how low-dimensional electronic structures enhance TE performance remains elusive. Single-walled carbon nanotube (SWCNT) is a very good model for studying relationships between one-dimensional (1D) electric structure and TE properties. Our recent study revealed the unique 1D characteristic in their TE properties.² For example, in conventional metallic materials, the increase of their conductivity induces the decrease of their Seebeck coefficient, which is known as TE trade-off. By contrast, in the case of metallic SWCNTs, the trade-off is violated. We can observe the enhancement of both Seebeck coefficient and conductivity because of the presence of van-Hove singularity (vHs) in the density of states, reflecting 1D metallic electronic structures.² In the case of semiconducting SWCNTs, however, it is difficult to discuss 1D characteristics in their TE properties, because we cannot distinguish three, two or one-dimensional characteristics in the line shapes of Seebeck coefficient as a function of Fermi-level.

However, a recent theoretical study pointed out the importance of “thermoelectrical conductivity,” L_{12} .³ Only in the case of 1D materials, a sharp peak structure can be observed around 1st vHs in L_{12} . Thus, in this study, we investigated L_{12} of semiconducting SWCNTs with various chiralities and 2D materials. Fig. 1 shows L_{12} as a function of gate voltages in semiconducting SWCNTs with various chiralities. Only when we prepare (6,5) SWCNTs with the purity more than 99%, we could observe a sharp peak structure in L_{12} . This sharp peak structure reflects vHs structure. In this talk, we will discuss the background.

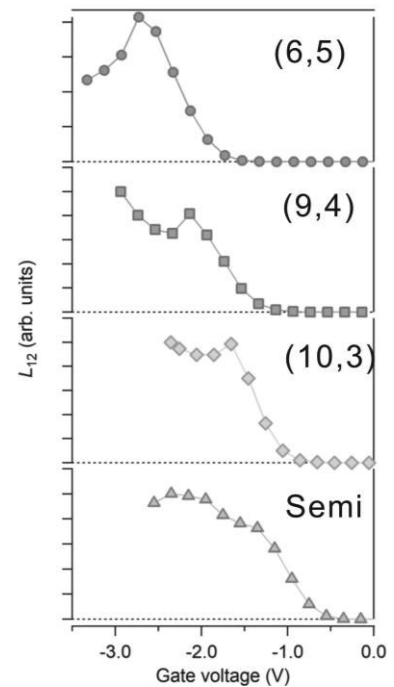


Fig. 1. Thermoelectrical conductivity, the L_{12} term, of (6,5), (9,4), (10,3) and Semi (semiconducting SWCNT with diameter of 1.4 nm) as a function of gate voltage.

References:

[1] Hicks & Dresselhaus, *PRB* **47**, 16631 (1993) [2] Ichinose et al., *Nano Lett.* **19**, 7370 (2019) [3] Yamamoto & Fukuyama, *JPSJ* **87**, 114710 (2018)

Corresponding Author: K. Yanagi, E-mail: yanagi-kazuhiro@tmu.ac.jp

Simple and Effective Method to Control Photoluminescence Properties of Single-walled Carbon Nanotubes by Ultrasonic Irradiation

○Yui Konno¹, Akane Nishino¹, Michio Yamada¹, Yutaka Maeda¹, Saki Okudaira², Yuhei Miyauchi², Kazunari Matsuda², Jun Matsui³, Masaya Mitsuishi⁴, Mitsuaki Suzuki⁵

¹ Department of Chemistry, Tokyo Gakugei University, Tokyo 184-8501, Japan

² Institute of Advanced Energy, Kyoto University, Uji 611-0011, Japan

³ Department of Material and Biological Chemistry, Yamagata University, Yamagata 990-8560, Japan

⁴ Institute of Multidisciplinary Research for Advanced Materials, Tohoku University, Sendai 980-8577, Japan

⁵ Department of Chemistry, Josai University, Saitama 350-0295, Japan

It has been reported that the sidewall functionalization is effective to control the local band structures of single-walled carbon nanotubes (SWNTs), resulting in emergence of new red-shifted photoluminescence (PL) peaks in the near-infrared region [1,2,3]. This allows the excitation with the E₁₁ energy to afford increase of the PL excitation efficiency, which is advantageous for bioimaging and so on. For the PL measurements, the use of low concentrated and individually dispersed solution of SWNTs is preferred for avoiding concentration quenching and unwanted interaction with other chiral SWNTs [4]. However, the sonication of SWNTs is also known to shorten and damage the SWNTs [5,6]. Meanwhile, surfactant decomposition has been studied and reported that the decomposition proceeds *via* generation of radical species from water upon ultrasonic irradiation [7]. Here we present the effects of ultrasonic irradiation on the PL properties of SWNTs under various conditions including different surfactants, concentration of SWNTs, and atmospheres.

In this study, sodium cholate (SC), sodium dodecylbenzene sulfate (SDBS), and sodium dodecyl sulfate (SDS) were selected as typical surfactants to disperse SWNTs in D₂O. To clarify the effect of ultrasonic irradiation, a small amount of SWNTs (initial concentration: 12.5 mg/L) was sonicated and centrifuged to prepare the SWNTs dispersion. The characteristic absorption and PL peaks of SWNTs were observed from the supernatant prepared using SC. On the other hand, the supernatant prepared using SDS exhibited low intrinsic absorption and PL peaks of SWNTs. When SDBS was used, the dispersibility of SWNTs was found to be as good as that obtained with SC. In this case, it is noteworthy that the new PL peaks at 1043 and 1118 nm emerged accompanied by decreasing the intrinsic PL peaks of SWNTs, as seen in the oxidation of SWNTs [1, 2]. The details of the control of the PL properties of SWNTs by ultrasonic irradiation will be discussed.

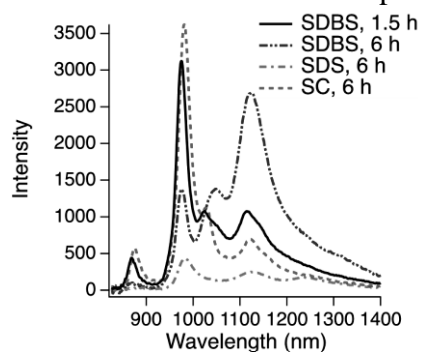


Fig. 1 PL spectra of SWNTs dispersion. Surfactant and sonication time are shown in the figure.

[1] R. B. Weisman *et al. Science* **330**, 1656 (2010) [2] Y. Maeda *et al. J. Am. Chem. Soc.* **135**, 6356 (2013) [3] Y. Wang *et al. Nat. Chem.* **5**, 840 (2013). [4] R. B. Weisman *et al. Science* **297**, 593 (2002). [5] M. D. Lay *et al. J. Phys. Chem. C* **114**, 12490 (2010). [6] F. Hennrich *et al. J. Phys. Chem. B* **111**, 1932 (2007). [7] M. Ashokkumar *et al. Aust. J. Chem.* **56**, 1045 (2003).

Corresponding Author: Y. Maeda

Tel: +81-42-329-7512

E-mail: ymaeda@u-gakugei.ac.jp

Utilization of transparent SWCNT films in 4-terminal perovskite-silicon tandem solar cells

*Ahmed Shawky*¹, *Kosuke Akino*¹, *Takuya Matsui*², *Taiki Inoue*¹, *Esko I. Kauppinen*³,
*Shohei Chiashi*¹, *Shigeo Maruyama*^{1,*}

¹ Department of Mechanical Engineering, The University of Tokyo, Tokyo 113-8656, Japan

² Research Center for Photovoltaics (RCPV), AIST, Tsukuba, 305-8568, Japan

³ Aalto University School of Science, Aalto, FI-00076, Finland

*Corresponding author: maruyama@photon.t.u-tokyo.ac.jp

Perovskite solar cells (PSC) recently showed much attention regarding easy fabrication and stability issues besides its high power conversion efficiency (PCE~25.2%). Also, single-walled carbon nanotubes (SWCNT) represent a great candidate to replace the metal electrodes and transparent conducting oxide (TCO) like ITO [1]. The SWCNT is a favourable electrode material, owing to its hydrophobic nature, earth-abundance, and mechanical robustness. The aerosol-synthesized SWCNT bottom electrode replacing TCO in PSCs has shown the most promising potential. Currently, numerous research is being conducted to improve the PCE of solar cells further, and one of the possibilities is the tandem structure, in which PSCs are stacked on silicon solar cells. To use PSC in a tandem structure, the electrode must have light transmissivity, and there have been reported examples of using a transparent conductive film as the electrode [2]. However, SWCNTs showed superior transparency in the longer wavelengths (800~1100 nm) [3]. We noticed a few works in which PSC using SWCNT electrodes applied to a tandem structure. In this study, we fabricated a tandem structure solar cell using an SWCNT-based PSC and silicon heterojunction (SHJ) solar cell [4]. The tandem structure solar cell device was prepared in advance, and conversion efficiencies of ~17.5% for SWCNT-PSC and ~6.5 % for bottom SHJ solar cells were obtained. The I-V characteristics and external quantum efficiency of the tandem structure solar cell with SWCNT-PSC confirmed that the perovskite-type solar cell using SWCNT is more transparent to light, and the SHJ solar cell as a tandem-structured bottom cell generates power by transmitted light depends on the transparency of SWCNTs. The obtained ~24.0% efficiency attituded among uppermost four-terminal perovskite-silicon tandem solar cells.

References

- [1] I. Jeon, T. Chiba, C. Delacou, Y. Guo, A. Kaskela, O. Reynaud, E. I. Kauppinen, S. Maruyama, Y. Matsuo, *Nano Lett.* 10 (2015) 6665.
- [2] I. Jeon, A. Shawky, S. Seo, Y. Qian, A. Anisimov, E. I. Kauppinen, Y. Matsuo, S. Maruyama, *J. Mater. Chem. A* 8 (2020) 11141.
- [3] C. Lee, S-W Lee, S. Bae, A. Shawky, V. Devaraj, A. Anisimov, E. I. Kauppinen, J.-W. Oh, Y. Kang, D. Kim, I. Jeon, S. Maruyama, H-S. Lee, *submitted*.
- [4] M. A. Green, E. D. Dunlop, J. Hohl-Ebinger, M. Yoshita, N. Kopidakis, A. W.Y. Ho-Bailli, *Prog. Photovoltaics* 28 (2020) 3

Simple and highly efficient intermittent operation circuit for triboelectric nanogenerator

○Atsushi Kawaguchi¹, Masahiro Matsunaga², Haruki Uchiyama¹,
Jun Hirotsu¹ and Yutaka Ohno^{1,2}

¹Department of Electronics, Nagoya University, Nagoya 464-8603, Japan

²Institute of Materials and Systems for Sustainability, Nagoya University, Nagoya 464-8601, Japan

With the arrival of the Internet of Things (IoT) society, there is an increasing demand for new power supply technologies to drive a large number of sensors. [1] Energy harvesting is attracting attention as an alternative of batteries for IoT sensors. In the previous study, we reported high output, transparent, and stretchable triboelectric nanogenerator (TENG) using carbon nanotube (CNT) thin film. [2] Since the TENGs generate the pulsed voltage, a power management circuit to generate DC voltage sufficient for driving sensor devices is necessary. To achieve this, we propose a simple and highly efficient intermittent operation circuit.

The proposed circuit is composed of bridge rectifiers, a capacitor, a programmable unijunction transistor (PUT), and two resistors as shown in Fig. 1. The pulsed output voltage of TENG is rectified and stored in the capacitor. The PUT acts as a switch which turns on when the voltage stored in the capacitor reaches a threshold determined by external resistors, so that, the stored energy is supplied to the load. Then, PUT returns to the off state and the capacitor starts being charged again.

We used the CNT based stretchable TENG. [2] The output voltage was generated by touching the surface of the TENG with a nitrile glove-worn hand at a frequency of 1 Hz. The peak power density was reached up to 8.0 W/m^2 at the load resistance of $30 \text{ M}\Omega$. Figure 2 shows the voltages across the capacitor and the load resistance of $1 \text{ M}\Omega$, respectively. The stored energy was intermittently supplied to the load with intervals of about 14 s. The efficiency through the PUT was reached up to 89%. We also demonstrated driving the electronic device using the TENG and proposed circuit.

[1] D. Oliveira *et al.*, *Electronics* **9**, 111 (2020).

[2] M. Matsunaga *et al.*, *Nano Energy* **67**, 104297 (2020).

Corresponding Author: Y. Ohno, Phone: +81-52-789-5387, E-mail: yohno@nagoya-u.jp

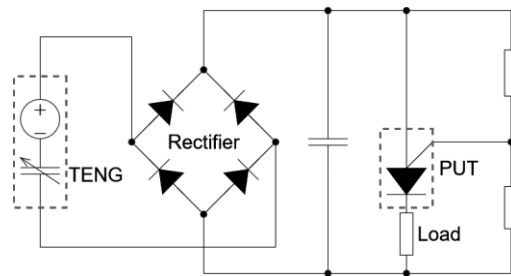


Fig. 1 Intermittent operation circuit consisting of TENG and PUT.

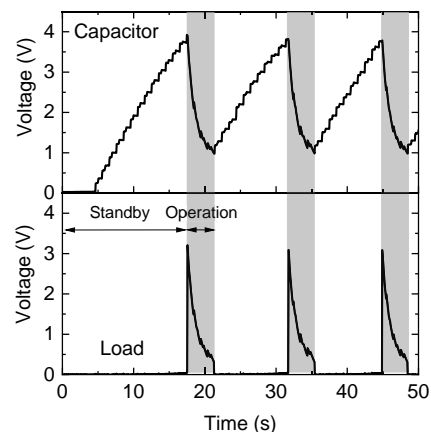


Fig. 2 Voltages across capacitor (upper) and load resistance (bottom).

Carbon nanotube-Cu through-Si-via interposer with Cu-level electrical conductivity and Si-comparable thermal expansion

○Guohai Chen¹, Rajyashree Sundaram¹, Atsuko Sekiguchi¹, Kenji Hata¹, Don N. Futaba¹

¹ CNT-Application Research Center, National Institute of Advanced Industrial Science and Technology (AIST), Tsukuba 305-8565, Japan

In microelectronic packaging, an interposer is an intermediate substrate acting as a bridge connecting the fine pitch I/Os at the dies to the coarse pitch package at the substrate. A through-silicon-via (TSV) interposer is a very common type with copper (Cu) filled inside the holes (“vias”) as interconnections. However, as the size of electronic devices decreases, heat generation significantly increases inside the miniature devices which results in deterioration in lifetime and reliability. Commonly, the deterioration originates from delamination or break at the interface due to the strain induced by the mismatch of the coefficient of thermal expansion (CTE) between Si and Cu. Therefore, the demands for interposer materials with high electrical conductivity but low CTE are growing.

Here, we demonstrate the fabrication of carbon nanotube-copper (CNT-Cu) composite TSV interposer (Fig. 1) to combine the high electrical conductivity of Cu with the low CTE of CNTs using a bottom-up and assembly approach. In short, an array of high aspect ratio CNT forest pillars was synthesized on lithographically patterned catalyst using water-assisted chemical vapor deposition [1-3]. Second, the CNT pillar arrays were infiltrated with Cu using a two-stage electrodeposition process developed previously [4-5]. Third, the CNT-Cu pillars were inserted into the prefabricated TSV wafer. Forth, the completed TSV interposer was released from the growth substrate. The CNT-Cu composite showed a Cu-level electrical conductivity ($\sim 2.5 \times 10^5$ S/cm) and Si-comparable CTE ($\sim 7 \times 10^{-6}$ /K). The CTE mismatch between CNT-Cu and Si was greatly reduced, less than 1/5 of that between Cu and Si. Finally, we demonstrate the operation in several applications highlighting the high electrical conductivity and small CTE mismatch. These results demonstrate the potential of the CNT-Cu TSV interposer in microelectronic packaging.

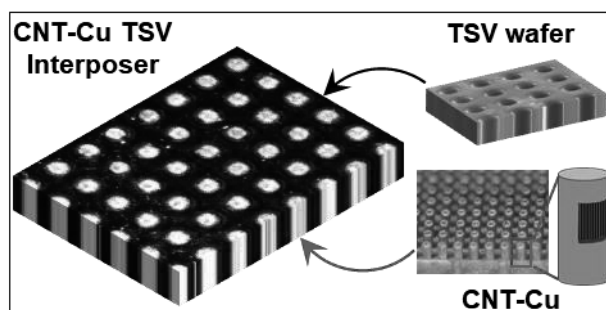


Fig. 1 CNT-Cu TSV interposer

- [1] G.H. Chen *et al.* ACS Nano, **7** (11), 10218 (2013).
- [2] G.H. Chen *et al.* Nanoscale, **8** (1), 162 (2016).
- [3] G.H. Chen *et al.* ACS Biomater. Sci. Eng., **4** (5), 1900 (2018).
- [4] C. Subramaniam *et al.* Nat Commun, **4**, 2202 (2013).
- [5] R. Sundaram *et al.* J Mater Res Technol, **9** (3), 6944, (2020).

Corresponding Author: G.H. Chen

Tel: +81-29-861-4416

Web: <https://unit.aist.go.jp/cnta/ja/member/Guohai.html>

E-mail: guohai-chen@aist.go.jp

Electrical detection of X-ray by using coplanar CNT thin-film electrodes on PEN substrate

○Satoru Suzuki¹, Hiroyuki Matsuda², Takahiro Ishikawa³, Teruaki Konishi³,
Tsuyoshi Hamano³, Hiroshi Ajiki¹, Yutaka Ohno^{4,5}, Toshio Hirao³, Satoshi Ishii¹

¹ Department of Physics, Tokyo Denki University, Saitama 350-0394, Japan

² Department of Engineering, Shinshu University, Nagano 380-8553, Japan

³ National Institute for Radiological Sciences, Chiba 263-8555, Japan

⁴ Department of Electronics, Nagoya University, Nagoya 464-8602, Japan

⁵ Institute of Materials and Systems for Sustainability, Nagoya University, Nagoya 464-8601, Japan

Radiation exposure to the eye lens has been a problem for a curer in the radiation therapy. Then, the transparent real-time dosimeter is required to measure the eye dose without disturbing their eyesight. In order to develop the transparent detector, transparency is necessary not only for the substrate but also for the electrode. Carbon nanotube is known to have transparency along with radiation tolerance [1]. In this study, we have fabricated the coplanar CNT thin-film electrodes on the PEN sheet and conducted the direct electrical detection of X-ray using these.

Figure 1 shows the schematic structure of the device, where the distance between the CNT thin-film electrodes was 1 mm. The electrodes were patterned on the PEN substrate by splay coating of the single-walled CNT dispersion in IPA (0.2 wt%) using the metal mask. The device was placed inside of the stainless chamber under a vacuum of 1.0×10^{-2} Pa. X-ray with an effective energy of 83 keV was irradiated to the device from outside of the chamber at a bias voltage of 10 V. The current of the device was measured in real time during turning on and off of the irradiation at each dose rate.

The current was confirmed to respond to the X-ray irradiation, as shown in Fig. 2. Moreover, the generated current increased linearly with the dose rate below 10.18 mGy/sec, as shown in Fig. 3, although it no longer changed linearly above 20.54 mGy/sec. It is thought that the generated current was the charges originated from the ionized residual gas inside the chamber, and that it did not reach the saturated region under the biased voltage. The CNT thin-film electrodes on the PEN sheet is applicable to the real-time transparent detector.

This work was supported partially by the joint usage/research program of the Institute of Materials and Systems for Sustainability (IMaSS), Nagoya University.

[1] S. Ishii *et al.* Physica E. **86**, 297 (2017).

Corresponding Author: S. Ishii

Tel: +81-49-296-1926, Fax: +81-49-296-2915,

E-mail: s.ishii@mail.dendai.ac.jp

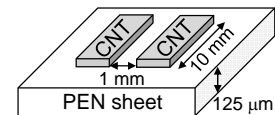


Fig.1 Device structure.

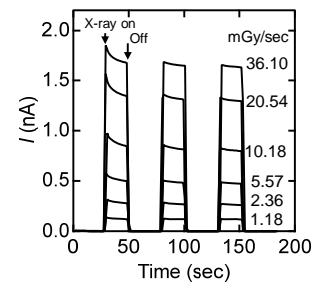


Fig.2 Time dependence of the current.

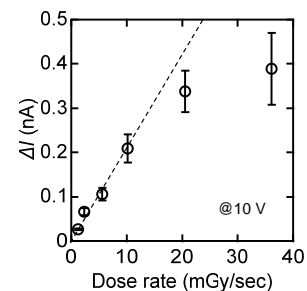


Fig.3 Dose rate dependence of the generated current.

Controlled synthesis of graphene nanoribbons from fluctuation-induced nanobar

○Naofumi Sato¹, Toshiro Kaneko¹, Toshiaki Kato^{1,2}

¹ Graduate School of Engineering, Tohoku University, Sendai 980-8579, Japan

² JST-PRESTO

In recent years, graphene nanoribbon (GNR), strips of two-dimensional (2D) graphene into one-dimensional (1D) structure gather intense attentions because of their superior electrical features. Although GNR can be made in a variety of ways, the reliable site and alignment control of GNR with high on/off current ratios remains a challenge.

Until now, we have developed a novel method based on the advanced plasma CVD with nanoscale Ni catalyst (Ni nanobar) for directly fabricating suspended GNR devices (Fig. 1(a) and (b)) [1, 2]. Further adjustments in the GNR structures such as the width, length and layer number can open up the application field of this novel material.

From our previous research, it can be conjectured that the locally-formed narrow part within the GNR may be the critical origin of high on/off current ratios. Such local structures can be formed by the Plateau-Rayleigh (P-R) instability during plasma CVD [2]. To improve the structure controllability of GNRs, controlling the P-R instability, especially initiation position of instability within nanoscale material, is one of the important subjects. Based on this background, we have developed a new approach introducing “fluctuation structures” within the initial Ni nanobar (Fig. 2). This structure includes circles and straight parts within single Ni nanobar. We expected that the straight (= narrower) part of Ni nanobar might be as a trigger for initiating P-R instability.

Based on this idea, we performed a GNR growth with changing the number of circles in the Ni nanobar. As a result, it was found that averaged on/off current ratios within the multiple GNR devices can be improved by adjusting the number of circles in the initial Ni nanobar, which can be explained by the balance between circle to circle distance and wavelength of P-R instability.

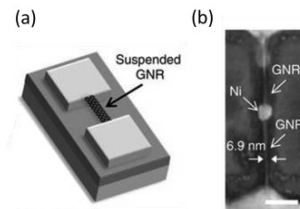


Fig. 1. (a) Schematic illustration of suspended GNR device. (b) Typical scanning electron microscope (SEM) image of suspended GNR grown by our plasma CVD. Scale bar in (b) shows 100 nm.

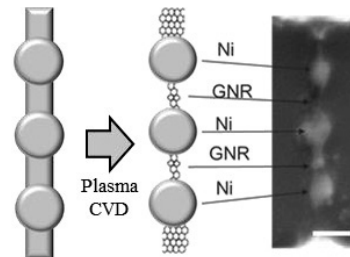


Fig. 2. Schematic illustration and SEM image of fluctuation structure of Ni nanobar and GNR. Scale bar in SEM image shows 100 nm.

[1] T. Kato and R. Hatakeyama, *Nature Nanotechnology*, **7**, 651-656 (2012).

[2] H. Suzuki, T. Kaneko, Y. Shibuta, M. Ohno, Y. Maekawa, T. Kato, *Nature Communications*, **7**, 11797-1-10 (2016).

Corresponding Author: N. Sato

Tel: +8122-795-7046, Fax: +8122-263-9225,

E-mail: naofumi.sato.s2@dc.tohoku.ac.jp

Fabrication of large Ni grain on sapphire substrate for graphene growth

○Asato Nakashima¹, Tatsuya Kashio¹, Tomoaki Murahashi¹, Tukasa Soga¹,
Takahiro Maruyama², and Shigeeya Naritsuka¹

¹ *Department of Materials Science and Engineering, Meijo University
Nagoya 468-8502, Japan*

² *Department of Applied Chemistry, Meijo University, Nagoya 468-8502, Japan*

Multilayer graphene (MLG) is a promising alternative to metal conductors in electrical conduction. Ni (111) is often used as a catalyst of graphene growth because it has a large carbon solubility befitting for the growth of multilayer graphene. Conventionally, Ni is used in a polycrystalline shape, which results in a poor quality of the grown MLG. On the other hand, in the case of single-crystalline Ni, superior MLG is expected to be grown with its orientation aligned to that of the catalyst. However, a single-crystalline Ni substrate is difficult to obtain and, moreover, very expensive.

We have been trying to crystallize Ni film with the aid of the crystal information of sapphire substrate. However, the Ni grains are not easy to be enlarged only by annealing. Therefore, in this study, we use an epitaxial Ni (111) layer grown on a sapphire substrate to crystallize the Ni layer deposited over it.

A 100 nm-thick Ni (111) layer was epitaxially grown on a c-plane sapphire substrate by MBE at a substrate temperature of 700 °C. In addition, 300 nm-thick Ni layer was deposited on the layer using electron beam deposition. Then, the sample was annealed at 1000 °C for 30 min to crystallize the whole Ni layer. The samples were investigated using Nomarski differential interference contrast microscopy (N-DICM) and X-ray diffraction (XRD) measurement.

Figure 1 shows (a) N-DICM image of the sample surface and (b) XRD in-plane spectrum of Ni (200) diffraction. From Fig. 1(a), it was found that a large Ni grain of about 5 mm×3 mm in size was obtained. The in-plane Ni (111) spectrum in Fig. 1(b) shows that its crystal orientation was well aligned to that of the sapphire substrate although it still contained twins. This can be attributed to the amorphous like Ni layer deposited by the electron beam deposition was successfully crystallized by the crystal information of the MBE grown Ni buffer layer during the subsequent annealing. At the time of the presentation, the graphene growth on the Ni layer will also be reported.

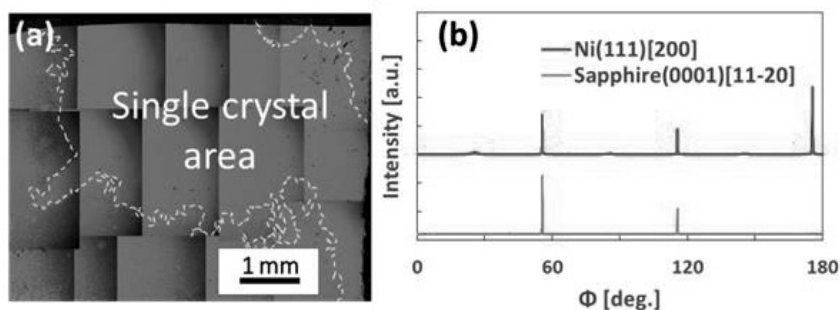


Fig.1 (a) N-IDCM image of Ni (111) layer after annealing and (b) XRD in-plane spectra.

Corresponding Author : A. Nakashima Tel: +81 90 9924 2059, E mail 193428014@c alumni.meijo-u.ac.jp

The Instructive Aspect of Moire-Patten Analysis of Rotation Less Than 0.5-degree on Twisted Bilayer Graphene by Tool for Computer Imaging

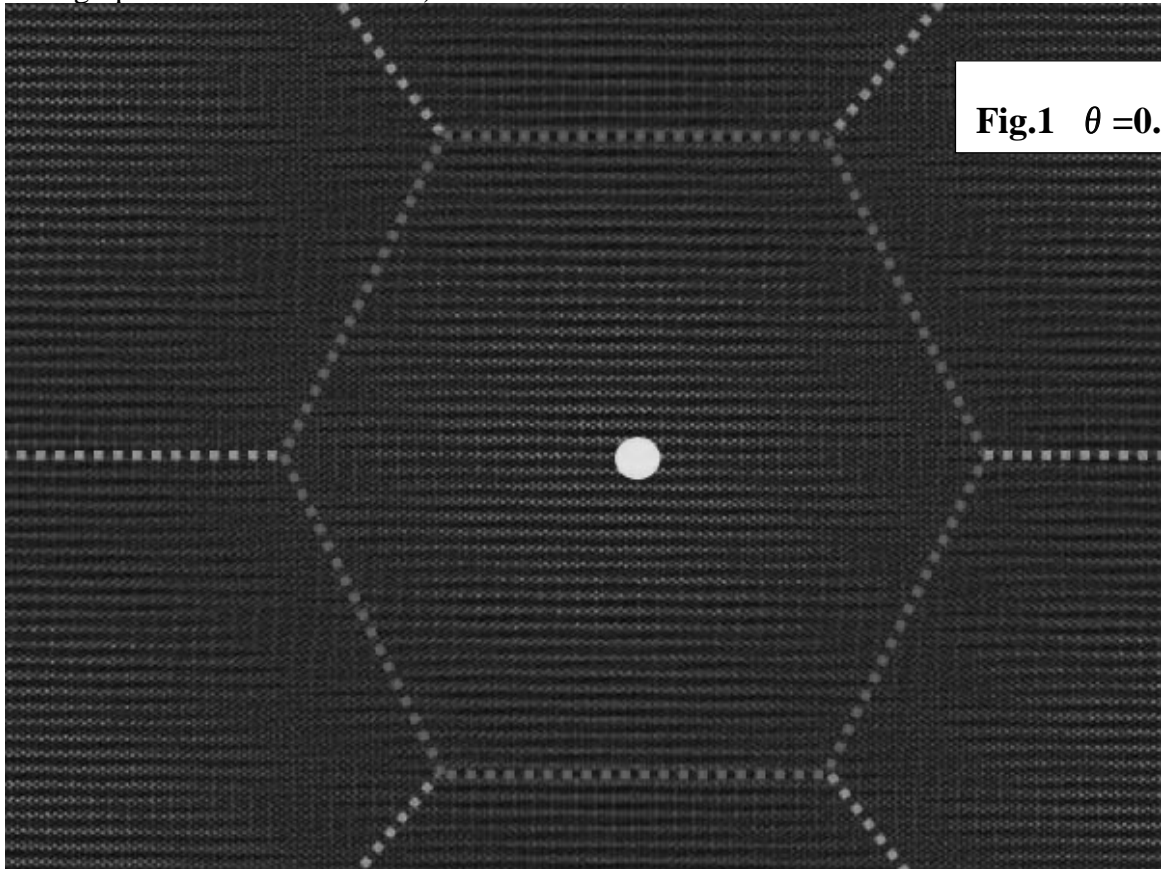
○Yuhei Natsume¹, Tohei Moritani²

¹International Education Center (IEC), Chiba University, Chiba 260-0033, Japan

²Yokohama Physics Circle, Japan

Recently, much attention has been paid to the relationship between moire-pattern and the superlattice structure in twisted bilayer graphene has been investigated from the viewpoint of appearance for flat bands originated from Dirac K-points in the single layer[1-3].

In these circumstances, we propose moire-pattern analysis by the use of tool for computer imaging from the viewpoint of the instruction. The typical example is shown in Fig.1, where the twisted angle θ is 0.3° . In this case, the super-lattice constant is $191a$. (Here, $a=0.246\text{nm}$ is the is graphene's lattice constant.)



Though there remains much problem as to the electronic properties in a quite large unit cell where the number of containing atoms is more than 100,000, the tool of computer imaging is quite powerful and instructive for the findings of super lattices. This tool should be used as the stimulating introduction to solid state electronics.

[1] R.Bistritzer and A.H. MacDonald, Proc. Natl. Acad. Sci. U.S.A. **108**, 12233 (2011).

[2] C.Berger, X. Song, X. Li, X. Wu, N. Brown, C. Naud, D. Mayou, T. Li, J. Hass, A.N. Marchenkov, E.H. Conrad, P.N. First and W.A. de Heer, Science **312**, 1191 (2006).

[3] M. Koshino et al., Phys Rev. X **8**, 031087 (2018).

Raman optothermal methods to measure interfacial thermal conductance of low-dimensional materials

○Qin-Yi Li^{1,2}, Koji Takahashi^{1,2}

¹ Department of Aeronautics and Astronautics, Kyushu University, Fukuoka 819-0395, Japan

² International Institute for Carbon-Neutral Energy Research (WPI-I2CNER), Kyushu University, Japan

Measurement and tuning of interfacial thermal conductance (ITC) between individual low-dimensional materials are of fundamental significance for a variety of applications including thermal management and thermoelectric energy conversion. However, the existing methods for measuring ITC at the nanoscale are extremely limited. Here, we present Raman based techniques to measure the ITC between 1D materials and layered 2D sheets. First, a totally non-contact transient Raman mapping method is developed to measure the ITC between individual 1D materials [1]. Focused laser is used to heat the sample and the laser absorptivity is experimentally determined by a transient Raman technique. The laser heating positions are changed along two connected 1D materials, and the change of temperature rise with varying positions is *in-situ* measured from the temperature dependent Raman band shifts. Further, a MEMS sensor is combined with Raman thermometry to improve the measurement accuracy of ITC between 1D materials. Second, a variable-spot-size transient Raman method is proposed to measure the ITC between atomic thin 2D layers in heterostructures [2]. Both pulsed and continuous-wave laser beams are used to heat the 2D heterostructure, and the temperature of each layer is detected from their distinct Raman shifts. By changing the laser spot sizes and pulse widths, both the in-plane thermal conductivity and ITC between every two layers can be simultaneously extracted from the multiple temperature curves.

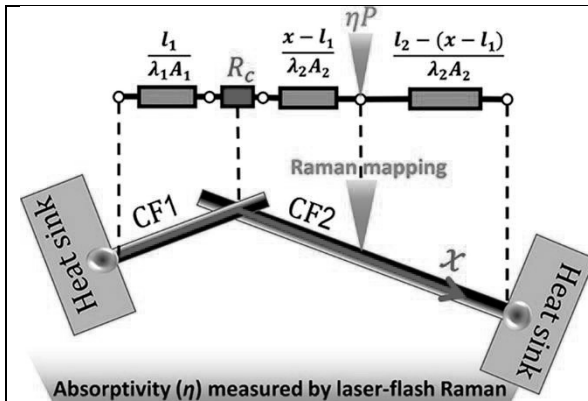


Fig. 1 Transient Raman mapping method to measure interfacial thermal conductance between 1D materials [1]

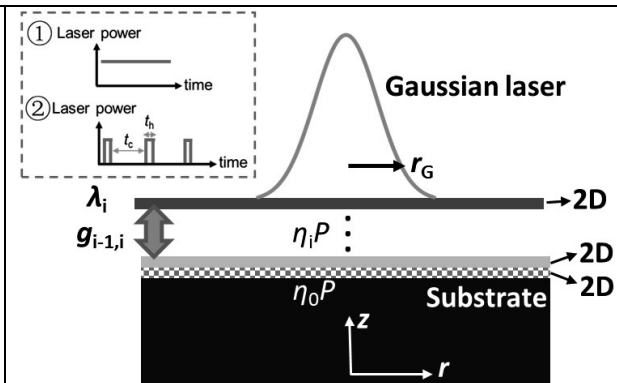


Fig. 2 Variable-spot-size transient Raman method to measure interfacial thermal conductance between 2D layers [2]

[1] Q.Y. Li *et al.*, Carbon, **141**, 92–98 (2019).

[2] Q.Y. Li *et al.*, Int. J. Heat Mass Transf., **125**, 1230–1239 (2018).

Corresponding Author: Q.Y. Li

Tel: +81-92-802-3016

E-mail: qinyi.li@aero.kyushu-u.ac.jp

Non-diffusive molecular transport in graphene liquid cells

Sota Hirokawa¹, Hideaki Teshima^{1,2}, Pablo Solis Fernandez³, Hiroki Ago³, Yoko Tomo⁴, Qin-Yi Li^{1,2}, Koji Takahashi^{1,2}

¹ Department of Aeronautics and Astronautics, Kyushu University, 744 Motoooka, Nishi-ku, Fukuoka 819-0395, Japan

² International Institute for Carbon-Neutral Energy Research (WPI-I2CNER), Kyushu University, 744 Motoooka, Nishi-ku, Fukuoka 819-0395, Japan

³ Global Innovation Center, Kyushu University, 6-1 Kasuga-koen, Kasuga-city, Fukuoka 816-8580, Japan

⁴ Department of Mechanical Engineering, Kyushu University, 744 Motoooka, Nishi-ku, Fukuoka 819-0395, Japan

Graphene liquid cells (GLCs) allows highest possible spatial resolution for liquid phase transmission electron microscopy (TEM)[1][2]. Here, we studied the nanoscale dynamics of bubbles induced by controllable damage of GLCs. The occurrence of graphene damage was ruled by electron dose rate depended on an acceleration voltage and a type of electron gun. Interestingly, during the observation of water pockets encapsulating no-bubbles, we never found the damage of GLC even with highest electron dose rate TEM. This fact indicates that electron beam induced damage in graphene depends on not only the electron dose rate but also whether there is bubbles in the GLC. After the graphene was damaged, air leakage caused dynamic behavior of bubbles, and we observed the unexpected the unexpected directional nucleation of new bubbles. This phenomenon is beyond the explanation of conventional diffusion theory. We attributed this to the effect of nanoscale confinement.

[1] J. M. Yuk *et al.*, *Science*, **336**, 61–64, (2012).

[2] D. Shin *et al.*, *Nat. Commun.*, **6**, 1–6, (2015).

Corresponding Author: K. Takahashi

Tel: +81-92-802-3015

E-mail: takahashi@aero.kyushu-u.ac.jp

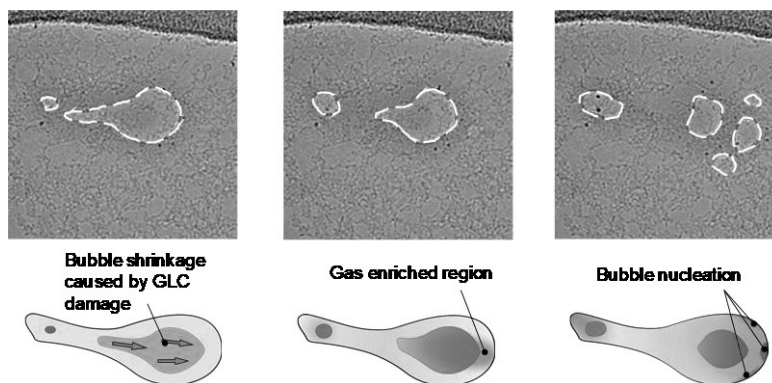


Fig.1. TEM images of dynamic bubble behavior and nucleation, and schematics of gas molecules transport in the GLC. White dash lines show outline of bubbles.

Layer-selective dopant implantation in van der Waals heterostructures

○Hiroto Ogura¹, Yuya Murai², Toshifumi Irisawa³, Zheng Liu⁴, Hiroshi Shimizu¹, Hong En Lim¹, Yusuke Nakanishi¹, Takahiko Endo¹, Ryo Kitaura², Yasumitsu Miyata¹

¹ Department of Physics, Tokyo Metropolitan University, Hachioji 192-0397, Japan

² Department of Chemistry, Nagoya University, Nagoya 464-8602, Japan.

³ Nanoelectronics Research Institute, AIST, Tsukuba, 305-8562, Japan

⁴ Innovative Functional Materials Research Institute, AIST, Nagoya, 463-8560, Japan

Two-dimensional (2D) transition metal dichalcogenides (TMDCs) have attracted much attention because of their unique physical properties and future device applications. To control their electronic properties, dopant implantation in TMDCs provides an effective way. For example, it is known that *p*-type doping can be achieved by Nb substitution for Mo or W atoms due to the formation of acceptor levels [1, 2]. However, the element substitution in channel layer has generally several issues such as reduced carrier mobility due to increased carrier scattering, and uncontrollable impurity levels. To address these issues, we focus our attention on the separation of impurity-doped layer and channel layer in van der Waals (vdW) heterostructures.

In this study, we have investigated the effect of Nb atomic beam irradiation in TMDC-based vdW heterobilayers. The heterobilayers such as MoS₂/WS₂ were prepared by chemical vapor deposition [3]. These samples were irradiated with atomic beams of Nb and Se at 500°C in ultrahigh vacuum (Fig.1a) [4]. As shown in Fig.1b, the Raman peaks of WS₂ around 350 and 420 cm⁻¹ are reduced after the irradiation. In contrast, there is almost no change in the Raman peaks of MoS₂ for 380~410 cm⁻¹ after the same treatment. Similar tendency is also observed for PL spectra of these samples. These results suggest that the effect of Nb irradiation is suppressed for bottom MoS₂ monolayer by the presence of top WS₂ monolayer in WS₂/MoS₂. In other words, the present process can preferentially implant the impurity atoms in the upper layer in vdW heterostructures, which could provide a promising way to realize controlled carrier doping of various 2D materials.

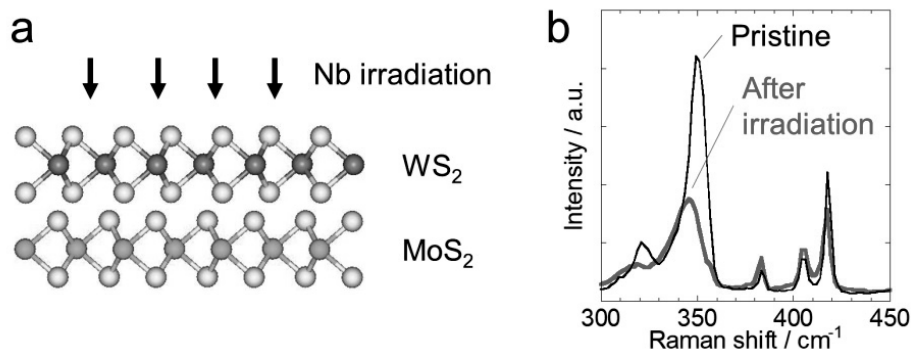


Figure 1 (a) Schematic illustration of Nb atomic beam irradiation for WS₂/MoS₂ heterobilayer. (b) Raman spectra of pristine and Nb-irradiated WS₂/MoS₂ heterobilayers.

[1] J. Suh *et al.*, Nano Lett, **14**, 6976 (2014). [2] L.-P. Feng *et al.*, Nanoscale, **8**, 6507 (2016).

[3] K. Kojima *et al.*, Nanoscale, **11** 12798 (2019). [4] Y. Murai *et al.*, in preparation.

Corresponding Author: Y. Miyata, Tel: +81-42-677-2508, E-mail: miyata-yasumitsu@tmu.ac.jp

Hydrogen adsorption effects on the electronic properties of TaS₂

○Yasushi Ishiguro¹, Naoko Kodama², Kirill Bogdanov³, Alexander Baranov³,
Kazuyuki Takai^{1,2}

¹ Dept. of Chemical Science and Technology, Hosei University, Tokyo 184-8584, Japan

² Graduate School of Science and Engineering, Hosei University, Tokyo 184-8584, Japan

³ St. Petersburg National Research University of Information Technologies, Mechanics and Optics, Saint Petersburg 197101, Russia

Tantalum disulfide (TaS₂) is a typical two-dimensional (2D) material that exhibits a charge density wave (CDW) phase transitions [1,2]. Recently, it has been reported that the transition temperatures and the electronic properties behave differently from those in bulk crystals when the dimensionality (number of layers) is modulated. In the case of 2D materials, it is known that the interfacial interactions with the substrate or adsorbed molecules has a great influence on the electronic properties of the 2D material. However, regarding TaS₂, the effects of the interfacial interactions on its electronic properties and the CDW phase transitions have not been clarified. In our study, the hydrogen adsorption effect in the Nearly-Commensurate (NC) CDW and Incommensurate (IC) CDW phases of exfoliated TaS₂ thin film, was investigated in terms of the change of electrical conductivity.

The TaS₂ thin films were prepared by mechanical exfoliation of bulk crystals of TaS₂ grown by the chemical transport synthesis on a SiO₂ (285 nm) / Si substrate. A FET device for the conductivity measurement were fabricated by EB-lithography process. Electrical conductivity measurements were conducted in a vacuum chamber equipped with a temperature-controlled stage and H₂ gas line. The partial pressure of H₂ and the device temperature were controlled throughout the measurements.

Figure 1 shows time dependence of electrical resistivity of TaS₂ thin film in the ICCDW phase (up to 500 K), where H₂ gas is intermittently introduced. The vertical axis represents the ratio of the change of the resistance $\Delta R = (R - R_0) / R_0$ (%), where R_0 and R are the resistance at $t = 0$ under vacuum, and the resistance at each time. When H₂ gas is introduced, the electrical resistance R decreases, and recovers after evacuation of the H₂ gas. The ratio of change ΔR increases as the pressure of introduced H₂ gas increases. The response times when hydrogen gas is introduced and when the gas is evacuated are obviously different. The response time for introduction of the gas takes more than 20 minutes, while the response time for the evacuation takes less than 5 minutes. The $I_{SD} - V_{SD}$ characteristics before and after introduction of H₂ gas maintain the linear characteristics and show no change in the slope, indicating ohmic contact between electrodes and the thin films maintains after H₂ adsorptions.

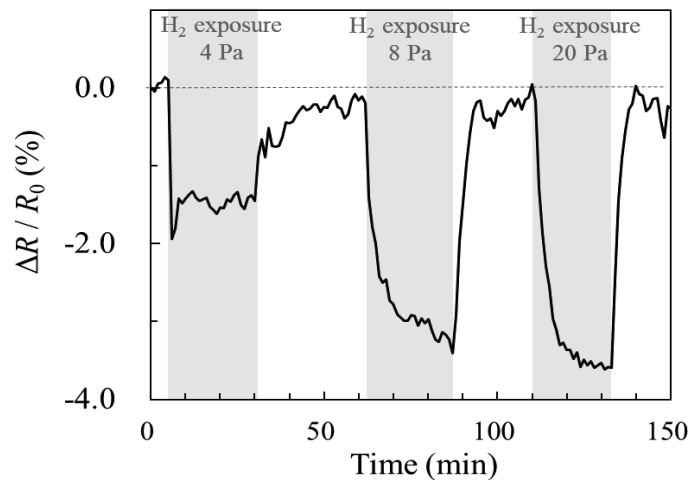


Fig. 1. The ratio of the change of the resistivity for different H₂ gas pressures

[1] Y. Yu *et al.*, Nat. Nanotechnol., **10**, 270 (2015)

[2] I. Lutsyk *et al.*, Phys. Rev. B., **98**, 195425 (2018)

Simple formula of enhancement of the electric field inside a hollow metallic cylinder

○Yuan Tian, M. Shoufie Ukhtary, Riichiro Saito

Department of Physics, Tohoku University, Sendai 980-8578, Japan

Hollow metallic cylinder with dielectric core (fig.1) is a good model in representing the character of tips used in tip enhancement Raman spectroscopy (TERS) [1]. Further, photovoltaic devices inside the metallic hollow core is synthesized for enhancing the photoelectric efficiency [2]. For such application, the enhancement of electric field inside the cylinder should be optimized. E. Devaux *et.al.* showed that the electric field is enhanced because the surface plasmon (SP) is excited [3]. Although the existence of SP in the cylinder and its relation with the enhancement are already studied, designing the cylinder which gives a large enhancement is still not easy because the SP is excited resonantly in which resonant condition is not given analytically and depends on the geometry of the cylinder. If the enhancement of electric field is given as a function of the geometry and the frequency of the light, we could design the hollow cylinder which gives the largest enhancement for a given frequency of light, which is our motivation.

In this work, we calculate the enhancement of the electric field inside the hollow core as function of geometry parameters and the frequency. Then we fit the enhancement to a simple formula for the previous purpose

In Fig. 2, we plot the enhancement of the electric field inside the hollow core as a function of the frequency. The enhancement plot can be fitted to a Lorentzian function of frequency. The parameters of the Lorentzian, such as the peak frequency and the peak value is further fitted by geometry parameters a_1 and d . We thus obtain a simple formula of enhancement as function of the light frequency and the geometry parameters (a_1, d) which is useful for finding the optimized geometry of cylinder to give the largest enhancement.

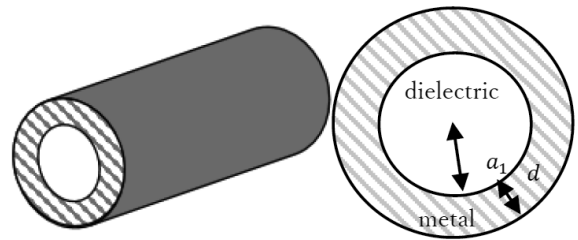


Fig. 1 The hollow metallic cylinder, with an inner radius a_1 and a thickness d .

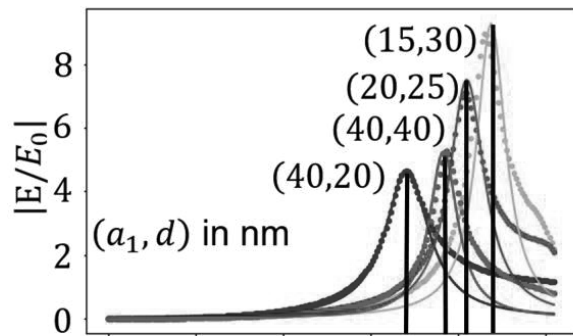


Fig. 2 The enhancement as a function of the frequency for several (a_1, d) . Dot represents the calculated result and the solid line represents the fitted function. Vertical lines represent the peak frequency.

Reference:

- [1] Alexander S. Mxleod *et.al.*, Phys. Rev. B 90, 085136 (2014)
- [2] Joseph D. Christesen *et.al.*, Nano Lett. 12, 11, 6024-6029 (2012)
- [3] U. Schroeter, E. Devaux *et.al.*, Phys. Rev. B 64, 125420 (2001)

Tellurization of solution-synthesized tungsten oxide nanowires

○Mai Nagano, Yohei Yomogida, Yasumitsu Miyata, and Kazuhiro Yanagi*

Department of Physics, Tokyo Metropolitan University, Tokyo 192-0397, Japan

Transition-metal dichalcogenide nanotubes have cylindrical structures of rolled MX_2 sheets (MX_2 , $\text{M} = \text{W}$, $\text{X} = \text{S}$, Se , Te) with unique physical properties. The physical properties of these inorganic nanotubes exhibit various properties depending on constituent elements. Among various compositions, tellurides such as WTe_2 attract a lot of interest because of their unique semi-metallic properties. However, synthesis of semi-metallic nanotubes such as WTe_2 nanotubes has not been achieved yet, although various semiconducting nanotubes such as WS_2 , MoS_2 and WSe_2 have been synthesized. One of approaches to synthesize such WS_2 (WSe_2) nanotubes is the sulfurization (selenization) of tungsten oxide nanowires [1,2]. Thus, in this study, we investigated whether WTe_2 nanotubes could be obtained by tellurization of the tungsten oxide nanowires.

The tungsten oxide nanowires obtained by solvothermal synthesis were reacted with Te for 30 min in Ar and H_2 flow. Te is known to be less reactive than S and Se. Thus, here we introduced NaOH as catalyst to promote tellurization, where NaOH produces highly reactive Na_2Te by the reaction with Te [3]. We varied the amount of NaOH and the temperature of tellurization.

Fig. 1 shows Raman spectra of samples synthesized with various amounts of NaOH. In the sample produced with 2 μmol of NaOH, we could observe the Raman peaks of WTe_2 , suggesting the success of tellurization. On the other hand, without NaOH or with a larger amount of NaOH, we cannot observe the Raman peaks of WTe_2 . These results indicate that the controlled amount of NaOH significantly influences the tellurization. However, we found that the produced samples were not nanotubes but nanowires according to the TEM measurements on the samples.

References:

- [1] Y. Yomogida et al, Appl. Phys. Express 12, 085001 (2019)
- [2] Y. Yomogida et al, Appl. Phys. Lett 116, 203106 (2020)
- [3] S. Yun et al, Nature Communications 8:2163 (2017)

Corresponding to Kazuhiro Yanagi
e-mail: yanagi-kazuhiro@tmu.ac.jp

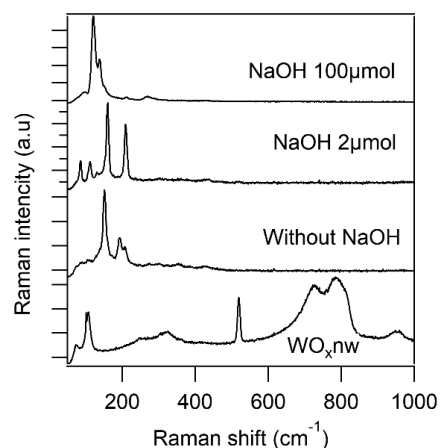


Fig 1: Raman spectra of samples after tellurization on WO_x nanowires with different amount of NaOH

First-principles calculation of excitonic effect in Raman spectra

○Pang Xiaoqi¹, Nguyen T. Hung², Riichiro Saito¹

¹*Department of Physics, Tohoku University, Sendai 980-8578, Japan*

²*Frontier Research Institute for Interdisciplinary Sciences, Tohoku University, Sendai 980-8578, Japan*

Coulomb interaction between a pair of electron and hole influences the optical properties of materials, which is known as excitonic effect. Usually, by optical absorption spectroscopy, we can observe the excitonic effect on many materials, especially for 2D materials. In fact, the observed absorption spectra show the existence of an exciton. Although experimental groups report the excitonic properties, the quantitative analysis by the theoretical calculation for Raman spectra is not yet possible for the transition metal dichalcogenide. Therefore, the theoretical analysis based on first-principles calculation which can calculate the exciton-photon interaction, is necessary to explore how excitons affect the optical Raman spectral.

In this work, we use Yambo code [1] to calculate the eigen values and eigen vectors of exciton. The optical absorption of monolayer and heterostructure transition metal dichalcogenide are discussed by the calculated results. Further, by using the eigen vector of exciton, we also discuss how to develop the program of excitonic Raman spectra (Fig.1).

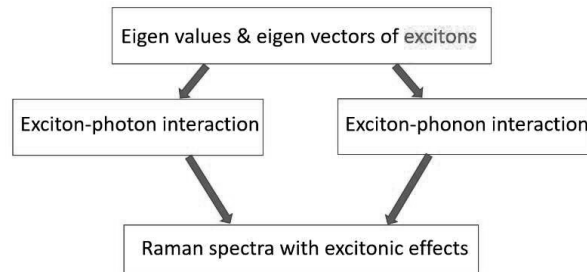


Figure 1: The flow chart to calculate resonant Raman intensity including excitonic effect

[1] Andrea Marini *et al* Comput. Phys. Commun. 180, 1392-1403 (2009)

Corresponding Author: Pang Xiaoqi

Tel: +81-22-795-6442, Fax: +81-22-795-6447,

E-mail: pang@flex.phys.tohoku.ac.jp

Photoluminescence property changes of locally functionalized single-walled carbon nanotubes using structural differences of proximal modifiers

○Haruka Aoki¹, Naoki Tanaka^{1,2}, Tsuyohiko Fujigaya^{1,2,3}, Tomohiro Shiraki^{1,2}

¹ Graduate School of Engineering, Kyushu University, Fukuoka 819-0395, Japan

² WPI-I2CNER, Kyushu University, Fukuoka 819-0395, Japan

³ Center for Molecular Systems, Kyushu Univ, Fukuoka 819-0395, Japan

Single-walled carbon nanotubes (SWNTs) with semiconducting features show photoluminescence (PL) in the near infrared regions (900-1600 nm), which is applicable to bioimaging probes and telecom devices. The PL properties of SWNTs are determined by the photogenerated exciton that is a bound state of an electron and a hole by Coulombic interactions. Recently, local chemical functionalization of SWNTs have been reported for sp^3 carbon defect doping to the crystalline sp^2 carbon lattice to produce locally functionalized SWNTs (lf-SWNTs). [1-3] The lf-SWNTs emit redshifted and brighter E_{11}^* PL than E_{11} PL, which is due to trapping and localization of the diffusive excitons at the defect doped sites having narrower bandgaps. We have reported proximal modification of SWNTs using bis-aryldiazonium salts (bADs) [2]. The synthesized lf-SWNTs (lf-SWNT-bA) showed largely redshifted PL (E_{11}^{2*}) than E_{11}^* PL over 100 nm. In addition, there is a strong correlation between the E_{11}^{2*} PL wavelength shifts and the chemical structures of bADs, which was observed by changing their methylene spacer lengths and connected positions on the aryl groups [3]. Therefore, proximal modification would provide unique techniques for PL property modulation of the lf-SWNTs.

In this study, we newly synthesize lf-SWNTs using multi points-aryldiazonium salts (mADs) that could allow proximal multipoint modification and investigate the effects of proximal modification structures on the PL properties of lf-SWNTs.

The SWNTs (CoMoCAT, (6,5) chirality-rich) were solubilized in D₂O containing sodium dodecyl sulfate by sonication. After ultracentrifugation, the supernatant was collected as a SWNT solution. The synthesized mAD was mixed with the SWNT solution for local chemical functionalization to produce lf-SWNTs-mA. In the PL spectrum of lf-SWNTs-mA, PL peaks were observed over 1200 nm wavelength regions. In vis/NIR absorption and Raman scattering measurements, absorbance at 980 nm decreased and the intensity of D-band that related to the defect introduction increased, respectively. These results show that the local chemical functionalization of SWNTs occurs by the reaction with mAD. In addition, we found that the reaction conditions such as solution concentrations significantly influenced such longer wavelength PL generation. The details regarding the chemical structure effects of the modifiers and the reaction condition dependency will be discussed at the symposium.

[1] Y. Wang *et al.*, *Nat. Chem.*, **5**, 840 (2013).

[2] T. Shiraki *et al.*, *Sci. Rep.*, **6**, 28393 (2016).

[3] T. Shiraki *et al.*, *Chem. Lett.*, **48**, 791 (2019).

Corresponding Author: T. Shiraki

Tel: +81-092-802-2841, Fax: +81-092-802-2840,

Web: <http://www.chem.kyushu-u.ac.jp/~fifth/jp/>

E-mail: shiraki.tomohiro.992@m.kyushu-u.ac.jp

Temperature dependence of Seebeck coefficients in Semiconducting and Metallic Single-Wall Carbon Nanotube film.

○Akari Yoshida, Yota Ichinose, Kengo Fukuhara,
Kan Ueji, Yohei Yomogida and Kazuhiro Yanagi

Department of Physics, Tokyo Metropolitan University, Tokyo 192-0397, Japan

Temperature dependence of Seebeck coefficient is a very important parameter to understand carrier transport mechanisms. According to the Mott's equation, in a variable range hopping (VRH) conduction, both the conductivity and Seebeck coefficient decrease as the decrease of temperature. Semiconducting single-walled carbon nanotube (SWCNT) thin films usually exhibit VRH conduction, so both the absolute value of the Seebeck coefficient and the conductivity usually decrease as the decrease of temperature. However, recent theoretical calculations suggested that when the chemical potential is located inside the semiconducting band gap of the van hove singularities, the Seebeck coefficient exhibits an opposite temperature dependence such as the increase of the Seebeck coefficient as the decrease of temperature.[1] Therefore, in order to understand the background of the thermoelectric properties of hopping conduction systems, we investigate the temperature dependence of Seebeck coefficients of semiconducting and metallic SWCNTs with controlled carrier injection by electrolyte gating approaches.

We employed our home-build thermoelectric measurement setups on the thin films of semiconducting and metallic SWCNT with a diameter of 1.4 nm. Here we used ionic gels as gate-electrolyte. The amount of injected carriers into the sample was controlled by the shift of the gate voltage (V_G) and the temperature dependence of the Seebeck coefficient at various V_G was investigated.

Figure 1 shows the temperature dependence of the Seebeck coefficient of semiconducting SWCNT thin films with a series of V_G . When the Fermi level is located in the band ($V_G = +0.8$ V: ◆, $+1.5$ V: ▲), the Seebeck coefficient decreases as the decrease of temperature. This is the conventional behavior of the hopping conduction system. Remarkably, when the Fermi level is located in the energy gap ($V_G = +0.3$ V: ▼ and $+0.4$ V: ■), the Seebeck coefficient increased as the decrease of temperature. In the case of metallic SWCNTs, we always observed the decrease of Seebeck coefficients at any V_G . Increase of Seebeck coefficient was only observed when the Fermi-level was properly tuned in semiconducting SWCNT thin films.

[1] Yamamoto&Fukuyama, JPSJ 87, 114710 (2018)

Corresponding Author: K. Yanagi

E-mail: yanagi-kazuhiro@tmu.ac.jp

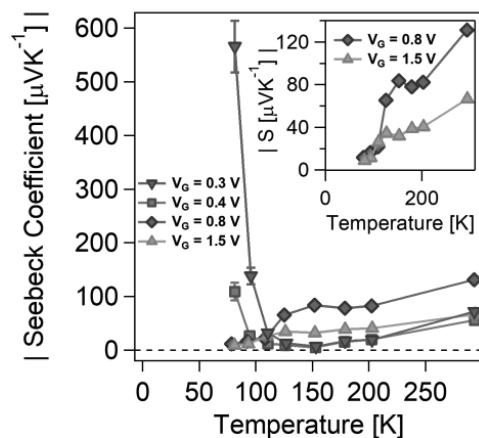


Fig. 1 Temperature dependence of Seebeck coefficient in semiconducting SWCNTs thin films.

Effects of pyrene derivatives on photoluminescence properties of single-walled carbon nanotubes

○Boda Yu¹, Tsuyohiko Fujigaya^{1,2,3}, Tomohiro Shiraki^{1,2}

¹ Graduate School of Engineering, Kyushu University, Fukuoka 819-0395, Japan

² WPI-F²CNER, Kyushu University, Fukuoka 819-0395, Japan

³ Center for Molecular Systems (CMS), Kyushu University, Fukuoka 819-0395, Japan

Semiconducting single-walled carbon nanotubes (SWNTs) show near-infrared (NIR) photoluminescence (PL) and are expected as promising materials for optical applications including bioimaging and telecommunication devices. Their PL properties are known to be influenced by surrounding materials such as solvent and surfactant molecules, which is recognized as microenvironmental effects [1]. In particular, aromatic molecules could strongly interact with SWNT surface by π - π interactions and, therefore, be used as a motif of dispersants for SWNTs in aqueous media [2]. Recently, we have reported strong interactions of such aromatic molecules with the SWNTs that were locally functionalized by defect doping through chemical functionalization with aryldiazonium salts (lf-SWNTs) [3]. This finding implies that aromatic molecules could be employed for the modulation of PL properties of not only pristine SWNTs but also lf-SWNTs.

In this study, we investigate the effects of pyrene derivatives on the PL properties of pristine SWNTs or lf-SWNTs by mixing these components. Firstly, we synthesized a cationic pyrene derivative (compound 1: **Fig. 1**) and mixed with solubilized SWNTs (CoMoCAT, (6, 5) chirality-rich) in D₂O using a surfactant. **Fig. 2** shows PL spectra of pristine SWNTs and the mixture of SWNTs and compound 1. In both spectra, we observed a PL peak around 986 nm, which was ascribable to E_{11} PL. The addition of compound 1 resulted in 12 nm redshift and decreased intensity of the E_{11} PL. Such phenomena is similar to the result reported from Dai *et al.* [4] and could be considered due to interactions between compound 1 and SWNTs providing dielectric environmental changes. Details including the results using lf-SWNTs will be discussed at the symposium.

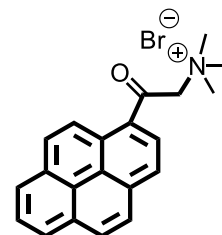


Fig. 1. Chemical structure of compound 1.

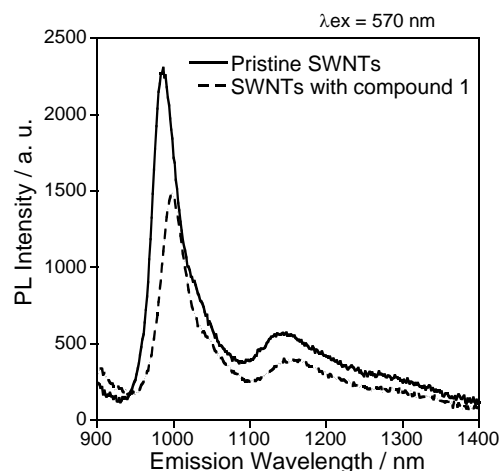


Fig. 2. PL spectra of pristine SWNTs (solid line) and the mixture of SWNTs with compound 1 (dashed line).

[1] Y. Ohno *et al.*, Phys. Stat. Sol. B **244**, 4002 (2007).

[2] N. Nakashima *et al.* Chem. Lett. **25**, 638 (2002).

[3] T. Shiraki *et al.* Chem. Commun. **55**, 3662 (2019).

[4] S. M. Tabakman *et al.* J. Phys. Chem. C **114**, 19569 (2010).

Corresponding Author: T. Shiraki

Tel: +81-092-802-2841, Fax: +81-092-802-2841,

Web: <http://www.chem.kyushu-u.ac.jp/~fifth/jp/>

E-mail: shiraki.tomohiro.992@m.kyushu-u.ac.jp

MoO₃ Doping of Carbon Nanotube Top Electrodes for Highly Efficient Metal-Electrode-Free Perovskite Solar Cells

Seungju Seo¹, Il Jeon¹, Kosuke Akino¹, Hiroki Nagaya¹, Esko I. Kauppinen², Yutaka Matsuo^{1,3}, Shigeo Maruyama^{1,4}

1. Department of Mechanical Engineering, School of Engineering, The University of Tokyo
2. Department of Applied Physics, Aalto University School of Science
3. Institutes of Innovation for Future Society, Nagoya University
4. Energy NanoEngineering Laboratory, National Institute of Advanced Industrial Science (AIST)

ABSTRACT

As an alternative to the metal electrodes, single-walled carbon nanotube (CNT) as the top electrode has been reported to achieve high stability in Perovskite Solar Cells (PSCs) owing to the hydrophobic nature of carbon and avoiding the ion migration. In addition, it drastically reduces the fabrication cost as it can be easily deposited onto devices by a simple mechanical transfer. Despite such advantages, there are three factors limiting the PCE of the CNT top electrode-based PSCs that need to be addressed: (1) the unfavorable work function of the CNT with respect to the active perovskite layer, leading to loss in voltage potential, (2) lower conductivity than the metal counterparts, limiting the fill factor (FF), and (3) less refractive nature with respect to incident light leading to loss in short-circuit current.

Here, we address those three issues by engineering the CNT top electrode. We tuned the work function of CNT electrodes and hole selectivity by depositing MoO₃ under vacuum, without damaging underneath perovskite layers. Using photoelectron yield spectroscopy, absorbance and raman spectroscopy, we determine the necessary MoO₃ thickness to efficiently dope the CNT top electrode and study underlying doping mechanism between CNTs and MoO₃ to achieve highly efficient CNT top electrode-based PSCs.

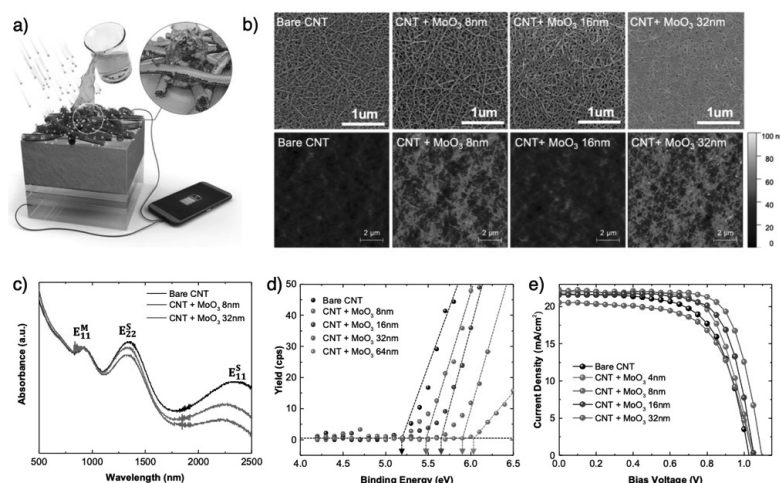


Figure 1 a) Schematics of PSC with MoO₃ doped CNTs. b) AFM and SEM images of CNT film with MoO₃. c) Absorbance spectra of CNTs with MoO₃. d) PYS Spectra of CNT film with MoO₃. e) J-V curve of PSC device with MoO₃ doped CNTs.

Corresponding Author: Prof. Shigeo Maruyama (maruyama@photon.t.u-tokyo.ac.jp)

Monitoring of adsorption behavior of serum albumin onto the single-walled carbon nanotube functionalized with fatty acid

○Kenta Nakamura¹, Yoshiaki Niidome¹, Yukiko Nagai¹, Naoki Tanaka¹, Tomohiro Shiraki^{1,2}, Takeshi Mori^{1,3}, Yoshiki Katayama^{1,3,4}, Tsuyohiko Fujigaya^{1,2,4}

¹ Department of Applied Chemistry, Kyushu University, Fukuoka 819-0395, Japan

² WPI-I2NER, Kyushu University, Fukuoka 819-0395, Japan

³ The Center for Future Chemistry, Kyushu University, Fukuoka 819-0395, Japan

⁴ CMS, Kyushu University, Fukuoka 819-0395, Japan

Single-walled carbon nanotubes (SWNTs) are attracting increasing attentions in biological applications because of their unique thermal, physical and optical properties. To use SWNTs for in vivo applications, SWNTs need to be biocompatible. Up to date, coating of SWNTs with biocompatible materials especially polyethylene glycol (PEG) has been investigated due to its stealth property [1]. However, it was pointed that the PEG-modified materials are rapidly excreted from the blood due to an immune reaction when they are repeatedly administered, which is known as accelerated blood clearance (ABC) phenomenon [2]. To avoid such a problem, serum albumin (SA) attracts recent attention as an alternative material of PEG since SA is a blood protein derived from a living body. However, since the adsorption coefficient of SA onto SWNT surface is lower than that of the other proteins [3], the increase of the adsorption to avoid the risk of the replacement might be necessary. Therefore, in this study, we introduced fatty acid onto the surface of SWNTs to improve the binding of SA by utilizing the strong binding between SA and fatty acid, where the introduction of the fatty acid was carried out by the radical grafting of the fatty acid derivative onto the SWNT sidewall. Here, the adsorption behavior was monitored by monitoring of the unique red-shifted and brighter photoemission (PL) compared to that of the non-functionalized SWNTs [4]. As the result, binding constant of SA onto fatty acid-site was 7.00×10^3 , while that of SA onto the non-modified surface was 3.29×10^3 . Since the control experiment carried out using phenyl-modified SWNTs showed binding constant of SA onto phenyl-site was 6.53×10^2 , recognition of SA onto fatty acid was clarified.

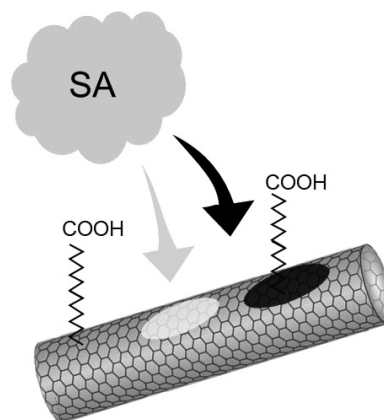


Figure 1 Schematic illustration of this study.

- [1] J. M. Harris et al., *Nat. Rev. Drug Discovery*, **2003**, 2, 214.
 [2] Dams, E. T. et al., *J. Pharmacol. Exp. Ther.* **2000**, 292, 1071.
 [3] Ge, C. et al., *Proc. Natl. Acad. Sci. U. S. A.* **2011**, 108, 16968.
 [4] Wang, Y. et al., *Nat. Chem.* **2013**, 5, 840.

Corresponding Author: T. Fujigaya

Tel/Fax: +81-92-802-2842

Web: <http://www.chem.kyushu-u.ac.jp/~fifth/jp/>

E-mail: fujigaya.tsuyohiko.948@m.kyushu-u.ac.jp

N-type doping from sulfhydryl groups of proteins to semiconducting single-wall carbon nanotube

○Tomohito Nakayama^{1,2}, Hiroataka Inoue³, Yuho Shigeeda³, Yasuhiko Hayashi³,
Takeshi Tanaka², Atsushi Hirano², Muneaki Hase¹

¹ Department of Applied Physics, Faculty of Pure and Applied Sciences, University of Tsukuba, Tsukuba, Ibaraki 305-8573, Japan

² Nanomaterials Research Institute, National Institute of Advanced Industrial Science and Technology (AIST), Tsukuba, Ibaraki 305-8565, Japan

³ Natural Science and Technology, Okayama University, Tsushima-naka, Kita, Okayama, 700-8530, Japan

Semiconducting single-wall carbon nanotubes (S-SWCNTs) have attracted much attention in their applications to thermoelectric devices because of their narrow bandgap and ultrahigh charge carrier mobility [1]. In principle, such thermoelectric devices require both p- and n-type of S-SWCNTs. Though some substances, including alkali metals, cobalt, nitrogen and organic molecules, are conventionally used for n-type doping into S-SWCNTs [2], they have problems such as instability at room temperature [3] and non-biocompatibility [4]. For realizing bio-implantable SWCNT-based thermoelectric devices, it is necessary to develop biocompatible dopants that are stable even at body temperature. Proteins are candidates for such dopants because they are biocompatible and typically have sulfhydryl groups with a high energy electron. In this study, we fabricated various SWCNT–protein composite films and evaluated their electric properties—Seebeck coefficients and ultrafast carrier responses—by the thermoelectric measurement and the femtosecond pump-probe spectroscopy (Fig.1a), respectively.

SWCNT–protein composite films were prepared using two proteins, *i.e.* hen-egg white lysozyme (LYZ) and bovine serum albumin (BSA), as dopant candidates [5,6]. LYZ lacks sulfhydryl groups, whereas BSA has a sulfhydryl group. The SWCNT–LYZ film showed a positive value of the Seebeck coefficient, which indicates that the semiconducting SWCNTs are p-type. In contrast, the SWCNT–BSA films showed a negative value (Fig.1b). This result suggests that BSA changes the electronic property of the semiconducting SWCNTs from p-type to n-type. The ultrafast carrier response of the SWCNT–LYZ film had a negative sign on the sub-picosecond time scale, whereas that of the SWCNT–BSA film had a positive sign (Fig.1c,d), which supports the suggestion that the SWCNT–LYZ film and the SWCNT–BSA film are p-type and n-type, respectively. We further investigated the ultrafast carrier response of the SWCNT film with reduced lysozyme (R-LYZ) which has artificially induced sulfhydryl groups. As expected, the response of the SWCNT–R-LYZ film had a positive sign (Fig.1e), which is consistent with the SWCNT–BSA film. In conclusion, sulfhydryl groups of proteins induce n-type doping in the SWCNTs. Our present findings are useful for realizing biocompatible thermoelectric devices.

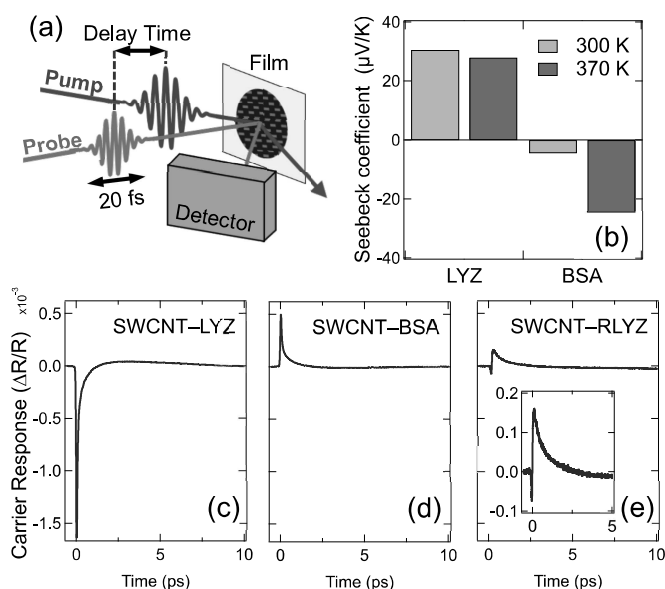


Fig.1 | (a) The experimental set-up of the pump-probe spectroscopy. (b) Seebeck coefficients of the SWCNT–protein composite films. (c–e) Carrier response of the SWCNT–protein composite films. The inset is an enlarged view of the carrier response in 0–5 ps.

[1] C. Yu, ACS Nano, 5,10.7885.(2011) [2] Y. Nonoguchi, Sci. Rep., 3,3344.(2013) [3] T. Fukumaru, Sci. Rep., 5,7951.(2014) [4] J. M. Gernand, Risk Analysis, 34,3.(2014) [5] T. Nakayama, APEX. 11,075101.(2018) [6] T. Nakayama, APEX. 10,125101.(2017)
Corresponding Author: T. Nakayama Tel: +81-29-853-5022, Fax: +81-29-853-5022, E-mail: s1930096@s.tsukuba.ac.jp

Time-resolved photoluminescence spectroscopy of epitaxial monolayer and bilayer graphene on SiC

○Kensuke Saito¹, Jianfeng Bao², Wataru Norimatsu², Michiko Kusunoki³,
Hideo Kishida¹, Takeshi Koyama¹

¹ *Department of Applied Physics, Nagoya University, Japan*

² *Department of Chemical Systems Engineering, Nagoya University, Japan*

³ *Institute of Materials and Systems for Sustainability, Nagoya University, Japan*

Graphene has various optical properties as two-dimensional material, and a study on light emission devices based on graphene has been conducted [1]. The emission band of a device can be tuned by using interference between thermal radiation of graphene and reflected light from substrate [2]. The emission intensity of thermal radiation increases as emitter temperature. Therefore, it is important to understand the cooling processes of graphene for application of thermal radiation.

An early study on time-resolved photoluminescence (PL) spectroscopy of transferred and epitaxial monolayer graphene indicated that the long distance between graphene and substrate reduces heat flow rate to the substrate [3]. Because slow heat flow leads to strong steady-state PL, it is preferred to use graphene with weak coupling to the substrate for light emission devices. The distance of the upper layer of bilayer graphene and the substrate is longer than that of monolayer graphene. It is expected that bilayer graphene has weaker coupling to the substrate. In this study, we compared PL from monolayer and bilayer graphene to investigate the coupling of the graphene to the substrate.

The epitaxial monolayer and bilayer graphene were prepared by thermal decomposition of 4H-SiC. The time-resolved PL measurements were conducted based on the frequency up-conversion method. The excitation photon energy and pulse duration were 1.55 eV and 90 fs, respectively. Figure 1 shows PL decay curves of the monolayer and bilayer graphene samples at a photon energy of 0.6 eV. The PL decay of bilayer graphene is slower than that of monolayer graphene, suggesting slower heat flow to the substrate in the bilayer graphene sample. We also obtained time-resolved PL spectra of the monolayer and bilayer graphene samples to investigate electron temperatures in the two samples. Comparison of the decay behavior and the intensity between the two samples and three-temperature model calculation enable us to estimate the strength of interaction between the graphene and the substrate.

- [1] Y. Miyoshi *et al.*, Nat. Commun. **9**, 1279 (2018).
[2] Y. D. Kim *et al.*, Nat. Nanotechnol. **10**, 676 (2015).
[3] H. Imaeda *et al.*, J. Phys. Chem. C **122**, 19273 (2018).

Corresponding Author: T. Koyama

Tel: +81-52-789-4450, Fax: +81-52-789-4450,

E-mail: koyama@nuap.nagoya-u.ac.jp

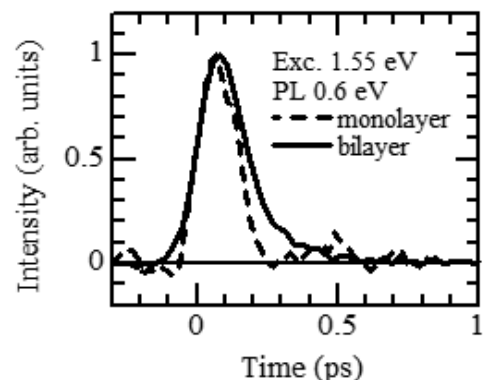


Fig.1 Photoluminescence decay of epitaxial monolayer and bilayer graphene on SiC at a photon energy of 0.6 eV.

A controllable post doping method for TMD atomic layers

○Yuya Murai¹, Shoji Yoshida², Zheng Liu³, Toshifumi Irisawa⁴, Hiroshi Shimizu⁵,
Takahiko Endo⁵, Yasumitsu Miyata⁵, Ryo Kitaura¹

¹Department of Chemistry, Nagoya University, Nagoya 464-8602, Japan

²Department of Pure and Applied Sciences, University of Tsukuba, Tsukuba 205-8573, Japan

³Innovative Functional Materials Research Institute, AIST, Nagoya 463-8560, Japan

⁴Nanoelectronics Research Institute, AIST, Tsukuba 305-8560, Japan

⁵Department of Physics, Tokyo Metropolitan University, Hachioji 192-0397, Japan

The purpose of this study is to develop a method for accurate doping of atomic layers, especially transition metal dichalcogenide (TMD) atomic layers. Control of p-type and n-type by introducing dopants is one of the essential techniques in semiconductor-device applications. In the case of silicon, the ion implantation technique has been widely used as a controllable doping method. It is, however, challenging to apply the ion implantation method to TMD atomic layers, which are ultrathin semiconductors with a sub-nanometer thickness; the high-energy ion beam significantly damages TMD atomic layers. In this work, we have focused on low-kinetic-energy atomic beam irradiation as a highly controllable doping method applicable to TMD atomic layers.

Figure 1 shows a HAADF-STEM image of a Nb-doped single-layer WSe₂. In HAADF-STEM images, image contrasts are proportional to the n th power of the atomic number (Z -contrast imaging). As shown in Fig. 1, W atoms are, therefore, imaged as bright spots, whereas Se atoms give image contrasts much weaker than those of W atoms. As you can see from Fig. 2, some of the W-sites are imaged as dark spots, which correspond to substituted Nb atoms; we confirmed the existence of Nb atoms by the elemental analysis based on EDX. Figure 3 shows transfer characteristics of a WSe₂ FET device before (the blue curve) and after (the red curve) a doping process. Although the transfer curve clearly shows ambipolar characteristic before the doping, the Nb-doped WSe₂ FET clearly shows the p-type characteristic with on current of 10^{-7} A. At the presentation, we will also discuss more detailed device characteristics and spectroscopic results.

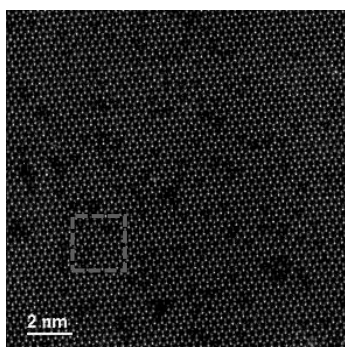


Figure 1 A HAADF-STEM image of Nb-doped WSe₂

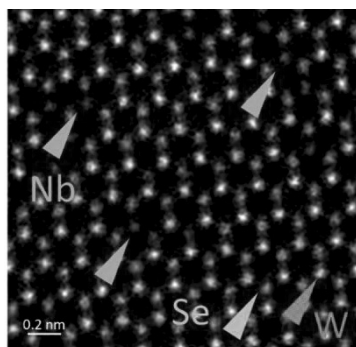


Figure 2 An enlarged image of the area indicated by the red box in Figure 1

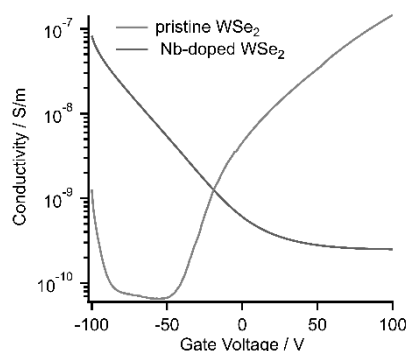


Figure 3 Transfer characteristics of pristine and Nb-doped WSe₂ devices

Corresponding Author: R. Kitaura

Tel: +81-52-789-2482, Fax: +81-52-747-6442

Web: <http://nano.chem.nagoya-u.ac.jp/>

E-mail: r.kitaura@nagoya-u.jp

Superconducting properties in three-dimensional networks of NbSe₂ films

○Togo Takahashi¹, Chisato Ando², Mitsufumi Saito³, Yasumitsu Miyata²,
Yusuke Nakanishi², Jiang Pu¹, Taishi Takenobu¹

¹ Department of Applied Physics, Nagoya University, Nagoya 464-8603, Japan

² Department of Physics, Tokyo Metropolitan University, Tokyo 192-0397, Japan

³ Department of Electrical Engineering, Tokyo Metropolitan University, Tokyo 192-0397, Japan

Increasing upper critical field, H_{c2} , in the superconductors is one of the most significant requirements for the superconducting device applications. In this regard, emerging two-dimensional (2D) noncentrosymmetric NbSe₂ is a promising candidate because their pair breaking is protected by the spin-momentum (spin-valley) locking effect, resulting in giant in-plane H_{c2} (~ 50 T) [1,2]. However, the strong anisotropy of 2D NbSe₂ suppress the robustness of out-of-plane H_{c2} (< 5 T) [2,3]. Although NbSe₂ offers a possible robust superconductor, this great anisotropy restricts the potential utility for future practical device designs. To overcome this issue, here, we propose synthetic approach to produce superconducting NbSe₂ film with nearly isotropic large H_{c2} . The scalable and thickness controlled chemical vapor deposition is developed to tailor 3D superconducting networks, in which 2D NbSe₂ flakes are vertically aligned to the substrates [4]. We investigate the relations between 3D structured films and their superconducting properties through by X-ray diffraction and magneto-transport measurements.

The direct selenization methods were introduced to synthesize large-area NbSe₂ films, and their morphologies can be tuned by just a two-step vapor-phase reaction of the initial thickness of evaporated Nb layers (Fig. 1a). The spectroscopic characterizations revealed the 3D structured films comprising of vertically stacked 2D flakes with random orientations, as shown in the SEM image of Fig. 1b. Using these samples, the angle-resolved magneto-transport realized the enhanced H_{c2} of 20 – 38 T for all directions of external magnetic fields. Figure 1c shows the comparison of the angle-dependent H_{c2} between our 3D structured films and reported 2D films [3], indicating that nearly isotropic large H_{c2} was observed in our samples. On the basis of X-ray diffraction measurements, the isotropic nature of H_{c2} is attributed to the averaging intrinsic anisotropy of 2D NbSe₂ flakes due to their 3D superconducting networks. Thus, the proposed synthetic approach provides a significant method to functionalize 2D superconducting materials for creating practical superconductors that can operate under high magnetic fields.

[1] X. Xi *et al.*, Nat. Phys., **12**, 139 (2016).

[2] H. Lin *et al.*, Nat. Mater., **18**, 602 (2019).

[3] H. Matsuoka *et al.*, Phys. Rev. Research, **2**, 012064 (2020).

[4] T. Takahashi *et al.*, submitted (2020).

Corresponding Author: J. Pu, T. Takenobu

E-mail: jiang.pu@ngoya-u.jp, takenobu@nagoya-u.jp, Tel/Fax: +81-52-789-5165

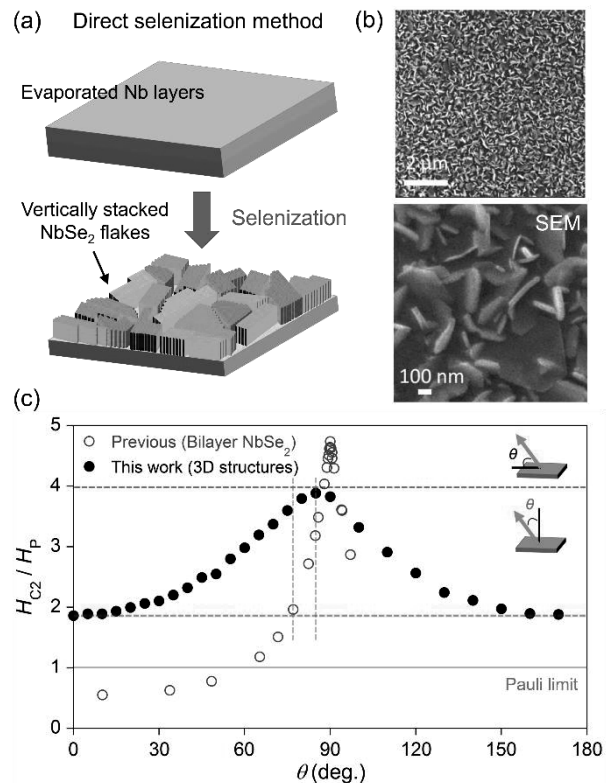


Fig. 1. (a,b) Growth of 3D structured NbSe₂ films (a) and their SEM image (b). (c) The comparison of H_{c2} between 3D and 2D films [3].

Crystallinity dependence on mechanical properties of aerographite particles

YUEXUAN LI¹, Hiromu Hamasaki¹, Kaori Hirahara¹

¹*Dept. of Mechanical Engineering, Osaka University, 565-0871, Japan*

Aerographite is an ultralight and highly-flexible carbon material [1]. The three-dimensional morphology can be controlled by choosing the template of zinc oxide (ZnO). Recently, hollow microparticles of aerographite with urchin-like shell structures have been synthesized by using ZnO nanorod-microsphere [2, 3]. This urchin-like microparticles exhibit a unique flexibility deserving to mention. Each particle can remain its original shape after large compression more than 73%, even when the shell was partially broken [2]. However, It was also indicated that the graphitic walls comprising the as-grown particles are defective, and improvement of the crystallinity may make the aerographite particles exhibit much excellent mechanical properties [2]. In this study, we studied on the relationship between mechanical properties and crystallinity of the aerographite particles by single-particle-level compressive tests in a scanning electron microscope (SEM). The particles used in this study were annealed at 800–2000°C in argon atmosphere for controlling the crystallinity. The crystallinity was evaluated by electron diffraction and transmission electron microscope images. A single particle was made compression between two parallel cantilevered probes in SEM, and the stress-strain curve of each sample was obtained. As the results, all particles performed a linear elastic behavior under 30% strain. The young's modulus of the particles annealed at 2000°C is 3 times higher than samples annealed at 1600°C and as-grown samples, probably related to the higher crystallinity. However, the critical point tend to be lower.

This work was supported by JSPS KAKENHI Grant Number 19K21920.

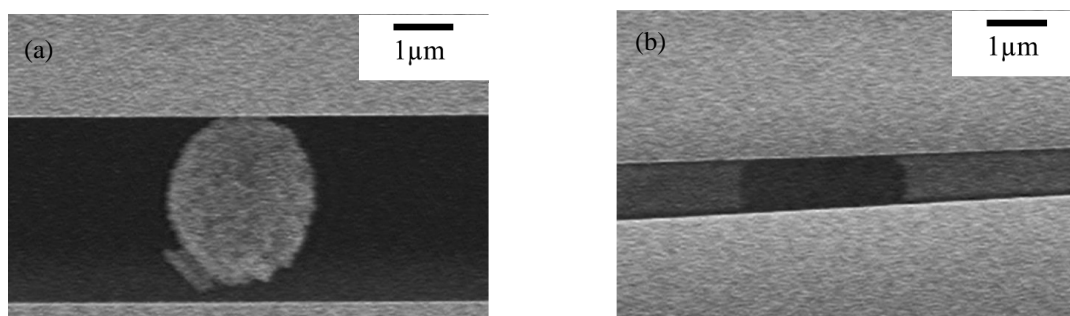


Fig. 1. SEM images of an aerographite particle (a) before compression, (b) during the compression test (70% strain)

[1] M. Mecklenburg, A. Schuchardt, Y. K. Mishra, et al. *Advanced materials*, **24**(26),3486 (2012) .

[2] K. Hirahara, K. Hiraishi, K. Imadate, et al. *Carbon*, **118**, 607-614(2017).

[3] Y. Hirota, M. Syafiq Elias, B. Dwijaya, et al. *Chem. Letters.*, **43**, 360-362(2014).

High-density CNT forest by multiple coating of iron oxide nano-colloid for dry-spinnable CNT forest

○Kento Tabata, Takayuki Nakano, Yoku Inoue

Department of Electronics and Materials Science, Shizuoka Univ., Hamamatsu 432-8561, Japan

In the conventional research on CNT forest synthesis, the catalyst thin film has been deposited on the substrate by, for example, sputtering. However, in the sputtering method, since the diameter of catalyst nanoparticle can be controlled only by the thickness of the catalyst film, the diameter and density of CNT cannot be controlled separately. In this study, we prepared a CNT forest by using catalyst nano-colloid. The diameter of catalyst nanoparticle was controlled by parameters of a polyol method, and density was increased by multiply coating the nano-colloid on a substrate.

Catalyst nano-colloid was synthesized by a polyol method using iron acetyl acetylacate as a precursor. By tuning the temperature ramping rate, the diameter of the nanoparticle was controlled. The diameter of iron oxide nanoparticles used was 3.05 nm. Al_2O_3 was deposited on a thermally oxidized Si substrate by sputtering first. Then, iron oxide nanoparticles were spin-coated. The substrate coated with the iron oxide nanoparticles was annealed in the air. The number of catalyst nanoparticles was increased by repeating the nanoparticle deposition process. A mixed solution of hexane and toluene was used as a solvent, and the concentration of the iron oxide nanoparticle solution was set to 0.5 mg/ml. The spin coating was performed at 1000 rpm for 30 seconds. The heat treatment was performed in the air at 400° C for 3 hours. CNT synthesis was carried out by thermal chemical vapor deposition using acetylene as a carbon source, hydrogen as a reducing agent for catalyst particles, and argon as a carrier gas.

Figure 1 shows the atomic force micrography(AFM) image of nanoparticles on the substrate. Figure 2 shows the scanning electron microscopy(SEM) image of the CNT forest. A CNT web is drawn from the forest. Figure 3 shows the relationship between mass density and the number of spin coating of the colloid. We found that two-times spin-coating increased the mass density of the CNT forest. Further deposition of nanoparticles induced a decrease in mass density resulted from the aggregation of nanoparticles.

Corresponding Author: Yoku Inoue
Tel: +81-53-478-1356
Web: <http://cnt.eng.shizuoka.ac.jp/>
E-mail: inoue.yoku@shizuoka.ac.jp

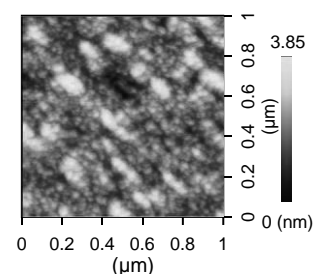


Fig.1 AFM image of iron oxide nanoparticles on substrate.

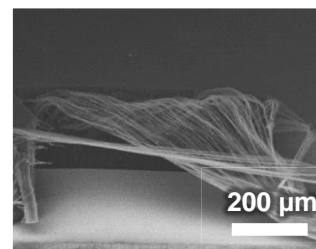


Fig.2 SEM image of CNT forest.

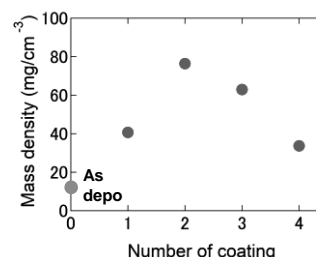


Fig.3 the relationship between mass density and the number of annealing.

Activation of Alkane for CVD Growth of Single-Wall Carbon Nanotubes

○Pengfei Chen¹, Mengju Yang¹, Rei Nakagawa¹, Hisashi Sugime¹, Hitoshi Mazaki², Suguru Noda^{1,3,*}

¹ Department of Applied Chemistry, School of Advanced Science and Engineering, Waseda University, 3-4-1 Okubo, Shinjuku-ku, Tokyo 169-8555, Japan

² Central Technical Research Laboratory, JXTG Nippon Oil & Energy Corporation, 8 Chidori-cho, Naka-ku, Yokohama, Kanagawa 231-0815, Japan

³ Waseda Research Institute for Science and Engineering, Waseda University, 3-4-1 Okubo, Shinjuku-ku, Tokyo 169-8555, Japan

Nowadays C₂H₂ is one of the commonly used carbon sources for the growth of single-wall carbon nanotubes (SWCNTs) due to its high activity [1]. However, the large-area synthesis of SWCNTs is still a problem because the C₂H₂ supply at high concentrations easily causes the catalyst deactivation [2]. We proposed the control of gas-phase reactions by combining two carbon sources of C₂H₂ and C₂H₄, which yielded SWCNTs at an improved areal yield [3]. In this study, instead of using the alkyne or alkene, we investigated less reactive alkane as the carbon source. Compared to the C₂H₂, n-hexane (n-C₆H₁₄) can be a better candidate because of the lower price and easier storage in liquid state. We studied the gas-phase reactions by gas chromatography (GC) and gas-phase kinetic simulation (CHEMKIN) to determine the factors that influence the SWCNT growth. We first checked the CNT synthesis using the combinatorial catalyst (0.2-5 nm Fe on 15 nm AlO_x) [2] and found that SWCNTs grow from thin Fe layer when n-C₆H₁₄ (2 vol%) is fed with H₂ at relatively high concentrations (20-40 vol%) (Fig. 1a). Then we examined the large-area synthesis of SWCNTs using the 18 substrates (1×1 cm²) with 0.7 nm Fe, and found that SWCNTs was produced at a higher average yield of 1.8 mg cm⁻² from n-C₆H₁₄ (Fig. 1b) than from C₂H₂ (1.4 mg cm⁻²). The analysis of the gas-phase species showed that C₂H₂ forms from n-C₆H₁₄ at a concentration similar to the optimum C₂H₂ concentration (0.3 vol%) in our previous works [2,3]. n-C₆H₁₄ is an effective carbon source that yields C₂H₂ *in situ* for the large-area synthesis of SWCNTs.

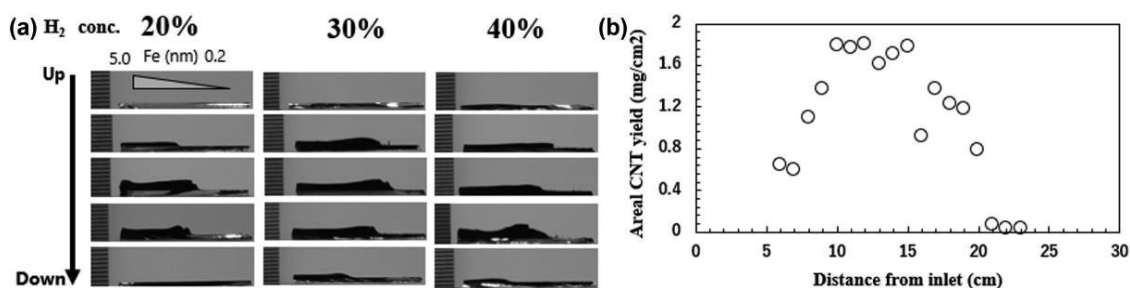


Fig. 1: (a) Side-view images of the CNT forests grown from 2 vol% n-C₆H₁₄ with different H₂ concentrations on Fe (gradient)/AlO_x/Si. (b) Areal mass of the SWCNTs grown with 20 vol% H₂ and 0.7 nm Fe. CVD was carried out at 800 °C for 30 min.

[1] H. Sugime and S. Noda, *Carbon* **50**, 2953 (2012). [2] K. Hasegawa and S. Noda, *ACS Nano* **5**, 975 (2011). [3] T. Sato et al., *Carbon* **136**, 143 (2018).

Corresponding Author: S. Noda, Tel: +81-3-5286-2769, E-mail: noda@waseda.jp

Growth mechanism of one-dimensional heterostructures

oYongjia Zheng¹, Yang Qian¹, Ming Liu¹, Akihito Kumamoto¹, Yuichi Ikuhara¹, Esko I. Kauppinen², Shohei Chiashi¹, Taiki Inoue¹, Rong Xiang¹, Shigeo Maruyama¹

¹ Department of Mechanical Engineering, The University of Tokyo, Tokyo 113-8656, Japan

² Department of Applied Physics, Aalto University, Otakaari 1, 02150 Espoo, FI-20742, Finland

In recent years researchers have focused on two-dimensional van der Waals (vdW) heterostructures, which have generated great interests recently due to the possibility of combining diverse atomic layers to create novel materials and devices [1-2]. In this work, we demonstrate a new one-dimensional structure with similar heterostructure interfaces that includes single-walled carbon nanotubes (SWCNTs), boron nitride nanotubes (BNNTs) and molybdenum disulfide (MoS₂) nanotubes. Techniques involving direct growth of 1D vdW heterostructures by chemical vapor deposition (CVD) will be presented in detail. Binary heterostructures in SWCNT-BNNT and SWCNT-MoS₂ order can be achieved with the aid of SWCNTs as a template, and ternary heterostructure in SWCNT-BNNT-MoS₂ was further demonstrated [3]. In addition, formation mechanism of 1D vdW heterostructures will be discussed with the open-end-chiral growth, the effect of isolation, and three kinds of growth models (Fig. a-g). The high quality of 1D heterostructure allows for further experimental exploration of its properties. We believe there is a great prospect for these new structures as they extended the concept of vdW heterostructures to 1D materials.

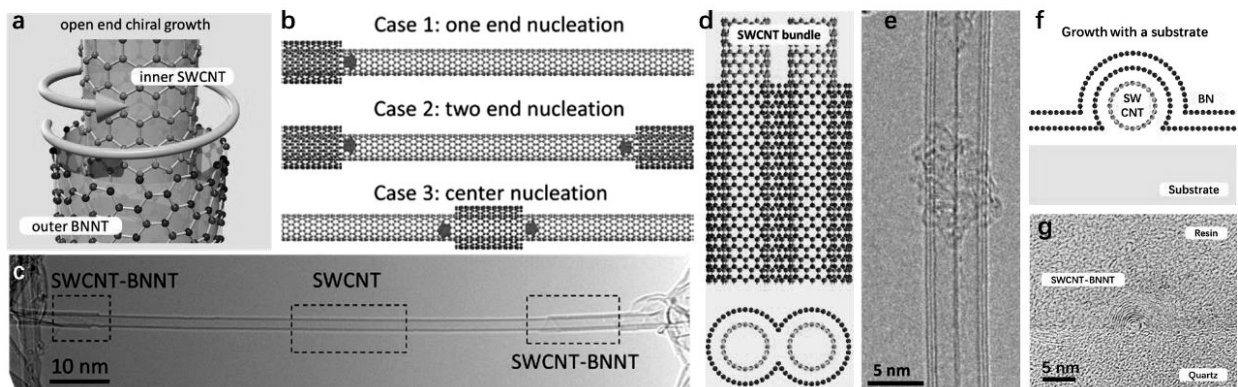


Fig. 1: (a) Atomic model of open-end growth mechanism. (b) Atomic 3D model for three cases refers to open-end chiral growth. (c) TEM image as an example for case 2, in which BNNT growth starts from both ends. (d) Atomic model of a BN coated bundle consisting of two SWCNTs, and its cross-section view. (e) TEM image for this bundle situation. (f) Atomic model of a BN coated bundle SWCNT on a flat substrate as the second situation. (g) Specimen based on the second situation made by a focused-ion-beam (FIB) system for TEM characterization.

[1] D. Jariwala *et al.*, *Nature materials*, **16**, 170 (2017).

[2] Z. Liu *et al.*, *Nature Nanotechnology*, **8**, 119 (2013).

[3] R. Xiang *et al.*, *Science*, **367**, 537 (2020).

Corresponding Author: S. Maruyama

Tel: +81-3-5841-6421,

Fax: +81-3-5841-6983,

E-mail: maruyama@photon.t.u-tokyo.ac.jp

Imaging of functional group distribution on carbon nanomaterials with highly spatially resolved SEM-EDS

○Hideaki Nakajima, Takahiro Morimoto, Ying Zhou,
Kazufumi Kobashi, Takeo Yamada, and Toshiya Okazaki

¹ National Institute of Advanced Industrial Science and Technology, Tsukuba 305-8565, Japan

Functionalization is a key technique for improving the dispersibility of carbon nanomaterials such as single-walled carbon nanotubes (SWCNTs) in solvents. Therefore, a robust and efficient characterization method is required to confirm spatial uniformity of their surface functionalization. Energy dispersive X-ray spectrometry (EDS) in scanning electron microscopy (SEM) is particularly suitable for evaluating the elemental distribution relating to functional groups on various nanomaterials with wide scanning area [1]. However, its low analytical sensitivity to light elements (*i.e.* C and O) limits the spatial resolution to around 1 μm , which hinders the spatial information on nanomaterial surfaces. Here, we demonstrate a highly spatially resolved SEM-EDS elemental imaging for carbon nanomaterials. Highly sensitive X-ray detection and drift-free EDS operation enable us to image light elements with a sufficient spatial resolution of < 10 nm. The technique clearly reveals the spatial distribution of surface functionalization on chemically reacted SWCNT bundle structures [2].

Figure 1(a) shows a schematic of SEM-EDS measurement setup. EDS equips annular type four-channel detectors, and thus light elements can be detected sensitively. Furthermore, due to the electrical contact between metal and CNT, the imaging drift during electron-beam irradiation is suppressed to within 10 nm. SWCNT sample was synthesized by water-assisted chemical vapor deposition and was chemically modified with $\text{KMnO}_4/\text{H}_2\text{SO}_4$ treatment.

Figure 1(b) indicates a typical EDS result. The SWCNT bundle structures are clearly reproduced by the C element mapping. In addition, the usage of a nitride substrate significantly suppresses the background of oxygen species that come from the substrate. Therefore, our approach can provide an accurate functional group distribution of a variety of carbon nanomaterials. The detailed analysis about the degree of functionalization and the spatial resolution of EDS imaging will be discussed in the symposium. Acknowledgments: This work was supported by a project (JPNP16010) commissioned by the New Energy and Industrial Technology Development Organization (NEDO).

[1] J. Ji *et al.*, Chem. Sci. **2**, 484 (2011). [2] H. Nakajima *et al.*, Nanoscale **11**, 21487 (2019).

Corresponding Author: Toshiya Okazaki

Tel: +81-29-861-4173 / E-mail: toshi.okazaki@aist.go.jp

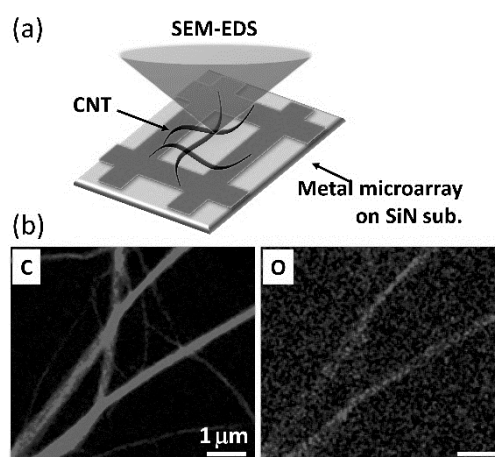


Figure 1. Highly spatially resolved SEM-EDS measurements. (a) Schematic diagram of measurement setup and (b) elemental images of C and O of SWCNT sample.

Foot Pressure Sensor System Made from MWCNT Coated Cotton Fibers to Monitor Human Activities and Sports Performance

Md. Abdul Momin^{*a}, Mohammad Jellur Rahman^b, Tetsu Mieno^a,

^aGraduate School of Science & Technology, Shizuoka University, Shizuoka 422-8529, Japan

^bDepartment of Physics, Bangladesh University of Engineering and Technology, Dhaka-1000, Bangladesh

Highly sensitive pressure sensors have been developed from multiwall carbon nanotube (MWCNT) coated cotton fibers to utilize them in monitoring of human activities and sporting performances [1]. The sensing mechanism of the pressure sensor is discussed through experimental and theoretical explanations. The principle of the sensing mechanism is related with the number of contacts among the MWCNT coated fibers, contact area among the fibers when a force is applied and the tunneling current among the MWCNTs coated on the cotton fibers. Using the three sensors a foot pressure sensor system has been developed, which can detect the exerted force of human foot during standing, walking, running, jumping, and other activities [1, 2]. The locus of the center of gravity is also measured by these sensors during these human activities. The exerted force increases instantaneously when a person jumps from an upper step of a ladder onto a floor, which is clearly recorded. The variations of force during kicking a football and basketball scoring are recorded. The foot pressure sensors can be used to monitor the real-time sporting performances. To prevent the ankle and knee injury of sportsmen and to monitor the activities of the patients, and old persons, the foot pressure sensors can be utilized.

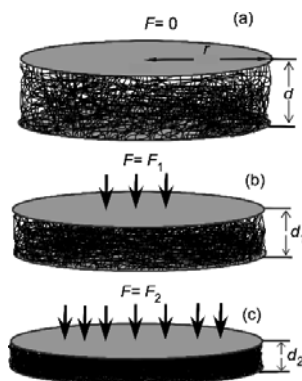


Fig. 1 A compression model of the sensor with an external force. (a) $F=0$, (b) $F=F_1>0$, and (c) $F=F_2>F_1$.

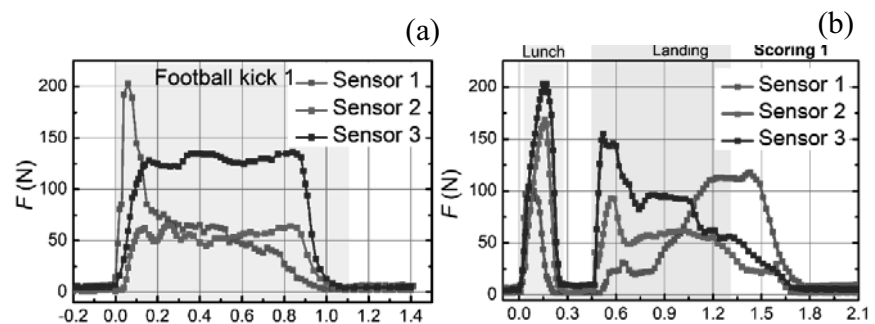


Fig. 2 (a) Time variations of forces, on the foot pressure sensors (right foot) during kicking a football by a left foot (b) Time variation of forces on the foot pressure sensors during basketball scoring.

[1] Momin M.A, Rahman, M. J. Mieno, T., J. Nanomater. 2019, ID 7658437, 2019.

[2] Momin M.A, Rahman, M. J. Mieno, T., Surf. Coat. Tech. 394, ID 125749, 2020.

*Corresponding author: Md. Abdul Momin

E-mail: mamomin89bd@gmail.com, Mobile: +8108041265887

Improvement of carbon nanotube filament formation efficiency by gas discharge breakdown using triode electrode configuration

○Hiro Hayama, Soichiro Magata, Hideki Sato

Graduate School of Engineering, Mie University, Tsu 514-8507, Japan

We have demonstrated that carbon nanotube (CNT) filaments, thin thread-like assemblies comprising many CNTs, can be efficiently formed by irradiating gas discharge breakdown to CNT mat attached to a planar electrode [1]. This method may be used as a simple method for CNT spinning. However, the efficiency of the CNT filament formation was low, and improvement of the filament formation efficiency was required. We recently found that CNT filaments were efficiently formed by using a collection electrode, which was additionally placed above the discharge electrodes (anode and cathode) [2]. In addition, it was confirmed that the shape of the collection electrode influences the formation efficiency of the CNT filaments. In this study, we examined the effect of the shape of the collection electrode on the CNT filaments formation by the gas discharge breakdown using triode electrode configuration.

The mat-shaped CNT sheet was attached on a stainless-steel plate by pressing and used as a cathode. A tungsten wire (0.15 mm diam.) was used as an anode, which was placed horizontally to the cathode. The distance between them was 1.0 mm. The square-shaped collection electrode (a stainless-steel plate, 0.5 mm thick.) was vertically positioned above the anode wire. The distance between the cathode and the collection electrode was 2.0 mm [Fig. 1(a)]. These electrodes were introduced to a discharge chamber that was filled with Ar gas at 6.2 kPa. DC voltage (-800 V) was applied to the cathode for ignition of the gas discharge breakdown.

A bias voltage of +150 V was applied to the collection electrode and a gas discharge was generated between anode and cathode. The discharge breakdown generated dust-like CNT bundles, and they formed long filaments around the electrodes [Fig. 1(b)]. After that, the collection electrode was gradually moved upward from the discharge area, floating CNT filaments adhered to the collection electrode [Fig. 1(c)]. This accompanied elongation of the CNT filaments on the collection electrode and aggregated near the corner of the stainless-steel plate [Fig. 1(d)]. The length of the CNT filament bundle formed at this time was about 1.5 cm. This result shows that the plate-shaped collection electrode is effective for formation of longer CNT filaments. It is considered that the CNT filaments were formed by efficient formation of the dust-like CNT bundles by the irradiation gas discharge breakdown to the CNT mat and the reconstruction of the CNT bundles to the filaments by an effect of the electrostatic induction.

This study was supported by JSPS KAKENHI Grant No. 19K05206.

[1] H. Sato *et al.*, *Appl. Phys. Lett.*, **110**, 033101 (2017).

[2] S. Hiromura *et al.*, *The 57th FNTG General Symposium*, 2P-21 (2019).

Corresponding Author: H. Sato E-mail: sato@elec.mie-u.ac.jp

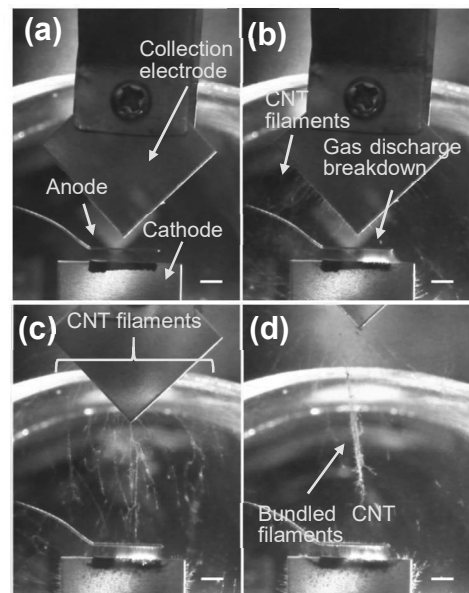


Fig.1 Photographs of (a) electrodes before ignition of gas discharge breakdown, (b) breakdown accompanied by the CNT filament formation, (c) elongation of CNT filaments and (d) formation of bundled CNT filaments by moving the collection electrode upward. Scale bars are 2.0 mm.

Quantitative study of sheet thermal conductance of Single-Walled carbon nanotube film

oPengyingkai Wang¹, Yongjia Zheng¹, Taiki Inoue¹, Rong Xiang¹, Shohei Chiashi¹, Watanabe Makoto¹, Shigeo Maruyama^{1,2}

1 Department of Mechanical Engineering, The University of Tokyo, Tokyo 113-8656, Japan

Single-walled carbon nanotube (SWNTs) film exhibits promising potential as thermal interface material due to the superior thermal conductivity [1]. However, tube density, bundle length, bundle diameter and junction conductance have great impacts on the thermal transport property of SWCNT film. SWCNT-BNNT heterostructure film has been studied and shown an enhanced sheet thermal conductance [2]. To deeply understand the mechanism of thermal transport in heterostructure film, it's essential to propose a proper model.

SWCNT films are consist of SWCNT bundles with various size. In this work, we put forward a new way in modeling the thermal transport in SWCNT film based on a quantitative model of SWCNT bundle. The bundle length, area contact conductance and bundle diameter have been studied as variables and the corresponding sheet thermal conductance of SWCNT film is discussed. With the statistic distribution of bundle size in 87% transparent SWCNT film, a modified random stick network (RSN) model with only parameter of line density and path conductance is established [3]. Finally, sheet thermal conductance is plotted as a function of film transparency according to the model, which fits well with the experimental result.

The non-monotonic increase of bundle conductance with bundle size and length, diameter, contact conductance dependent sheet thermal conductance is presented. Based on the understanding of SWCNT film, thermal transport mechanism of SWCNT-BNNT heterostructure film is further discussed.

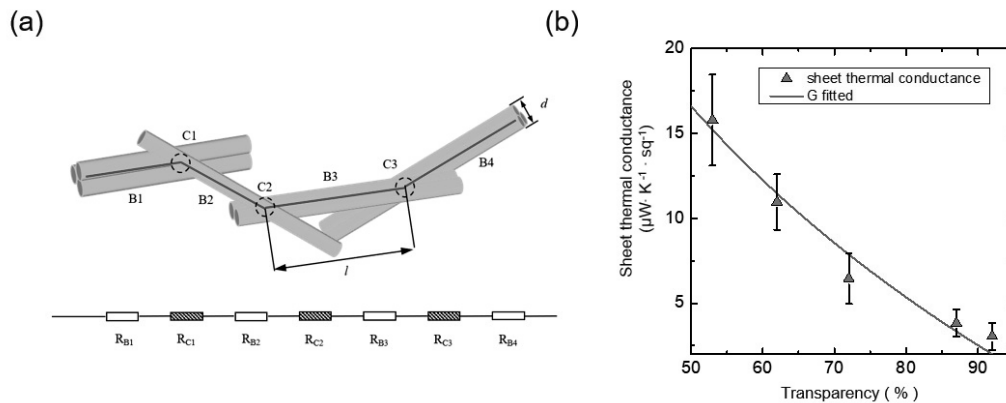


Fig.1 (a) Thermal resistance of RSN model. (b) Fitting line (blue) and experimental result (red triangle).

[1] J Hone *et al.*, *Appl.Phys.Lett*, **77**, 666 (2000)

[2] P.Wang *et al.*, *ACS Nano*, **14**,4298 (2020)

[3] M. Tsukuda *et al.*, *Appl. Phys. Express*,**12** (2019)

Corresponding Author: S. Maruyama

Tel: +81-3-5841-6421, Fax: +81-3-5841-6421,

E-mail: maruyama@photon.t.u-tokyo.ac.jp

In-situ X-ray diffraction monitor of multi-layer graphene precipitated from nanodiamonds

○Tatsuya Kashio¹, Asato Nakashima¹, Yuki Ueda¹, Takahiro Maruyama², and Shigeya Naritsuka¹

¹ *Department of Materials Science and Engineering, Meijo University
Nagoya 468-8502, Japan*

² *Department of Applied Chemistry, Meijo University, Nagoya 468-8502, Japan*

Precipitation method is one of the useful ways of graphene growth where graphene is obtained by simple processes; deposition of catalytic and carbon materials, and subsequent heating. We have succeeded in a direct growth of multilayer graphene on various substrates by the precipitation method using nanodiamond [1]. In order to improve the graphene quality, it is necessary to reveal the growth mechanism. Therefore, in this study, in-situ observation of graphene precipitation was carried out using a high intensity X-ray beam from the synchrotron radiation facility of SPring-8.

Firstly, 100nm-thick Ni layer was deposited on c-plane sapphire using MBE, and nanodiamond was coated on the surface. The sample was heated in ultra-high vacuum chamber, which was installed on a manipulator for X-ray diffraction measurement. The temperature was incrementally increased from 600°C to 700°C by the steps of 50°C with the annealing periods of 30 min. At the same time, the peak intensity of the graphite (002) diffraction was insitu monitored to investigate the behavior of the graphene precipitation. The temperature was cooled at a rate of 100°C/min after the annealing. The Ni catalytic layer was etched off using nitric acid to directly characterize the precipitated graphene by Raman scattering spectroscopy.

Figure 1a shows a typical Raman spectrum of the precipitated graphene. The intensity difference of the G and G' peaks indicates that multilayer graphene was soundly precipitated. Fig.1b shows the intensity change of the diffraction peak of graphite (200) during the sample annealing. Areas (I), (II), and (III) correspond to (I) 600°C, (II) 650°C, and (III) 700°C annealings for 30 min. The change rates of the diffraction intensity indicate that the growth rate of graphene monotonously increased with increasing the temperature, which suggests the temperature change of the diffusion constant of the carbons through the Ni catalytic layer.

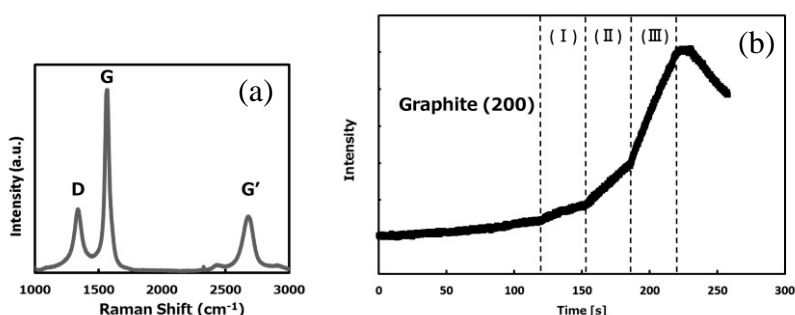


Fig.1 (a) Raman spectrum of grown sample (b) intensity dependence of graphite (002) diffraction.

[1] T. Kashio et al., The 57th FNTG Symposium 1P-26.

Acknowledgement: This work was supported by the QST Advanced Characterization Nanotechnology Platform (A-19-QS-0028). The X-ray diffraction measurements were performed at BL11XU, SPring-8 with the approval of JASRI (No.2019B3587). Corresponding Author: T. Kashio E-mail: 193428007@ccmailg.meijo-u.ac.jp

Non-destructive, Uniform, and Continuous Electrochemical Functionalization of Graphite Sheet

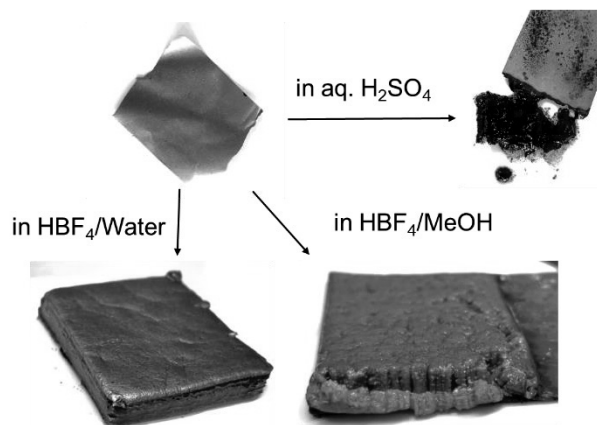
○Yuta Nishina,^{1,2} Benoît D. L. Campéon,¹ Masato Komoda¹

¹ Graduate School of Natural Science and Technology, Okayama University, 3-1-1 Tsushima-ka, kita-ku, Okayama, 700-8530, Japan.

² Research Core for Interdisciplinary Sciences, Okayama University, 3-1-1 Tsushima-ka, kita-ku, Okayama, 700-8530, Japan.

To exploit superior properties of graphene in specific applications, it is necessary to improve its production methods (top-down approach or bottom-up approach) and the modulation of its structure (atom doping, covalent functionalization, or non-covalent functionalization). Current methods to prepare graphene possess several disadvantages in terms of scalability, cost, homogeneity, and structural controllability. These drawbacks have restricted the mass production and practical uses of graphene. Recently, the electrochemical method has become attractive for producing and functionalizing graphene as an easy, fast, safe, scalable, and green procedure.¹⁻³

The electrochemical functionalization of graphite to graphene oxide was developed by using HBF_4 as an electrolyte.⁴ The non-destructive nature of the intercalated species (BF_4^-) results in the expansion of graphite while preventing the exfoliation and formation of un-oxidized graphite domain before functionalization. HBF_4 aqueous electrolyte and that diluted by methanol produced materials with similar morphology and oxygen content. Introduction of the methoxy functional group allowed to be dispersed in organic solvents, thus extending its processability. Additionally, promising results were obtained in using the graphene oxides by electrochemical methods for energy storage and water filtration, thus guaranteeing their wide scope of application. Finally, this process was adapted to a flow system to enable continuous production. This research will contribute to allowing the fine-tuning of the functional groups, functionalization degree, and large-scale production of 2D carbons in the future.



[1] K. Parvez *et al.*, *J. Am. Chem. Soc.* **136**, 6083 (2014). Fig. 1 Electrochemically produced graphene oxides.

[2] Y. L. Zhong *et al.*, *J. Am. Chem. Soc.* **134**, 17896 (2012).

[3] S. Pei *et al.*, *Nature Commun.* **9**, 145 (2018).

[4] B. D. L. Campeon, M. Akada, M. S. Ahmad, Y. Nishikawa, K. Gotoh, Y. Nishina, *Carbon* **158**, 356 (2020).

Corresponding Author: Y. Nishina

Tel: +81-86-251-8718, Fax: +81-86-25-8718,

Web: <http://www.tt.vbl.okayama-u.ac.jp/publication.html>

E-mail: nisina-y@cc.okayama-u.ac.jp

If the format of this page is broken, Select Printing Layout in “Display” tab.

Resolution of the phonon scattering by transient phonon spectra of graphene in molecular dynamics calculations

○Tatiana Zolotoukhina¹, Shohei Hokazono¹

¹ *Department of Mechanical Engineering, University of Toyama, Toyama 930-8555, Japan*

The study of plasmons in 2D monolayer atomic crystals reveals the production of hybridized plasmon-phonon modes. On the lifetime of the existence of coupled plasmon-phonon modes, the propagation of phonons within a few ps can be considered as guided by the interaction process [1-3]. In order to resolve the coupling of electronic excitation with phonons, one has to be able to distinguish dynamic changes such as 3-phonon processes. The phonon dispersion relation in thermal energy transfer is regarded primarily as an equilibrium process. However, the phonon dynamics is dependent on temperature in 2D materials as it is shown in Raman spectroscopic measurements [4]. The dynamics of the phonon scattering influences thermal conductivity at ps time intervals by transient changes in the phonon mode population that we aim to trace and qualitatively assess in the framework of the classical equation of motion. We use an approach where transient calculations in molecular dynamics (MD) method estimate variation in the transient density of states (DOS) of the graphene samples at selected sets of the sampling regions through which the transient phonon modes move. The mode propagation changes energy distribution between phonon modes in the graphene sample. The MD method with REBO potential for graphene nanoribbon that was thermally excited in a small area at one end has been tested. The energy distribution between basic and transient phonon modes in the 1st Brillouin zone in ΓM direction is calculated. We test mode resolution and probable energy exchange between modes at the transient time that proves the presence of the phonon scattering in the ps time scale.

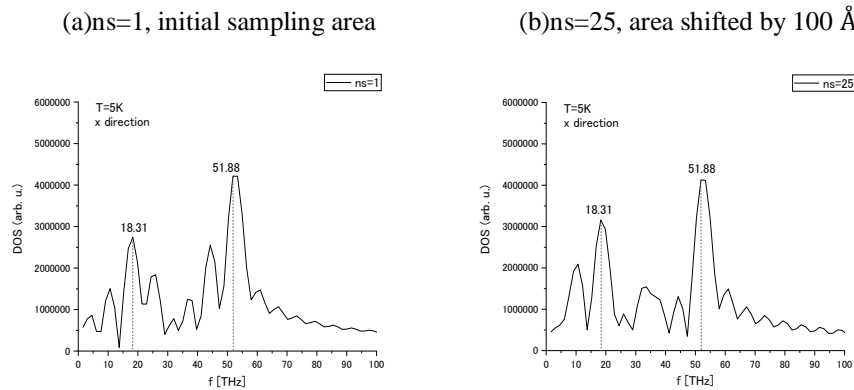


Fig1 Density of states of graphene nanoribbon ($T=5K$, padding=4 for FFT transfer)

- [1] H. Tornatzky, R. Gillen, H Uchiyama, and J. Maultzsch, *arXiv:1809.03381v1*, (2018).
- [2] A. Kınacı, J. B. Haskins, C. Sevik, T. Cagin, *Phys. Rev. B* 86, 115410 (2012).
- [3] I. M. Felix & L. F. C. Pereira, *Scientific Reports*, 8, 2737, (2018).
- [4] Z.-Y. Cao, X.-J. Cheng, *App. Phys. Lett.*, 114(5):052102 (2019).

Corresponding Author: T. Zolotoukhina

Tel: +81-76-445-6739, Fax: +81-76-445-6739, E-mail: zolotu@eng.u-toyama.ac.jp

Raman spectroscopy of graphene oxide and reduced graphene oxide flakes on Si-based substrates

○K. Kanishka H. De Silva¹, Seiya Suzuki², Pamarti Viswanath¹, Masamichi Yohimura¹

¹ Graduate School of Engineering, Toyota Technological Institute, Nagoya 468-8511, Japan

² International Center for Young Scientists (ICYS), National Institute for Materials Science (NIMS), 1-1 Namiki, Tsukuba, Ibaraki 305-0044, Japan

The optical visibility of mono- and few-layer graphene oxide (GO) under optical microscope (OM) is challenging even by using 300 nm SiO₂/Si substrate, which is the current standard for the visualization of pristine graphene. This is because of the large optical band-gap caused by higher degree of oxidation and intercalated water [1,2]. However, the optical contrast of GO can be improved by annealing GO on 300 nm SiO₂/Si substrate. Apart from the optical visualization, the effect of the substrate on intrinsic properties of GO or reduced graphene oxide (RGO) should be taken into consideration. Raman spectroscopy is a versatile tool to characterize structural, electronic, and optical properties of graphene-based materials [3]. A strong dependence of the Raman spectroscopy of monolayer pristine graphene on the thickness of the SiO₂ layer has been reported [4]. Yet, an in depth report on the effect of SiO₂ thickness or the type of substrate on the Raman spectra of GO and RGO has not been reported. In this work, we show the influence of the substrate on Raman spectral properties (peak position, intensity, etc.) of GO and RGO mono- and few-layer flakes, which is useful in interpreting the Raman spectra of these materials.

Individual GO flakes were obtained by spin coating an aqueous dispersion of GO on four different substrates, Si and Si with a SiO₂ thickness of 50, 90, and 300 nm. Two more sets of GO were prepared. One set was annealed at 800 °C/30 min in Ar/H₂ atmosphere (RGO) and the other set was annealed in ethanol vapour environment (EtOH-RGO) to restore the lattice defects (as we reported previously [5]). Figure 1 shows the Raman spectra of GO, RGO, and EtOH-RGO on different substrates. A dependence of the substrate on the Raman peak intensities and positions were observed. This has a strong relationship to the multilayer interference of light and multilayer reflection of Raman signal. The study gives a new insight to interpret Raman spectra of GO and RGO by considering the underlying substrate properties, in addition to the contribution for optical visibility.

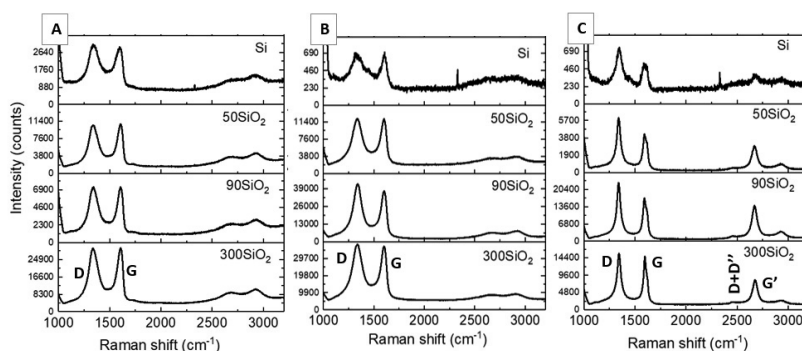


Figure 1: Raman spectra of (A) GO, (B) RGO, and (C) EtOH-RGO on different substrates.

[1] P. Blake and E. W. Hill, *Appl. Phys. Lett.*, **91**, 063124 (2007).

[2] X. Guo *et al.* *Nanotechnology*, **30**, 295704 (2019).

[3] J.B. Wu *et al.* *Chem. Soc. Rev.*, **47**, 1822 (2018).

[4] D. Yoon *et al.*, *Phys. Rev. B*, **80**, 125422 (2009).

[5] K.K.H. De Silva *et al.*, *Jap. J. Appl. Phys.*, **57**, 08NB03 (2018).

Corresponding Author: K.K.H. De Silva

Tel: +81-52-809-1852 E-mail: sd16501@toyota-ti.ac.jp

Synthesis of Mo₂C/C composite films as electrocatalyst for the hydrogen evolution reaction by microwave-plasma CVD method

○Shunsuke Numata¹ and Hironori Ogata^{1,2}

¹ Department of Chemical Science and Technology, Hosei University

² Research Center for Micro-Nano Technology, Hosei University

Electrocatalytic water splitting is one of the suitable methods for hydrogen production. However, this process relies on the electrocatalysis of the hydrogen evolution reaction (HER).

It is well known that Pt-based electrocatalysts show high current density at low overvoltages and are efficient HER electrocatalysts. However, since they are rare and expensive, transition metal carbide (TMC) such as molybdenum carbide has been proposed as an alternative to Pt, and much research has been done so far. It has been reported that the penetration of carbon atoms into the transition metal lattice increases the density of d-band electrons at the Fermi level, leading to Pt-like properties. In addition, it has been reported that HER and conductivity are improved by synthesizing TMC using nanocarbon materials [1].

In this study, we prepared Mo₂C / C composite films by directly laminating a nanocarbon materials on a molybdenum substrate by a microwave plasma chemical vapor deposition (MPCVD) method and investigated the possibility of application to a catalyst electrode for HER. Fig. 1 shows the Mo 3d XPS spectrum of the fabricated material. It was found that a Mo₂C/C composite film was formed. Detailed experimental results will be reported at the meeting.

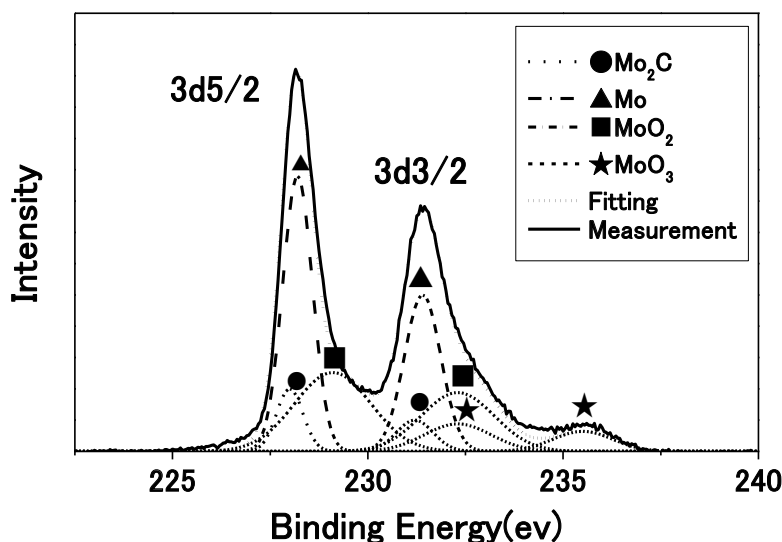


Fig. 1 Mo 3d XPS spectrum of prepared material

[1] Qiufang Gong *et al.*, *Nature Communication*, **7**, 2 (2016).

[2] Hongyang Zhao *et al.*, *Journal of Applied Physics*, **123**, 053301 (2018).

Corresponding Author: H. Ogata

E-mail: hogata@hosei.ac.jp

Anomalous electroluminescence from WS₂/WSe₂ in-plane heterostructures

○Naoki Wada¹, Jiang Pu², Tomoyuki Yamada², Wenjin Zhang³, Zheng Liu⁴, Yusuke Nakanishi¹, Yutaka Maniwa¹, Kazunari Matsuda³, Yuhei Miyauchi³, Taishi Takenobu², Yasumitsu Miyata¹

¹ Department of Physics, Tokyo Metropolitan University, Hachioji 192-0397, Japan

² Department of Applied Physics, Nagoya University, Nagoya 464-8603, Japan

³ Institute of Advanced Energy, Kyoto University, Uji, 611-0011, Japan

⁴ Inorganic Functional Materials Research Institute, AIST, Nagoya, 463-8560, Japan

Heterostructures of transition metal dichalcogenides (TMDCs) are an attractive system to realize high-performance devices such as light-emitting diodes and tunnel field-effect transistors. To investigate their electronic properties and device performance, we have developed growth processes of various in-plane heterostructures based on TMDC monolayers. In our previous studies, we have demonstrated the electric double layer light emitting diodes (EDLEDs) using these in-plane heterostructures [1-3]. In particular, we recently found that some samples show unique electroluminescence (EL) peaks, which have never been observed for photoluminescence spectra. However, the origin of these EL peaks is still unknown. In this study, we have investigated the spatially-resolved EL spectra of WS₂/WSe₂ in-plane heterostructures. The samples were grown by chemical vapor deposition (Fig.1a), and then EDLEDs were fabricated (Fig.1b). The device shows linear EL along the heterointerface by applying bias voltage (Fig. 1c). Interestingly, multiple EL peak components can be observed at a specific position along the interface as shown in Fig.1d. This suggests that the interface EL could be used to probe interface-derived electronic states and optical transitions. In this presentation, we will discuss about the detail of voltage- and site-dependent EL properties.

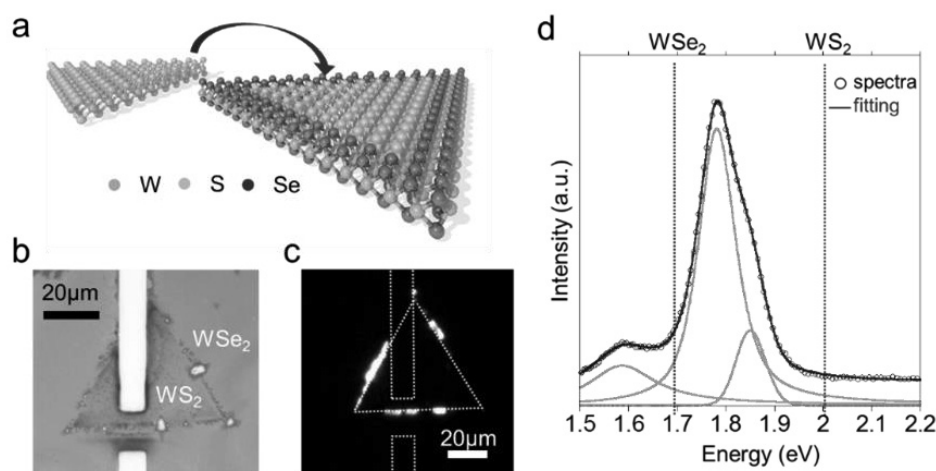


Fig.1 (a) Illustration of growth model of WS₂/WSe₂ in-plane heterostructures. (b) Optical and (c) EL images of WS₂/WSe₂-based EDLED device. (d) EL spectrum obtained at the interface.

[1] J. Pu et al., *Adv. Mater.*, 29, 1606918 (2017). [2] Y. Takaguchi et al., 56th FNTG symposium.

[3] N. Wada et al., 57th FNTG symposium.

Corresponding Author: Yasumitsu Miyata, Tel: 042-677-2508, E-mail: ymiyata@tmu.ac.jp

Effects of defect formation in monolayer MoS₂ by low energy Ar⁺ ion beam irradiation

○Yangzhou Zhao¹, Hiroki Yokota², Haruna Ichikawa², Yasushi Ishiguro², Kazuyuki Takai^{1,2}

¹ Graduate School of Science and Engineering, Hosei University, Tokyo 184-8584, Japan

² Dept. of Chemical Science and Technology, Hosei University, Tokyo 184-8584, Japan

MoS₂ is a kind of promising material in the application of electronic devices using two-dimensional (2D) materials, but the structural defects of MoS₂ always exist in either of samples by CVD-grown or exfoliated from natural mineral. The presence of defects has a great influence on the structure, and electronic properties of MoS₂ having 2D nature. In this study, in view of verifying the influence by defects on the structure and electronic properties, the monolayer MoS₂ is irradiated with low energy Ar⁺ ion beam in order to introduce defects under a well-controlled condition, and then evaluated by Raman spectroscopy, photoluminescence, and electrical conductivity.

A field effect transistor using MoS₂ obtained by exfoliation is fabricated on the SiO₂ / Si substrate. For defect-introduction, atomic vacancies are introduced into the surface of MoS₂ by low energy Ar⁺ beam irradiation at 100 eV accelerating voltage after annealing. After Ar⁺ ion irradiation, both of the line widths of E_{2g} and A_{1g} peaks in Raman spectra increase and become broad as the increase of irradiation time. The observed increase of the line width is considered mainly because of the increase of the contribution of satellite peaks caused by the introduction of defects [1]. Interestingly, the effect of the irradiation is more significant for E_{2g} in spite of its less sensitivity to charge transfer by molecular adsorption, where A_{1g} peak is much more sensitive due to the larger electron-phonon coupling [2].

As for photoluminescence (PL), after Ar⁺ ion irradiation, with the increase of irradiation time, the intensity of the peak at 1.84 to 1.88 eV decreases significantly with the emerging of a tail at the lower energy side. Interestingly, the peak around 1.35 eV assigned to the emission related to impurity levels also rapidly decreases upon ion beam irradiation.

The electrical conductivity measurements indicate that the shift of threshold voltage for MoS₂-FET “V_g shift” increases upon the irradiation time, suggesting the hole doping formation during the Ar⁺ ion irradiation. This might be explained by charge transfer from terminating oxygen atoms of defects originating from the residue oxygen gas in the measurement vacuum chamber.

[1] Soungmin Bae *et al.*, Phys. Rev. App., **7**, 024001(2017).

[2] B. Chakraborty *et al.*, Phys. Rev. B, **85**, 161403(2012).

Corresponding Author: Kazuyuki Takai

E-mail: takai@hosei.ac.jp

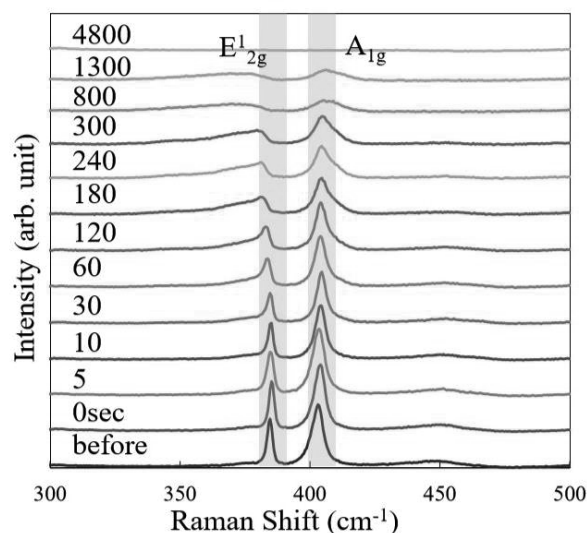


Fig.1 Raman spectra for monolayer MoS₂ irradiated Ar⁺ ion beam for 0-4800 sec and before annealing

Synthesis of NbSe₂ nanowires by selenization of niobium oxide nanowires

○Ryoga Tanaka, Yohei Yomogida, Yasumitsu Miyata, Kazuhiro Yanagi

Department of Physics, Tokyo Metropolitan University, Tokyo 192-0397, Japan

Transition-metal dichalcogenides (MX₂, M = Mo, W, Nb, X = S, Se) can form cylindrical structures of rolled MX₂ sheets, which show unique physical properties different from 2D materials. Their physical properties are expected to depend on constituent elements, but investigated elements so far have been limited. For example, synthesis and transport properties of semiconducting nanotubes such as WS₂ and WSe₂ have been studied [1,2]. On the other hand, those of superconducting nanotubes such as NbSe₂ nanotubes, which are interesting because of their low dimensional structures, have not been well investigated. These inorganic nanotubes are typically synthesized by chalcogenation of metal oxide nanowire precursor [1,2]. Thus, in this study, we applied chalcogenation to synthesized niobium oxide nanowires [3] and investigated whether niobium oxide nanowires are converted to chalcogenide cylindrical structures.

Niobium oxide nanowire precursors were synthesized by annealing Nb foils in a low vacuum (400 Pa) while supplying a small amount of air. Here we investigated the synthesis of niobium oxide nanowires by changing growth temperature (800-1000°C) and amount of supplied air (0.2-1.6 sccm). Thereafter, the obtained nanowire precursor was reacted with Se precursor for 30 min in 200 sccm Ar/H₂ flow (with 2% H₂).

The niobium oxide nanowires have a length of 10-50 μm and it is straightly grown from the surface of foil. Fig.1 shows a typical TEM image of the selenized sample. The structure of the selenized sample is similar to that of the oxide sample. This suggests that conversion took place without significant change of the structure. Considering Raman spectra shown in Fig.2, the selenized sample shows clear peaks of NbSe₂, which is different from those of Nb₂O₅. This result indicates that Nb₂O₅ nanowires are successfully converted to NbSe₂ nanowires. Interestingly, the selenized sample shows layered outer shells, suggesting the presence of rolled NbSe₂ sheets. In the poster, we will discuss specific content of synthesis and consideration of some conditions of synthesis.

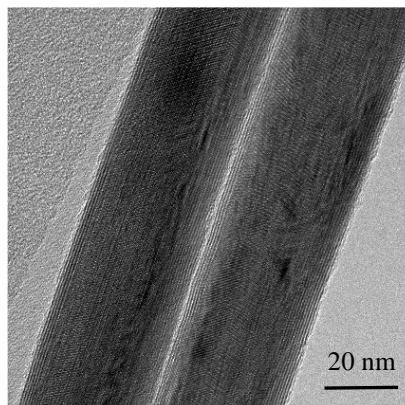


Fig. 1 TEM image of NbSe₂ nanowires.

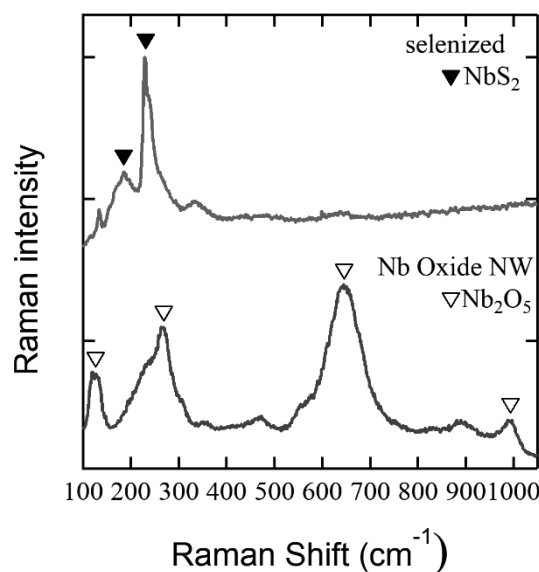


Fig. 2 Raman spectra of the selenized samples and Nb oxide nanowires.

- [1] Y. Yomogida *et al.*, Appl. Phys. Express **12**, 085001 (2019).
 [2] Y. Yomogida *et al.*, Appl. Phys. Lett. **116**, 203106 (2020).
 [3] J. H. Lim *et al.*, J. Ind. Eng. Chem. **15**, 860-864 (2009).

Polarized Raman Spectra of LaAlSi

○Tong Wang¹, Xiaoqi Pang¹, Nguyen T. Hung², Riichiro Saito¹

¹*Department of Physics, Tohoku University, Sendai 980-8578, Japan*

²*Frontier Research Institute for Interdisciplinary Sciences, Tohoku University, Sendai 980-8578, Japan*

LaAlSi is a type-II Weyl semimetal which has the Weyl nodes crossing the Fermi energy. In order to investigate the symmetry of phonon modes, polarized Raman spectroscopy is a useful tool. In this study, we present the calculated polarized Raman spectra and polar plot of Raman intensity for LaAlSi.

The resonant Raman spectra of LaAlSi are shown in Figure 1 for five polarization angles. There are five phonon modes which include 3 B_1 modes and 2 A_1 modes. For $B_1^{2^2}$ mode at 303 cm^{-1} , the peaks appear at 0, 90, 180 degrees and disappear at 45, 135 degrees. By analyzing with group theory, the B_1 mode has four-fold symmetry for the Raman intensity as a function of the angle, and the main peaks in polar plot appear at 0, 90, 180 degrees. However, the four-fold symmetry is broken in the calculated polar plot of the Raman intensity. In the poster section, we discuss the reason of the broken for four-fold symmetry.

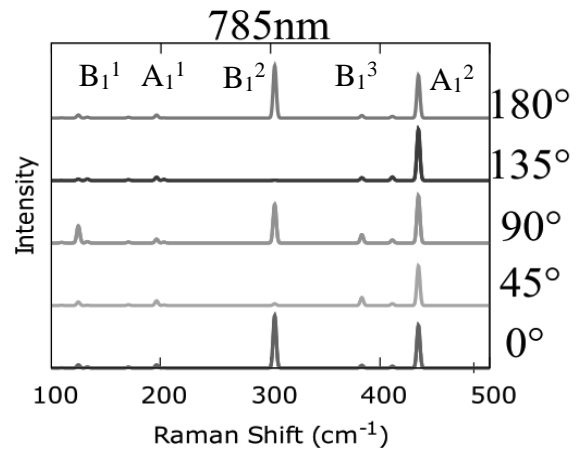


Figure 1. Polarized Raman spectra of LaAlSi by using laser energy 785nm.

In order to calculate the Raman intensity, we have used our own program [1] combined with the first-principle calculation, in which the electron-photon and electron-phonon interaction matrix elements are obtained by the Quantum-Espresso package [2] and EPW package [3], respectively.

[1] Y. Tatsumi, R. Saito, Phys. Rev. B 97, 115407 (2018).

[2] P. Giannozzi, *et al.*, J. Phys.: Condens. Matter 21, 395502 (2009)

[3] J. Noffsinger, *et al.*, Compt. Phys. Commun. 181, 2140 (2010)

Corresponding Author: Tong Wang

E-mail: wang@flex.phys.tohoku.ac.jp

Electronic and geometric structures of carbon nano-boxes of centrohexaquinane

○Yasumaru Fujii, Mina Maruyama, and Susumu Okada

Graduate School of Pure and Applied Sciences, University of Tsukuba, 1-1-1 Tennodai, Tsukuba, Ibaraki 305-8571, Japan

Polyquinane has been attracting much attention as building block of various real and hypothetical carbon allotropes covering all dimensions. Because of the unsaturated π electron states of pentagonal ring, covalent networks of polyquinane occasionally possess unusual electronic structures that are absent in the networks solely consisting of hexagonal rings. In addition to the electronic structure, the large number of possible combinations and arrangements of polyquinane and other hydrocarbons causes the rich morphological variety of polyquinane derivatives. For example, D. Kuck et al. reported that a cubic structure could be synthesized using a centrahexaindane which have a polyquinane structure in the center.

In this work, using the density functional theory with generalized gradient approximation, we theoretically designed three-dimensional covalent networks by copolymerizing centrohexaquinane [Fig1. (a)], which are arranged at the vertexes of cubic covalent network, and cyclooctatetraene, which are arranged at faces of the cubic network. Accordingly, the copolymers are three-dimensional carbon allotropes consisting of both sp^2 and sp^3 C atoms, forming C nano-boxes which are connected each others with $P\bar{4}3m$ [Fig1. (b)] and $Fm\bar{3}m$ [Fig1. (c)] symmetries, owing to two possible arrangements of centrohexaquinane. Our DFT calculation and MD simulation show that the both of copolymers are energetically and thermally stable, respectively. The electronic structure of copolymers are metals.

Corresponding Author: Y. Fujii
E-mail: yfujii@comas.frsc.tsukuba.ac.jp

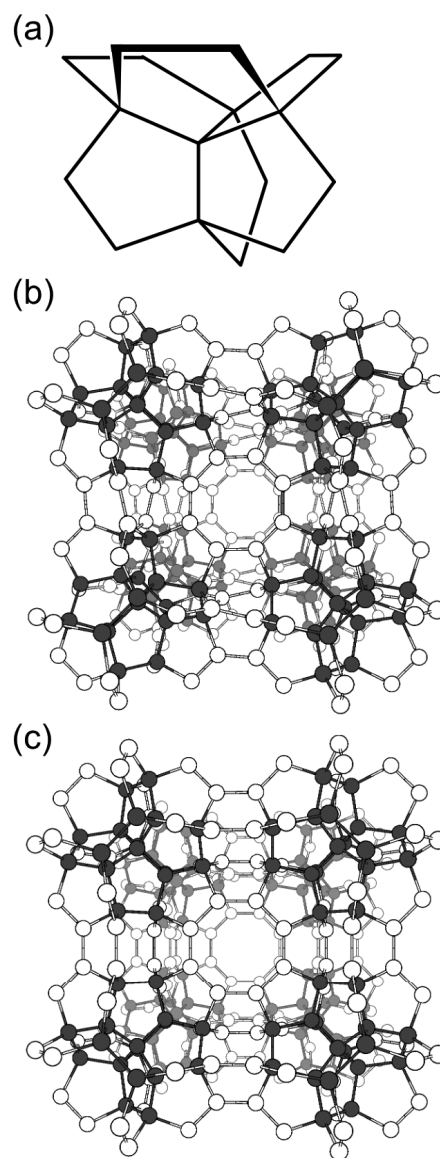


Fig.1 Geometric structure of (a) Centrohexaquinane, (b) C nano-boxes with $P\bar{4}3m$ and (c) C nano-boxes with $Fm\bar{3}m$ symmetry. Gray and white spheres denote sp^3 and sp^2 C atoms, respectively.

Elucidation of adsorption state of polybenzimidazole on carbon surface by adsorption isotherm measurement

○Nana Kayo¹, Tsuyohiko Fujigaya^{1, 2, 3}

¹ Department of Applied Chemistry, Kyushu University, Fukuoka 819-0395, Japan

² WPI-I2CNER, Kyushu University, Fukuoka 819-0395, Japan

³ CMS, Kyushu University, Fukuoka 819-0395, Japan

In polymer electrolyte fuel cells (PEFC), a composite of carbon black (CB) with platinum particles (Pt) is widely used as an electrode catalyst after mixing with acidic electrolyte. However, low platinum utilization efficiency because of the uneven distribution of acid electrolyte on the CB surface that caused the insufficient, protons transport was the issue [1]. We reported the improvement of platinum utilization efficiency and power density by coating of polybenzimidazole (PBI) onto CB surface prior to the platinum loading [2], in which the distribution of the electrolyte become uniform by the coating of PBI (Fig. 1). However, coating state such as homogeneity and coverage ratio of PBI onto CB has not been clarified yet.

In this study, the adsorption state of PBI on carbon materials such as CB (Vulcan) and carbon nanotube (CNT) was studied by the adsorption isotherm and the interaction between the CB and PBI was investigated. Fig. 2 showed the adsorption isotherm of PBI on CB measured at 25 °C using *N,N*-dimethylacetamide (DMAc) as a solvent. It was revealed that PBI adsorption reached adsorption equilibrium from a low concentration (0.005 mg/mL), suggesting that PBI was adsorbed in a monolayer manner on the CB quite efficiently. In addition, the PBI coverage ratio calculated from the Langmuir equation showed as high as 99.9% at the concentration of 0.50 mg /mL used for the PBI coating. Therefore, we concluded PBI uniformly coats CB in monolayer.

Based on the adsorption isotherm experiments at different temperature, ΔH and ΔS were estimated to be 14 kJ/mol and 0.11 kJ/mol, respectively. The temperature dependence of the isotherm revealed that this adsorption process was entropy-driven process since the PBI adsorption amount was increased with increasing the temperature. The adsorption behavior and interaction of PBI with other carbon materials including CNT will be discussed in the presentation.

[1] S. Jayawickrama et. al., *Electrochim. Acta*, **312**, 349 (2019).

[2] T. Fujigaya, et al., *ACS Appl. Mater. Interfaces*, **8**, 14494 (2011)

Corresponding Author: T. Fujigaya

Tel/Fax: +81-92-802-2842,

Web: <http://www.chem.kyushu-u.ac.jp/~fifth/jp/>

E-mail: fujigaya.tsuyohiko.948@m.kyushu-u.ac.jp



Fig. 1 Schematic illustration of this research.

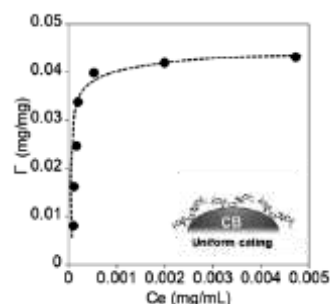


Fig. 2 Adsorption isotherm of PBI onto CB.

Understanding the Effect of Sulfur on the Synthesis of Carbon Nanotubes

○ Rei NAKAGAWA¹, Michiko EDO¹, Hisashi SUGIME¹, Suguru NODA^{1,2,*}

¹Department of Applied Chemistry, ²Waseda Research Institute for Science and Engineering, Waseda University, Tokyo, Japan

Carbon Nanotubes (CNTs) are attractive with high hopes in many different fields for their excellent properties. However, the practical applications of CNTs has been a challenge due to their high price and/or insufficient quality. Floating catalyst chemical vapor deposition (CVD) enables the synthesis of high quality CNTs, but it has had an issue with its low catalyst usage. To combat this situation, many groups have conducted research to improve the productivity of this process, and as a result it has been reported that the implementation of sulfur can increase the overall yield of floating catalyst CVD [1]. Many groups have proposed positive roles of sulfur; Fe-S to be the active site for catalytic reaction or reduced surface energy of Fe-S for nucleation of small Fe particles. However, these models are not supported by clear evidences and are not applicable to supported catalysts.

Here, we propose an opposite model where sulfur deactivates the Fe catalyst. Small amount of sulfur forms an inactive region on a Fe particle, and the inactive region works as an entrance for the carbon source without being covered with graphitic carbon. The analysis of this is difficult for floating catalysts, therefore for this research, supported catalysts were used by implementing graphite sheets as substrates to replicate the floating catalysts with spherical structure. Scanning electron microscope (SEM) shows that CNTs were only synthesized when S was supplied during synthesis (Fig. 1a). Additionally, to confirm the importance of having an inactive region within the catalyst particle for CNT synthesis, a thin Al₂O₃ layer was deposited on top of the Fe catalysts. The thin Al₂O₃ layer significantly enhanced the CNT growth (Fig. 1b) in a similar manner as sulfur. These results suggests a new approach for future catalyst design.

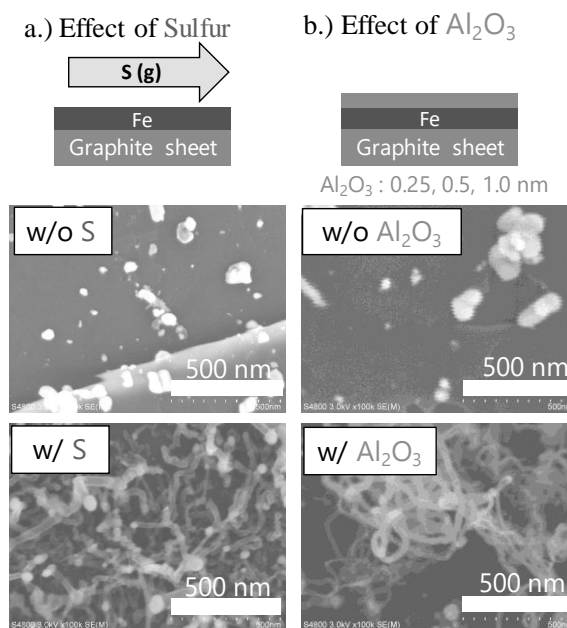


Fig. 1. SEM analysis of graphite substrates after CNT synthesis. (a) Sulfur vapor was supplied to the Fe catalyst during synthesis. (b) Al₂O₃ thin layer was deposited on the Fe catalyst.

[1] H.M. Cheng, et al., *Appl. Phys. Lett.* **72**, 3282 (1998).

Corresponding Author: S. Noda, Tel&Fax: +81-3-5286-2769, E-mail: noda@waseda.jp

Directional exciton diffusion in pentacene-decorated carbon nanotubes

○Zhen Li^{1,2}, Keigo Otsuka², Daiki Yamashita¹, Yuichiro K. Kato^{1,2}

¹*Quantum Optoelectronics Research Team, RIKEN Center for Advanced Photonics,
Saitama 351-0198, Japan*

²*Nanoscale Quantum Photonics Laboratory, RIKEN Cluster for Pioneering Research,
Saitama 351-0198, Japan*

Photoluminescent carbon nanotubes are anticipated to become versatile room-temperature single-photon sources that are crucial for quantum information processing. The optical processes in carbon nanotubes are dominated by the so-called excitons, whose binding energies are sensitive to the surrounding dielectric environment. To modify the exciton properties in carbon nanotubes, molecular adsorption has been proven as an effective approach [1-3]. When suitable molecules are adsorbed onto a nanotube, excitons nearby are expected to accumulate at the adsorbed site and engage in enhanced exciton-exciton annihilation, leading to single-photon emission at wavelengths modulated by the molecules.

Here, by decorating individually suspended single-walled carbon nanotubes with isolated pentacene particles, we demonstrate tuning of the excitonic energies and directional exciton diffusion induced by molecular screening. Pentacene particles with controllable sizes in the range of tens of nanometers are deposited onto the nanotubes via thermal evaporation. Bright photoluminescence is observed, and peaks corresponding to the pristine region and the pentacene-adsorbed site on the nanotube can be distinguished in the photoluminescence excitation spectra. The excitonic energies are lowered at the adsorbed site compared to that in the pristine region as evidenced by the redshifted emission wavelengths. Importantly, directional exciton diffusion is achieved, where excitons transfer from the pristine region to the adsorbed site on the nanotube due to the energy difference. Time-resolved photoluminescence measurements reveal the exciton lifetimes, and photon antibunching is demonstrated in the adsorbed region.

Work supported in part by MIC (SCOPE 191503001), JSPS (KAKENHI JP20H02558, JP20K15121, JP20K15137, and JP20K15199), and MEXT (Nanotechnology Platform JPMXP09F19UT0079). K. O. and D. Y. are supported by the JSPS Research Fellowship. We acknowledge the Advanced Manufacturing Support Team at RIKEN for technical assistance.

[1] T. Uda, A. Ishii, Y. K. Kato, *ACS Photonics* **5**, 559-565 (2018).

[2] T. Uda, S. Tanaka, Y. K. Kato, *Appl. Phys. Lett.* **113**, 121105 (2018).

[3] S. Tanaka, K. Otsuka, K. Kimura, A. Ishii, H. Imada, Y. Kim, Y. K. Kato, *J. Phys. Chem. C* **123**, 5776-5781 (2019).

Corresponding Author: Yuichiro K. Kato

Tel: +81-48-462-1449

Web: <http://katogroup.riken.jp>

E-mail: yuichiro.kato@riken.jp

Locally functionalized single-walled carbon nanotubes synthesized by azide compounds and their photoluminescence properties

○Keita Hayashi¹, Tsuyohiko Fujigaya^{1,2,3}, Tomohiro Shiraki^{1,2}

¹ Department of Applied Chemistry, Kyushu University, Fukuoka 819-0395, Japan

² WPI-I2CNER, Kyushu University, Fukuoka 819-0395, Japan

³ CMS, Kyushu University, Fukuoka 819-0395, Japan

Single-walled carbon nanotubes (SWNTs) with semiconducting features show photoluminescence (PL) in the near infrared (NIR) region and are promising for applications such as optical communication devices. The PL arises from the recombination of exciton generated by the photoexcitation of SWNTs. Recently, local chemical functionalization has been conducted for structural defect doping to the crystalline semiconducting structures of SWNTs. As a result, new emissive sites that have narrower bandgaps and exciton trapping features are created and the locally functionalized SWNTs (lf-SWNTs) emit redshifted and brighter E_{11}^* PL compared to E_{11} PL of pristine SWNTs. The E_{11}^* PL wavelengths of lf-SWNTs are changed with the dependence on the functionalized molecules of the doped sites. For example, oxygen doping using ozone treatment produced ether and/or epoxide structures in the lf-SWNTs, which showed different PL wavelengths depending on its structure [1,2]. Aryldiazonium salts created sp^3 carbon defects for the lf-SWNTs, in which substituents of the functionalized aryl groups and proximal doping were found to shift E_{11}^* PL wavelengths [3-5].

Here, we utilized organic azide compounds to synthesize lf-SWNTs. For the local chemical functionalization, SWNTs were solubilized in a surfactant solution of D_2O and reacted with an azide compound. Fig. 1 shows PL spectrum of the synthesized lf-SWNTs. Two PL peaks were observed at 977 nm and 1116 nm. The former one is assigned as E_{11} PL and the latter one that appears after the chemical reaction is considered as E_{11}^* PL from the doped sites. Interestingly, the intensity of E_{11} PL after the reaction hardly decreased compared to the typical lf-SWNTs. This result indicates that not only E_{11}^* PL wavelengths but also conversion efficiency of exciton to PL could be changed depending on the doped site structures. It may relate to the difference in electron and exciton localization at the doped sites, which was indicated by density functional theory calculation results. Thus, azide compounds would be useful to functionalize and modulate NIR PL properties of lf-SWNTs based on the unique exciton behaviors.

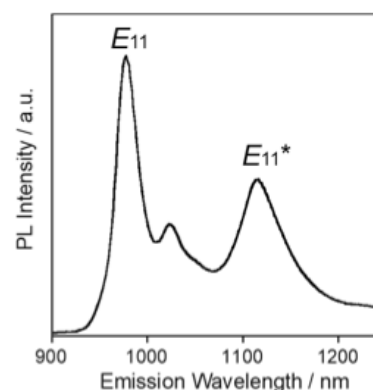


Fig. 1 PL spectrum of the synthesized lf-SWNT. $\lambda_{ex} = 570$ nm.

- [1] R. B. Weisman *et al.*, *Science*, **330**, 1656 (2010).
- [2] H. Htoon *et al.*, *ACS Nano*, **8**, 10782 (2014).
- [3] Y. Wang *et al.*, *Nat. Chem.*, **5**, 840 (2013).
- [4] T. Shiraki *et al.*, *Chem. Commun.*, **53**, 12544 (2017).
- [5] T. Shiraki *et al.*, *Sci. rep.*, **6**, 28393 (2016).

Corresponding Author: T. Shiraki

Tel/Fax: +81-92-802-2841,

Web: <http://www.chem.kyushu-u.ac.jp/~fifth/jp/>

E-mail: shiraki.tomohiro.992@m.kyushu-u.ac.jp

Temperature dependence of Raman G-band shift in defective single-walled carbon nanotubes

○Masanori Endo¹, Haruki Uchiyama¹, Yutaka Ohno^{1,2} and Jun Hirotsu¹

¹ Department of Electronics, Nagoya University, Nagoya 464-8601, Japan

² Institute of Materials and Systems for Sustainability, Nagoya University, Nagoya 464-8601, Japan

Carbon nanotubes (CNTs) are considered good thermal management devices, [1] and the thermophysical properties of CNTs have been explored by various methods such as Raman spectroscopy, IR thermometry, and scanning thermal microscopy. Raman spectroscopy is a powerful tool for simultaneously heating samples and measuring sample temperature. Temperature of CNTs inside the laser spot can be obtained by the G-band shift. In a previous study, the Raman shift of the G-band was found to exhibit universal temperature dependence in several CNT samples grown by different methods. [2] However, the relationship between a wide range of quality of CNTs and temperature dependence of G-band shift is still unclear. In this work, we have investigated temperature dependence of Raman G-band shift and estimated thermal and electrical conductivities of CNT thin film of various degree of defect densities.

High-quality single-walled CNTs with a G/D ratio of ~90 were grown by floating-catalyst chemical vapor deposition. A CNT thin film was formed on a Si substrate by the dry transfer process. Raman measurement was conducted in vacuum of 3×10^{-2} Pa. A 532-nm excitation laser was used for Raman measurement. The excitation power was set to be 10^3 W/cm² so as not to elevate the temperature of the CNT thin film. Temperature of the sample was controlled by a Peltier module. Defects were induced by UV/ozone treatment. [3]

Figure 1 shows the temperature coefficient of Raman G⁺-peak frequency as a function of G/D ratio. As G/D ratio decreased, the temperature coefficient was increased, which might be attributed to bond-softening due to increased defects. In addition, we investigated the effect of the defect introduction on both thermal and electrical conductivities. It was found that the electrical conductivity was degraded more significantly with a decrease in G/D ratio than thermal conductivity was.

[1] B. Kumanek and D. Janas, *J. Mater. Sci.* **54**, 7397 (2019).

[2] S. Chiashi et al., *Jpn. J. Appl. Phys.* **47**, 2010 (2008).

[3] Y. Nonoguchi et al., *J. Appl. Phys.* **126**, 135108 (2019).

Corresponding Author: J. Hirotsu, Phone & Fax: +81-52-789-5455, E-mail: hirotsu@nuee.nagoya-u.ac.jp

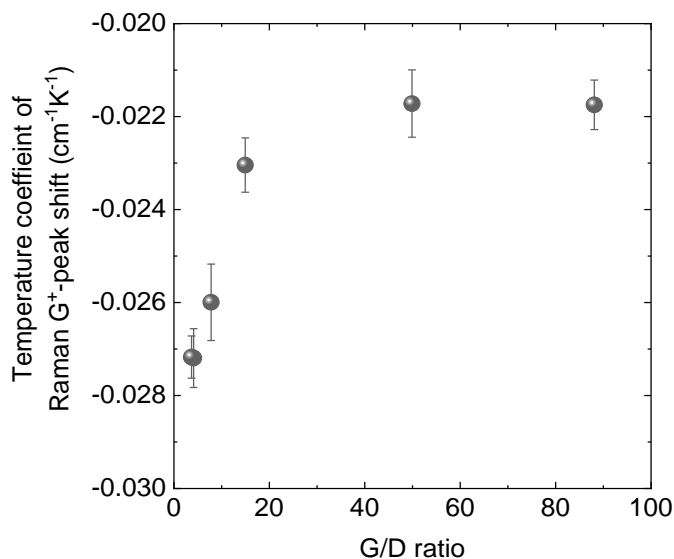


Figure 1. Relationship between G/D ratio and temperature coefficient of Raman G⁺-peak shift.

Doping of single-walled carbon nanotube by thermal evaporation method

○Ryohei Yamaguchi¹, Kaito Oda^{2,3}, Motohiro Tomita^{2,3}, Takanobu Watanabe^{2,3}, Tsuyohiko Fujigaya^{1,4,5}

¹ Graduate School of Engineering, Kyushu University, Fukuoka 819-0395, Japan

² Faculty of Science and Engineering, Waseda University, Tokyo 169-8555, Japan

³ Japan Science and Technology Agency (JST) CREST, Tokyo 102-0076, Japan

⁴ WPI- I²CNER, Kyushu University, Fukuoka 819-0385, Japan

⁵ Center for Molecular Systems (CMS), Kyushu University, Fukuoka 819-0395, Japan

Single-walled carbon nanotubes (SWNTs) is ideal materials for thermoelectric (TE) conversion because of their high Seebeck coefficient and electrical conductivity. Development of the wearable thermoelectric device using SWNTs is now investigated by taking advantage of their film toughness and flexibility. Up to date, π -shape structure has been proposed for the SWNT thermoelectric devices. However, this structure needs to attach on a skin vertically and not preferable for the wearable application. Therefore, we proposed a new planar-type structure using SWNT sheet (Fig. 1a) [1]. The planar-type SWNT TE device can attach on the skin surface and preferable as a wearable device.

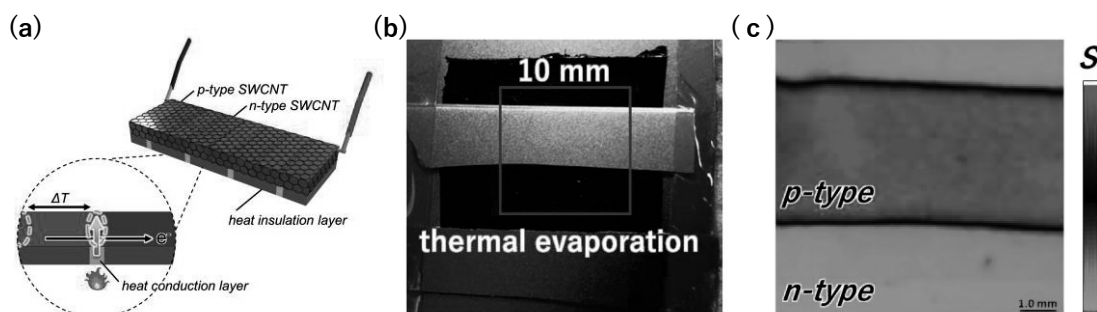


Fig.1 (a) Schematic illustration of planar type TE device using SWNT sheet. (b) Photograph and (c) Seebeck coefficient imaging of the DMBI-I-doped SWNT sheet covered mask.

Since sequential repeating of p-type and n-type properties are necessary for the devices, in this study, we investigated the patterned doping of p-type SWNT sheet into n-type using thermal evaporation method. To realize this idea, 2-(2-Methoxyphenyl)-1,3-dimethyl-1H-benzimidazol-3-ium iodide (DMBI-I) was used as a dopant [2]. We deposited DMBI-I to SWNT sheet having a thickness of 50 nm by masking a part of the sheet as shown in Fig. 1b. Seebeck coefficient of the obtained SWNT sheet was mapped by thermal probe micro image (ADVANCE RIKO Inc.; STPM-1000) and found that the masked area kepted p-type, while exposed area was turned to n-type (Fig. 1c) [3].

[1] T. Watanabe et al., *IEEE EDTM.*, **86** (2017).

[2] Z. Bao et al., *Proc. Natl. Acad. Sci. USA*, **111**, 4776 (2014).

[3] R. Yamaguchi et al., in preparation.

Corresponding Author: T. Fujigaya

Tel: +81-92-802-2842, Fax: +81-92-802-2842,

Web: <http://www.chem.kyushu-u.ac.jp/~fifth/jp/>

E-mail: fujigaya.tsuyohiko.948@m.kyushu-u.ac.jp

Growth of Monolayer MoS₂ Lateral *p-n* Junction with *p*-type Substitutional Nb Doping

○Mitsuhiro Okada¹, Toshifumi Irisawa², Naoya Okada², Wen-Hsin Chang², Tetsuo Shimizu¹, Toshitaka Kubo¹, Masatou Ishihara¹

¹ Nanomaterials Research Institute, AIST, Tsukuba 305-8565, Japan

² Device Technology Research Institute, AIST, Tsukuba 305-8568, Japan

The development of carrier doping is one of the most significant issues in achieving high performance two-dimensional (2D) transition metal dichalcogenides (TMDs) based devices. Substitutional doping technique is a common carrier doping method in conventional semiconductors due to its thermodynamic stability. However, for TMDs, the substitutional doping method is still in infancy. In this work, we report the chemical vapor deposition (CVD) growth of monolayer MoS₂ *p-n* lateral homojunction. Local doping of Nb, an acceptor of Group-VI TMDs by substitution for Mo or W [1], has allowed us to obtain monolayer MoS₂-based *p-n* diode: the obtained crystal shows current rectification behavior at the interface between Nb-doped and non-doped MoS₂ layers.

MoS₂ lateral *p-n* junction has been grown by a CVD method with alkali-metal assistance [2]. As metal precursors, we have used MoO₃ and Nb for Mo and Nb source, respectively. Due to the large vapor pressure difference of these precursors, we have succeeded in doping Nb locally at an edge of a MoS₂ crystal. Partially-Nb-doped MoS₂ crystal was confirmed, using scanning electron microscope (SEM), whose image is shown in Fig. 1. The contrast difference between inner and outer regions of a triangular crystal is caused by the electronic structural difference.

Field-effect transistor (FET) characteristics of an Nb-doped (outer) and a non-doped (inner) region of a MoS₂ crystal is shown in Fig. 2. FET characteristics measured in the outer and the inner region shows *p*- and *n*-type operation, respectively. Figure 3 shows an I_{ds} - V_{ds} characteristic of the Nb-doped MoS₂-non-doped MoS₂ interface. The result shows current rectification behavior, indicating that *p-n* junction is formed at the interface.

In summary, we have grown monolayer Nb-doped MoS₂-non-doped MoS₂ lateral homojunction by the CVD method. The obtained homojunction shows a diode behavior, indicating the *p-n* junction formation at the interface. Our findings would be a basis of doping technology on TMDs.

This work was supported by JSPS KAKENHI Grant No. 19K15403 and JST-CREST Grant No. JPMJCR16F3, MEXT, Japan.

[1] K. Dolui *et al.*, Phys. Rev. B, **88**, 075420 (2013).

[2] S. Li *et al.*, Appl. Mater. Today, **1**, 60 (2015).

Corresponding Author: M. Okada

Tel: +81-29-861-2880, Fax: +81-29-861-3005,

Web: <https://unit.aist.go.jp/nmri/index.html>

E-mail: mi.okada@aist.go.jp

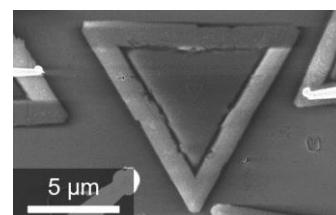


Fig. 1. SEM image of a partially-Nb-doped MoS₂.

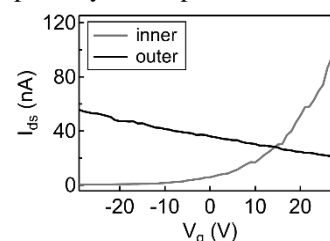


Fig. 2. I_{ds} - V_g characteristics of an obtained crystal.

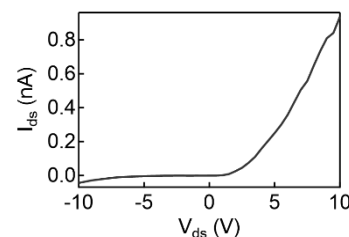


Fig. 3. I_{ds} - V_{ds} characteristic of Nb-doped MoS₂-non-doped MoS₂ interface.

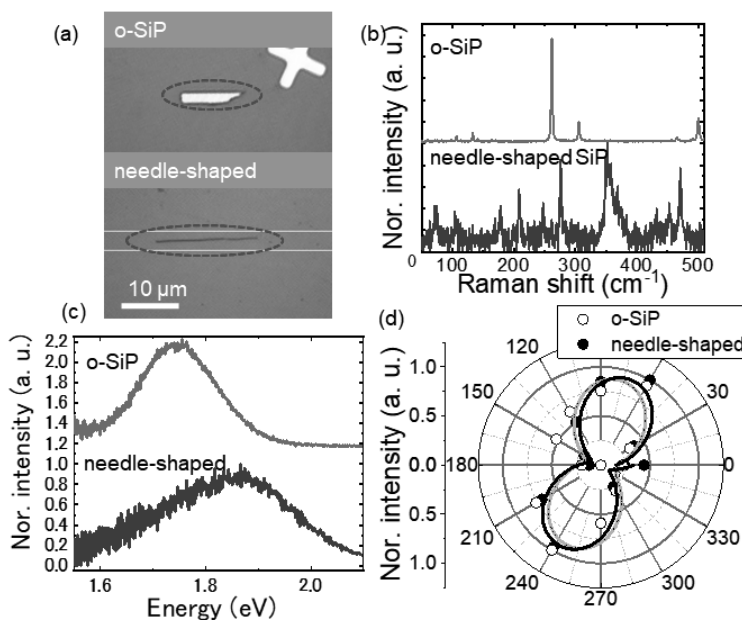
Two-dimensional silicon phosphide with anisotropic optical and electronic properties

○Mikio Kobayashi, Keisuke Shinokita, Yuhei Miyauchi, Kazunari Matsuda

Institute of Advanced Energy, Kyoto University, Uji 611-0011, Japan

Two-dimensional layered semiconductors have recently attracted tremendous interest, because of their novel optical and electronic properties. Layered silicon phosphide (SiP) is a promising candidate for the next-generation optoelectronic devices because it is theoretically predicted to have unique properties including high stability in air, high carrier mobility ($2.034 \times 10^3 \text{ cm}^2 \text{V}^{-1} \text{s}^{-1}$), anisotropic electronic properties, and bandgap in visible region [1-2]. However, the intriguing properties are not well verified experimentally, since the synthesis of the SiP crystals was succeeded quite recently [1]. Here we studied the electronic and optical properties of layered SiP by using optical absorption, Raman scattering, and photoluminescence (PL) spectroscopy.

Fig. 1(a) shows optical image of the mechanically exfoliated SiP crystal synthesized using Flux zone technique. The different flake shapes of plane- and needle-shape indicate the layered SiP crystal contains two allotropes in growth process. Fig. 1(b) shows Raman spectra of the two allotropes. The different Raman spectra indicate the two allotropes have different crystal structure: The plane- and needle-shaped SiP can be assigned to orthorhombic structure with Cmc2 space group (o-SiP) and lower-symmetry crystal structure, respectively. The PL spectra have peaks at 1.74 eV and 1.87 eV for plane- and needle-shaped SiP, respectively, as shown in Fig. 1(c), suggesting different bandgap transition energy and electronic state of two crystal structures. Figure 1(d) shows the polarization dependence of PL intensity of two allotropes. Both the plane- and needle-shaped SiP show polarization-dependence, indicating the anisotropic optical properties originating from the crystal structure of two allotropes. Our experimental results of optical and electronic properties of layered SiP suggest the possibility of tunable optical and electronic properties while retaining the anisotropic properties by changing crystal structure of 2D materials.



[1] C. Li *et al.*, *CrystEngComm*, **19**, 6986 (2017).

[2] S. Zhang *et al.*, *2D Mater.* **4**, 015030 (2017).

Corresponding Author: K. Matsuda

Tel: +81-774-38-3465

E-mail: matsuda@iae.kyoto-u.ac.jp

Fig1 (a) Optical images of SiP crystal. (b) Raman scattering spectrum and (c) PL spectrum of SiP.

(d) Polar plot of the integrated PL intensity.

Electron transport properties of WTe nanowire networks

○Hiroshi Shimizu¹, Jiang Pu², Hong En Lim¹, Yusuke Nakanishi¹, Zheng Liu³,
Takahiko Endo¹, Taishi Takenobu², Yasumitsu Miyata¹

¹ Department of Physics, Tokyo Metropolitan University, Hachioji 192-0397, Japan

² Department of Applied Physics, Nagoya University, Nagoya 464-8603, Japan

³ Innovative Functional Materials Research Institute, AIST, Nagoya 463-8560, Japan

Transition metal chalcogenide (TMC) nanowires (Fig.1a) have attracted much attention in recent years because of their one-dimensional metallic properties and electronic device applications. To date, many groups have reported the preparation and properties of individual and bundled TMC nanowires including as Mo₆S₆, Mo₆Se₆, and Mo₆Te₆ [1-5]. Recently, our group has achieved large-area growth of TMC nanowires using chemical vapor deposition (CVD) [6]. Depending on the affinity with substrate surface, this technique also enables network formation of either aligned atomically thin two-dimensional (2D) sheets or random network of three dimensional (3D) bundles composing of individual nanowires. For these samples, it is expected that the morphology such as bundle size will strongly affect the electron transport properties of TMC nanowire networks.

In this study, we have investigated the temperature dependence electron transport of WTe nanowire networks with various densities and morphologies. The samples were grown on SiO₂ or Al₂O₃ surface using CVD, and the network formation was confirmed using scanning electron microscope (SEM)(Fig.1b). At room temperature, the sheet resistances of samples vary from 2 kΩ to 75 MΩ depending on the nanowire density. The high-density network shows a metallic behavior from room temperature to 20 K, whereas almost no temperature dependence is observed for the low-density network (Fig.1c). In the presentation, we will discuss a possible mechanism for the temperature dependence electron transport.

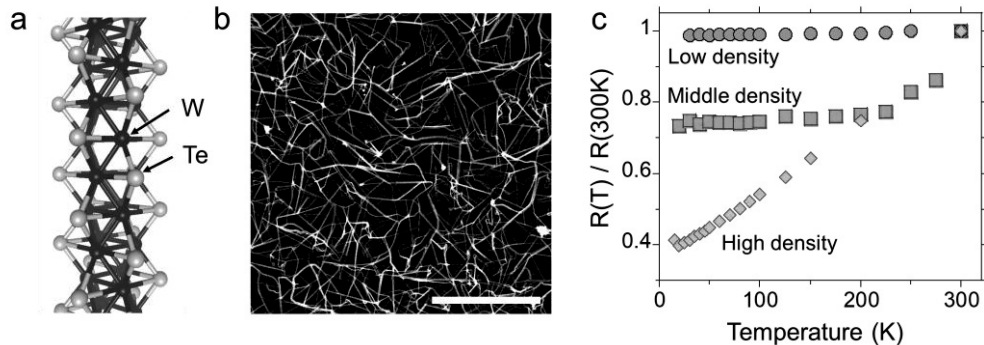


Figure 1 (a) Structure model of the WTe nanowire. (b) SEM image of WTe nanowire network. Scale bar is 10 μm. (c) Temperature-dependent resistance (normalized to 300 K) of the random networks of WTe nanowires with various nanowire densities (Low, middle, and high densities).

- [1] L. Venkataraman *et al.*, Phys. Rev. Lett., **83**, 5334 (1999).
- [2] L. Venkataraman *et al.*, Phys. Rev. Lett., **96**, 076601 (2006).
- [3] J. Kibsgaard *et al.*, Nano Lett., **8**, 11 (2008).
- [4] J. Lin *et al.*, Nat. Nanotechnol., **9**, 436 (2014).
- [5] M. Nagata *et al.*, Nano Lett., **19**, 4845–4851 (2019).
- [6] H.-E. Lim *et al.* Submitted.

Corresponding Author: Y. Miyata, Tel: +81-42-677-2508, E-mail: miyata-yasumitsu@tmu.ac.jp

Preparation of ruthenium oxide-[C₆₀]fullerene nanowhiser composites and their photocatalytic activity for degradation of azo dyes

○Jeong Won Ko¹, Sugyeong Jeon², Weon Bae Ko^{1,2,3}

¹Nanomaterials Research Institute, ²Department of Convergence Science, Graduate School, ³Department of Chemistry, Sahmyook University, 815 Hwarang-ro, Nowon-gu, Seoul 01795, Republic of Korea

Ruthenium (III) chloride hydrate (RuCl₃·nH₂O) and polyvinyl pyrrolidone(PVP) were dissolved in mixed solvents of distilled water and methanol. Then, sodium borohydride (NaBH₄) was put into it. The solution was continuously stirred to prepare ruthenium oxide for 6 h [1]. Ruthenium oxide-[C₆₀]fullerene nanowhiser composite was synthesized by using ruthenium oxide solution, C₆₀-saturated toluene, and isopropyl alcohol by liquid-liquid interfacial precipitation (LLIP) method [2]. The surface morphology, particle size, and properties of ruthenium oxide-[C₆₀]fullerene nanowhiser composites were examined using scanning electron microscopy (SEM), X-ray diffractometer (XRD), Raman spectrometer and UV-vis spectrophotometer.

Ruthenium oxide-[C₆₀]fullerene nanowhiser composite as photocatalyst for degradation of various azo dyes were irradiated ultraviolet light at 254 nm. The order of photocatalytic degradation efficiency of azo dyes with ruthenium oxide-[C₆₀]fullerene nanowhiser composites was Methyl Orange (MO) > Acid Orange 7 (AO7) > Acid Yellow 23 (AY23). Kinetic study for photocatalytic degradation of azo dyes was followed a pseudo-first order reaction.

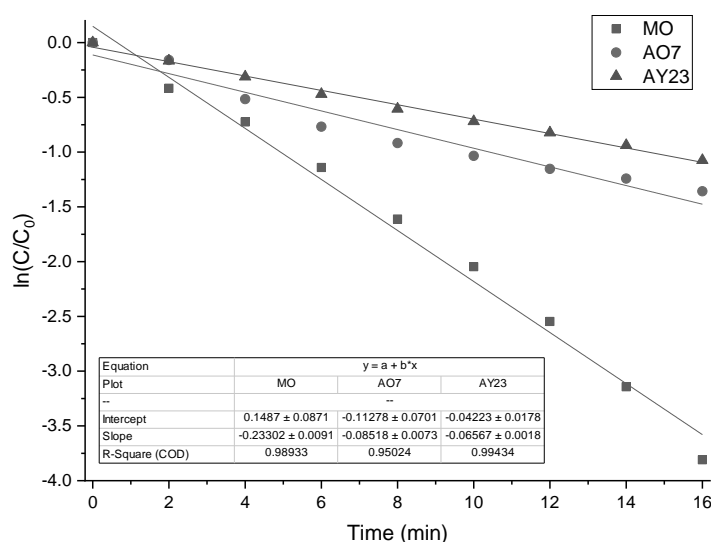


Fig.1 Kinetics study for degradation of azo dyes with ruthenium oxide-[C₆₀]fullerene nanowhiser composites.

[1] L. Xu and J. Yang, Phys. Sci. Rev. doi.org/10.1515/psr-2017-0080 **3**, 12 (2018).

[2] K. Miyazawa *et al.* Surf. Eng. doi.org/10.1080/02670844.2017.1396779 (2017).

Corresponding Author: W. B. Ko

Tel: +82-2-3399-1700, Fax: +82-2-979-5318,

E-mail: kowb@syu.ac.kr

CNT/copper composite yarn made from metallic nanoparticle-decorated spin-capable CNT forest

○Kosuke Tanaka, Takayuki Nakano, Yoku Inoue

Department of Electronics and Materials Science, Shizuoka University, Hamamatsu 432-8561, Japan

Carbon nanotubes (CNTs) are lightweight and have excellent mechanical, thermal, and electrical properties. Since it can be upsized using the dry spinning, it is being researched to apply to various fields. In particular, CNT yarn is expected to play a role as an alternative to the currently used wire rods. However, the electrical conductivity of the CNT yarn is smaller than that of metallic wires. To solve this problem, a composite of CNT and copper has been researched. Previously, it has been reported that the current capacity is significantly improved by uniformly depositing copper even inside the CNT structure.

Therefore, in this research, we aimed to improve the electrical properties by producing a composite material that contained copper evenly inside the CNT yarn.

FeCl_2 was used as a precursor to synthesize a CNT forest by chlorine mediated chemical vapor deposition (CVD). Then, copper nanoparticles were wholly deposited on CNTs by decomposing Cu precursor. A CNT web was pulled out from a CNT forest to prepare a CNT yarn. Here, CNTs are decorated with the Cu nanoparticles, and therefore, Cu nanoparticles were incorporated inside the yarn. Then, the CNT yarn was dipped in a copper sulfate aqueous solution and subjected to electroplating treatment to fabricate a CNT/Cu composite yarn. The CNT/Cu composite yarn after the electroplating treatment was finally reduced by hydrogen.

Figure 1 shows an SEM image of a CNT forest decorated with copper nanoparticles. The number of Cu nanoparticles was controlled by some deposition parameters. It confirmed that Cu nanoparticles were entirely decorating CNTs inside the forest. Figure 2 shows a cross-sectional SEM image of a CNT/Cu composite yarn. It can be seen that copper is filled inside the CNT yarn. We found that the incorporated Cu nanoparticles attracted Cu ions inside yarns during the electroplating, and it resulted in the present uniform composition of Cu and CNT. Fabrication of the uniform CNT/Cu composite yarn and its electrical properties will be discussed.

Corresponding Author: Yoku Inoue

Tel: +81-53-478-1356, Web: <http://cnt.eng.shizuoka.ac.jp/>, E-mail: inoue.yoku@shizuoka.ac.jp

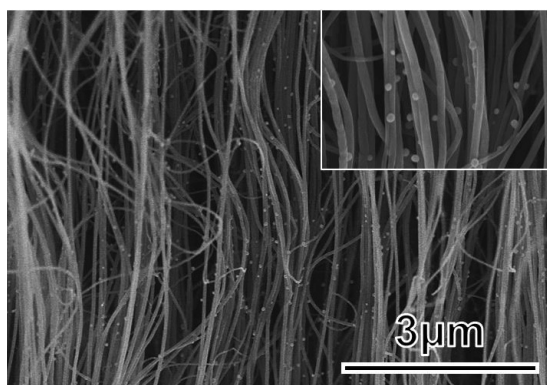


Fig.1 SEM image of CNT forest supporting copper nanoparticles. Inset shows a high magnification image of CNTs

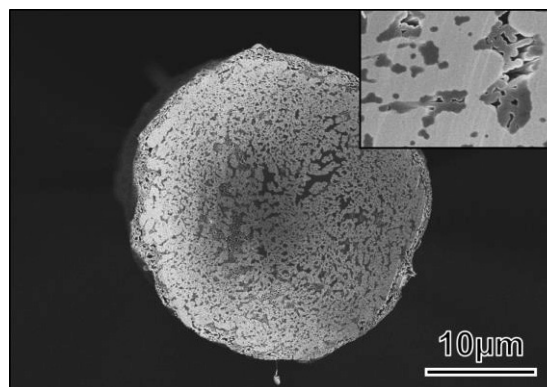


Fig.2 SEM image of cross-section of CNT/Cu composite yarn. Inset shows a high magnification image of the cross-section.

Raman scattering spectroscopy of gas-flow oriented single-walled carbon nanotubes on hexagonal boron-nitride

○Shu Sato, Satoshi Yotsumoto, Masanori Bamba, Taiki Inoue, Shigeo Maruyama, Shohei Chiashi

Department of Mechanical Engineering, The University of Tokyo, Tokyo 113-8656, Japan.

It is known that the properties of single-walled carbon nanotubes (SWCNTs) are affected by the environmental conditions around them. For example, the semiconducting SWCNTs that are suspended [1] or dispersed in solution [2] emit photoluminescence (PL), while those on silicon substrates do not. On the other hand, semiconducting SWCNTs on hexagonal boron nitride (h-BN) show PL emission [3]. Recently, the synthesis of the heterostructure of SWCNTs and boron nitride nanotubes (BNNTs) [4] is reported. These complex systems of SWCNT and h-BN are interesting, however, their properties are veiled. In this study, we directly synthesized SWCNTs on h-BN based on the gas-flow oriented CVD method [5] and investigated the optical properties by using Raman scattering spectroscopy.

SWCNTs were synthesized from Fe catalyst. Using the gas-flow oriented growth technique, SWCNTs were directly synthesized on exfoliated h-BN (Fig. 1(a)). The scanning Raman measurement (Fig. 1(b, c)) shows that a SWCNT was clearly lying on the surface of h-BN and that the G-band of the SWCNT on h-BN exhibited the downshift comparing to that on SiO₂ (Fig. 1(d)). In addition, in the point marked with (B) in Fig. 1(b), the G-band was locally split to G⁺ and G⁻ peaks and the intensity of the G⁻ peak was relatively strong. The features of the G-band may come from the interaction between SWCNTs and the surface of h-BN.

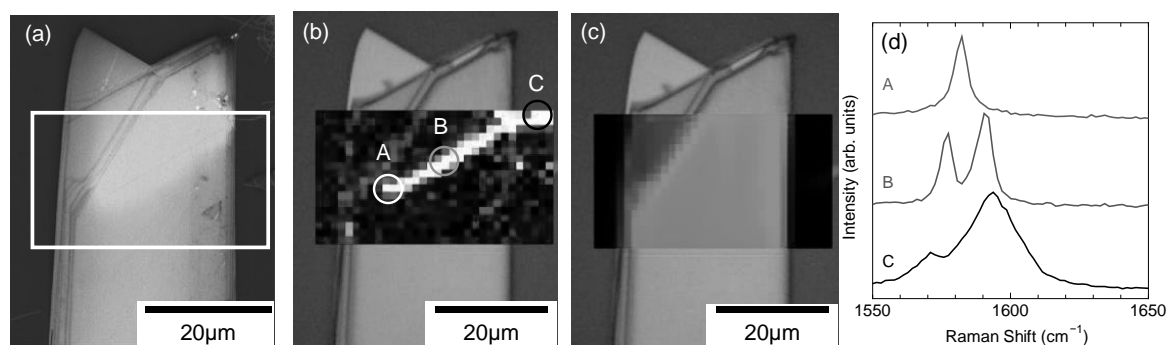


Figure 1 (a) SEM image of SWCNT on h-BN. (b, c) Scanning Raman images of (b) the G-band and (c) E_{2g} peak of h-BN intensity, respectively. (d) G-band of SWCNT on h-BN (A, B in Fig. 1(b)) and on SiO₂ substrate (C in Fig. 1(b)).

- [1] J. Lefebvre, et al., *Phys. Rev. Lett.*, **90**, 217401 (2003). [2] S. M. Bachilo, et al., *Science*, **298**, 2361 (2002). [3] J. C. Noé, et al., *Nano Lett.*, **18**, 4136 (2018). [4] R. Xiang, et al., *Science*, **367**, 537 (2020). [5] S. M. Huang, et al., *Nano Lett.*, **4**, 1025 (2004).

Tel/Fax: +81-3-5841-6408, E-mail: chiashi@photon.t.u-tokyo.ac.jp

Fermi-level dependence of high-harmonic generation in semiconducting single-walled carbon nanotubes with different bandgaps

○Hiroyuki Nishidome¹, Kohei Nagai², Kent Uchida², Yota Ichinose¹, Junko Eda¹, Hitomi Okubo¹, Yohei Yomogida¹, Koichiro Tanaka^{2,3}, Kazuhiro Yanagi¹

¹ Department of Physics, Tokyo Metropolitan University, Tokyo 192-0397, Japan

² Department of Physics, Kyoto University, Kyoto 606-8502, Japan

³ Institute for Integrated Cell-Material Sciences, Kyoto University, Kyoto 606-8501, Japan

High-harmonic generation (HHG), which is the generation of light with multiple optical harmonics, is an unconventional nonlinear optical phenomenon beyond the perturbation regime. HHG has recently been demonstrated in solid state materials,[1] and then how to control such extreme nonlinear optical phenomena is one of challenging subjects. The HHG in solid are caused by two distinct dynamics: one is related to nonlinear optical transitions between bands (interband dynamics) and the other is to nonlinear current within a band (intraband dynamics) [2]. In both processes, the electronic structure of materials and the location of Fermi-level will strongly influence on HHG. Recently, we clarified remarkable characteristics of HHG in single walled carbon nanotubes (SWCNTs) with different electronic structures.[3] We observed higher HHG in SWCNTs with larger band-gap. In addition, we observed enhancement of 3rd order HHG, but reduction of the other HHG by carrier injection into (6,5) SWCNTs (Fig. 1(a)). The enhancement or the reduction occurred whether the energy of high-harmonics is below or above (Fig. 1(a)) [3]. If so, when we use the semiconducting SWCNT with small energy gap E_g , which is smaller than the energy of 3rd harmonics, the enhancement will be suppressed. To understand the detailed mechanism of HHG in SWCNTs, here we investigated the Fermi-level dependence of HHG in semiconducting SWCNTs with different E_g .

We prepared a semiconducting-SWCNT thin film (Semi, $E_g = 0.7$ eV) and employed side-gating device using ionic liquid, which enable to tune Fermi level by shift of gate voltage V_G . The sample was irradiated with 0.26 eV mid-infrared fs pulse laser, and we investigated the relationships between HHG and carrier injection.

Figure 1(a) and (b) show the high-harmonic intensities as a function of V_G in (6,5) and Semi, respectively. In Semi, 5th and 7th harmonics just decreased as the shift of V_G . However, the 3rd harmonics at first increased and then decreased as the shift of V_G . In this presentation, we will discuss the background using temporal evaluation of wave-packets in two band model.

[1] S. Ghimire *et al.*, Nat. Phys. 7, 138 (2010)

[2] O. Schubert *et al.*, Nat. Photon., 8, 119 (2014)

[3] H. Nishidome *et al* Nano Lett. accepted (2020)

Corresponding Author: K. Yanagi, yanagi-kazuhiro@tmu.ac.jp

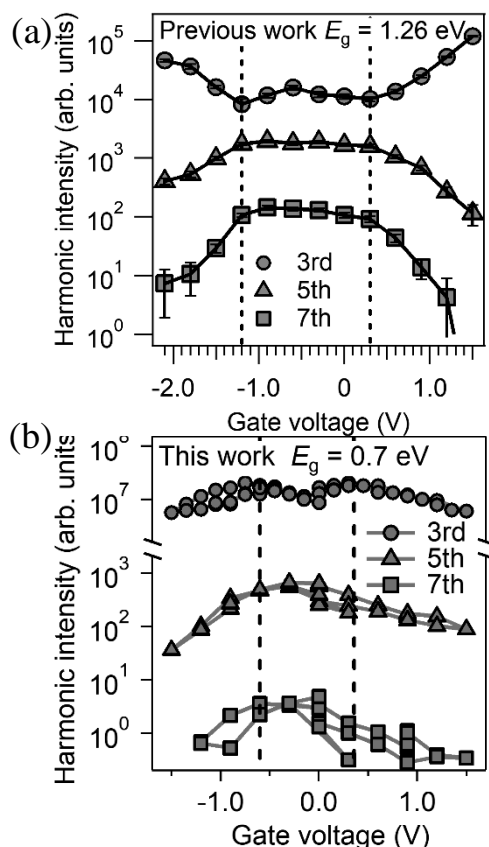


Fig. 1 Fermi-level dependence of high-harmonic intensity in (a) (6,5) and (b) Semi.

Effects of deposition method on the states of Pt nanoparticles on carbon materials and their electrocatalytic properties toward methanol oxidation

○Yuho Abe¹ and Hironori Ogata^{1,2}

¹ *Department of Chemical Science and Technology, Hosei University*

² *Research Center for Micro-Nano Technology, Hosei University*

E-mail: hogata@hosei.ac.jp

Direct methanol fuel cells (DMFCs) are one of the most promising transportable power sources which can be used in mobiles, laptops, and small power generation. The most important advantage of DMFCs over other types of fuel cells is that methanol can integrate effectively with transmission and distribution systems that already exist. However, there are technological challenges for the commercialization of DMFCs that remain unsolved [1,2]. The basic operation principle of DMFCs involves methanol oxidation and oxygen reduction on the precious metal catalysts, which are loaded on the support surfaces. As is well-known, the dispersion of Pt-based nanoparticles on carbon supports as well as catalyst particle size and shape plays a dominant role in the electrochemical performance for fuel cells. We have explored the electrocatalytic properties of Pt-based nanoparticles supported on the carbon materials by one-step electrodeposition [3]. In this study, we investigated the effects of deposition method and conditions on the shape and dispersion state and electrocatalytic properties of Pt-based nanoparticles supported on the carbon materials. Especially we picked up the electrodeposition method and the liquid phase reduction method as the loading method of Pt nanoparticles on single walled carbon nanotubes (SWNTs) and compared the dispersion state of Pt nanoparticles on the nanocarbon materials and the oxygen reduction reaction activities. The surface state of SWNTs, the loading state of Pt nanoparticles and the catalytic properties of electrode were investigated using TEM, XPS, and cyclic voltammogram (CV).

The detailed results will be presented.

References:

- [1] N. Pongpichyakul *et al.*, *Springer Nature*, **50**, 51-62 (2019).
- [2] I. Martinalou *et al.*, *Applied Catalysis B: Environmental*, Elsevier, 2019
- [3] Zhipeng Wang, Mao Shoji and Hironori Ogata, *Appl. Surf. Sci.* **259**(2012)219-224.

Corresponding Author: H.Ogata

Tel: +81-42-387-6229, Fax: +81-42-387-6229,

E-mail: hogata@hosei.ac.jp

F4-TCNQ Vapor-doped Single Walled Carbon Nanotubes for Thermoelectric Applications

○ Mariamu kassim Ali¹, Naofumi Okamoto², Ryo Abe², Ahmed Abdel Moneim¹, Masakazu Nakamura²

¹*Department of Materials Science and Engineering, Egypt-Japan University of Science and Technology, New Borg El Arab City, Alexandria 21934, Egypt*

²*Division of Materials Science, Nara Institute of Science and Technology, 8916-5 Takayama-cho, Ikoma, Nara 630-0192, Japan*

Single-walled carbon nanotubes (SWCNT) has emerged as a potential candidate material for thermoelectric (T.E) applications owing to its unique and outstanding electronic properties [1] since its discovery by Iijima [2]. Despite the low power factor associated with CNTs, its robustness and lightweight nature make it a promising candidate for flexible thermoelectric applications. From previous study [3], it was shown that CNT yarns have a potential to be integrated into thermoelectric fabric for wearable energy harvesters. Doping which is a versatile technique for tuning the carrier concentration of SWCNTs and the effect of charge transfer organic molecule F4-TCNQ was investigated.

Herein, we successfully synthesized CNT yarns through wet spinning and further vapor-doped the yarns by varying amounts of F4-TCNQ. The morphological studies by SEM revealed that the dopant molecules can successfully penetrate into the porous CNT network and thus modify the morphology which is expected to influence the T.E characteristics. Furthermore, Seebeck coefficient and the electrical conductivity were evaluated using four-probe technique while the thermal analysis was done through 3- ω and laser pit techniques, the results of which will be reported.

This work was supported by JST CREST Grant Number JPMJCR18I3, Japan.

[1] Blackburn, J. L. *et al.*, *Advanced Materials*, **30**: p. 1704386. (2018).

[2] Iijima, S., *Nature*, **354**: p. 56-58, (1991).

[3] M. Ito *et al.*, *J. Mater. Chem. A* **5**: 12068-12072 (2017)

Corresponding Author: M. Nakamura

Tel: +81- 743-72-6031, Fax: +81-743-72-6047,

E-mail: mnakamura@ms.naist.jp

Operation speed enhancement in carbon nanotube thin film transistors by self-aligned process

○Saya Ishimaru¹, Taiga Kashima¹, Hiromichi Kataura², and Yutaka Ohno^{1,3}

¹Department of Electronics, Nagoya University, Nagoya 464-8603, Japan

²Nanomaterials Research Institute, National Institute of Advanced Industrial Science and Technology 305-8565, Japan

³Institute of Material and Systems for Sustainability, Nagoya University, Nagoya 464-8601, Japan

Carbon nanotube thin film transistors (CNT TFTs) are promising for flexible electronics applications because of the high carrier mobility and outstanding flexibility. Since conventional photolithography process on a plastic film requires an alignment margin due to the thermal shrinkage during the device fabrication process, large parasitic capacitances are formed by the overlaps between the source/drain and gate electrodes. This can be one of causes of the operation speed degradation in CNT TFTs.

In the previous work, we reported a self-aligned process for flexible CNT TFTs which was effective to reduce the parasitic capacitances. [1] In this work, we evaluate the operation speed of the self-aligned flexible CNT TFTs by measuring the scattering (S) parameters.

We fabricated CNT TFTs with a bottom gate structure on a polyethylene naphthalate (PEN) film by the self-aligned process (Fig. 1). Semiconducting CNTs purified by the gel-chromatography were used as the channel. The channel length (L_{ch}) was from 20 to 50 μm and channel width was 12 mm. A 45-nm-thick Al_2O_3 gate oxide was deposited by the atomic-layer deposition. We also fabricated CNT TFTs with overlaps of 20 μm by the conventional process for comparison. S -parameter measurements were carried out by using a vector network analyzer (Keysight, E5061B).

The parasitic capacitance C_p was reduced from 780 to 35.8 pF by introducing the self-aligned process. Figure 2 shows the dependence of current gain cutoff frequency (f_T) on L_{ch} at V_{DS} of -5 V and V_{GS} of -3 V. f_T was significantly improved by the introduction of the self-aligned process. The curves in the figure show calculated f_T with assuming the carrier mobility of 12 cm^2/Vs . Here, a both channel capacitance (C_{ch}) and C_p were taken into account as expressed by $f_T = g_m/2\pi(C_{ch} + C_p)$, confirming that C_p is a dominant cause of a degradation in operation frequency of conventional flexible CNT TFTs.

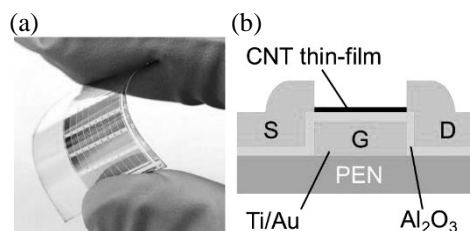


Fig.1 (a) Schematic of device.
(b) Device structure.

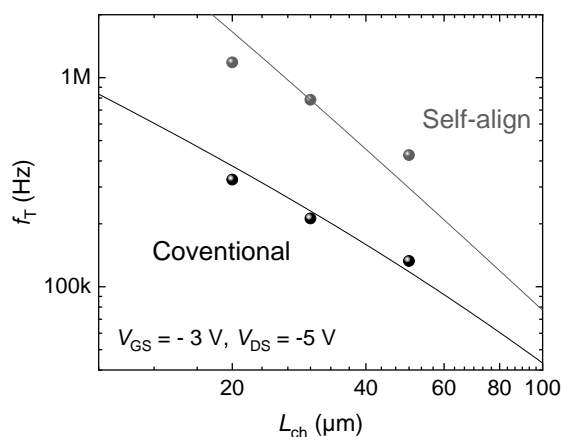


Fig. 2 f_T versus L_{ch} .

[1] T. Kashima *et al.*, The 79th JSAP Autumn meeting, 18p-211A-7

Corresponding Author: Yutaka Ohno, Phone: +81-52-789-5387, E-mail: yohno@nagoya-u.jp

Radical polymerization in the presence of carbon nanotubes (CNTs): Radical scavenging by CNTs

○Taiyo Shimizu¹, Ryoichi Kishi¹, Takeo Yamada¹, Kenji Hata¹

¹ National Institute of Advanced Industrial Science and Technology (AIST), Tsukuba Central 5, 1-1-1 Higashi, Tsukuba, Ibaraki 305-8565 Japan

Carbon materials, e.g. carbon black, generally show radical scavenging activities for various radical species. Among carbon materials, fullerenes show prominent radical scavenging activities and have been extensively studied for the applications such as biomedicines. In recent research concerning composite materials [1], it has been found that carbon nanotubes (CNTs) are also capable of scavenging radicals. Radical scavenging activity of CNTs is of great importance because this property is highly beneficial not only for fabricating thermally stable CNT composites but for surface functionalization of CNTs. However, limited numbers of research have been conducted so far, and the details of radical scavenging by CNTs are still unclear.

In this study, we investigated the radical scavenging activities of CNTs by means of radical polymerization in the presence of CNTs in the reaction systems. Bulk polymerization of styrene dispersing CNTs was conducted by using commonly used radical initiators under N₂ atmosphere.

As shown in Fig. 1, we found that the yields of polystyrene (PSt) have been affected by the kinds of radical initiators. In the case of azobisisobutyronitrile (AIBN), the yield of PSt in the presence of CNTs is not so much lowered as compared to that in the absence of CNTs. When using peroxide type initiators such as benzoyl peroxide (BPO), however, the yields reach almost zero when CNTs exist in the reaction systems. This result indicates that CNTs possess high affinity for the radicals from peroxides and not for carbon radicals. Further discussions on the results such as the effect of the kinds of CNTs, molecular weight distributions of obtained PSt, surface analysis of the CNT after radical reactions etc., will be performed on the presentation.

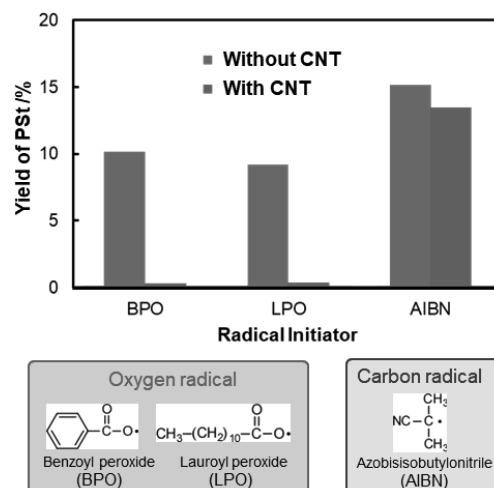


Fig. 1 Yields of polystyrene (PSt) obtained by using different kinds of radical initiators with and without CNTs.

[1] X. Shi *et al.*, Carbon, **50**, 1005 (2012).

Corresponding Author: T. Shimizu

Tel: +81-29-861-5712 Web: <https://unit.aist.go.jp/cnta/ja/organization/index.html>

E-mail: shimizu-t@aist.go.jp

Effect of Chemical Etching Treatment on Copper Foils for Single-Layer Graphene CVD Growth

○Naoki Yoshihara¹, Masaru Noda¹

¹ Department of Chemical Engineering, Fukuoka University, Fukuoka, 8-19-1 Nanakuma, Jonan-ku, Japan

Single-layer graphene growth on commercially available copper foils by chemical vapor deposition (CVD) is paid the most attention as a mass production technique for practical applications in numerous fields. Chemical etching treatment of the copper foils is essential as a pre-treatment for the graphene CVD growth. This chemical etching plays the role of between the surface flatness and the removal of impurities and the naturally copper oxide layer. However, the graphene CVD growth on etched copper foils is still unclear. Here, we investigated the effect of the chemical etching treatment on copper foils for single-layer graphene CVD growth.

Figure 1 showed the optical micrographs of graphene domains grown on the copper foil (thickness: 25 μm) treated with 0.2 mol/L iron trichloride (FeCl_3) aqueous solution for the different etching time. We synthesized graphene on the etched copper foil under a mixed flow of CH_4 , H_2 , and Ar atmosphere at 1000 $^\circ\text{C}$ for 1 hr. In all etching conditions, the hexagonal graphene domains were observed on etched copper foils. Interestingly, the graphene domain size increased with extending the etching time and the graphene domain on copper foils etched for 120 sec is around 4 orders of magnitude larger than that for 15 sec.

It is likely that the observed effect of chemical etching treatment on the copper surface reflects the graphene nucleation density. Recently, it has been reported that the presence of oxygen in copper foils is a key factor for decreasing the graphene nucleation density and accelerating graphene domain growth [1-2]. However, our results cannot account for only this explanation because a large amount of copper oxide layer on subsurface of copper foils is eliminated by the longer etching treatment. This might be related to surface morphology of the copper foil after the chemical etching treatment.

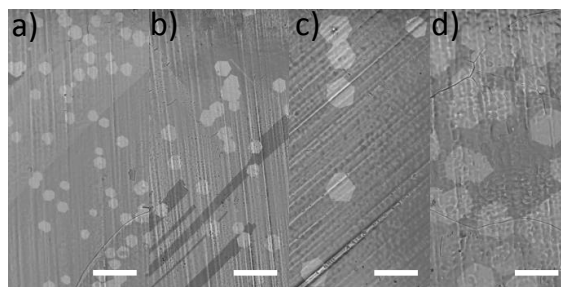


Fig. 1 The optical micrographs of graphene domains on the etched copper foil treated with FeCl_3 aqueous solution for a) 15, b) 30, c) 60, and d) 120 sec. All scale bars are 100 μm .

[1] Y. Hao *et al.*, Science **342**, 720 (2013).

[2] D. Ding *et al.*, Appl. Surf. Sci. **408**, 142 (2017).

Corresponding Author: N. Yoshihara

Tel: +81-92-871-6631, Fax: +81-92-865-6031

E-mail: nyoshihara@fukuoka-u.ac.jp

Thermal transport property of suspended twisted bilayer graphene

J. Doi*, S. Mouri and T. Araki

The Graduate School of Science and Engineering, Ritsumeikan University,

Nojihigashi 1-1-1, Kusatsu, Shiga, Japan

*email: re0110ev@ed.ritsumei.ac.jp

Graphene has interesting characteristics such as high electron mobility [1] and high thermal conductivity [2]. Especially, bilayer graphene could transmute from superconductivity [3] to insulator with changing twisted angle [4]. Thermal transport property could be modulated with twisting as well as electronic properties. Thermal conductivity of suspended twisted bilayer graphene (tBLG) with specific twisted angle was reported [5], however, precise properties depending on twisted angle have been unveiled so far. Therefore, here, we studied laser heating effect of suspended tBLGs having different twisted angles using Raman spectroscopy.

We prepared suspended tBLG on TEM grid which has 2.5 μm diameter aligned holes by wet transfer method using PMMA [6]. CVD grown monolayer graphene (Graphenea Co.) used here contains variety of domains with several micron meter square, then, twisted angles of tBLG on each hole were different. They were determined by electron beam diffraction pattern measured with TEM as shown in Fig. 1. We measured Raman spectra of tBLGs having different twisted angles with changing laser power. Peak position of G mode signal was shifted with increasing laser power due to the laser heating effect as shown in Fig. 2. The slope of Raman shift via laser power was different according to its twisted angle, which suggests that thermal conductivity of tBLG depends on the twisted angle.

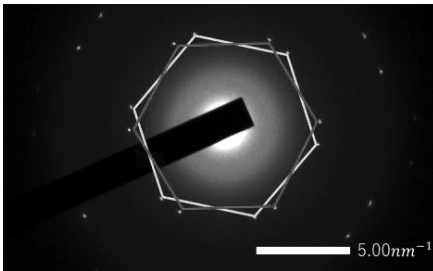


Figure 1 Electron beam diffraction pattern of tBLG measured by TEM.

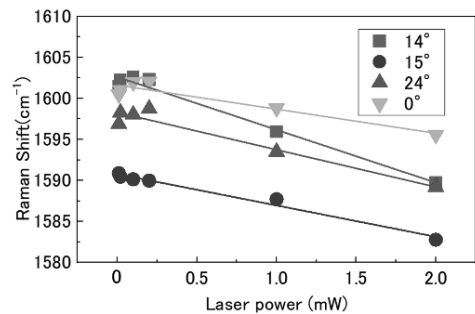


Figure 2 Peak position of Raman peak (G mode) measured at different laser powers.

References

- [1] K. I. Bolotin *et al.*, *Solid State Commun*, **146**, 351 (2008).
- [2] A.A. Balandin *et al.*, *Nano Lett*, **8**, 902 (2008).
- [3] Y. Cao *et al.*, *Nature*, **556**, 43 (2018).
- [4] Y. Cao *et al.*, *Nature*, **556**, 80 (2018).
- [5] H. Li *et al.*, *Nanoscale*, **6**, 13402 (2014).

This work was supported by JSPS, KAKENHI, #16H06415, #18H04294.

Carrier control in bilayer graphene dual-gate field effect transistors by interlayer atomic arrangement

○Yanlin Gao, Susumu Okada

Department of Physics, University of Tsukuba, Tsukuba 305-8571, Japan

Bilayer graphene is an important material in the field of physics and material science owing to its unusual electronic structures, which depend on the interlayer stacking arrangement and perpendicular electric field. For instance, bilayer graphene with the AB interlayer stacking arrangement is a semiconductor under the perpendicular electric field, while twisted bilayer graphene with a particular magic angle is a superconductor by injecting carriers through the external electric field. Although our previous work excluded the dependence of carrier distribution in bilayer graphene on the interlayer stacking arrangement [1], comprehensive knowledge about the correlated effect of the stacking arrangement, external electric field, and carrier concentration on the carrier distribution in bilayer graphene is still absent. Therefore, in this work, we aim to elucidate the carrier distribution on the bilayer graphene under the perpendicular electric field in terms of the field strength, doping concentration, and interlayer stacking arrangement, using density functional theory combined with the effective screening medium method (Fig.1).

Our calculations show that the carrier distribution is sensitive to the stacking arrangement, external electric field, and carrier concentration. Under a strong electric field with low electron doping concentration, doped electrons are mainly accommodated in the lower layer situated at the positively charged electrode side of bilayer graphene with a twisted stacking arrangement, while those are in the opposite layer situated at the negatively charged electrode side of bilayer graphene with an AB stacking arrangement. In the bilayer graphene with an AA stacking arrangement, the injected electrons are almost equally accommodated in both layers. By injecting holes in the bilayer graphene, their distribution is symmetric to the case of electron doping. These characteristic asymmetric and symmetric carrier distributions depending on the stacking arrangements and doping concentration, respectively, is ascribed to the electronic structures of these bilayer graphene under an external electric field.

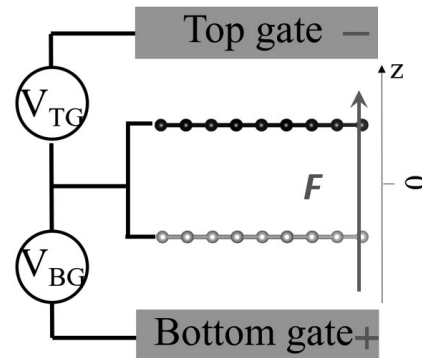


Fig.1 Structural model of bilayer graphene dual-gate field effect transistor.

Reference

[1] Y. Gao and S. Okada, *Appl. Phys. Express* **13**, 065006 (2020)

Corresponding Author: Y. Gao

TEL: +81-29-853-5921, FAX: +81-29-853-5924

E-mail: ylgao@comas.frsc.tsukuba.ac.jp

Difference of functional groups in Graphene oxide in terms of chemical activity

○Riku Kondo¹, Yoshiaki Matsuo², Kazuyuki Takai¹

¹*Dept. of Appl. Chem., Hosei Univ.*, ² *Dept. of Appl. Chem., Univ. of Hyogo.*

Graphene oxide (GO) has oxygen-containing functional groups such as epoxy group, carboxyl group and hydroxyl group. The major GO synthesis methods are the Brodie method [1] and the Hummers method [2, 3] in which different oxidizing agents are used. Our group found that the ratio of quantities of each kinds of oxygen-containing functional groups depends on the oxidation methods greatly, suggesting that chemical reactivity such as catalytic activity depends on the GO synthesis methods [4]. In this study, we precisely determined the quantity of each acidic functional groups in HGO oxidized by the Hummers method and BGO oxidized by the Brodie method by Boehm titration to clarify their chemical activity.

GO was synthesized by oxidation of natural graphite using concentrated sulfuric acid and potassium permanganate followed by the modified Hummers method [3], and using potassium chlorate and fuming nitric acid according to the Brodie method.

The Boehm method based on neutralization titration was used to determine the quantity of acidic functional groups. In the Boehm method, the synthesized either of HGO or BGO was added to NaOH (aq), Na₂CO₃ (aq), and NaHCO₃ (aq) at a concentration of 0.1 mol / L at a ratio of 20 mg / 40 mL, respectively, followed by dispersing by ultrasonication for 1 h. After standing for 3 days, the mixture was centrifuged for 2.0 h. The acid-base titration was performed for the filtrate of the supernatant by adding 0.1 mol / L of HCl (aq) dropwisely.

The amount of hydroxide ions consumed by carbon materials indicates the amount of total acidic functional groups when neutralized by NaOH (aq). Similarly, the amount of moderate and strong acid groups is obtained when neutralized by Na₂CO₃ (aq). Strong acid content is also estimated by using NaHCO₃ (aq) [3].

Table 1 shows the amount of acidic functional groups of different strengths in GO calculated from the amount of HCl (aq) added until reaching the equivalent point obtained from the titrations. The total amount of acidic functional groups, strongly, moderately acidic groups in HGO and BGO are 9 mEq/g and 5 mEq/g, 6 mEq/g and 3 mEq/g, 3 mEq/g and 2 mEq/g, respectively. Almost no weak acid group were found in both of HGO and BGO. The fact that HGO has more acidic functional groups than BGO acidic functional groups suggests a difference in catalytic activity between HGO and BGO.

Table 1 Neutralization of acidic surface-oxides

Sample	Total acidic group	Strong acidic group	Moderate acidic group
	(mEq / g)	(mEq / g)	(mEq / g)
HGO	9	6	3
BGO	5	3	2

[1] B. C. Brodie, *Philos. Trans. R. Soc. London*, **149**, 249–259 (1859)

[2] W.S. Hummers, R.E. Offeman, *Preparation of graphitic oxide*, *J. Am. Chem. Soc.* **80** (6) (1958), 1339-1339

[3] D. C. Marcano et al, *ACS Nano*, **4**, 8, 4806–4814 (2010)

[4] K.Tajima, et al., *Polyhedron*, **136**, 155-158 (2017)

Corresponding Author: Kazuyuki Takai

E-mail: takai@hosei.ac.jp

Tailor-made two-dimensional nano-scale super-structures

○Nanami Ichinose¹, Satoshi Iida¹, Liu Zheng², and Ryo Kitaura¹

¹*Department of Chemistry, Nagoya University, Nagoya 464-8602, Japan*

²*Innovative Functional Materials Research Institute, AIST, Nagoya 463-8560, Japan,*

Two-dimensional (2D) heterostructures have attracted plenty of attention. To fully explore the enormous potential of 2D heterostructures, the development of a highly-controllable fabrication technique is crucial. Although 2D van der Waals stackings have been intensively studied the research on the lateral heterostructures is still limited due to the difficulty in fabrication. In this work, we focus on lateral heterostructures, in which different 2D materials are joined multiple heterojunctions. These are novel low-dimensional materials, whose electronic states can show crossover from 2D to 1D depending on the junction width.

In this study, we focused on metal organic chemical vapor deposition (MOCVD) growth of lateral heterostructures composed of transition metal dichalcogenide (TMD). Since various TMDs, including metals, semiconductors, superconductors, and topological insulators, are available, it is possible to realize novel 2D superstructures with different electronic states. The MOCVD equipment used in this research can rapidly switch supply of source materials on the order of milliseconds to realize multiple lateral heterostructures with nanometer-scale periodicity.

In this study, we fabricated lateral heterostructures of WS₂/MoS₂, on hexagonal boron nitride by sequential growth of WS₂ and MoS₂ through rapid switching of supply of W and Mo source. Figure 1 shows HAADF-STEM images of a lateral heterostructures WS₂/MoS₂. In the HAADF-STEM images, W atoms are images as bright spots, whereas Mo and S atoms are images as much darker spots. As clearly seen, the MOCVD-grown multi-step lateral heterostructure possesses atomically steep interfaces with width down to 3 nm. A trace amount of W atoms is seen in the MoS₂ region, and the number of W atoms can be reduced through increasing the interval time during consecutive MOCVD growth. In the presentation, further details of the MOCVD setup and results of the characterization will be shown.

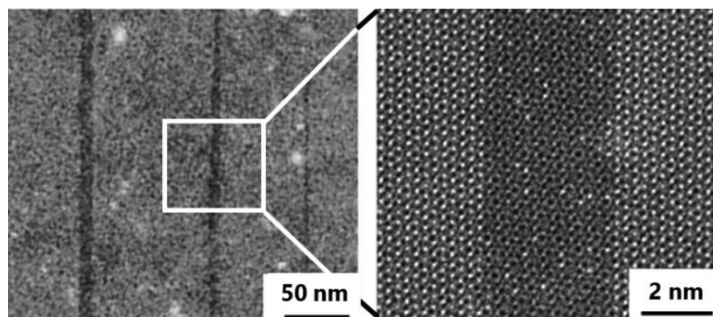


Fig. 1 Left: A low-magnification HAADF-STEM image of WS₂/MoS₂ super structure. Right: A high-resolution HAADF-STEM image of interface between WS₂ and MoS₂.

Corresponding Author: R. Kitaura

Tel: +81-52-789-2482, Fax: +81-52-747-6442

Web: <http://nano.chem.nagoya-u.ac.jp/>

E-mail: r.kitaura@nagoya-u.jp

Chemically tuned p- and n-type WSe₂ monolayers with improved carrier mobility for electronic applications

^oHyun Goo Ji¹, Pablo Solís-Fernández², Daisuke Yoshimura³, Mina Maruyama⁴, Takahiko Endo⁵, Yasumitsu Miyata⁵, Susumu Okada⁴, Hiroki Ago^{1,2}

¹Interdisciplinary Graduate School of Engineering Sciences, Kyushu University, Fukuoka 816-8580

²Global Innovation Center (GIC), Kyushu University, Fukuoka 816-8580

³Kyushu Synchrotron Light Research Center, Saga 841-0005

⁴Graduate School of Pure and Applied Sciences, University of Tsukuba, Ibaraki 305-8571

⁵Department of Physics, Tokyo Metropolitan University, Tokyo 192-0397

Semiconducting transition metal dichalcogenides (TMDCs), such as WSe₂ and MoS₂, have attracted great interest due to their unique physical properties. Although both p- and n-type materials are required for electronic applications, most of semiconducting TMDCs exhibit n-type or ambipolar behaviors. Therefore, several approaches have been reported to control the electrical polarity of semiconducting TMDCs, such as substitutional doping of transition metals and metal nanoparticle deposition [1,2]. However, both methods were found to have critical disadvantages such as carrier scattering or photoluminescence quenching. As an alternative, chemical doping can be a promising method. Although the usefulness of chemical doping has been demonstrated [3], the controlled p- and n-type doping of a single TMDC material has not been reported so far.

In this work, we demonstrate the doping of CVD-grown WSe₂ for selective conversion from ambipolar to p- or n-type semiconductors [4]. This was done by using 4-nitrobenzenediazonium tetrafluoroborate (4-NBD) and diethylene triamine (DETA) molecules as p- or n-type dopants, respectively. Spectroscopic studies proved p- and n-type doping as shown in Figure 1. After doping, WSe₂ showed clear p- or n-type transport properties (Figure 2) and the effective carrier mobility showed significant increase up to 10³~10⁴ times. To demonstrate the usefulness of our chemical doping technique, a complementary metal-oxide-semiconductor (CMOS) inverter was fabricated which showed a sharp inversion between input and output voltages, as shown in Figure 3 together with an extremely low power consumption. Also, a p-n junction was fabricated within a single WSe₂ grain by developing a spatially controlled doping technique, and it showed clear rectification behavior as well as optical response under laser illumination.

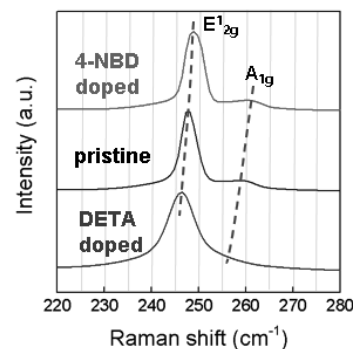


Fig. 1 Raman spectra of pristine and doped WSe₂.

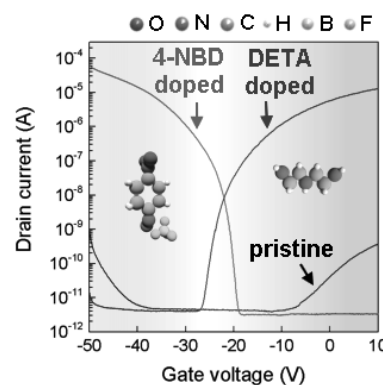


Fig. 2 Transfer curves of pristine and doped WSe₂.

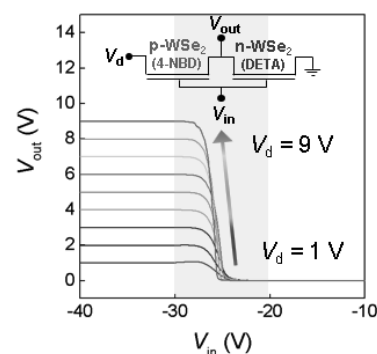


Fig. 3 V_{in} - V_{out} characteristics of a CMOS inverter made of p- and n-doped WSe₂.

References: [1] K. Zhang *et al.*, *Nano Lett.*, **2015**, *15*, 6586. [2] C. H. Chen *et al.*, *2D Mater.*, **2014**, *1*, 034001. [3] S. Zhang *et al.*, *Adv. Mater.*, **2018**, *30*, 1802991. [4] H. G. Ji *et al.*, *Adv. Mater.*, **2019**, *31*, 1903613.

Correspondence: H. Ago (Tel&Fax: +81-92-583-8815, E-mail: h-ago@gic.kyushu-u.ac.jp)

Electrical Conductivity of Chemical-Vapor-Deposition Grown WTe Nanowire Bundles

○Chisato Ando¹, Yusuke Nakanishi¹, Hiroshi Shimizu¹, Hong En Lim¹,
Zheng Liu², Takahiko Endo¹, and Yasumitsu Miyata¹

¹*Department of Physics, Tokyo Metropolitan University, Hachioji 192-0397, Japan*

²*Innovative Functional Materials Research Institute, AIST, Nagoya 463-8560, Japan*

One-dimensional (1D) conducting nanowires are required as a building block to realize an integrated circuit at the nanoscale, but the studies and applications have never been fully investigated due to the lack of well-defined materials. Very recently, we have achieved the wafer-scale production of transition metal chalcogenide (TMC) nanowires (Figure 1a) by using chemical vapor deposition (CVD) [1]. Although we have demonstrated that these nanowires are metallic, their electrical properties still remain to be fully clarified. Understanding the transport properties of these ultrathin wires is of critical importance for future electronics applications.

Here we report the electrical properties of isolated bundles of the CVD-grown WTe nanowires. We have investigated the electrical conductivity of single bundles with various diameters by the four-point probe method (Figure 1b). The resistivity of WTe bundles with a diameter of 20 nm was estimated to be approximately $100 \text{ cm}\mu\Omega$, comparable to Cu nanowires [2]. In contrast, the current-carrying capacity ($7.8 \times 10^7 \text{ A cm}^{-2}$) of WTe bundles is superior to bulk copper ($2.0 \times 10^6 \text{ A cm}^{-2}$). Our findings suggest that conducting TMC nanowires could serve as robust 1D electron channels for flexible integrated nanocircuits. In the conference, the conductivity of isolated bundles and their network will also be presented.

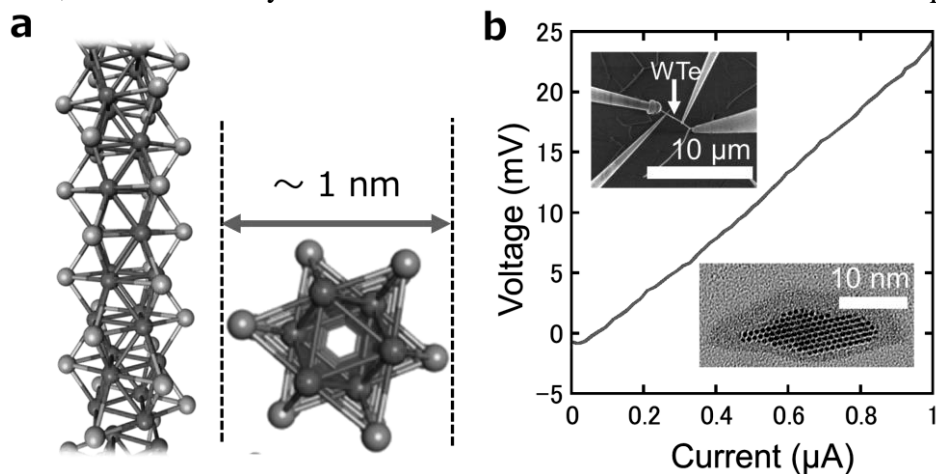


Fig. 1 (a) A schematic illustration of transition metal chalcogenide nanowire. (b) I - V characteristic curve for a single WTe bundle: (inset) a typical scanning electron micrograph of the four-point probe measurement and cross section transmission electron micrograph of a single WTe bundle.

[1] H.-E. Lim *et al.* *Submitted*

[2] M. E. Toimil-Molaes *et al.* *Appl. Phys. Lett.* **82**, 2139 (2013)

Corresponding Author: Y. Nakanishi, Y. Miyata

Tel: 042-677-2508, E-mail: naka24ysk@tmu.ac.jp, ymiyata@tmu.ac.jp

First-principle calculation of the electronic state of a 2D covalent network of 1,3,5-triamino benzene and benzene-1,3,5-tricarboxaldehyde

Hiroyuki Yokoi

Institute of Industrial Nanomaterials, Kumamoto University, Kumamoto 860-8555, Japan

Bottom-up fabrication of two-dimensional nanostructures is one of promising approaches to tailor-made creation of new functional materials. Kunitake et al. recently succeeded to synthesize monolayer covalent honeycomb nanosheets comprising small 1,3,5-triamino benzene (TAB) and benzene-1,3,5-tricarboxaldehyde (BTA) aromatic building blocks on Au(111) in a pH-controlled aqueous solution [1]. This material is very interesting in that it resembles graphene with periodical opening of regular pores and substitution. In this study, we have conducted first-principle calculations to investigate the electronic states of this unique material. The arrangement of atoms were optimized in the condition that the lattice constant of the hexagonal lattice is kept 1.13 nm, which was determined experimentally [1]. The optimized structure is as shown in Fig. 1. We have calculated the electronic structure and clarified that this material has a metallic band structure as shown in Fig. 2. Opening of band gap by about 0.02 eV is recognized at the Dirac point located approximately 0.1 eV above the Fermi level. We think that this electronic structure is very interesting as the π -conjugated electronic states appears around the Fermi level in spite that the six-membered rings are linked indirectly through $-C=N-$ bridges.

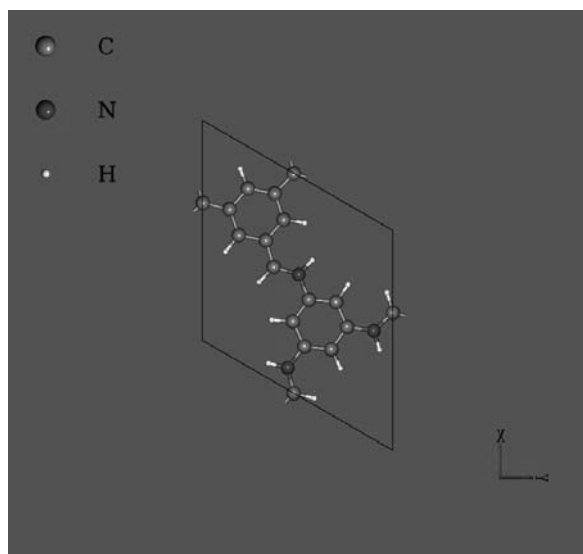


Fig. 1 Optimized structure of covalently bonded TAB-BTA nanosheet

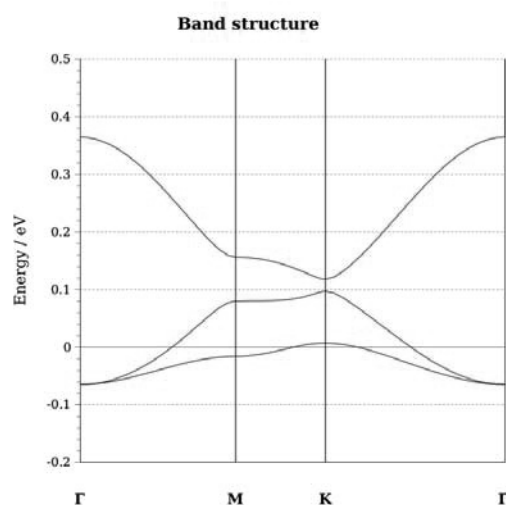


Fig. 2 Electronic structure of the covalently bonded TAB-BTA nanosheet around the Fermi level.

[1] M. Kunitake *et al.*, *Nanoscale Advances*, DOI: 10.1039/d0na00180e, (2020).

Corresponding Author: H. Yokoi

Tel: +81-96-342-3727, Fax: +81-96-342-3710,

Web: <http://www.msre.kumamoto-u.ac.jp/~yokoi-gr/index-j.html>

E-mail: yokoihr@kumamoto-u.ac.jp

Two-channel model for low thermal conductivity of Mg_3Bi_2

○ Nguyen T. Hung¹, Riichiro Saito²

¹*Frontier Research Institute for Interdisciplinary Sciences, Tohoku University, Sendai
980-8578, Japan*

²*Department of Physics, Tohoku University, Sendai 980-8578, Japan*

Materials with low thermal conductivity κ are of great interest for thermoelectricity (TE). Although κ in a given material can be reduced by alloying or nanostructuring, finding materials with intrinsically low κ is still necessary to avoid the expensive fabrication of nanostructure. Recently, Mao et al. [1] experimentally showed that replacing Te with Mg in a commercial TE material Bi_2Te_3 , a new TE material Mg_3Bi_2 can perform a figure of merit $ZT \sim 0.9$ with a low $\kappa \sim 2$ W/mK at 300K. Since a low κ is important for obtaining a large ZT , theoretical analysis to understand the low κ of Mg_3Bi_2 is essential.

In this work, we calculate the κ of Mg_3Bi_2 by using the density functional theory (DFT). When we consider the phonon-phonon interaction to calculate the κ , we obtained the $\kappa \sim 0.6$ W/mK at 300K, which is smaller than that in the experimental data. It suggests that the other term might contribute to the κ of Mg_3Bi_2 . As shown in Fig. 1, Mg_3Bi_2 has a

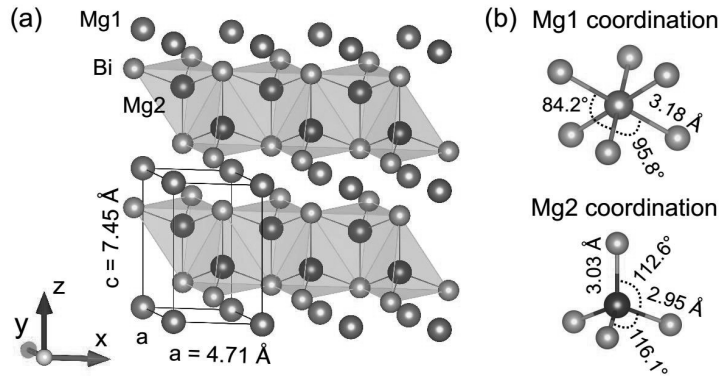


Figure 1: (a) Structure of Mg_3Bi_2 . (b) Mg1 and Mg2 coordinations

structure as a crystal with glass-like, in which the structure of Mg_3Bi_2 can be expressed as $\text{Mg}^{2+}\text{-}[\text{Mg}_2\text{Bi}_2]^{2-}$. For such glass-like system, Mukhopadhyay et al. [2] showed that the κ can be expressed as $\kappa = \kappa_c + \kappa_g$, where κ_c and κ_g are thermal conductivities by crystal and glass, respectively, which is called two-channel model [2]. Here, κ_c is evaluated by the lattice anharmonicity with phonon-phonon interaction from DFT, while κ_g is calculated by using the Einstein model for glass systems. By adopting the two-channel model, the theoretical results of the thermal conductivity of Mg_3Bi_2 is well consistent with experimental data [1].

[1] J. Mao et al., *Science* 365, 6452 (2019).

[2] S. Mukhopadhyay et al., *Science* 360, 1455 (2018).

Corresponding Author: Nguyen Tuan Hung

Tel: +81-22-795-6442, Fax: +81-22-795-6447, E-mail: nguyen@flex.phys.tohoku.ac.jp

発表索引
Author Index

Author Index

< A >

AbdelMoneim, Ahmed	2-10, 3P-15
Abe, Ryo	1-9, 3P-15
Abe, Yuho	3P-14
Ago, Hiroki	2-2, 2-4, 1P-22, 3P-23
Aizaki, Motoki	2-3
Ajiki, Hiroshi	1P-17
Akino, Kosuke	1P-14, 2P-4
Akita, Seiji	1-6, 3-4
Alejandro, Criado	2-5
Ali, Mariamu	2-10, 3P-15
Ando, Chisato	2-3, 2-6, 2P-9, 3P-24
Ando, Hiroshi	3-1, 1S-3
Angana, Borah	1P-6
Antoku, Daiki	1S-2
Aoki, Haruka	2P-1
Araki, Tsutomu	3P-19
Arie, Takayuki	1-6, 3-4

< B >

Bamba, Masanori	3P-12
Bao, Jianfeng	2P-7
Baranov, Alexander	1P-24
Barnard, Amanda S.	2-8
Bhattacharya, Maireyee	1-9
Bogdanov, Kirill	1P-24

< C >

Campeon, Benoit	2P-19
Chang, Wen-Hsin	3P-7
Chen, Guohai	3-5, 1P-16
Chen, Pengfei	2P-12
Chiashi, Shohei	1-2, 1P-14, 2P-13, 2P-17, 3P-12

< D >

De Silva K. Kanishka H.	2P-21
Doi, Juntaro	3P-19

< E >

Eda, Junko	3P-13
Edo, Michiko	3P-2
Endo, Masanori	3P-5
Endo, Takahiko	2-6, 1P-23, 2P-8, 3P-9, 3P-23, 3P-24

< F >

Feng, Ya	1-7
Fortner, Jacob	1-3
Fujigaya, Tsuyohiko	3-10, 1P-2, 1P-4, 1P-6, 2P-1, 2P-3, 2P-5, 3P-1, 3P-4, 3P-6
Fujii, Yasumaru	2P-27
Fukuhara, Kengo	2P-2
Fukushima, Tomohiro	2-11 , 2-12
Futaba, Don N.	1-10, 3-5, 3-12, 1P-16

< G >

Gao, Yanlin	1P-10
Ghali, Mohsen	2-10

< H >

Hamano, Tsuyoshi	1P-17
Hamasaki, Hiromu	1P-5 , 2P-10
Hamasuna, Aoi	3-10
Harano, Koji	1-11
Hase, Muneaki	2P-6
Hata, Kenji	1-10, 3-5, 3-12, 1P-16, 3P-17
Hatao, Shunya	2-5
Hayama, Hiro	2P-16
Hayami, Shinya	2S-2
Hayashi, Keita	3P-4
Hayashi, Shingo	3-1
Hayashi, Tatsuhiro	1P-1
Hayashi, Yasuhiko	2P-6
He, Jinping	3-12
He, Xing	1P-8
Hibino, Hiroki	2-4

Hirahara, Kaori	1P-5, 2P-10	Jeon, Sugyeong	3P-10
Hirano, Atsushi	2P-6	Ji, Hyun Goo	3P-23
Hirao, Toshio	1P-17		
Hirokawa, Sota	1P-22	< K >	
Hirotani, Jun	1P-3, 1P-15, 3P-5	Kajiwara, Takashi	1S-3
Hisama, Kaoru	1-2	Kanahashi, Kaito	1P-12
Hokazono, Shohei	2P-20	Kanda, Naoyuki	2-3
		Kaneko, Toshiro	1-5, 1P-8, 1P-18
< I >		Kashima, Taiga	3P-16
Ichikawa, Haruna	2P-24	Kashio, Tatsuya	1P-19, 2P-18
Ichinose, Nanami	3P-22	Katagishi, Daiki	2-9
Ichinose, Yota	3-9, 1P-12 , 2P-2,	Kataura, Hiromichi	3-8, 3P-16
	3P-13	Katayama, Yoshiki	2P-5
Iida, Satoshi	3P-22	Kato, Toshiaki	1-5, 1P-8, 1P-18
Iimori, Takushi	1S-3	Kato, Yuichi	3-11
Iizumi, Yoko	1P-7	Kato, Yuichiro K.	1-3, 3-6, 3P-3
Ikeda, Atsushi	1S-2	Kauppinen, Esko I.	1P-14, 2P-4, 2P-13
Ikemoto, Hirofumi	1-6	Kawaguchi, Atsushi	1P-15
Ikuhara, Yuichi	2P-13	Kawahara, Kenji	2-2, 2-4
Imamura, Hitoshi	1S-3	Kawai, Tsuyoshi	1P-2
Inaba, Takumi	1-1	Kawasaki, Riku	1S-2
Inoue, Hirotaka	2P-6	Kayo, Nana	3P-1
Inoue, Taichi	1-6	Khozami, Mohsen	2-10
Inoue, Taiki	1-3, 1-7, 1P-14,	Kim, Jaeho	1-10
	2P-13, 2P-17, 3P-12	Kishi, Ryoichi	3P-17
Inoue, Tsukasa	2-5	Kishida, Hideo	2-2, 2P-7
Inoue, Yoku	1P-1, 2P-11, 3P-11	Kitada, Takahito	1-5
Inukai, Daiki	2-2	Kitaura, Ryo	1P-23, 2P-8, 3P-22
Irisawa, Toshifumi	1P-23, 2P-8, 3P-7	Ko, Jeong Won	3P-10
Ishiguro, Yasushi	1P-24 , 2P-24	Ko, Weon Bae	3P-10
Ishihara, Masatou	3P-7	Kobashi, Kazufumi	3-11, 2P-14
Ishihara, Yoshiaki	3-3	Kobayashi, Mikio	3P-8
Ishii, Akihiro	1-3	Kodama, Naoko	1P-24
Ishii, Satoshi	1P-17	Kojima, Keiko	1P-7
Ishii, Taiki	1P-6	Kokubo, Ken	3-5
Ishikawa, Takahiro	1P-17	Komai, Takaha	2-11, 2-12
Ishimaru, Saya	3P-16	Komoda, Masato	2P-19
Ishizaka, Kyoko	1P-9	Komori, Fumio	3-1, 1S-3
Iwasa, Yoshihiro	1P-9	Kondo, Riku	3P-21
Iwasaki, Yuya	3-7	Konishi, Teruaki	1P-17
Iwata, Kota	1S-3	Konno, Yui	1P-13
		Koyama, Takeshi	2-2, 2P-7
< J >		Kozawa, Daichi	1-3
Jeon, IL	1-8, 2P-4	Kubo, Toshitaka	3P-7

Kubota, Yoshiyuki	3S-3	Mieno, Tetsu	2P-15
Kumamoto, Akihito	2P-13	Mitsuishi, Masaya	1P-13
Kusunoki, Michiko	2P-7	Miyamachi, Toshio	1S-3
		Miyamoto, Yoshiyuki	1P-11
< L >		Miyata, Yasumitsu	2-3, 2-6, 1P-23, 1P-26, 2P-8, 2P-9, 2P-23, 2P-25, 3P-9, 3P-23, 3P-24
Li, Henan	1-7	Miyauchi, Yuhei	3-8, 1P-13, 2P-23, 3P-8
Li, Qin-Yi	1P-21 , 1P-22	Momin, Md. Abdul	2P-15
Li, Yuexuan	2P-10	Mori, Takeshi	2P-5
Li, Zhen	3P-3	Morimoto, Takahiro	1-1, 3-11, 2P-14
Lim, Hong En	2-6 , 1P-23, 3P-9, 3P-24	Morimoto, Yusuke	3-4
Lin, Hao-Sheng	1-8	Moritani, Tohei	1P-20
Lin, Yung-Chang	2-4	Mouri, Shinichiro	3P-19
Liu, Ming	2P-13	Murahashi, Tomoaki	1P-19
Lungerich, Dominik	1-11	Murai, Yuya	1P-23, 2P-8
		Murakoshi, Kei	2-11, 2-12
< M >		Murayama, Mitsuhiro	1-11
Maeda, Taisei	3-7		
Maeda, Yutaka	1P-13	< N >	
Magata, Soichiro	2P-16	Nagai, Kohei	3P-13
Majima, Yuki	1P-9	Nagai, Yukiko	2P-5
Maniwa, Yutaka	2P-23	Nagano, Mai	1P-26
Maruyama, Mina	1-2, 1-4 , 1P-10, 2P-27, 3P-23	Nagashio, Kosuke	2-4
Maruyama, Shigeo	1S-1 , 1-2, 1-3, 1-7, 1-8, 1P-14, 2P-4, 2P-13, 2P-17, 3P-12	Nagata, Masa	2-3
Maruyama, Takahiro	1P-19, 2P-18	Nagaya, Hiroki	2P-4
Mase, Kazuhiko	1S-3	Nakagawa, Kaito	1-6
Mashino, Tadahiko	2-9	Nakagawa, Rei	2P-12, 3P-2
Matsubara, Manaho	1P-12	Nakagawa, Yasuto	1P-2
Matsuda, Hiroyuki	1P-17	Nakajima, Hideaki	2P-14
Matsuda, Kazunari	Tutorial, 3-8, 1P-13, 2P-23, 3P-8	Nakamura, Eiichi	1-11
Matsui, Jun	1P-13	Nakamura, Junji	3S-1
Matsui, Takuya	1P-14	Nakamura, Kenta	2P-5
Matsumoto, Kaisei	1P-3	Nakamura, Koichi	2-10
Matsunaga, Masahiro	1P-15	Nakamura, Masakazu	1-9, 3P-15
Matsuo, Yoshiaki	3P-21	Nakamura, Shigeo	2-9
Matsuo, Yutaka	1-8, 2P-4	Nakanishi, Yusuke	2-3 , 2-6, 1P-23, 2P-9, 2P-23, 3P-9, 3P-24
Matsuoka, Hideki	1P-9	Nakano, Masaki	2S-1 , 1P-9
Matsuoka, Yuya	3-9	Nakano, Takayuki	1P-1, 2P-11, 3P-11
Mazaki, Hitoshi	2P-12	Nakashima, Asato	1P-19 , 2P-18

Nakashima, Hiroshi	2-4	Prato, Maurizio	2-5
Nakashima, Takuya	1P-2	Pu, Jiang	2-6, 1P-12, 2P-9,
Nakatsuji, Kan	1S-3		2P-23, 3P-9
Nakayama, Tomohito	2P-6		
Naritsuka, Shigeya	1P-19, 2P-18	< Q >	
Natsume, Yuhei	1P-20	Qian, Yang	2P-13
Nguyen, T.Hung	1P-27, 2P-26, 3P-26		
Niidome, Yoshiaki	1P-4 , 2P-5	< R >	
Nishidome, Hiroyuki	3P-13	Rahman Mohammad Jellur	2P-15
Nishihara, Taishi	3-8		
Nishina, Yuta	2P-19	< S >	
Nishino, Akane	1P-13	Saika Bruno Kenichi	1P-9
Nishiyama, Wataru	2-4	Saito, Kensuke	2-2, 2P-7
Noda, Masaru	3P-18	Saito, Mitsufumi	2P-9
Noda, Suguru	2P-12, 3P-2	Saito, Riichiro	3-2, 3-7 , 1P-25,
Norimatsu, Wataru	2P-7		1P-27, 2P-26, 3P-26
Nouchi, Ryo	3-3	Saito, Susumu	2-1
Numata, Shunsuke	2P-22	Sakakita, Hajime	1-10
		Sakurai, Shunsuke	1-10, 3-12
< O >		Sato, Hideki	2P-16
Oda, Kaito	3P-6	Sato, Naofumi	1P-18
Ogata, Hironori	2P-22, 3P-14	Sato, Shu	3P-12
Ogura, Hiroto	1P-23	Sekiguchi, Atsuko	1P-16, 3-5
Ohe, Tomoyuki	2-9	Sekimoto, Yuki	1-9
Ohno, Yuaka	1P-3, 1P-15, 1P-17,	Senga, Ryosuke	3S-4
	3P-5, 3P-16	Seo, Mizuki	1-5
Okada, Mitsuhiro	3P-7	Seo, Seungju	2P-4
Okada, Naoya	3P-7	Shaanan, Nageh	2-10
Okada, Susumu	1-2, 1-4, 1P-10 ,	Shawky, Ahmed	1P-14
	2P-27, 3P-20, 3P-23	Shiga, Takuma	2-3
Okamoto, Naofumi	1-9, 3P-15	Shigeeda, Yuho	2P-6
Okazaki, Toshiya	1-1, 3-11, 1P-7,	Shimizu, Hiroshi	2-6, 1P-23, 2P-8,
	2P-14		3P-9 , 3P-24
Okubo, Hitomi	3P-13	Shimizu, Taiyo	3P-17
Okudaira, Saki	1P-13	Shimizu, Tetsuo	3P-7
Omachi, Haruka	2-5 , 1P-3	Shimizu, Toshiki	1-11
Osawa, Eiji	2-8	Shimizu, Yoshiki	1-10
Otsuka, Keigo	1-3, 3-6 , 3P-3	Shinohara, Hisanori	2-3, 2-5
Otsuka, Tomohiro	1-5	Shinokita, Keisuke	3P-8
		Shiraki, Tomohiro	1P-2, 1P-4, 2P-1,
< P >			2P-3, 2P-5, 3P-4
Pandey, Manish	1-9	Shirasawa, Tetsuroh	1S-3
Pang, Xiaoqi	1P-27 , 2P-26	Shoufie Ukhtary Muhamma	1P-25
Pichler, Thomas	3S-4	Soga, Tsukasa	1P-19

Solís-Fernández, Pablo	2-4, 1P-22, 3P-23	Ueno, Kazuki	1P-3
Stuckner, Joshua	1-11	Ukhtary, M. Shoufie	3-2, 3-7
Suenaga, Kazu	3S-4, 2-3, 2-4	Uotani, Ryosuke	1S-3
Sugikawa, Kouta	1S-2	Uwanno, Teerayut	2-4
Sugime, Hisashi	2P-12, 3P-2		
Sugimoto, Wataru	3-3	< V >	
Sundaram, Rajyashree	3-5, 1P-16	Visikovskiy, Anton	3-1, 1S-3
Suzuki, Mitsuaki	1P-13	Viswanath, Pamarti	2P-21
Suzuki, Satoru	1P-17		
Suzuki, Seiya	2P-21	< W >	
Syrgiannis, Zois	2-5	Wada, Naoki	2P-23
		Wakabayashi, Tomonari	2-7
< T >		Wang, Pengyingkai	2P-17
Tabata, Kento	2P-11	Wang, Sake	3-2, 3-7
Taguchi, Yuta	2-1	Wang, Tong	2P-26
Takahashi, Koji	1P-21, 1P-22	Wang, YuHuang	1-3
Takahashi, Kyoko	2-9	Watanabe, Makoto	2P-17
Takahashi, Togo	2P-9	Watanabe, Takanobu	3P-6
Takai, Kazuyuki	1P-24, 2P-24, 3P-21	Wu, Xiaojian	1-3
Takakura, Akira	3-8		
Takei, Kuniharu	1-6, 3-4	< X >	
Takenobu, Taishi	2-6, 1P-12, 2P-9, 2P-23, 3P-9	Xiang, Rong	1-3, 2P-13, 2P-17
Takimoto, Seiya	1P-5	< Y >	
Tanaka, Koichiro	3P-13	Yagi, Ryuta	3S-2
Tanaka, Kosuke	3P-11	Yagi, Takashi	3-9
Tanaka, Naoki	3-10, 1P-6, 2P-1, 2P-5	Yaji, Koichiro	3-1
Tanaka, Ryoga	2P-25	Yamada, Michio	1P-13
Tanaka, Satoru	1S-3, 3-1	Yamada, Takeo	3-5, 2P-14, 3P-17
Tanaka, Takeshi	3-8, 2P-6	Yamada, Tomoyuki	2P-23
Tanaka, Toshihiko	2-8	Yamaguchi, Ryohei	3P-6
Terao, Yuri	2-4	Yamamoto, Keisuke	2-4
Teshima, Hideaki	1P-22	Yamamoto, Takahiro	1P-12
Tian, Yuan	1P-25	Yamashita, Daiki	3P-3
Tomita, Motohiro	3P-6	Yamazaki, Satoshi	1-1
Tomo, Yoko	1P-22	Yanagi, Kazuhiro	2-6, 3-9, 1P-12, 1P-26, 2P-2, 2P-25, 3P-13
Tsuji, Takashi	1-10		
		Yang, Mengju	2P-12
< U >		Yanlin, Gao	3P-20
Uchida, Kento	3P-13	Yokoi, Hiroyuki	3P-25
Uchiyama, Haruki	1P-15, 3P-5	Yokota, Hiroki	2P-24
Ueda, Yuki	2P-18	Yomogida, Yohei	3-9, 1P-12, 1P-26, 2P-2, 2P-25, 3P-13
Uji, Kan	3-9, 1P-12, 2P-2		

Yoshida, Akari	3-9, 1P-12, 2P-2
Yoshida, Satoshi	1P-9
Yoshida, Shoji	2P-8
Yoshihara, Naoki	3P-18
Yoshikawa, Hirofumi	2-5
Yoshimura, Daisuke	3P-23
Yoshimura, Masamichi	2P-21
Yotsumoto, Satoshi	3P-12
Yu, Boda	2P-3

< **Z** >

Zhang, Minfang	1P-7
Zhang, Wenjin	2P-23
Zhao, Yangzhou	2P-24
Zheng, Liu	2-3, 2-6, 1P-23, 2P-8, 3P-9, 2P-23, 3P-22, 3P-24
Zheng, Yongjia	2P-13 , 2P-17
Zhou, Ying	2P-14
Zolotoukhna, Tatiana	2P-20

複写をご希望の方へ

フラーレン・ナノチューブ・グラフェン学会では、複写複製および転載複製に係る著作権を学術著作権協会に委託しています。当該利用をご希望の方は、学術著作権協会 (<https://www.jaacc.org/>) が提供している複製利用許諾システムもしくは転載許諾システムを通じて申請ください。

注意：著作物の引用、翻訳等に関しては、(社)学術著作権協会に委託致しておりません。直接、フラーレン・ナノチューブ・グラフェン学会へお問い合わせください。

Reprographic Reproduction outside Japan

Fullerenes, Nanotubes and Graphene Research Society authorized Japan Academic Association For Copyright Clearance (JAC) to license our reproduction rights and reuse rights of copyrighted works. If you wish to obtain permissions of these rights in the countries or regions outside Japan, please refer to the homepage of JAC (<http://www.jaacc.org/>) and confirm appropriate organizations to request permission.

In order to obtain permission to quote and/or translate, please contact the copyright holder directly.

2020年9月10日発行

第59回フラーレン・ナノチューブ・グラフェン総合シンポジウム 講演要旨集

《フラーレン・ナノチューブ・グラフェン学会》

〒464-8601 愛知県名古屋市千種区不老町

名古屋大学 未来材料・システム研究所

未来・エレクトロニクス集積研究センター 大野研究室内

E-mail : secretariat@fntg.jp

URL : https://fntg.jp/jp_new/

印刷 / 製本 社会福祉法人 福岡コロニー

GEMINI *an ultra-stable interferometer*

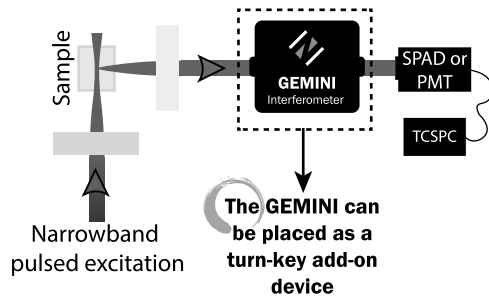
GEMINIは新しくコンパクトで堅牢な干渉計です。
 時間分解蛍光スペクトル、コヒーレントラマン分光、ポンププローブ測定、単一分子分光などのさまざまなアプリケーションで優れた性能を発揮します。

主な特徴

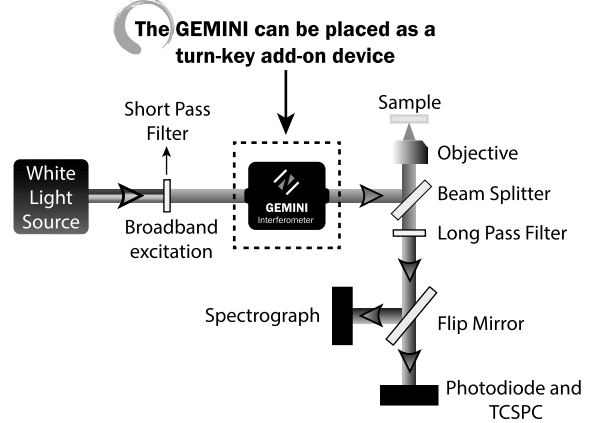
- ・ 高効率、高感度
- ・ 1秒以内の高速スキャン
- ・ コンパクト、定価価格
- ・ 優れた耐振動性能
- ・ 波長範囲 250 ~ 3500 nm
- ・ 外形寸法 100 x 110 x 65 mm



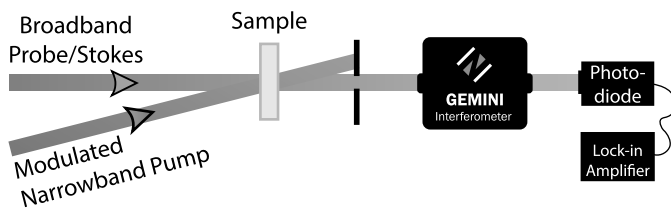
発光側に使用して時間分解蛍光スペクトルに



励起側に使用してEEM測定に



ポンププローブ過渡吸収測定に





科学技術と生産技術の進歩に貢献し、
お客様の研究開発や品質管理をサポートします。

「私達に、ご相談ください！」

分析・計測機器の販売
試薬・工業薬品の販売
各種工事（ユーティリティ・移設）
メンテナンス（修理・点検）
中古品販売

★特注商品 設計・製作



運用解析



納入・稼働



品質チェック



設計・製作



カスタマイズ



桜木理化学機械株式会社

本社・福岡営業所
北九州営業所
鳥栖営業所

福岡市博多区千代4-4-23
北九州市戸畑区牧山5-1-2
鳥栖市布津原町11-16

TEL 092-651-9561
TEL 093-883-6616
TEL 0942-82-6728

～スマートなデザインに簡単操作～

BRANSON 超音波ホモジナイザー

主な特長

- 1.電気エネルギーから超音波振動への変換効率が95%以上
→ 無駄なエネルギーロスが小さく、安定した振幅が得られる。
- 2.通常では、液体の種類によって振幅が安定し難い。
→ 条件を変えても一定の振幅を保つ機能がついている。
- 3.ジュール (watt/sec) による発振制御が可能
→ Total何ジュールでこの処理が完了するという情報が論文に掲載できる。

20kHz超音波ホモジナイザー
BRANSON SONIFIER SFX250,550

40kHz超音波ホモジナイザー
BRANSON SONIFIER SFX150HH



主なアプリケーション

分散

カーボンナノチューブ 有機顔料 無機顔料 セラミック セメント 感光体 記録材料
磁性粉 粉末冶金 酸化鉄 金属酸化物 シリカ アルミナ カーボンブラック
ポリマー ラテックス 製紙 ファンデーション
研磨剤 電池 フィラー 光触媒 触媒 ワクチン 体外診断薬 歯磨き粉 シャンプー
半導体 電子基盤 液晶 貴金属 金属 宝石 タイヤ 発酵菌類 その他

乳化

エマルジョン製剤 農薬 トナー ラテックス 界面活性剤 クリーム 乳液 その他

日本国内販売総代理店



株式
会社

セントラル科学貿易

東京本社: 〒136-0071 東京都江東区亀戸1-28-6 タニビル3F

TEL 03-5627-8150 FAX 03-5627-8151

技術物流センター: 〒272-0146 千葉県市川市広尾2-1-9

TEL 047-701-6100 FAX 047-701-6116

大阪支店: 〒533-0031 大阪府大阪市東淀川区西淡路1-1-36 新大阪ビル

TEL 06-6325-3171 FAX 03-6325-5180

福岡営業所: 〒812-0016 福岡県福岡市博多区博多駅南1-2-15 事務機ビル

TEL 092-482-4000 FAX 092-482-3797

札幌出張所: 〒001-0911 北海道札幌市北区新琴似11条13-7-13-2

TEL 011-764-3611 FAX 011-764-3612

<https://www.cscjp.co.jp>

GRAND ARM™ over GRAND ARM™

原子分解能分析電子顕微鏡

JEM-ARM300F2

"GRAND ARM™ 2"

原子分解能電子顕微鏡 JEM-ARM300F

"GRAND ARM™" をさらに進化させ、

低加速から高加速までさまざまな加速電圧にて、

超高空間分解能観察と高感度分析を両立させた

原子分解能分析電子顕微鏡登場！

JEOL  **日本電子株式会社**

本社・昭島製作所 〒196-8558 東京都昭島市武蔵野3-1-2 TEL:(042)543-1111(大代表) FAX:(042)546-3353
www.jeol.co.jp ISO 9001-ISO 14001 認証取得

JEOLグループは、「理科学・計測機器」「産業機器」「医用機器」の3つの事業ドメインにより事業を行っております。
【理科学・計測機器事業】電子光学機器・分析機器・計測検査機器 【産業機器事業】半導体関連機器・産業機器 【医用機器事業】医用機器



**TELEDYNE
PRINCETON INSTRUMENTS**
Everywhere you look™

高感度近赤外線
2次元 InGaAs ハイスピードカメラ

NIRvana® HS

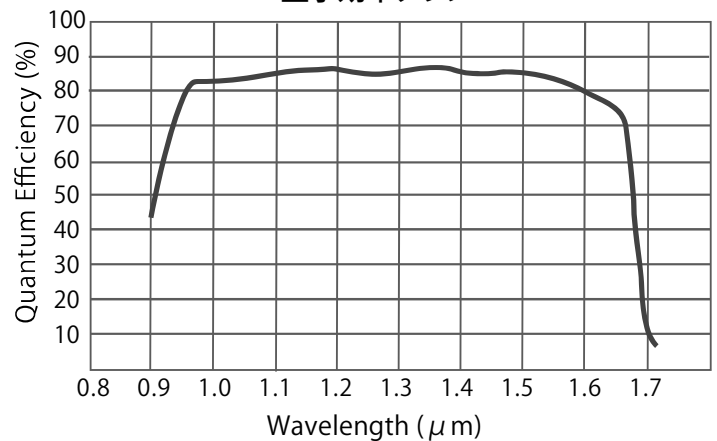
- **ハイスピード**
250 fps (full 640x512 pixels)
1200 fps (200x200 pixels)
- **多彩な読み出しモード**
Integrate While Read (IWR) mode搭載
マルチROI
- **低読み出しノイズ**
- **USB3.0接続**



アプリケーション例

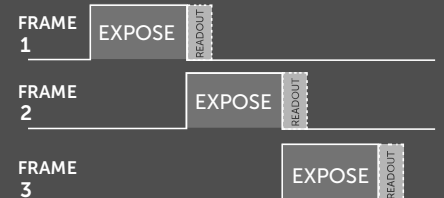
- ・フォトリソ結晶PLイメージング及びスペクトル
- ・一重項酸素イメージング及びスペクトル
- ・太陽電池PLイメージング及びスペクトル
- ・天体観測微弱光イメージング
- ・食品断面イメージング
- ・In-Vivoイメージング など

量子効率グラフ



仕様

モデル	NIRvana HS	NIRvana:640	NIRvana:640LN
センサー	640 x 512 x InGaAs		
素子サイズ	20 μm x 20 μm		
波長範囲	0.9 ~ 1.7 μm		
冷却温度	-55°C (-50°C空冷)	-80°C	-190°C
ダークチャージ	700 e-/p/sec	300 e-/p/sec	<8 e-/p/sec
読み出しノイズ	<60 e-rms	<120 e-rms	15 e-rms
ダイナミックレンジ	16 Bit (>15Bit@1 素子)		
フレームレート	250 fps	110 fps	2.77 fps@250KHz
インターフェース	USB3.0	Gig E	



Integrate While Read (IWR) mode
for maximum duty cycle

www.pi-j.co.jp

テレダイン・ジャパン株式会社 プリンストンインスツルメンツ

〒170-0013 東京都豊島区東池袋 3-4-3 池袋イースト13F TEL 03-6709-0631 FAX 03-6709-0632